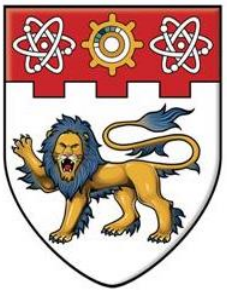

NANYANG TECHNOLOGICAL UNIVERSITY

THE ROLE OF IRON IN *ENTEROCOCCUS FAECALIS* BIOFILM FORMATION

LAM LING NING

School of Biological Sciences

2018

The role of iron in *Enterococcus faecalis* biofilm formation

LAM LING NING

School of Biological Sciences

A thesis submitted to the Nanyang Technological University in partial fulfillment of the requirement for the degree of Doctor of Philosophy

2018

Acknowledgement

I would like to express my heartfelt gratitude to Assoc Professor Kimberly Kline for her patience and guidance, as well as the valuable insights and expertise, which contributed to the development of my project and Dr Damien Keogh, former colleague, who pioneered the project. I appreciate the freedom Kimberly has given me to freely explore and develop my research throughout these years. I am also grateful for all the advice and guidance in developing my leadership skills and interpersonal skills, which have been a great asset. The help and experience sharing in the search for academic postdoctoral position is a good learning experience which I will lean upon moving forward in academic research.

I am also grateful to have wonderful thesis advisory committee members, namely Assoc Prof Scott Rice and Assoc Prof Zbynek Bozdech who have given great suggestions in developing my research project. The journey in academic research has been fruitful and a great learning experience. I especially like to express my gratitude to Pei Yi, Wei Hong, Kelvin, Jun Jie, Irina, Sumitra and Adeline, who I have bothered numerous times for help as well as all other members in the Kline lab who have made my PhD journey full of joy and excitement, and together made Kline lab my second home and family. I am also appreciative to have parents who are supportive in my studies and life decisions that I made over the years.

Last but not least, I would like to thank the staff and students working in Singapore Centre on Environmental Life Science Engineering (SCELSE) for guiding me in term of logistic, administrative and laboratory needs. I have fostered many friendships and gained invaluable memories throughout this journey. As such, I would like to express my gratitude to everyone for their encouragement, companionship and support. I would like to thank School of Biological Sciences, Nanyang Technological University for its Research Scholarship. This work was also funded by the National Research Foundation and Ministry of Education Singapore under its Research Centre of Excellence Programme, by the National Research Foundation under its Singapore NRF Fellowship programme (NRF-NRFF2011-11), and by the Ministry of Education Singapore under its Tier 2 programme (MOE2014-T2-2-124).

Table of Contents

Acknowledgement 3

Table of contents 4

List of figures 8

List of tables 10

Abbreviations 11

Abstract 13

Chapter 1: Introduction and literature review 15

1.1 Emergence of Enterococci 15

1.2 Enterococcus biofilm associated infections 15

1.3 Enterococcus biofilm formation 16

1.3.1 Quorum sensing systems 16

1.3.2 Surface attachment 19

1.3.3 Microcolony formation 20

1.3.4 Biofilm growth and maturation 21

1.4 Role of transition metals in infection 23

1.5 Host-pathogen competition for iron 24

1.6 Putative iron acquisition systems in Enterococci 25

1.7 Role of iron in Enterococcus physiology 27

1.8 Oxidative stress resilience in Enterococcus physiology 28

1.9 Significance of this study 30

Chapter 2: Extracellular electron transfer powers *E. faecalis* biofilm metabolism 32

2.1 Statement of contribution 32

2.2 Abstract 33

2.3 Introduction 34

2.4 Materials and methods 36

2.5 Results 44

2.5.1 Iron supplementation augments *E. faecalis* biofilm and alters biofilm architecture 44

2.5.2 *E. faecalis* biofilm biomass augmentation is a biofilm-specific phenotype 46

2.5.3 Iron mediated *E. faecalis* biofilm augmentation is biometal specific and dose dependent 47
2.5.4 Iron deposits are present in iron supplemented *E. faecalis* biofilm 49
2.5.5 Genes associated with *E. faecalis* metabolism contribute to iron mediated biofilm growth 52
2.5.6 L-lactate dehydrogenase drives extracellular electron transfer and increased energy production through modulating NAD/NADH substrate 55
2.5.7 Iron mediated extracellular electron transfer is biometal specific and genus specific mechanism 61
2.6 Discussion 64
2.7 Acknowledgements 66
2.8 Supplementary figures and tables 67
Chapter 3: Iron-pili interaction facilitates electron transfer, biofilm augmentation and intracellular iron accumulation to promote *Enterococcus faecalis* biofilm formation 69
3.1 Statement of contribution 69
3.2 Abstract 70
3.3 Introduction 72
3.4 Materials and methods 75
3.5 Results 83
3.5.1 Iron-augmented *E. faecalis* biofilm formation requires pilus expression 83
3.5.2 Iron drives aggregation of pilus expressing cells in *E. faecalis* biofilm 87
3.5.3 Iron induces pilus expression in *E. faecalis* in a biometal specific manner 89
3.5.4 Iron co-localized to pili on cell surface and is dependent on MIDAS motif on EbpA 91
3.5.5 Pili and electron transport systems contribute to extracellular electron transfer (EET) 96

3.5.6 Global transcriptional analysis of iron supplemented *E. faecalis* biofilm reveals 90 genes which are differentially regulated in response to iron 99
3.5.7 Global transcriptional analysis of iron supplemented *ebpA*^{AWAGA} mutant biofilm reveal 734 genes which are differential regulated compared to wild type OG1RF 106
3.5.8 High iron diet promotes Ebp-dependent *E. faecalis* colonization in the murine colon 111
3.6 Discussion 115
3.7 Acknowledgements 119
3.8 Supplementary figures and tables 120
Chapter 4: *E. faecalis* manganese efflux transporter (MntE) prevents manganese toxicity and contributes to fitness in murine gastrointestinal (GI) colonization 122
4.1 Statement of contribution 122
4.2 Abstract 123
4.3 Introduction 124
4.4 Materials and methods 127
4.5 Results 132
4.5.1 *OG1RF_10589* cation efflux transporter is a manganese efflux pump (MntE) 132
4.5.2 Upregulation of *mntE* under high manganese conditions alleviates intracellular metal accumulation and modulates *E. faecalis* pathogenicity 138
4.5.3 Magnesium supplementation alleviates manganese mediated growth inhibition 139
4.5.4 MntE efflux pump exhibits dual manganese and iron specificity which modulates growth and virulence gene expression 141
4.5.5 Absence of MntE does not alter oxidative stress tolerance 144
4.5.6 MntE efflux pump contribute to fitness in murine gastrointestinal (GI) tract colonization 145
4.6 Discussion 147

4.7 Acknowledgements 149
Chapter 5: Conclusion 150
5.1 Significance of findings 150
5.2 Future directions 152
Conference presentation and publications 154
References 156

List of figures

Chapter 2: Extracellular electron transfer powers *Enterococcus faecalis* biofilm metabolism

Figure 2.1: *E. faecalis* flow cell biofilms in iron supplemented media

Figure 2.2: *E. faecalis* planktonic growth under metal supplementation

Figure 2.3: *E. faecalis* biofilm growth under metal supplementation

Figure 2.4: Electron micrographs of the *E. faecalis* biofilm matrix grown in iron supplemented media

Figure 2.5: Transposon library screen for mutants exhibiting changes in biofilm accumulation under iron supplementation

Figure 2.6: Extracellular electron transfer in *E. faecalis* biofilm

Figure 2.7: *E. faecalis ldh1* mutant biofilm growth in iron supplementation

Figure 2.8: MALDI MS/MS analysis of NAD/NADH ratios

Figure 2.9: Model for fermentation and EET-dependent respiration metabolism in *E. faecalis* biofilm

Figure 2.10: Biometal specificity of extracellular electron transfer in *Enterococcus spp*

Figure S2.1: Electron micrographs of the *E. faecalis* biofilm matrix in the absence or presence of metal supplementation

Figure S2.2: Biofilm biomass and metal-dependence of *E. faecalis* EET

Chapter 3: Iron-pili interaction facilitates electron transfer, biofilm augmentation and intracellular iron accumulation to promote *Enterococcus faecalis* biofilm formation

Figure 3.1. Contribution of pilus to iron mediated *E. faecalis* biofilm growth

Figure 3.2. Analysis of complemented Δ*ebpABC* pGCP123::*ebpABCsrtC* ability to form biofilm in iron supplemented media

Figure 3.3. *E. faecalis* biofilm growth in iron supplemented media

Figure 3.4. Quantification of pilus-expressing cell population in *E. faecalis* biofilm

Figure 3.5. Electron micrographs of *E. faecalis* biofilm

Figure 3.6. Iron quantification in pilus extract from *E. faecalis* biofilm

Figure 3.7. Extracellular electron transfer in *E. faecalis* biofilm

Figure 3.8. Global transcriptional response of *E. faecalis* biofilm exposed to iron for 24 hrs

Figure 3.9. qRT-PCR of RNA transcript abundance of genes associated with pilus biogenesis
Figure 3.10. Intracellular iron quantification of *E. faecalis* mutants
Figure 3.11. Quantification of ability for ferric iron reduction in *E. faecalis* mutants
Figure 3.12 Global transcriptional response of *E. faecalis ebpA*^{AWAGA} deletion mutant biofilm exposed to iron for 24 hrs
Figure 3.13. Venn diagram of genes responsive to iron and MIDAS motif
Figure 3.14 *E. faecalis* colonization in lower gastrointestinal tract

Chapter 4: *E. faecalis* manganese efflux transporter (MntE) prevents manganese toxicity and contributes to fitness in murine gastrointestinal (GI) colonization

Figure 4.1. Cation sensitivity of MntE transposon mutant
Figure 4.2. Manganese supplementation results in planktonic growth inhibition
Figure 4.3. Manganese supplementation results in biofilm growth inhibition
Figure 4.4. Intracellular manganese and magnesium content in 24 hr *E. faecalis* biofilm
Figure 4.5. Magnesium supplementation rescue manganese mediated growth inhibition
Figure 4.6. Comparison of gene expression in *E. faecalis* biofilm under manganese and iron condition
Figure 4.7. Iron quantification in *E. faecalis* biofilm grown in 2 mM iron
Figure 4.8. Oxidative stress tolerance against menadione and hydrogen peroxide
Figure 4.9. Hydrogen peroxide production under manganese and iron stress
Figure 4.10. *E. faecalis* colonization in lower gastrointestinal tract of murine

Chapter 5: Conclusion

Figure 5.1. Model for the role of iron in *E. faecalis* biofilm
Figure 5.2. *E. faecalis* colonization in lower gastrointestinal tract of murine.

List of tables

Chapter 2: Extracellular electron transfer powers *Enterococcus faecalis* biofilm metabolism

Table 2.1: *E. faecalis* genes involved in iron-induced biofilm growth

Chapter 3: Iron-pili interaction facilitates electron transfer, biofilm augmentation and intracellular iron accumulation to promote *Enterococcus faecalis* biofilm formation

Table 3.1: List of bacterial strains used

Table 3.2: Primers used in qRT-PCR

Table 3.3: *E. faecalis* iron uptake and oxidative stress homeostasis genes transcriptionally regulated in response to 2 mM iron

Table 3.4: List of *E. faecalis* virulence gene transcriptionally regulated in response to iron

Table 3.5: *E. faecalis ebpA*^{AWAGA} mutant iron uptake and oxidative stress homeostasis genes transcriptionally regulated in response to 2 mM iron

Table 3.6 List of gene transcriptionally regulated in response to iron and MIDAS motif

Table S3.1: List of *E. faecalis* virulence gene transcriptionally regulated in response to iron in *E. faecalis ebpA*^{AWAGA} mutant

Table S3.2: List of cell division and respiration-associated genes transcriptionally regulated in response to iron in *E. faecalis ebpA*^{AWAGA} mutant

Chapter 4: *E. faecalis* manganese efflux transporter (MntE) prevents manganese toxicity and contributes to fitness in murine gastrointestinal (GI) colonization

Table 4.1: List of bacterial strains used

Table 4.2: Primers used in qRT-PCR

Table 4.3. Global transcriptional changes in *mntE:Tn* grown in 2 mM iron in comparison with OG1RF

Abbreviations

Enterococcus faecalis (*E. faecalis*)

Pseudomonas aeruginosa (P. aeruginosa)

Endocarditis and biofilm associated pili (Ebp)

Iron (Fe)

Manganese (Mn)

Magnesium (Mg)

Copper (Cu)

Zinc (Zn)

Extracellular electron transfer (EET)

Urinary tract infections (UTI)

Catheter-associated UTI (CAUTI)

Extracellular polymeric substances (EPS)

Quorum sensing (QS)

Alarmones guanosine tetraphosphate and guanosine pentaphosphate ((p)ppGpp)

Gelatinase biosynthesis-activating pheromone (GBAP)

Auto-inducer 2 (AI-2)

Aggregation substance (Agg)

Biofilm-associated glycolipid synthesis A (BgsA)

Enterococcal surface protein (Esp)

Extracellular DNA (eDNA)

Multiple peptide resistance factor (mprF*)*

Reactive oxygen species (ROS)

Gastrointestinal tract (GI)

Tryptone soya broth supplemented with 10 mM glucose (TSBG)

Phosphate buffered saline (PBS)

Tryptone soya broth (TSB)

Brain heart infusion (BHI)

Colony forming units (CFU)

Optical density (OD)

Genomic DNA (gDNA)

SYTO 9 green fluorescent nucleic acid stain (SYTO9)

Propidium iodide (PI)

Transmission electron microscopy (TEM)

Adenosine triphosphate (ATP)

Energy-dispersive X-ray spectroscopy (EDS)

High-angle annular dark-field scanning transmission (HAADF STEM)

Three dimensional (3D)

Inductive coupled plasma mass spectroscopy (ICP-MS)

Nicotinamide adenine dinucleotide (NAD – oxidized, NADH – reduced)

Confocal laser scanning microscopy (CLSM)

Green fluorescence protein (GFP)

L-lactate dehydrogenase 1 (ldh1)

Milicoulomb (mC)

Current (Q)

Standard error margin (SEM)

Hydroxy-1,4-naphthoquinone (HNQ)

Extracellular matrix (ECM)

Quantitative real time PCR (qRT-PCR)

Cation diffusion facilitator (CDF)

Abstract

Enterococcal biofilm-associated infections are a major challenge in hospitals due to their tolerance to host defenses and their intrinsic and acquired antimicrobial resistance. *Enterococcus faecalis* is a member of the gut microbiota and is a clinically important opportunistic pathogen associated with endocarditis, and several other nosocomial infections such as wound and urinary tract infections. Owing to its malleable genome and metabolic flexibility, *E. faecalis* is well adapted to colonize a variety of niches in the host. Furthermore, *E. faecalis* possesses several cell surface virulence factors including endocarditis and biofilm associated pili (Ebp) which are important for host colonization. Many pathogenic organisms require iron (Fe) for essential metabolic processes, and the host has multiple mechanisms to restrict iron availability to limit bacterial growth. Even though *E. faecalis* is highly tolerant to both iron restriction and high iron concentrations, its homeostatic response to iron availability has been minimally studied and the role of iron in enterococcal biofilm physiology and infection has been largely overlooked.

In this thesis, we show that iron augments *E. faecalis* biofilm formation and alters biofilm structure. Using a transposon library screen, we identified genes associated with respiration and metal efflux that contribute to iron-augmented biofilm growth. Using chronocoulometry assay, we also uncovered that *E. faecalis* uses iron for extracellular electron transfer (EET), and absence of *ldh1* attenuate electron transfer. Presence of Ldh1 contributes to generate growth-promoting energy. In addition to Ldh1, further characterization of other genes identified through the library screen uncovered additionally mechanisms driving iron-augmented biofilm growth. We demonstrate that pili, which are important for surface adherence and host colonization, contribute to both iron mediated biofilm growth and EET. We also show that MenB and Ndh3 which are essential for demethylmenaquinone (DMK) biosynthesis and flavin-mediated electron transfer respectively are involved in iron-mediated EET. Global transcriptional analysis of *E. faecalis* biofilm grown in iron supplemented media revealed upregulation of *feoB* iron transporter which is important for intracellular iron uptake. Furthermore, we demonstrate that iron co-purifies with Ebp on cell surface, and presence of Ebp and FeoB are essential for iron uptake in *E. faecalis* biofilm cells. We also show that a high iron diet promoted *E. faecalis* gastrointestinal tract (GI) colonization in the mouse colon, in an *ebp*-dependent manner. Together, these findings demonstrate that iron-pili

interaction facilitate electron transfer, biofilm augmentation and intracellular iron accumulation in *Enterococcus faecalis* biofilm.

In addition to iron uptake, we also found that iron and manganese export have a profound effect on biofilm growth. Among the genes identified in the transposon library screen, we uncovered that *E. faecalis* has a dual specificity MntE-like manganese exporter (*OG1RF_10589*) which contributes to iron-augmented biofilm growth. We show that MntE functions as a manganese (Mn) and iron (Fe) efflux pump in *E. faecalis.* Deletion of *mntE* results in accumulation of intracellular Mn and Fe which can be reverted either with *mntE* complementation or magnesium (Mg) supplementation. However, metal-induced growth inhibition is only observed in response to Mn, which suggest that MntE contributes to a larger extent, in Mn homeostasis. In support of this, we also observed upregulation of *mntE* in response to Mn, but not in Fe. Global transcriptional analysis of *mntE* mutant grown in high iron-supplemented media resulted in upregulation of three glycerol catabolic genes (*glpF2, glpK, glpO*), which leads to enhanced iron-mediated biofilm growth. Furthermore, we also demonstrate that deletion of *mntE* resulted in attenuated colonization in mouse gastrointestinal tract (GI) model.

These findings represent the first mechanistic description of extracellular electron transfer (EET) by *Enterococcus faecalis*, a gastrointestinal tract commensal and opportunistic pathogen, and support a previously unappreciated, additional role for *E. faecalis* endocarditis and biofilm associated pili in this process, beyond their adhesive function. Moreover, this is also the first study describing the importance of manganese tolerance by the manganese exporter MntE (*OG1RF_10589*) in *E. faecalis.* Through these findings, we better understand *E. faecalis* biofilm physiology and the role for transition metals in *E. faecalis* colonization, biofilm formation, and persistence in the host.

Chapter 1: Introduction and literature review

2.1 Emergence of Enterococci

Enterococcus faecalis is a gram positive diplococcal bacterium. The *Enterococcus* genus is in the *Enterococcaceae* family, and consists of species that commonly inhabit human and animal gastro-intestinal tracts (Lebreton et al., 2014). Enterococci can also be found in a variety of environments including plants, soil and water. A key factor for their broad distribution in different habitats stems from their remarkably resilient nature. Enterococci are highly tolerant of harsh environmental conditions such as high temperature, acidity, alkalinity, salt concentration, and nutrient scarcity which in turn may allow colonization at unfavourable niches (Fisher and Phillips, 2009).

Even though they constitute less than 1% of the adult human gut microbiome, Enterococci are ubiquitous and fastidious (Lebreton et al., 2014). For optimal growth, *E. faecalis* requires the amino acids valine, leucine, isoleucine, serine, methionine, glutamic acid, arginine, histidine, and tryptophan, as well as the vitamins biotin, nicotinic acid, pantothenate, pyridoxine, riboflavin, and folic acid. Despite its fastidious nutritional demands, it is one of the earliest gut colonizers in newborn humans (Lebreton et al., 2014). For decades, *E. faecalis* has been thought to be part of the commensal, non-pathogenic microbiome within the gastrointestinal tract, thus has been deemed largely medically insignificant. However, in the 1980s, the prevalence of Enterococci rose in hospital-acquired infections, the majority of which occurred in immuno-compromised individuals (Arias and Murray, 2012; Higuita and Huycke, 2014; Hollenbeck and Rice, 2012). The emergence of antibiotic resistance strains worldwide has exacerbated the challenge in treating enterococcal infections (Higuita and Huycke, 2014) and highlighted the need to understand the ecology, epidemiology and virulence of *E. faecalis* in order to identify new therapeutic strategies.

1.2 Enterococcus biofilm-associated infections

E. faecalis is an opportunistic pathogen and is involved in numerous nosocomial infections such as bacteraemia and urinary tract infections (UTI) (Higuita and Huycke, 2014; Kristich et al., 2014). *E. faecalis* can also colonize and infect the bloodstream, endocardium, surgical wounds, and implanted medical devices (Higuita and Huycke, 2014). Among these nosocomial infections, many are often biofilm associated and are polymicrobial in nature (Dunny et al., 2014). Biofilms

are defined by their coordinated community-like interactions of bacterial cells existing as microbial communities adhered on a surface, which display increased antimicrobial tolerance and which makes treatment of biofilm-associated infections extremely challenging (O'Toole et al., 2000). Biofilms were first associated with *E. faecalis* clinical infections when the organism was found alone or mixed with other bacterial species on catheter implants and in vegetations from endocarditis (Jansen et al., 1993; Keane et al., 1994; Reid et al., 1992; Stickler et al., 1993). Given their clinical significance, concerted efforts over the years have aimed to determine biofilm associated genetic factors and the mechanisms underlying enterococcal biofilm formation.

Biofilms, unlike planktonic cells, secrete extracellular polymeric substances (EPS) that are a major constituent of the biofilm extracellular matrix, encasing the bacterial cells and protecting them from environmental stresses. In the context of clinical infections, this leads to both enhanced antimicrobial tolerance and evasion from killing by immune cells (Stewart, 2002). Moreover, bacterial cells within a biofilm use quorum sensing to mediate coordinated response to environmental stimuli (Flemming et al., 2016), which can in turn impact virulence. Understanding the virulence factors contributing to biofilm development in response to iron have considerable implications for current antibacterial treatments (Flemming et al., 2016; Phillips and Schultz, 2012). This rationale drives the work in this thesis, and aimed at understanding enterococcal biofilm development in order to advance alternative therapeutic treatments for biofilm associated infections.

1.3 Enterococcus biofilm formation

Biofilm development involves multiple stages: surface attachment, microcolony formation, biofilm maturation and dispersal. Enterococci are able to form biofilms both *in vitro* and *in vivo*.

1.3.1 Quorum sensing systems

In many bacteria, biofilm development is driven by population density dependent quorum sensing (QS). Quorum sensing is a means for bacteria in a community to communicate and coordinate responses (Solano et al., 2014). Identification of QS inhibitors in other bacteria species (Aggarwal et al., 2015) has demonstrated that QS are promising targets for developing anti-biofilm treatments. The identification of small signaling molecules and metabolites in QS have been described

recently. Chavez de Paz and colleagues have shown that alarmones guanosine tetraphosphate and guanosine pentaphosphate, collectively known as (p)ppGpp, which is regulated by (p)ppGpp-synthetase/hydrolase RelA and the alarmone synthetase RelQ, contribute to virulence, stress response and biofilm formation in *E. faecalis*. Deletion of *relA*, which resulted in complete loss of (p)ppGpp, consequently decreased antibiotic tolerance and resulted in decreased antibiotic tolerance, attenuated biofilm formation *in vitro*, attenuated virulence and consequently increases survival of infected *C. elegans* (Chávez de Paz et al., 2012). The role of small signaling molecules such as cyclic di-GMP (Camilli and Bassler, 2006; Krasteva et al., 2012) and cyclic di-AMP (Corrigan et al., 2013; Gries et al., 2016; Peng et al., 2016a; Peng et al., 2016b; Townsley et al., 2018) in modulating biofilm formation has been demonstrated in other bacterial species; however these cyclic dinucletodide signaling molecules in Enterococci have not been well-studied. However, Davlieva and colleagues have recently shown that Enterococci also produces cyclic di-AMP which is hydrolyzed by a cyclic dinucleotide phosphodiesterase of the GdpP family. Moreover, the cyclic dinucleotide phosphodiesterase is a part of LiaFSR membrane stress pathway. Mutating the cyclic dinucleotide phosphodiesterase results in loss of hydrolysis activity, led to accumulation of cyclic di-AMP level which consequently led to increased susceptibility to daptomycin (Wang et al., 2017). To date, the underlying mechanism between these small molecules and (p)ppGpp in driving enterococcal biofilm development remains to be elucidated.

Several quorum sensing (QS) systems are utilized by Enterococci. Peptide pheromone secretion can drive a coordinated response in a bacterial community, and is a conserved system observed across many prokaryotes and eukaryotes (Wyatt, 2014). Hence, it is not unexpected that Enterococci are also equipped with the ability to respond to peptide pheromones (Cook and Federle, 2014). Among the peptide pheromone systems identified in Enterococci, the cCF10 peptide pheromone conjugative system is the most well studied to date. Secretion of the cCF10 peptide pheromone out of donor cells is mediated by an ABC transporter (Varahan et al., 2014). The mechanism underlying peptide pheromone-mediated gene regulation and plasmid transfer has been well described (Chen et al., 2017b) and was recently shown to mediate pCF10 transfer between *E. faecalis* cells in the GI tract of mice (Hirt et al., 2018). Moreover, pheromone mediated plasmid transfer occurs between *E. faecalis* cells at a high efficiency in the intestinal tract, which suggest that pCF10 carriage provides a fitness advantage; however, its role in colonization and

infection remains to be answered. A membrane protease, Eep, processes immature peptide pheromones cAD1 and cCF10 (An et al., 1999; Chandler and Dunny, 2008). Eep also mediates proteolytic processing of RsiV which is the anti-sigma factor for SigV (extra-cytoplasmic function sigma factor), leading to enhanced environmental stress resistance (Varahan et al., 2013). Similar biofilm phenotypes were observed for both an *eep* and a *sigV* mutant (Varahan et al., 2013), consistent with *eep* regulation of SigV production. Eep, along with AhrC (an ArgR family transcriptional regulator), contributes to *in vitro* biofilm formation (Frank et al., 2013) and deletion of either gene attenuates colonization in a rat osteomyelitis model *in vivo* (Frank et al., 2015), and significantly reduces bacterial burden in UTI (Frank et al., 2013) and endocarditis infection model (Frank et al., 2012).

Another quorum sensing system present in Enterococci is *fsrABC*, which encodes a two-component system, comprised of *fsrC* (membrane sensor kinase) and *fsrA* (response regulator), as well as *fsrB* (soluble secreted peptide) which activates FsrAC in a density-dependent manner (Ali et al., 2017). The *fsr* quorum-sensing system also governs FsrD production, which is a precursor for the cyclic peptide GBAP (gelatinase biosynthesis-activating pheromone) (Nakayama et al., 2006). Similar to the peptide pheromone system, the growth and multiplication of bacterial cells drive the extracellular accumulation of GBAP, which in turn is sensed by FsrC and consequently phosphorylates intracellular response regulator FsrA (Ali et al., 2017). This cell-cell communication system regulates several biofilm-associated genes and operons including *bopABCD*, *ebpABC*, *gelE*, and *sprE* (Dunny et al., 2014), and deletion of *fsrABC* completely abolishes biofilm formation (Hancock and Perego, 2004b). Another secreted small molecule involved in biofilm formation is the CylL cytotoxin, located on pheromone responsive plasmids (Hallgren et al., 2009). However, the roles of CylL in quorum-dependent biofilm formation remain to be explored.

More recently, the auto-inducer 2 (AI-2) quorum sensing system, which is dependent on *luxS* (S-ribosylhomocysteine lyase) was demonstrated to be involved in the re-structuring of *Enterococcus* biofilms. AI-2 mediated cell-cell communication is involved in virulence and biofilm formation in *E. coli* (Li et al., 2007) and *S. aureus* (Zhao et al., 2010). Shao and colleagues have shown that AI-2 supplementation increases *E. faecalis* biofilm formation *in vitro* (Shao et al., 2012), and that

deletion of *luxS* results in aberrant biofilm formation consisting of aggregates and dense structures compared to confluent monolayer biofilms typically seen for wild type *E. faecalis* (He et al., 2016). Although quorum-sensing is also involved in triggering biofilm dispersal in other organisms (Guilhen et al., 2017), this has not been reported for enterococcal biofilms.

1.3.2 Surface attachment

Like all pathogenic bacteria, *E. faecalis* adherence to a surface (abiotic or biotic) drives the initial establishment of a biofilm. For the past two decades, concerted efforts and resources have been devoted to identify key surface adhesins that serve important roles in host surface attachment, which is the first step driving biofilm formation.

To date, one of the most well characterized surface adhesins is the endocarditis and biofilm associated pilus (Ebp). Ebp mediates surface adherence *in vitro* and *in vivo* and is composed of three different subunits: EbpA (the tip of the pilus), EbpB (basal subunit which is anchored to cell wall), and EbpC (major subunit which comprises the pilus fiber) (Bourgogne et al., 2010; Nallapareddy et al., 2011a; Nallapareddy et al., 2006; Nallapareddy et al., 2011b; Nielsen et al., 2012; Singh et al., 2007). Mutant strains in which *ebpABC* is deleted are attenuated for binding to platelets (Nallapareddy et al., 2011b), binding fibrinogen and collagen (Nallapareddy et al., 2011a), display reduced surface attachment and consequently display impaired biofilm formation *in vitro* (Nallapareddy et al., 2006). Significantly attenuated colonization in urinary tract infection (UTI), catheter-associated UTI (CAUTI), and infective endocarditis models (Nallapareddy et al., 2011a; Nallapareddy et al., 2006; Nallapareddy et al., 2011b; Nielsen et al., 2013b) also corroborated the *in vitro* findings. Together these findings suggest that Ebp is a promising target for developing alternative anti-biofilm treatments. In **Chapter 3** of this thesis, we will look at alternative roles of Ebp, in addition to its role in adhesion and host colonization, which further emphasize the importance of Ebp as a target for developing alternative anti-biofilm treatments.

Several similar studies have also looked into other surface adhesins such as aggregation substance, enterococcal surface protein (Esp), and adhesin to collagen from enterococci (Ace), and showed that lack of these surface adhesins significantly reduced surface adherence which consequently reduced biofilm formation (Mohamed et al., 2006; Rozdzinski et al., 2001; Sillanpaa et al., 2010;

Sussmuth et al., 2000; Toledo-Arana et al., 2001). Shankar and colleagues have also demonstrated that deletion of *esp* resulted in reduced bacterial burdens in murine bladder using an ascending UTI model (Shankar et al., 2001) which was expected since Esp is important for fibrinogen and collagen binding, and these ligands are present in bladders. Likewise, Ace is involved in collagen, laminin, and dentin binding (Kowalski et al., 2006; Nallapareddy et al., 2000a; Nallapareddy et al., 2000b), and deletion of *ace* leads to attenuated colonization in rat endocarditis (Singh et al., 2010) and UTI models (Lebreton et al., 2009), but does not reduce bacterial burden in peritonitis model (Singh et al., 2010), which suggests that Ace-mediated biofilm formation is not relevant in peritoneal infection. By contrast, deletion of aggregation substance (Agg) leads to reduced adherence to renal epithelial cells (Rozdzinski et al., 2001; Sussmuth et al., 2000), reduced binding to lipoteichoic acid of other *E. faecalis* cells, and thus reduced inter-bacterial clumping (Waters et al., 2004) and reduced bacterial titers recovered from endocarditis vegetations on aortic heart valves (Johnson et al., 2004). However, Agg is not involved in colonization of the urinary tract suggesting that Agg-mediated biofilms are not necessary for ascending UTI (Johnson et al., 2004).

Biofilm-associated glycolipid synthesis A (BgsA) also contributes to initial adherence and biofilm formation *in vitro,* but its contribution *in vivo* has yet to be determined (Theilacker et al., 2009). Deletion of the extracellular secreted protein *salB* (SagA-like protein B*)* enhanced fibronectin and collagen binding but paradoxically decreased biofilm formation (Mohamed et al., 2006), which was suggested to be due to decreased hydrophobicity of the cell wall of *salB*-mutant cells.

Collectively, these studies demonstrate that *E. faecalis* surface adhesins are important for initial surface attachment; however, they are niche dependent since each adhesin binds a different repertoire of ligands, which may be differentially available on different substrates. The use of appropriate *in vivo* models to understand how and where these factors act is an important consideration, and thus anti-biofilm treatments for Enterococci biofilm associated infections have to be tailored depending on the infection site and the target adhesin.

1.3.3 Microcolony formation

After establishing surface adherence, initial bacterial growth drives microcolony formation (Monds and O'Toole, 2009). In contrast to *P. aeruginosa*, the model organism whereby biofilm

development has been clearly described (Lee and Yoon, 2017), the mechanism underlying microcolony formation in Enterococci has not been characterized to date. However, several studies have described the peculiar phenomenon whereby *E. faecalis* biofilm structure changes in specific circumstances. Unlike typical 2-3 cell thick confluent biofilms typically observed in *in vitro* models, electron microscopic images of *E. faecalis* colonization of the GI tract of germ-free mice revealed numerous discrete clusters of cell aggregates covered in a fibrous sweater-like matrix (Barnes et al., 2017), which appears to mirror microcolonies being formed. Another recent study also showed similar biofilm structure mirroring enterococcal microcolonies when *E. faecalis* biofilm is exposed to antibiotic treatment. Biofilms exposed to sub-inhibitory levels of daptomycin form a complex structure, unlike the typical *in vitro* two-dimensional biofilms (Dale et al., 2017; Dale et al., 2015). Moreover, deletion of *epaOX*, a glycosyltransferase involved in production of cell-wall associated rhamnopolysaccharide also formed numerous microcolonies, in the absence of antibiotics (Dale et al., 2015), which are easily dislodged; a phenotype speculated to be due to reduced structural integrity. Although the precise role of EpaOX in microcolonies remains to be answered, it is clear that specific mechanisms, likely associated with environmental stress response, may be driving changes in biofilm structure.

1.3.4 Biofilm growth and maturation

Although the factors required for transition from microcolony formation to biofilm maturation has not been clearly elucidated for *E. faecalis*, it is theorized that biofilm maturation is driven by cell division and increased secretion of exopolymer substances such as extracellular DNA (eDNA), polysaccharides, lipoteichoic acid and extracellular proteases. The best characterized enterococcal biofilm matrix component is eDNA. Early studies have shown that eDNA contributes to biofilm integrity and the loss of eDNA either by deletion of autolysin or prevention of cell lysis increases surface detachment, and is conserved across several bacterial species (Montanaro et al., 2011). More recently, eDNA was observed at the *E. faecalis* septum, as part of intercellular filamentous structures, and also as part of the wider biofilm matrix (Barnes et al., 2012). Moreover, eDNA release from cells is dependent on autolysin (*atlA*) (Guiton et al., 2009; Thomas et al., 2009) which is not unexpected as this mechanism appears to be conserved. Biochemical assays and SEM imaging revealed both a lack of significant cell lysis and the presence of a membrane potential in cells associated with eDNA (Barnes et al., 2012), suggesting that eDNA is released from

metabolically active cells. Accordingly, treatment with Dnase reduced biofilm stability and increased detachment (Dunny et al., 2014; Vorkapic et al., 2016), and the deletion of *atlA* diminished eDNA release and resulted in reduced biofilm formation (Guiton et al., 2009). While there is no evidence that eDNA directs the spatial organization of enterococcal biofilm, as has been suggested for other bacterial species (Gloag et al., 2013), eDNA remains a potential therapeutic target.

Polysaccharides and glycoproteins are biofilm matrix components for many bacteria. Fabretti and colleagues hypothesized that lipoteichoic acid, which is an important constituent of gram positive bacterial cell wall, contributes to biofilm formation, and indeed deletion of *dltABCD* resulted in reduced biofilm formation *in vitro*, decreased adherence to epithelial cells, and increased susceptibility to antimicrobial peptides (Fabretti et al., 2006). Additionally, Hufnagel and colleagues showed that absence of *bopABC*, upstream of the putative sugar-binding transcriptional regulator *bopD*, resulted in enhanced biofilm growth in glucose but reduced biofilm growth when grown in maltose and attenuated virulence in murine GI colonization (Creti et al., 2006; Hufnagel et al., 2004). These data suggest that maltose is necessary for biofilm growth in the GI tract. Furthermore, deletion of multiple peptide resistance factor (*mprF)* paralogs (*mprF1* and *mprF2*), which are involved in cationic antimicrobial peptides resistance by modification of phosphatidylglycerol to reduce the net negative charge of membrane surface, results in increased sensitivity to several antimicrobial peptides, yet enhanced eDNA release and biofilm growth (Bao et al., 2012). Although *mprF1/2* deletion mutants are not attenuated in virulence in the murine bacteremia model (Bao et al., 2012), the *mprF1/2* deletion mutant is less fit during coinfection with parent strain at 3 days post infection in wound infection model (Chong et al., 2017) which demonstrate that cell membrane modification and membrane charge contribute to biofilm growth in a niche-dependent manner. Collectively, cell surface glycoproteins, membrane lipids, and polysaccharides likely contribute to the biofilm matrix in *E. faecalis* but their involvement in the organization and development of enterococcal biofilms is not well-characterized.

By contrast, extracellular proteases such as *gelE*, *sprE* and *atlA*, under the regulation Fsr quorum sensing system, are involved in matrix modification during biofilm growth (Dunny et al., 2014; Kristich et al., 2008; Qin et al., 1998; Thomas et al., 2009; Waters et al., 2003). Deletion of *gelE*

and *sprE* resulted in reduced biofilm formation *in vitro* and reduced bacterial burden in several *in vivo* models (Hancock and Perego, 2004a; Kristich et al., 2004; Thomas et al., 2008; Thurlow et al., 2010). However, in a rabbit endocarditis model, absence of *gelE* alone increases fibrinous matrix deposits in aortic vegetations (Thurlow et al., 2010), leading to the speculation that gelatinase may be digesting the biofilm matrix to facilitate dispersion (Thurlow et al., 2010). Interestingly, *sprE* deletion is associated with increased autolysis, eDNA release, and accelerates biofilm formation while *gelE* deletion prevents eDNA release (Thomas et al., 2008) and increases *ace* expression (Pinkston et al., 2011), which may increase surface attachment but make the biofilm susceptible to detachment by external stimuli.

Together, these findings provide some insights into the mechanism underlying the development of enterococcal biofilm but their contribution to disease remains poorly characterized. Nevertheless, targeting the mechanisms underlying these development stages are key to treating Enterococci biofilm associated infections.

1.4 Role of transition metals in infection

Enterococci are highly resilient and are exquisitely equipped to thrive in a variety of environmental and host niches (Hollenbeck and Rice, 2012; Ramsey et al., 2014b), which presumably enable colonization and infection. In the context of bacterial pathogenesis, the host represents a rich reservoir of nutrients which bacteria can acquire and use for survival and replication. Host-mediated environmental cues such as transition metal bioavailability can be exploited by bacteria to establish infection. Transition metals have variable oxidation states and readily accept or lose electrons, thus they typically drive redox reactions in biological processes. Of these transition metals, iron, copper, zinc and manganese are physiological relevant in host-pathogen infection (Hood and Skaar, 2012). These metals serve as cofactors for diverse families of metalloproteins. The change in oxidation states stem from the Fenton reaction and Haber Weiss reaction e.g. Fe^{2+} to Fe^{3+} or vice versa produces oxygen radical if the reactive species freely associate and react with proteins or DNA. Hence, strict regulation of intracellular metal is key to growth and virulence during infection (Palmer and Skaar, 2016).

There is limited literature describing role of transition metals during enterococcal infection to date. However, there have been some studies characterizing enterococcal physiology and resilience in the context of metals, using *Enterococcus hirae* as a model system despite its relatively limited metabolic capability, as compared to *E. faecalis* (Palmer et al., 2014; Ramsey et al., 2014b). *E. faecalis*, which colonise the gastrointestinal tract, possess several cation metal exporters such as ABC transporters, cation efflux transporter, major facilitator family transporter and divalent metal cation transporter yet there is no direct study of metal homeostasis during enterococcal infections. By understanding how Enterococci regulate the import, export and use of transition metals, as well as the dynamics of a changing host microenvironment during infection, we may gain insight into how these processes contribute to successful colonisation and infection. In this thesis, we will focus primarily on the role of iron on *E. faecalis* biofilm physiology and how this may impact clinical disease manifestation. To address this, in **Chapter 2**, we will show how iron drive *E. faecalis* biofilm formation, and in **Chapter 3**, we will discuss in details on the underlying mechanisms involved in iron-mediated biofilm growth and transcriptionally changes in response to iron. By contrast, **Chapter 4** will demonstrate the importance of exporting transition metals and how dysregulation of metal export have a profound effect on growth and biofilm formation in *E. faecalis*.

1.5 Host-pathogen competition for iron

Total iron content within a human adult is approximately 4 g and the majority of iron is found in haemoglobin, in the liver and spleen, while the rest is distributed among iron-binding proteins including transferrin, lactoferrin and ferritin (Ganz and Nemeth, 2012a, b). Iron is an essential metal for most organisms and is obtained in the form of dietary iron, primarily absorbed by the duodenum in the lower gastrointestinal tract (Benito and Miller, 1998). The predominant means of obtaining iron is through intestinal iron absorption where iron loss is replaced by dietary iron. Regulation of iron absorption still remains poorly understood, however there is a linear correlation between iron absorption, iron storage and iron loss (Hallberg, 2001). Typically, daily dietary intake contains 10-20 mg iron, and approximately 5-35% is absorbed to drive biological processes and replace daily iron loss (Abbaspour et al., 2014). Re-utilization of iron recycled from senescent cells account for most of the iron flux in the host (Bird, 2015; Drakesmith et al., 2015; Lamarche et al., 2008; Taketani, 2005). The unabsorbed fraction is excreted through the lower

gastrointestinal tract, hence it is conceivable that the colon could have a large iron reserve which *E. faecalis* and other gut anaerobic microbes can sense and respond to.

In most organisms, iron serves as a cofactor for cellular functions such as aerobic respiration, amino acid synthesis and stress resistance (Andrews et al., 2003; Frawley and Fang, 2014). However, iron is not readily accessible in the natural environment, as it is generally present in the insoluble Fe^{3+} (ferric) form (Weber et al., 2006). Thus, *E. faecalis*, as well as many other microbes, has evolved intrinsic mechanisms for iron acquisition from various sources, and convert ferric iron to Fe^{2+} (ferrous) iron which is then transported intracellularly by iron-transporting proteins (Andrews et al., 2003; Wooldridge and Williams, 1993)

Iron is an essential nutrient for the host and most microbes (Frawley and Fang, 2014), and its availability is one of the key factors in driving bacterial infection within a host (Bullen et al., 2006; Schaible and Kaufmann, 2004). Natural deterrence against infection is essential for host survival, and one key system used by the host is the tight regulation of iron availability (Bullen et al., 2006; Ganz and Nemeth, 2012a, b). Resistance to bacterial infection depends on an extremely low level of free iron (10^{-24} M) in mammalian systemic circulation (Carrondo, 2003; Valko et al., 2005). Restriction of labile iron hinges on iron-binding proteins (e.g. ferritin, lactoferrin, hepicidin, ferroportin, calprotectin), which have high affinity for binding to ferric iron (Drakesmith et al., 2015; Ganz and Nemeth, 2012a; Hentze et al., 2004; Nakashige et al., 2015; Taketani, 2005). However, in circumstances where iron is freely available in the circulatory system, when the bacteriostatic mechanism of the host (e.g. human) iron regulation system is impaired, an increased incidence of bacterial infections is observed (Weinberg, 1999, 2010). Iron overload can arise from altered metabolism such as haemochromatosis and hepatic disease, as well as from lysis of red blood cells resulting in release of haem compounds (Borgna-Pignatti and Marsella, 2015; Shiwei et al., 2015). Patients suffering from iron overload conditions, such as haemochromatosis and hepatic diseases, are more susceptible to infection by *Vibrio vulnificus* and *Candida albicans* among other pathogens (Borgna-Pignatti and Marsella, 2015; Kuo et al., 2009; Weinberg, 1999). The association of haemochromatosis with an increased prevalence of infections have been reviewed, however mechanisms driving virulence for different microbes in this setting varies

(Khan et al., 2007). However, an association between iron overload and *E. faecalis* infection has not been reported.

1.6 Putative iron acquisition systems in Enterococci

There have been no studies which primarily focus on characterization of enterococcal iron acquisition systems, particularly in the context of biofilms. However, *E. faecalis* genome encodes several putative iron uptake systems that are homologous to iron uptake systems in other bacteria (Ramsey et al., 2014b). Regulation of iron, in both gram positive and negative bacteria, has been associated with *fur* (ferric uptake regulator), a transcriptional repressor which drives expression of iron uptake associated genes in iron starved conditions (Troxell and Hassan, 2013). Many bacteria species utilise a number of ferrous iron uptake systems and siderophore systems, regulated by *fur*, to transport iron across the cell membrane and into the cell (Andrews et al., 2003).

The *E. faecalis* OG1RF genome encodes a number of putative cation transporters. By comparing with model organisms such as *Bacillus*, *Streptococcus* and *Escherichia spp*, four putative iron associated uptake systems are present – OG1RF 11352-11354 (approximately 36% protein sequence similarity to *Escherichia spp* FepBDE involved in ferric enterobactin import proteins) (Sprencel et al., 2000), OG1RF 10136-10139 (approximately 40% protein similarity to *Bacillus spp* FhuBGCD involved in ferric iron hydroxamate import) (Ollinger et al., 2006), OG1RF 10359-10360 (approximately 40% protein similarity to *Escherichia spp* FeoAB involved in ferrous iron import) (Kammler et al., 1993), and OG1RF 12351-12354 (54% protein similarity to *Bacillus spp* YclNOPQ iron petrobactin import) (Zawadzka et al., 2009); however these putative iron associated uptake systems have not been characterized. In contrast to iron uptake transporters, iron efflux transporters are less well studied due to the speculation that iron abundance in host-pathogen interaction during infection is unlikely to occur due to host iron sequestration. However, *E. faecalis* OG1RF genome encodes three putative efflux transporters – OG1RF_10589 (30% protein similarity to *Streptococcus spp* MntE manganese exporter) (Rosch et al., 2009), OG1RF_10301 (29% protein similarity to *Bacillus spp* RND efflux transporter) (Hassan et al., 2017), and OG1RF_10391 (32% protein similarity to *Bacillus spp* MATE efflux transporter) (Hassan et al., 2017). Among these efflux exporters, only OG1RF_10589 (MntE) manganese exporter has been shown to be upregulated when iron is in excess (Lopez et al., 2012) and downregulated when is

iron depleted (Abrantes et al., 2011; Vebo et al., 2009), together suggesting that MntE is iron responsive and functions to regulate iron export.

Taken together, we know that *E. faecalis* is equipped with the ability to uptake and efflux iron; however, it is unclear how does these iron acquisition systems work concertedly to regulate iron homeostasis. Moreover, the underlying mechanism in iron acquisition has not been clearly characterized. To address this, in **Chapter 3 and 4** of this thesis, we will elucidate the underlying mechanisms for iron acquisition.

1.7 Role of iron in Enterococci physiology

Remarkably, *E. faecalis* does not utilise iron to drive cellular growth, instead manganese is thought to be used as the essential cofactor for most enzymes required for biological processes (Archibald, 1986; Bruyneel et al., 1989; Marcelis et al., 1978; Weinberg, 1997). The use of alternative metals in the absence of iron, is unique in Lactobacillus species and a few other closely related lactic acid producing species (Weinberg, 1997). In serum, iron availability is severely restricted (Cassat and Skaar, 2013), which suggests that serum mimics an iron limited condition. However, iron depletion does not significantly attenuate *E. faecalis* growth (Colomer-Winter et al., 2017; Keogh et al., 2016b), which demonstrates that *E. faecalis* does not depend heavily on iron for growth.

Although the mechanism underlying sensing iron cues still remains unclear, several studies have shown the transcriptional changes in *E. faecalis*, in response to blood (Vebo et al., 2009) and high (1mM) iron concentrations (Lopez et al., 2012) *in vitro*. Exposure to blood leads to upregulation of genes associated with oxidative stress response (*ohr*, *dps*, *npr*, *msrB*, and *sodA),* and may drive virulence since *sodA* has been shown to contribute to intracellular survival in macrophages *in vitro* (Verneuil et al., 2006). Moreover, genes associated with fatty acid biosynthesis, lipases, putative lysis inhibitory systems, cardiolipin and membrane phospholipid synthesis are upregulated, while DltA and DltB, which are responsible for polymerization of teichoic acid and lipoteichoic acid are downregulated (Vebo et al., 2009), suggesting that remodelling of cell wall and membrane occurs in response to blood exposure. Upregulation of biofilm associated maltose metabolic genes, *bopAB/malPB, malT*, and manganese-dependent *efaABC* operon (Vebo et al., 2009) which encodes for endocarditis-associated virulence factor EfaA (Low et al., 2003), indicates that exposure to

blood may induce virulence and biofilm formation. Moreover, putative iron uptake transporters *feo* and *ycl* and other ABC transporters *mntH, yclQ, yclP, yclN, feoA, feoB*; a fur homolog (*perR*), as well as several stress response proteins (*nal, ohrA, trx, msrA, dps*) are upregulated, while *czcD* is downregulated to restrict cation efflux (Lopez et al., 2012), which further demonstrate that iron uptake and concomitant oxidative stress responses are important for growth in blood. Glycerol catabolism and glycolysis genes such as *gap-1*, glycerate kinase and *pgm* were up-regulated in response to growth in blood in addition to several metabolic systems governed by catabolite control protein A (CcpA) (Vebo et al., 2009), reflecting the metabolic flexibility of *E. faecalis* to acquire alternative carbon sources in blood which has limited glucose availability (Roder et al., 2016). Together, these findings suggest that *E. faecalis* respond to environmental iron limitations, which may be particularly important for growth in blood. However, blood also contains other nutritional cues which may also influence the transcriptional changes in *E. faecalis*. There are no studies to date which primarily characterize the *E. faecalis* response to iron depletion.

Conversely, Lopez and colleagues showed that exposure to excess (1 mM) iron leads to the downregulation of putative iron associated ABC transporters (*fhuC, fhuB, feoB, mntH, yclP, yclN*), suggesting that iron uptake is turned down when iron is abundant. *Fur* homologs (*perR, zurR*), oxidative stress response genes (*sodA, ohrA, msrA, trx*), and a cation efflux family protein (*czcD*) were upregulated in excess iron (Lopez et al., 2012) suggesting that excess iron is associated with oxidative stress, likely from release of radical species from the Fenton reaction, necessitating the export of excess intracellular iron. Because ferric iron is insoluble and unable to diffuse freely across bacterial membrane, bacteria have evolved mechanisms to synthesize high affinity iron-binding siderophores which sequester iron from host iron-binding proteins (Ahmed and Holmstrom, 2014; Saha et al., 2016) for its own use. Identification of iron-binding hydroxamate siderophores in Enterococci have been reported; however, genes associated with siderophore production have not been identified (Lisiecki, 2014; Lisiecki and Mikucki, 2006; Lisiecki et al., 2000; Maskell, 1980). Interestingly, *E. faecalis* possesses the arginine deaminase pathway (*arcABCRD*) which encodes for ornithine transcarboxylase, carbamate kinase, putative Crp/Fnr-type regulator, and a ornithine-arginine antiporter, which can synthesize ornithine (Barcelona-Andres et al., 2002), a cofactor required for hydroxamate-type siderophores. The binding of

ornithine to hydroxamate moiety in the sideropohore allows for subsequent iron binding (Robbel et al., 2011).

Overall, *E. faecalis* is able to sense and respond to iron availability, and associated transcriptional changes do indeed contribute to virulence. Although iron does not play a major role in *E. faecalis* growth as compared to other bacterial species, our overall understanding of the role of iron in Enterococci physiology still remains unclear. At the end of this thesis, we will demonstrate the role of iron and present a model for iron acquisition and utilization in *E. faecalis* biofilm.

1.8 Oxidative stress resilience in Enterococci physiology

Accompanying metal excess environment is the release of reactive oxygen species that can be stressful to most microbes. Encountering reactive oxygen species (ROS) is not uncommon, as it is generated from ATP generation with oxygen as the final electron acceptor during cellular growth (Cabiscol et al., 2000). Moreover, reactive oxygen species (ROS) is also produced as a result of the host immune response during infection (Paiva and Bozza, 2014). In the context of infection, *E. faecalis* encounters a variety of immune effectors in the human host, and its virulence is dependent on its ability to sense and respond to ROS.

E. faecalis is highly tolerant to oxidative stress, significantly surpassing other members of the phylogenetically similar Lactococci and Streptococci (Riboulet et al., 2007b), due to the presence of an extensive arsenal of ROS detoxification enzymes – three peroxidases (NADH peroxidase, alkyl hydroperoxide reductase and thiol reductase) (La Carbona et al., 2007), a heme dependent catalase (KatA) (Frankenberg et al., 2002b), a manganese-containing superoxide dismutase (SodA) (Britton et al., 1978), a NADH oxidase, a glutathione reductase, and the thioredoxin complex (Paulsen et al., 2003), which have been reviewed extensively (Ramsey et al., 2014c; Riboulet et al., 2007b). These detoxification enzymes are transcriptionally regulated by *perR*, a homolog of the Fur family (Verneuil et al., 2005a).

Given the metabolic flexibility and inherent ROS resilience of *E. faecalis*, it is therefore not surprising that *E. faecalis* can survive within macrophages, where concentration of reactive oxygen species is high, for up to 72 hours post infection (hpi) (Gentry-Weeks et al., 1999). Verneuil and

colleagues have shown that deletion of *perR* attenuates colonization in murine peritonitis model but has no effect on intracellular macrophage survival (Verneuil et al., 2005b), suggesting that other factors may be contributing to intracellular macrophage survival. Indeed, regulators of oxidative stress such as *hypR* (Verneuil et al., 2005a; Verneuil et al., 2004), s*px* (Kajfasz et al., 2012) and *soxS* contribute to intracellular macrophage survival. Additionally, deletion of *hypR*, hydrogen peroxide regulator, which positively regulates *hypR* and the *ahpCF* operon, results in decreased virulence in murine peritonitis model (Verneuil et al., 2005a).

Moreover, *E. faecalis* undergo transcriptional response when exposed to oxidative stress. A global transcriptional analysis of *E. faecalis* V583 exposed to 1.75 mM hydrogen peroxide revealed 132 differentially regulated genes, of which 39 were upregulated and 93 were downregulated (Yan et al., 2015). Genes associated with oxidative stress response were unchanged. Interestingly, four putative iron associated transporters (*feoA, ef0188, ef0191* and *ef3085)* and high affinity ABC potassium transport system (*Kdp*) were among the highly upregulated genes, while genes responsible for ethanolamine (*eutQ, eutX, eutY, eutE, eutG, eutP, eutB*) and methylglyoxal (*ef0358, ef0939, ef0630, ef0656, ef0666, ef0745, ef0867, ef1669, ef2591, ef3092*) metabolism were downregulated (Yan et al., 2015). Since iron can serve an co-factor for enzymes such as KatA and Dps, both of which are involved in the oxidative stress response, it is not unexpected that iron transport is upregulated under these conditions as well. Moreover, a similar adaptive response was also observed in *Bacillus spp* whereby iron uptake genes were upregulated in response to superoxide stress (Mostertz et al., 2004), suggesting that upregulation of iron uptake genes contribute to the oxidative stress response.

Overall, these findings reveal the inherent resilience of *E. faecalis* to environmental stresses and its remarkably ability to tolerate oxidative stress. However, to what extent this ability drives infection and contributes to biofilm formation still remains to be explored further.

1.9 Significance of this study

Enterococcus faecalis, as an opportunistic pathogen, is the causal agent for several nosocomial infections including bacteremia, endocarditis, wound and urinary tract infections. Of these infections, many are often biofilm associated and thus display biofilm associated properties such

as increased tolerance to antibiotics and reduced killing by immune cells. To advance treatments strategies, we need to better understand enterococcal biofilm physiology. Iron account for one of the environmental cues in the host which can influence virulence and disease outcomes, depending on the colonization niche and its iron availability. In **Chapter 1**, we have discussed that to date, studies which characterize Enterococci respond to iron depletion and abundance have been limited to planktonic cell cultures *in vitro*, and have not been performed in the context of Enterococcal biofilms. Moreover, studies on metal homeostasis in *E. faecalis* have so far been limited to global transcriptional data, and underlying mechanisms have not been characterized. In this thesis, we will attempt to address these unanswered questions. In **Chapter 2** of this thesis, we will demonstrate that iron promotes *E. faecalis* biofilm growth using iron-mediated extracellular electron transfer (EET) and this requires presence of L-lactate dehydrogenase (Ldh1). In **Chapter 3**, we will further characterize the role of pilus, EbpABC and electron transport systems (MenB, Ndh3) in driving EET and explore the iron-responsive transcriptionally changes in *E. faecalis* biofilm. Additionally, we will show that FeoB iron transporter drives intracellular iron uptake. Furthermore, in **Chapter 4**, we will show that MntE is a dual iron and manganese exporter, and regulation of intracellular iron and manganese have profound effect on growth and biofilm formation. This is the first mechanistic study characterizing the impact of iron abundance on *E. faecalis* biofilm physiology, of relevance to clinical biofilm associated infections, and our findings will provide meaningful insights for advancing treatment strategies for treating Enterococci biofilm associated infections.

Chapter 2: Extracellular electron transfer powers *Enterococcus faecalis* biofilm metabolism

2.1 Statement of contributions

D.K. conceptualized the study. D.K., L.N.L., E.M., and K.A.K. designed the experiments, analysed data, and prepared the manuscript. L.N.L. performed biofilm experiments, confocal imaging of biofilms and analysed data. A.M. analysed confocal data and generated 3D reconstruction models. Y.S. and S.P.N. performed and analysed mass spectrometry experiments. D.K., L.E.D., L.N.L., P.M.L., and E.M. performed the electrochemistry experiments and analysed data. L.N.L and C.B. performed EDS TEM. J.D. and G.D. provided the transposon library. All authors reviewed the manuscript and has been published on mBio.

2.2 Abstract

The emergence of Enterococci biofilm associated infections and the increasing antibiotic resistance worldwide has highlight the need to understand Enterococci biofilm physiology. Given its contribution to several nosocomial infections such as endocarditis, urinary tract infection, wound infection, and infections related to medical implants, advancing alternative therapeutic treatments towards Enterococci biofilms is of significance importance. Moreover, owing to its metabolic flexibility and resilient nature, *E. faecalis* is well adapted to colonize a variety of niches in the host. Despite the abundance of literatures associating iron availability and prevalence of clinical infections, the lack of knowledge on the role of iron in enterococcal biofilm physiology and infection has driven the need to examine this in greater context.

Here, we report a form of iron-dependent metabolism for *Enterococcus faecalis* where, in the absence of heme, extracellular electron transfer (EET) and increased ATP production augments biofilm growth. We show that the *ldh* gene encoding l-lactate dehydrogenase is required for iron-augmented energy production, biofilm formation, and promotes EET. We show that *E. faecalis* biofilm augmentation is biometal specific and is dose dependent. Furthermore, ferric iron forms deposits in the biofilm extracellular matrix and we demonstrate that ferric iron-mediated EET can be detected in *E. faecalis* biofilm. These findings represent the first mechanistic description of extracellular electron transport by *Enterococcus faecalis*, a gastrointestinal tract commensal and opportunistic pathogen, which may play a role in its ability to colonize, persist and cause infections in a variety of niches.

2.3 Introduction

Enterococci associated biofilms often present itself in clinical manifestations such as endocarditis, urinary tract infections, wound and surgical site infections, and including medical implants associated infections. Furthermore, Enterococci, is also one of the earliest colonizer in the gastrointestinal tract (GI), and remains as part of the GI commensal microbiota throughout life (Hufnagel et al., 2007). In the gastrointestinal tract, enterococci are present in the lumen as well as in more specialized niches in the physicochemically complex mucus epithelial layer and epithelial crypts in the small intestine (Sekirov et al., 2010). The ability to produce exopolymeric substances which forms a barrier-like matrix surrounding the bacterial community enhances tolerance to antimicrobial treatments. Moreover, its metabolic flexibility allows for environmental adaptation and niche colonization at sites which may be unfavorable for other microbes. Understanding Enterococci biofilm physiology which drive biofilm development, niche colonization and persistence will reveal novel factors associated with Enterococci biofilm pathogenesis.

The metabolic versatility in *E. faecalis* allows for aerobic respiration, which utilize heme dependent electron transport chain, or alternatively anaerobic fermentation in the presence of carbon sources. Since *E. faecalis* does not synthesize heme *de novo*, acquisition of heme is essential to drive cytochrome *bd* activity during aerobic respiration (Baureder and Hederstedt, 2012; Frankenberg et al., 2002a). Though *E. faecalis* do not have major requirement for iron in cellular growth (Archibald, 1986; Bruyneel et al., 1989; Marcelis et al., 1978; Weinberg, 1997), its ability to sense and respond to iron availability suggest that iron play a role in *E. faecalis* physiology (Keogh et al., 2016a; Vebo et al., 2009; Vebo et al., 2010). Moreover, the ability to withstand oxidative stress from O_2^-, hydroxyl radicals ($OH^\cdot$), and hydrogen peroxide (H_2O_2) sources (Riboulet et al., 2007a; Verneuil et al., 2006), suggest that *E. faecalis* may be able to tolerate iron concentrations which are considered toxic to other bacterial species. Although iron bioavailability in the host systemic circulation is restricted (Andrews et al., 2003), iron abundance have been reported in human spleens and gastrointestinal tracts (Kopani et al., 2015; Lee et al., 2016) which may be sufficient to support *E. faecalis* growth but restrict growth of other bacterial species. In this study, we hypothesize that the ability to tolerate higher iron concentrations provide a metabolic advantage and allow for colonization at a diverse range of niches. We show that iron can accumulate in the *E. faecalis* biofilm matrix and augments biofilm growth using extracellular

electron transfer (EET), in an *ldh1*-dependent manner. Together, these data support a model in which *E. faecalis* biofilm matrix harbours iron sinks which in turn promote EET, altered metabolism, and augmented biofilm growth. Understanding the metabolic factors that promote colonization and biofilm formation in different environmental conditions may inform mechanisms governing the transition from free-living planktonic to biofilm in a number of ecological reservoirs and clinical context.

2.4 Materials and methods

2.4.1 Bacterial strains and growth conditions

Enterococcus faecalis OG1RF (ATCC47077) (Dunny et al., 1978) was grown in Brain Heart Infusion broth (BHI) and cultured at 37 ^{o}C under static conditions. *E. faecalis* SD234 is an OG1RF strain derivative harbouring a constitutively expressed *gfp* gene (Debroy et al., 2012). Overnight cultures were normalized to 2-4x10^{8} CFU/ml in phosphate buffered saline (PBS), equivalent to OD_{600nm} 0.7 for *E. faecalis*. For planktonic and biofilm assays, bacteria were cultured at 37 ^{o}C (under 200 rpm orbital shaking or static conditions, respectively) with tryptone soya broth supplemented with 10 mM glucose (TSBG) and solidified with 1.5 % agar when appropriate (Oxoid Technical No.3). Planktonic assays were inoculated from the normalized stocks to a starting CFU of 2-4x10^{5} CFU/ml. *E. faecalis* strains harbouring pMSP3535 (source Gary Dunny, Addgene plasmid # 46886) or pMSP3535::*ldh1* (source Axel Hartke, (Rana et al., 2013)) were selected for using 300 µg/ml erythromycin and induced with 5 µg/ml nisin supplemented BHI. BHI was supplied by Becton, Dickinson and Company, Franklin Lakes, NJ. TSB and agar was supplied by Oxoid Inc., Ontario, Canada. Metals for supplementation were added during medium preparation. Ferric citrate hydrate ≥98%, magnesium chloride anhydrous ≥98%, copper chloride dihydrate ≥99%, ferrous sulphate heptahydrate ≥99%, ferric sulphate hydrate ≥97%, ferric chloride anhydrous ≥99%, heme ≥90% and the chelator 2,2'dipyridyl ≥99% were all supplied by Sigma Aldrich, St Louis, MO, USA. Manganese chloride tetrahydrate and zinc chloride were supplied by Merck Millipore, Singapore. The chelator 2,2'dipyridyl was supplied by Sigma Aldrich, St Louis, MO, USA.

2.4.2 Static biofilm assay

Bacterial cultures were normalized as described above and inoculated at 1.6-3.2x10^{6} CFU/200µl microtiter well in TSBG in a 96-well flat bottom transparent microtiter plate (Thermo Scientific, Waltman, MA, USA), and incubated at 37^{o}C under static conditions. Uninoculated media controls with metals supplemented to the highest concentration relevant to the assay were included to check for supplemented metal precipitation. Supernatants were discarded and the microtiter plate washed twice with PBS. To stain surface adherent bacteria, 200 µl of crystal violet solution at 0.1% w/v (Sigma-Aldrich, St Louis, MO, USA) was added to each well and incubated at 4 ^{o}C for 30 minutes. This solution was discarded and the microtiter plate washed twice with PBS followed by crystal

violet solubilization with 200 µl per well ethanol-acetone (4:1) for 45 minutes at room temperature. The intensity of crystal violet staining was measured by absorbance at OD_{595nm} using a Tecan Infinite 200 PRO spectrophotometer (Tecan Group Ltd., Männedorf, Switzerland).

2.4.3 Planktonic kinetic assay

Bacterial cultures were normalized as described above and serial diluted by dilution factor of 200. Diluted cultures were inoculated into the media at a ratio of 1:25, which is 8 µL of inoculum in 200 µL of media, incubated at 37^{o}C for 18 hrs, and absorbance at OD_{600nm} was measured using a Tecan Infinite 200 PRO spectrophotometer (Tecan Group Ltd., Männedorf, Switzerland) at 15 minutes interval. Growth curve was plotted to determine the exponential growth and doubling time.

2.4.4 Bacterial cell enumeration

A normalized cell suspension of 100 µL was added to each well of the 96-well microtiter plates. Serial dilution of $1:10^1$, $1:10^2$, $1:10^3$, $1:10^4$, $1:10^5$, $1:10^6$, $1:10^7$, $1:10^8$ and $1:10^9$ was performed using 1X phosphate saline buffer (PBS) within the 96-well plate. 5 µL per spot for each dilution factor, up to a total of five spots (technical replicates) were pipetted onto agar plates, and incubated at 37 ^{o}C for 24 hrs. After incubation, the colony-forming unit (CFU)/mL was counted.

2.4.3 Flow cell biofilm assay

Flow cell biofilm studies were performed as previously described with minor modifications (Paganelli et al., 2013). Bacterial cultures were normalized to 2-4x10^6 CFU/ml in PBS and 250 µl of this stock injected through the Stovall flow cell system inlet silicon tube connected to the flow cell chamber. This inoculation was performed when the system flow was halted by clamping both the inlet and outlet silicon tubes. The chamber was inverted for one hour to facilitate bacterial adherence to the glass slide surface. The flow cell assay was run for 120 hrs, at a speed of 4.5 mL/hr per flow cell channel. The flow cell system was then disassembled as described (Paganelli et al., 2013).

2.4.4 Transposon library screen

The cryogenically stocked, 96-well format *E. faecalis* OG1RF mariner transposon library consisted of 14978 individual mutants (Kristich et al., 2008). This library was cultured using a cryo-replicator (Adolf Kühner AG) to inoculate DeepWell blocks (Greiner Bio-One) containing 1ml BHI medium for overnight incubation at 37 ºC with shaking at 220 rpm. Cultures were normalized to OD_{600nm} 0.1 (2-4x10^8 CFU/ml) in PBS with the Tecan Infinite® 200 PRO spectrophotometer (Tecan Group Ltd., Switzerland) using a 96 well microtiter plate. The primary screen of the library was performed by inoculating a microtiter well with 1.6-3.2x10^6 CFU/200µl in TSBG medium supplemented with 2 mM $FeCl_3$. The microtiter plates were then incubated at 37 °C, statically, inside a moistened chamber to prevent evaporation of media. Biofilm was quantified by crystal violet staining as described above. Mutants with either reduction or further enhancement of biofilm signal compared to wild type controls were then validated using two independent biological replicates for each mutant in TSBG biofilm assays. This primary validation was followed by a planktonic growth validation in TSBG and TSBG medium supplemented with 2 mM $FeCl_3$. A secondary validation using three independent biological replicates for each mutant was performed in biofilm assays with TSBG and TSBG medium supplemented with 2 mM $FeCl_3$ to eliminate any mutants exhibiting defects in biofilm formation under normal conditions. Mutants harbouring multiple transposon insertions were excluded from the screen.

2.4.5 Mapping transposon insertions sites

Genomic DNA was extracted using the Wizard® Genomic DNA Purification Kit (Promega) from transposon mutants that were not originally mapped. The gDNA quantified and assessed for nucleic acid quality by Qubit High Sensitive dsDNA assay (Invitrogen) and NanoDrop. Sequencing was performed using an Illumina MiSeq. *De novo* reads were assembled using CLC Genomics Workbench version 8.0 and *E. faecalis* OG1RF as a template. The Tn insertion site was identified by BLAST using the mariner transposon sequence and identification of the flanking genomic sequence. Transposon mutant strains were named to include library location information, gene name or intergenic information, followed by "TnMar". For example, (4.2A1 F1) 10589:TnMar indicates the transposon mutant for OG1RF_10589 located in block 4.2A1 of the library in position F1 of the microtiter plate.

2.4.6 Electrochemical setup and analysis

Screen printed electrodes (SPE) (model DRP-C110; DropSens, Spain) consisting of a carbon working electrode, carbon counter electrode, and Ag pseudo-reference electrode were controlled by a multichannel potentiostat (VSP, Bio-Logic, France) in an electrochemical cell of 9 mL working volume sealed with a Teflon cap. Chronocoulometry was used to characterize the electrochemical activity of live microbial cultures by measuring the charge Q passed over the course of growth, with Q (mC) at 40 hr used for comparison. During chronocoulometry, the working electrode was maintained at 200 mV vs. the Ag pseudo-reference electrode of the SPE. Bacterial stocks of 2-4x10^8 CFU/ml for electrochemical experiments were prepared as described above, and electrochemical cells inoculated to 2-4x10^5 CFU/ml. All electrochemical experiments were conducted at 37 ^oC using TSBG medium supplemented with 2 mM $FeCl_3$ unless otherwise stated. The iron chelator, 2,2′dipyridyl (Sigma Aldrich, USA), was spiked in selected experiments to quench EET.

2.4.7 Electrode biofilm biomass quantification

Biofilm biomass was analysed by CLSM directly from screen printed electrodes with 5 individual Z-stack images per biological replicate. Images were acquired using LSM780 confocal microscope (Zeiss, Germany) equipped with 20x/0.8 Plan-Apochromat objective. Viability staining was performed using 5 mL of 200 µM propidium iodide (PI) and 33.4 µM SYTO 9 nucleic acid incubated in the dark for 15 minutes. After staining, the screen printed electrodes were washed with 5 mL of 1X phosphate buffered saline (PBS) twice, mounted inverted on the glass slide, and viewed using a LSM 780 confocal microscope. Imaging of propidium iodide-stained cells was performed using excitation/emission wavelength at 561 nm and 633 nm while SYTO9 nucleic acid-stained cells were imaged using excitation/emission wavelength at 488 nm and 500 nm. Image analysis was performed using Carl Zeiss Micro-Imaging software. Analysis of biomass was performed using Imaris software.

2.4.8 Thin-section transmission electron microscopy (TEM)

Biofilms were grown using the flow cell protocol or the standard biofilm protocol described, but with the latter using a 6-well plate. The flow cell biofilm was resuspended in a 2 % paraformaldehyde-2.5 % glutaraldehyde solution (Polysciences Inc., Warrington, PA) in 100 mM

PBS (pH 7.4) for 1 hr at room temperature. The samples were then embedded in 2 % low-melt agarose, washed in PBS and post-fixed in 1 % osmium tetroxide for 1 hr. Samples were rinsed extensively in distilled water (dH_2O) prior to *en bloc* staining with 1 % aqueous uranyl acetate (Ted Pella, Inc., Redding, CA, USA) for 1 hr. Following several rinses in dH_2O, samples were dehydrated in a graded series of ethanol and embedded in Eponate 12 resin (Ted Pella, Inc., Redding, CA, USA). Sections of 95 nm were cut with a Leica Ultracut UCT ultramicrotome (Leica Microsystems, Inc., Bannockburn, IL, USA), stained with uranyl acetate and lead citrate, and viewed on a JEOL 1200 EX transmission electron microscope (JEOL USA, Inc., Peabody, MA, USA).

2.4.9 Energy-dispersive X-ray spectroscopy (EDS) TEM

Samples were prepared as described above for TEM and viewed on an aberration-corrected JEOL ARM 200 cold field-emission gun transmission electron microscope in high-angle annular dark-field scanning transmission (HAADF STEM) mode using spot size 6. The sample was held in a JEOL Be double tilt holder tilted by about 12° towards the X-ray detector. STEM images were collected using a JEOL annular dark-field detector on a Gatan Digiscan with 2048×2048 pixels and a dwell time of 10 µs. Energy dispersive X-ray maps were collected using an Oxford Aztec system with a 0.7-sr collection solid angle by scanning the beam with multiple frames over a period of about 5 minutes at a resolution of 512×512 pixels.

2.4.10 ATP quantification

Biofilms were grown in 6-well microtiter plates at 37 °C for 24 hr under static conditions as described above. Spent medium was removed and the adherent biofilm was washed with 1 mL of 1X PBS, disrupted into a single cell suspension, and normalized to OD 0.5. 100 uL of normalized biofilm sample was added to 100 uL of prepared BacTiter-Glo™ Reagent from BacTiter-Glo™ Microbial Cell Viability Assay Kit (Promega), and incubated at room temperature for 5 minutes before measuring luminescence using a Tecan Infinite 200 PRO spectrophotometer (Tecan Group Ltd., Männedorf, Switzerland). An integration time of 0.25–1 second per well

2.4.11 Confocal laser scanning microscopy and 3D reconstruction

Biofilm morphology, biomass, and cell distribution were analysed by CLSM directly from flow cell chamber glass microscope slides at three separate locations (inlet, middle and outlet areas) with 3 individual Z-stack images per technical replicate. Images were acquired using LSM780 confocal microscope (Zeiss, Germany) equipped with 20x/0.8 Plan-Apochromat objective and controlled by ZEN software. Samples were illuminated with a 488 nm Argon laser line and the GFP emitted fluorescence was collected in the 507-535 nm range. Optical sections (425x425 µm) were collected every 5 µm through the entire biofilm thickness and signal from each section was averaged 2-4 times. Fiji software (Schindelin et al., 2012) was used for further processing (levels adjustment, stack reslice). For the 3D biofilm reconstructions, optical slices (85x85 µm) were acquired with 63x/1.4 Plan-Apochromat oil immersion lens every 0.3µm through entire biofilm thickness or until loss of the fluorescence signal (due to light scattering, absorption, and possible fluorescence quenching of thick iron-supplemented biofilms). The center of mass for each cell in 3D space was found using MosaicSuite for Fiji (Sbalzarini and Koumoutsakos, 2005), then coordinates were filtered in R (Team, 2016). To visualize the biofilm matrix and spatial organization coordinates were plotted as spheres with cell-size diameter and color coded Z-depth.

2.4.12 Inductive coupled plasma mass spectroscopy (ICP-MS)

E. faecalis cultures were prepared as previously described with minor modifications (Rolfe et al., 2012). Overnight cultures were normalized as described above and 1-2x10^5 CFU/well was inoculated into DeepWell blocks (Greiner Bio-One) containing 2 ml TSBG medium and incubated overnight at 37 ^oC under static conditions. Three biological replicates with five technical replicates were prepared for each *E. faecalis* strain and, following incubation, the technical replicates were pooled prior to preparation for ICP-MS. Harvested cell pellets were washed with 10 mM EDTA (Ambion^{TM} Thermofisher Scientific, USA) prepared in LC-MS grade dH_2O (Sigma Aldrich, St Louis, MO, USA) and washed three times with LC-MS grade dH_20. Cells were then concentrated to 2-4x10^8 CFU/ml in LC-MS grade dH_2O. Each cell pellet was digested in 500 µl of 69 % nitric acid and 250 µl of 31 % hydrogen peroxide. Following sample digestion, all the samples were diluted with LC-MS grade dH_20 to a 2 % (w/v) nitric acid concentration in the final solution. An Agilent 7700 series model ICP-MS system (Agilent, Santa Clara, CA, USA) was used for simultaneous determination of selected elements [Mg, Al, P, K, Ca, V, Cr, Mn, Fe, Co, Ni, Cu,

Zn] in prepared *E. faecalis* samples. Prior to sample measurement and quantification, stock solutions of a multi-element calibration standard (Inorganic Ventures, VA, USA) were serially diluted (0 µg/L to 1000 µg/L) and run on the system. For each measurement (standards, samples, blanks, and quality controls), addition of internal standard (Sc; 100 mg/L, Agilent, USA) was performed to correct for physical matrix effects. Blanks were determined together with samples for every run and the mean of three runs was determined for each sample. Full quantitative analysis was performed against calibration standards for each element. Quality control samples (multi-element calibration solution; 100 µL) were inserted and run at regular intervals during the experiment to ensure reliability of the data and to eliminate signal drift or interference. For statistical analysis, 10 metals were measured for 22 phenotypes (*E. faecalis* OG1RF wild type and 21 mutants) in three nutrient conditions, with 3 biological replicates for each mutant and in each condition. The concentration of the metals in a blank control (500 µl of 69% nitric acid and 250 µl of 31% hydrogen peroxide) was subtracted from the concentration of metals in the samples.

2.4.13 MALDI-MSI quantification of NAD/NADH ratio

100 µL of HPLC grade water (Fisher-Scientific, USA) was added to bacterial pellet and vortexed. Matrix solution (2,5-Dihydroxybenzoic acid) was prepared in methanol/water/formic acid (69.5/29.5/1, v/v) at 40 mg/mL. The matrix was mixed with the bacteria-water mixture at a 1:1 ratio and spotted at 1 µL spot on a glass slide. The droplets then were air dried for 20 mins so that it crystalizes as the solvent evaporates. MALDI MSI: MALDI-MSI was performed using a Synapt G2-Si mass spectrometer with a MALDI interface. The mass spectrometer was calibrated over a range of 50-1200 m/z using Sodiated PEG at 1 mg/mL. The glass slide containing the crystalized mixture was then loaded into the machine. The MALDI mass spectra was acquired with a 355 nm laser operating at 1 kHz in positive sensitive mode over a range of 50 m/z to 1200 m/z with an step rate of 50 µm/s. The laser ablation diameter is 50 µm, and an acquisition was performed on a square area slightly larger than the dried up sample area. For structural identification, reference spectra were acquired with the NAD and NADH standards by spotting 1 µL of 10 µM of each standard in HPLC grade water and matrix mix at a 1:1 ratio on a glass slide. Data processing of the MSI data: The data acquired from the mass spectrometry imaging experiments were viewed using Waters Mass Lynx software's [Spectrum] function.

2.4.14 Statistical analysis

All experiments were performed with at least three biological replicates and the mean value was calculated using GraphPad software. Statistical analysis was performed using either one-way ANOVA, two-way ANOVA or unpaired t-test unless stated otherwise. (* $p<0.05$, ** $p< 0.01$, *** $p<0.001$; **** $p<0.0001$, ns: $p>0.05$).

2.5 Results

2.5.1 Iron supplementation augments *E. faecalis* biofilm and alters biofilm architecture

To test the hypothesis that iron impact *E. faecalis* biofilm growth, *E. faecalis* biofilm was cultured in a flow cell biofilm system using diluted (10%) media enriched with 0.2 mM ferric chloride ($FeCl_3$) which is continuously supplied, and allowed for removal of planktonic cells and biological waste produced by the biofilms. *E. faecalis* biofilm was analyzed at 8 hrs, 12 hrs and 18 hrs post incubation in 37 ^oC, and at 120 hrs post incubation in 22 ^oC using confocal laser scanning microscopy (CLSM). Using *E. faecalis* SD234, a chromosomal encoded GFP-expressing strain, we observed numerous irregular, complex aggregates of micro colonies formation in media supplemented with 0.2 mM $FeCl_3$ compared to normal media (**Figure 2.1A)** which have fewer and smaller aggregates of micro colonies as our control at 8 hr post incubation in 37 ^oC, which indicate that iron supplementation enhances *E. faecalis* biofilm development. Iron mediated biofilm growth sustained for 18 hrs, and we observed increase in z-depth which indicate increase in biomass thickness, as compared to the normal media which showed a flat monolayer confluent biofilm, typically seen in *E. faecalis* biofilms (Dale et al., 2015; Seneviratne et al., 2013). Using the confocal z-stack images, 3-dimensional reconstruction reveal that iron supplemented *E. faecalis* biofilm is more spatially distributed and increased cell density as compared to the control **(Figure 2.1B)**. Furthermore, we speculate that iron-mediated biofilm growth is dependent on temperature as *E. faecalis* grows optimally at physiologically relevant temperature of 37 ^oC. To test the hypothesis that temperature modulate iron-mediated biofilm growth, *E. faecalis* biofilm was similarly cultured using the same set up and biofilm was analyzed 120 hrs post incubation, but under room temperature at 22 ^oC using confocal laser scanning microscopy (CLSM). Iron supplemented *E. faecalis* biofilm also showed increased spatial distribution and cell density, in contrast to our normal media which showed sparse monolayer biofilm **(Figure 2.1B),** and hence indicate that temperature indeed modulate the rate of iron mediated biofilm growth.

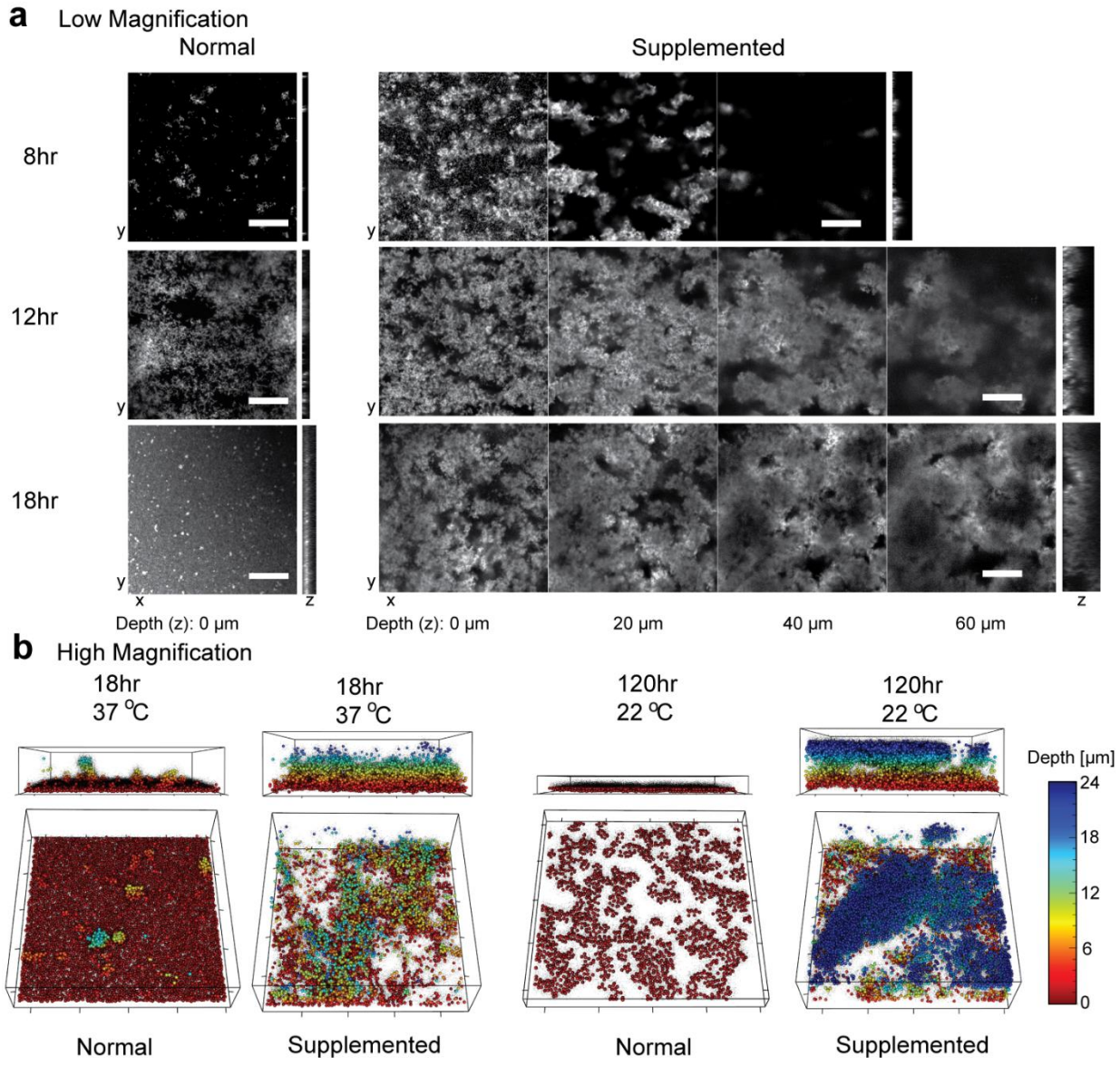

Figure 2.1: ***E. faecalis*** **flow cell biofilms in iron supplemented media.** (**A**) CSLM images at 8, 12, and 18 hr for normal (10 % TSBG) and supplemented (10% TSBG with 0.2 mM $FeCl_3$). Selected optical sections at the indicated depths are followed by representative lateral view in YZ at the right of each image set. Scale bar 100 µm. (**B**) 3D reconstructions of high magnification CLSM stacks of *E. faecalis* flow cell biofilms grown in normal or supplemented medium for 18 hr at 37 °C or 120 hr at 22 °C. Biofilm depth is color-coded as indicated on z-depth scale (0 to 24 µm) and the lateral box dimensions are 85 x 85 µm (20 µm between ticks).

2.5.2 *E. faecalis* biofilm biomass augmentation is a biofilm-specific phenotype

We have shown that iron enhance *E. faecalis* biofilm growth, and hence we speculate that iron-mediated growth is linked to increased metabolism and cellular growth. To assess whether iron mediated *E. faecalis* biofilm growth is driven by cellular growth, we performed planktonic growth assay to culture *E. faecalis* under shaking conditions which prevent biofilm formation and count the colony forming units (CFU) at specific time points. We did not observe significant increase in CFU numbers across 2, 4, 6 ,8 and 24 hrs time points **(Figure 2.2A)** and the rate of increase in optical density between normal and supplemented media is not significantly different **(Figure 2.2B)**, indicating that iron mediated augmentation of *E. faecalis* growth is a biofilm specific phenotype.

A **B**

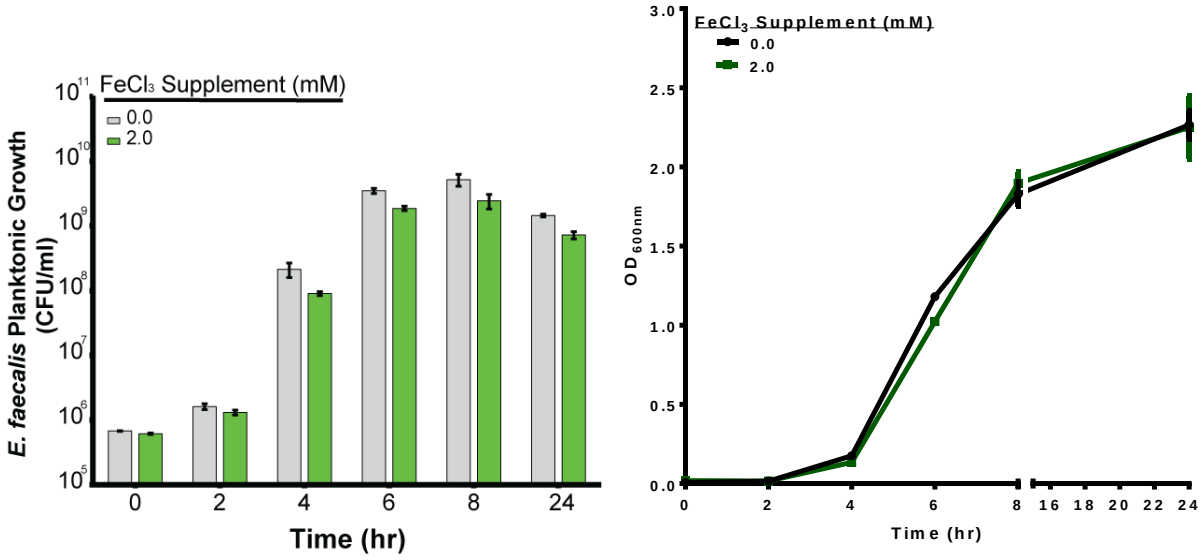

Figure 2.2: *E. faecalis* planktonic growth under metal supplementation. Time course (**A**) enumeration and (**B**) optical density of *E. faecalis* planktonic growth over 24hr in TSBG and TSBG supplemented with 2mM $FeCl_3$. N = 3, error bars represent standard error margin (SEM) from the mean.

2.5.3 Iron mediated *E. faecalis* biofilm augmentation is biometal specific and dose dependent

Since iron mediated biofilm growth is a biofilm specific phenotype, we next ask to what extent iron concentration drive enhanced biofilm growth, and the toxicity limit in which *E. faecalis* can tolerate iron. We speculated that the concentration of iron supplemented and incubation time post exposure to iron can modulate the enhanced *E. faecalis* biofilm growth rate. To test this hypothesis, we performed static biofilm assays using media supplemented with increasing concentration of ferric chloride in 96-well microtiter plates and quantified resultant adherence biofilm biomass using crystal violet staining at post 24 hrs, 48 hrs, 72 hrs, 96 hrs and 120 hrs incubation at 37 ^{o}C, static. Consistent with the enhanced biofilm growth observed in the flow cell biofilm assay **(Figure 2.1)**, we observed a dosage dependent growth enhancement in *E. faecalis* biofilm supplemented with ferric chloride from 0.5 mM to 3 mM, as compared to the normal media with no additional iron supplement **(Figure 2.3A)**. However, at 4 mM and higher concentrations of iron, we observed dosage dependent reduction in adherence biomass, suggesting that concentrations above 4 mM do not favor enhanced biofilm growth and may be the result of metal toxicity **(Figure 2.3A)**. At 0.5 mM iron concentration, significant enhanced biofilm growth (**** $p< 0.00001$) is observed at post 96 hrs incubation, while at 3 mM iron concentration, significant enhanced biofilm growth (* $p<0.05$) is observed at post 72 hrs incubation **(Figure 2.3A)**, which demonstrate that exposure to higher levels of ferric chloride drive enhanced biofilm formation at earlier time points. Next, we hypothesized that the mechanism underlying iron mediated biofilm growth specifically requires iron and other redox-reactive cationic metals do not promote *E. faecalis* biofilm growth. If iron drives enhanced biofilm growth, alternative sources of iron should exhibit similar enhanced biofilm growth. To address this, we performed static biofilm assays using media supplemented with manganese chloride, magnesium chloride, zinc chloride, coper chloride, ferric citrate, ferric sulphate, ferrous sulphate and heme in 96-well microtiter plates and quantified resultant adherence biofilm biomass using crystal violet staining post 120 hrs incubation at 37 ^{o}C, static. Consistent with our speculation, we found that supplementation with ferric sulphate and ferrous sulphate also enhanced *E. faecalis* biofilm growth; whereas ferric citrate do not enhance *E. faecalis* biofilm growth **(Figure 2.3B)**. Heme supplementation at 50 µM and above significantly (**** $p < 0.0001$) biofilm growth, which is expected because of enhanced activity in cytochrome *bd* which utilized heme as a cofactor for aerobic respiration (Borisov et al., 2011). In contrast, supplementing with 0.5 mM zinc chloride and 2 mM copper chloride results in reduced biofilm formation, which could

indicate metal toxicity. We also observed that magnesium supplementation do not impact *E. faecalis* biofilm growth; whereas manganese supplementation at 4mM significantly (** $p < 0.01$) enhanced biofilm growth **(Figure 2.3B)** which is not unexpected as manganese is utilized as cofactor for several cellular processes (Archibald, 1986; Bruyneel et al., 1989; Marcelis et al., 1978; Weinberg, 1997) which in turn could increase *E. faecalis* growth and metabolism.

A

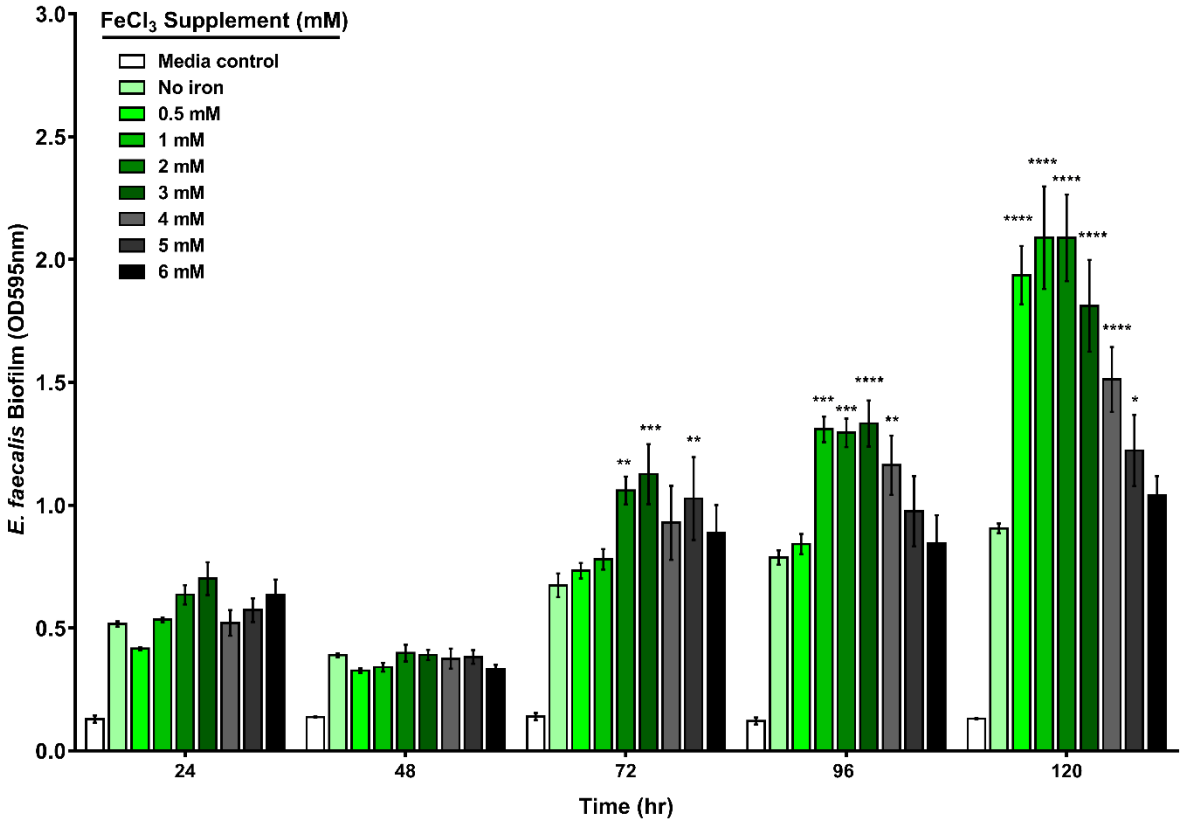

B

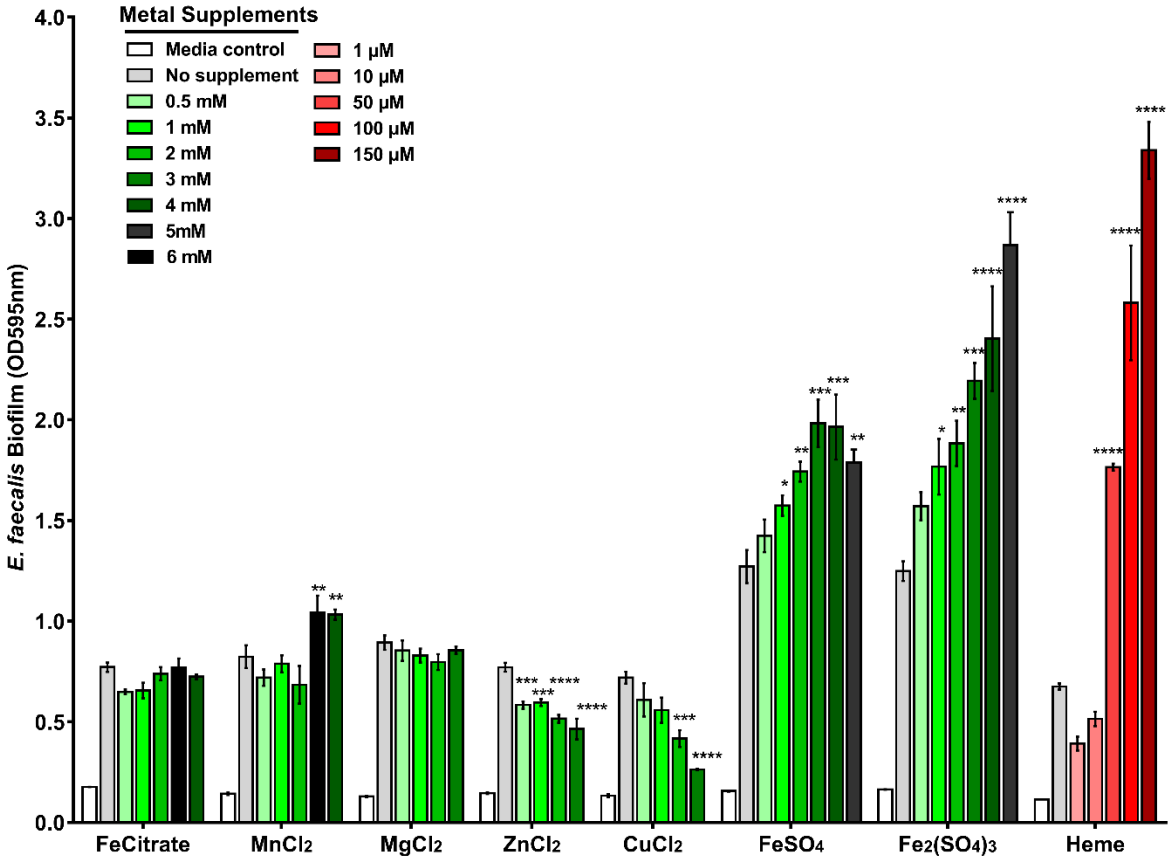

Figure 2.3: *E. faecalis* biofilm growth under metal supplementation. (**A**) Time course of *E. faecalis* biofilm growth in TSBG supplemented with $FeCl_3$. (**B**) *E. faecalis* biofilm growth at 120hr in TSBG supplemented with metals as indicated. Data at each time point or metal supplement represents an independent experiment, with the data merged for representation. N=9. Statistical significance was determined by two-way ANOVA with Tukey's test for multiple comparisons, N = 6 and error bars represent standard error margin (SEM) from the mean. * $P \leq 0.05$, ** $P \leq 0.01$, *** $P \leq 0.001$, **** $P \leq 0.0001$

2.5.4 Iron deposits are present in iron supplemented *E. faecalis* biofilm

Since high concentration of iron promotes *E. faecalis* biofilm growth, we sought to determine whether iron impact morphological changes to *E. faecalis* cells. To address this, we performed transmission electron microscopy (TEM) to visualize biofilm cells growth in flow cell biofilm assay. We observed typical diplococcus shaped *E. faecalis* cells with no morphological defects in

both the normal and iron supplemented biofilms **(Figure 2.4)**. Abundance of fibrous extracellular material is observed in the normal media grown biofilm **(Figure 2.4C)**. Using electron microscopy, to visualize bacterial cells, allow us to observe morphological defects but do not provide meaningful information on the constituents of *E. faecalis* biofilm matrix. Constituents of *E. faecalis* biofilm matrix have not been extensively characterized to date. However, eDNA is a major component of the *E. faecalis* biofilms matrix, and studies have demonstrated that DNase treatment, which cleaves DNA, disrupt the structural integrity of the biofilm thus makes *E. faecalis* biofilms easier to dislodge (Barnes et al., 2012; Guiton et al., 2009; Thomas et al., 2009). In the iron supplemented biofilm, we observed electron dense particles associated with extracellular fibrous matrix material **(Figure 2.4D-F)**. Using energy dispersive X ray spectroscopy (EDS) to analyse the electron dense particles, we showed that these particles are enriched in iron **(Figure 2.4G-M)**. We speculate that these iron deposits play an important role and contribute to iron-mediated biofilm growth. Electron microscopy images of *E. faecalis* biofilms supplemented with heme do not have electron dense particles, hence demonstrate that only iron supplementation results in formation of iron deposits **(Figure S2.1)**.

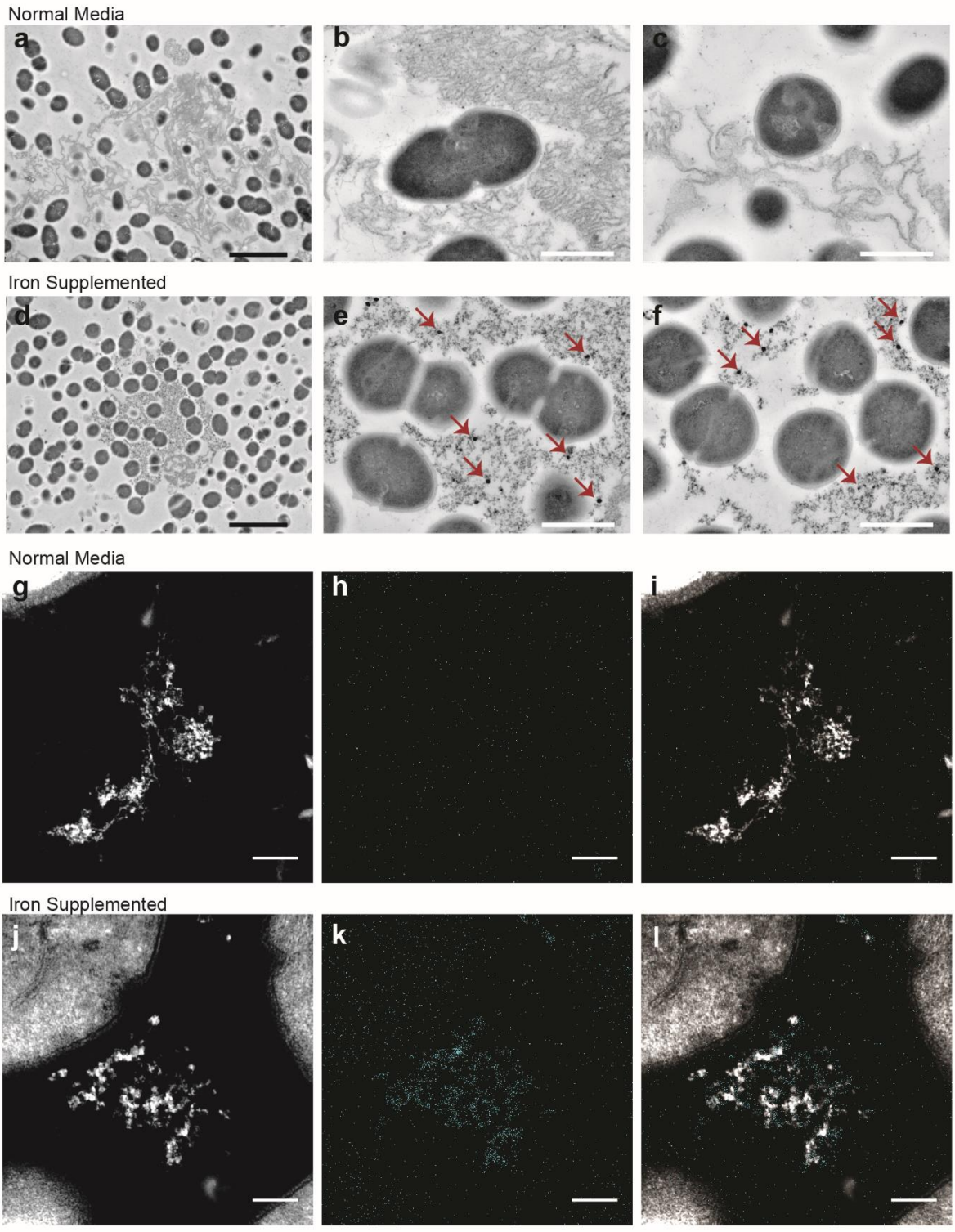
Normal Media
a
b
c
Iron Supplemented
d
e
f
Normal Media
g
h
i
Iron Supplemented
j
k
l

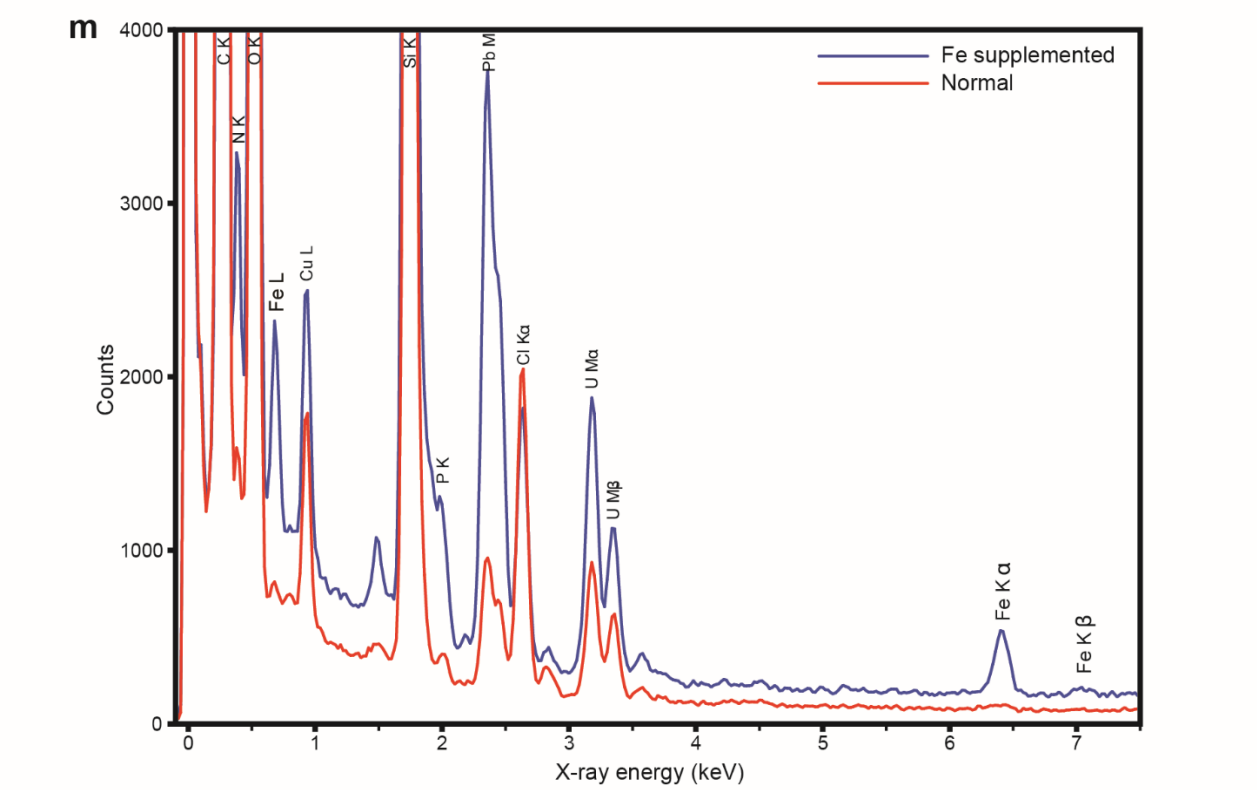

Figure 2.4: Electron micrographs of the *E. faecalis* biofilm matrix grown in iron supplemented media. Representative images from TEM of *E. faecalis* biofilm from flow cell in normal 10 % TSBG (**A**, **B**, **C**) or 10 % TSBG supplemented with 0.2 mM $FeCl_3$ (**D**, **E**, **F**). In a-f, scale bars represent 2 µm (black) and 0.5 µm (white), and red arrows highlight examples of electron dense particles. The biofilm matrix from biofilms grown in normal media (**G**, **H**, **I**) or with iron supplementation (**J**, **K**, **L**) was examined by HAADF STEM and EDS mapping at 300,000x magnification: HAADF STEM (**G, J**), iron EDS map (**H, K**), and merged EDS-STEM images (**I, L**) are shown at 300,000x magnification. Scale bars in g-l represent 1 µm. The EDS spectra for iron, corresponding to the images are shown in **M**.

2.5.5 Genes associated with *E. faecalis* metabolism contribute to iron mediated biofilm growth

From these findings **(Figure 2.1-2.4)**, we hypothesize that *E. faecalis* respond to extracellular iron present and an uncharacterized mechanism may be driving iron mediated biofilm growth. To determine the mechanism underlying iron enhanced *E. faecalis* biofilm growth, we screened a saturated *E. faecalis* mariner transposon library. Using static biofilm assays with ferric chloride

supplemented media, we screened for transposon mutants exhibiting loss of iron mediated enhanced biofilm growth and transposon mutants exhibiting further enhanced biofilm growth. The criteria guideline allow us to pick out mutants which are not significantly altered in ability to form biofilm under normal condition (<25% difference in biomass), but are significantly altered in iron supplemented condition (>25% different in biomass) **(Figure 2.5A)**. Planktonic growth assay was performed to eliminate transposon mutants who display growth defects in normal media, and secondary validation screen was performed to eliminate general biofilm defective mutants grown under normal media as we are seeking genes specifically involved in biofilm formation under iron enriched condition **(Figure 2.5B-2.5G)**. The final *E. faecalis* transposon mutants that specifically display altered biofilm formation in iron enriched condition have single gene disruption in *phoH*, *ldh1*, *trxB2*, *OG1RF_10589*, *OG1RF_11340* and an intergenic region Intergenic2A2C6:TnMar **(Table 2.4)**. Since *OG1RF_11340* has a morphological defect (data not shown) and the mutant with transposon insertion in the intergenic region likely might have polar effect on downstream genes, we rule these out for further characterization. Predicted functions for these genes are associated with electron transport chain, redox control, membrane transport and energy production.

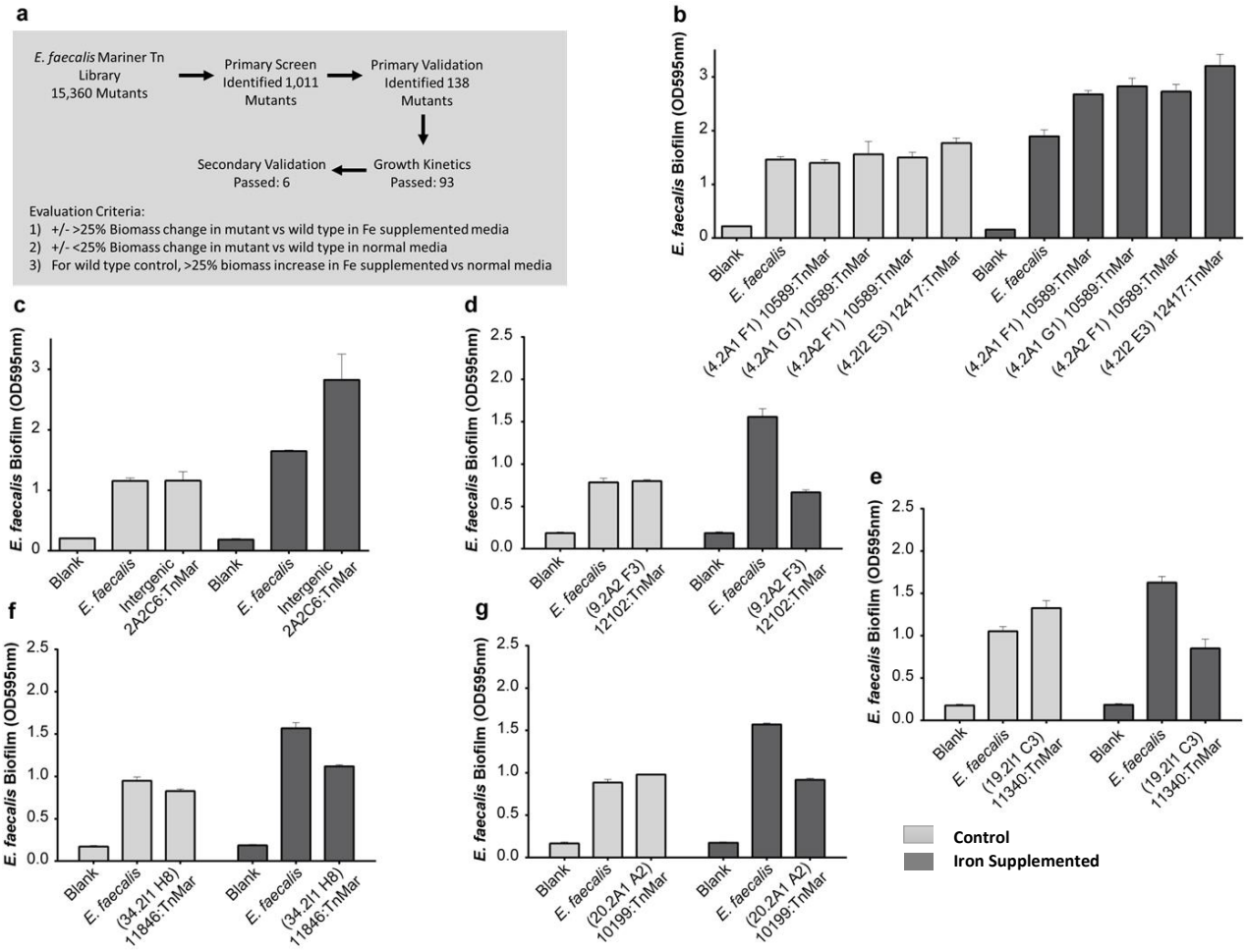

Figure 2.5: Transposon library screen for mutants exhibiting changes in biofilm accumulation under iron supplementation. (**A**) Flow chart of screen process including evaluation criteria for biofilm assays. (**B-G**) Secondary validation data for mutants passing primary evaluation. Light grey indicates normal medium and dark grey indicates iron supplemented medium. Secondary validation bar charts represent individual experiments and are separately presented, rather than being pooled, for greater clarity.

Mutant ID	Gene Locus / Name	Intergenic Location	Predicted/Annotated Function	Biofilm Phenotype*	Number of Hits	Description
Intergenic2A2C6:TnMar	n.a.	1427310-1427493	Between OG1RF_11362 & OG1RF_11363	Enhanced (+71.0%)	1	n.a.
10589:TnMar	OG1RF_10589	n.a.	Cation efflux protein	Enhanced (+37.0%)	3	Cation transporter
11340:TnMar	OG1RF_11340	n.a.	Acetaldehyde dehydrogenase	Reduced (-47.0%)	1	NADH-dependent
12102:TnMar	OG1RF_12102 / *trxB2*	n.a.	Thioredoxin-disulfide reductase	Reduced (-60.0%)	1	NADH-dependent, Redox control
10199:TnMar	OG1RF_10199 / *ldh1*	n.a.	L-lactate dehydrogenase	Reduced (-39.5%)	1	NADH-dependent

11846:TnMar	OG1RF_11846 / *phoH*	n.a.	PhoH family protein	Reduced (-28.0%)	1	Induced by phosphate starvation

Table 2.1: *E. faecalis* genes involved in iron-induced biofilm growth

Notes: n.a. = not applicable; * = mutant compared to wild type biofilm in the iron supplemented medium

2.5.6 *E. faecalis* L-lactate dehydrogenase drive extracellular electron transfer and increased energy production through modulation of NAD/NADH substrates

From the results obtained **(Figure 2.1-2.4)**, and given that the genes involved in iron mediated biofilm growth are associated with electron transport chain and are involved in the maintaining the cycling of nicotinamide adenine dinucleotide during redox change (NAD/NADH) **(Figure 2.5 and Table 2.4)**, we hypothesized that *E. faecalis* biofilm utilize ferric iron as terminal electron acceptor, in the absence of oxygen, to drive EET for respiration and biofilm growth. To address this, we performed chronocoulometry to measure charge transferred from *E. faecalis* biofilm grown in electrochemical cells maintained at high oxidative potential. *E. faecalis* biofilm, grown on carbon electrode, generated extracellular current in iron supplemented media **(Figure 2.6A)**. Next, we theories that the transposon mutants with altered biofilm formation in iron enriched condition should exhibit attenuation in EET. To address this, we then tested the transposon mutants identified through the library screen using chronocoulometry assay in iron supplemented media, and observed that only *ldh1* transposon mutant displayed significantly (**** $p<0.0001$) attenuated current production, indicating that *ldh1* contribute to the iron mediated EET (**Figure 2.6A**). Supplementing 10 mM metal chelator 2 2′-dipyridyl, to sequester exogenous supplemented iron, results in diminished current production, hence demonstrate that current detected from *E. faecalis* biofilm is produced in the presence of iron **(Figure 2.6B)**. To ensure that chelator supplementation do not impact cell viability leading to the observed loss of current production, we performed CLSM with live dead staining to verify that chelation did not alter viability (data not shown). Extracellular current was detected only in the presence of *E. faecalis* biofilm and with iron supplemented media **(Figure 2.6A)**. Moreover, *E. faecalis* biofilm grown in presence of manganese, magnesium and heme did not yield current production, while iron supplemented *E. faecalis* biofilm yielded current production and enhanced biovolume **(Figure S2.2)**. Complementing the *ldh1* transposon mutant with nisin inducible pMSP3535 vector with *ldh1* gene insert restores current production to wild type levels, and is not observed in the mutant complemented with empty pMSP3535 vector

(Figure 2.6C). We next tested the complemented *ldh1::Tn* p*ldh1* strain in static biofilm assay and observed that iron mediated biofilm growth in iron supplemented media was restored **(Figure 2.7)**.

Since our findings demonstrate that iron mediated EET promote E. faecalis biofilm growth, we next sought to determine whether energy production increased with biofilm growth. To address this, we performed quantification of total adenosine triphosphate (ATP) production in *E. faecalis* biofilm. Comparing between the normal and iron supplemented condition, we observed a non-significant increase in ATP in wild type, but not for the *ldh1* mutant **(Figure 2.6D)**. The complemented ldh1::Tn p*ldh1* strain however showed significantly (**$p<0.01$) increased ATP levels in iron supplemented media compared to the mutant complemented with empty pMSP3535 vector suggesting that energy was more abundant in iron supplemented media when *ldh1* was present **(Figure 2.6D)**. We also observed non-significant increase in ATP levels and adherence biofilm biomass in normal media for *ldh1* mutants harbouring the nisin inducible plasmids, which we speculate is attributed to the presence of the plasmid.

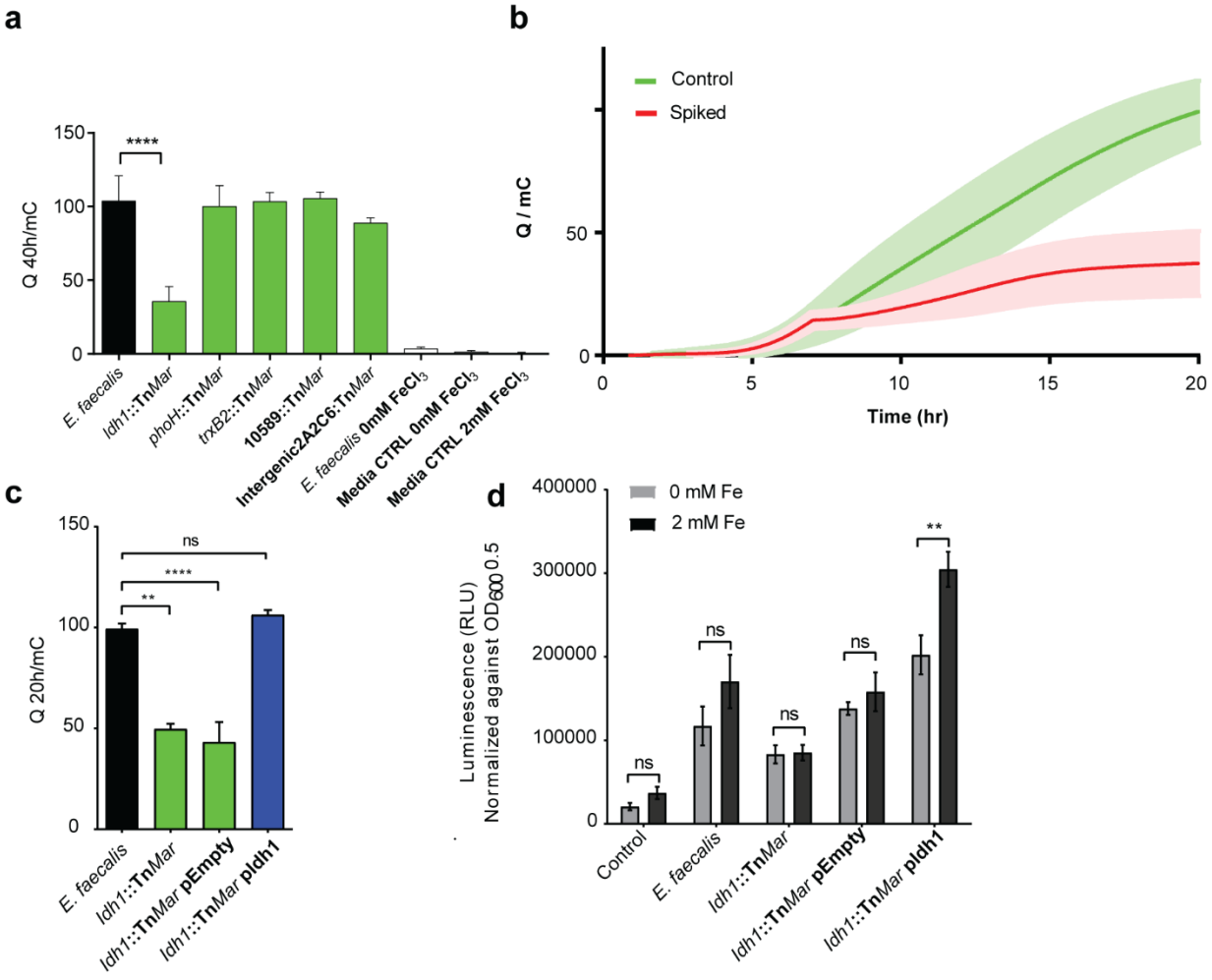

Figure 2.6: Extracellular electron transfer in *E. faecalis* biofilm. (**A**) Chronocoulometry current (Q) measurement, expressed in milicoulombs (mC), of *E. faecalis* biofilm on a screen-printed electrode over 40 hr in TSBG supplemented with 2mM $FeCl_3$ (Supplemented). Abiotic controls and media controls are indicated. Statistical significance was determined by one-way ANOVA with Tukey's test for multiple comparisons, N=6 biological replicates, error bars represent SD from the mean, **** $P \leq 0.0001$. (**B**) Chronocoulometry of *E. faecalis* biofilm in iron supplemented medium with a chelator spike (4 mM 2,2′dipyridyl) at 7.5 hr. Representative data from four independent experiments are shown, where the trend is consistent among all experiments. Statistical significance was determined by a paired two-tailed t-test, error bars (light-green or -red shading) represent SD from the mean, **** $P \leq 0.0001$. (**C**) Chronocoulometry current (Q) measurement, expressed in milicoulomb (mC), of *E. faecalis* wild type, *ldh1* mutant, and *ldh1* mutant complemented biofilm on a screen-printed electrode over 40 hr in TSBG

supplemented with 2mM $FeCl_3$. Statistical significance was determined by one-way ANOVA with Tukey's test for multiple comparisons, n = 3 biological replicates, error bars represent SD from the mean, **** $P \leq 0.0001$. (**D**) ATP quantification within biofilm grown in TSBG and TSBG supplemented with 2 mM $FeCl_3$ for 24 hr. Nisin was included at 5µg/mL for all samples, and erythromycin at 300 µg/mL for strains carrying a plasmid. Statistical significance was determined by one-way ANOVA with Sidak's test for multiple comparisons, n = 3 biological replicates, error bars represent SD from the mean, **** $P \leq 0.0001$.

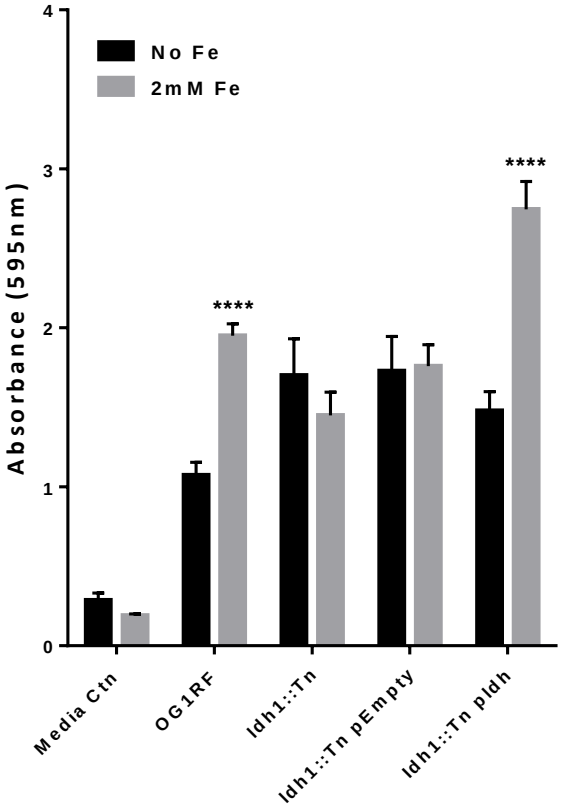

Figure 2.7: *E. faecalis ldh1* mutant biofilm growth under iron supplementation. *E. faecalis* biofilm growth at 120 hr in TSBG and TSBG supplemented with 2 mM $FeCl_3$. Nisin was included at 5µg/mL for all samples, and erythromycin at 300 µg/mL for strains carrying a plasmid. N = 9 biological replicates. Statistical significance was determined by two-way ANOVA with Sidak's test for multiple comparisons, N = 3, * $P \leq 0.05$, ** $P \leq 0.01$, *** $P \leq 0.001$, **** $P \leq 0.0001$, error bars represent standard error margin (SEM) from the mean.

From the literature, we know that *ldh1* functions in conversion of NADH to NAD^+, we hypothesize that conversion of NADH to NAD^+ is a critical step to ensure that intracellular NAD pools are balanced. To address this, we performed MALDI MS/MS and quantified the NAD/NADH ratio in iron supplemented *E. faecalis* biofilm. In the 12hr biofilm, we observed that *ldh1* mutant and *ldh1* mutant complemented with empty pMSP3535 vector displayed significantly (**$p<0.01$) reduced NAD/NADH ratio, which is consistent with our hypothesis **(Figure 2.8)**. By contrast, no significant differences in NAD/NADH ratio is observed in the 24hr biofilm **(Figure 2.8)**. We speculate that at 24hrs, biofilm growth has likely slowed down due to glucose depletion since NAD/NADH ratio changes during active growth and replication. However, the mechanism underlying electron transfer remains unanswered. Nevertheless, we propose two theories based on our findings and literatures describing EET mechanisms (Gorby et al., 2006; Marsili et al., 2008b; Okamoto et al., 2011; Reardon and Mueller, 2013a; Reguera et al., 2007; Smith et al., 2014a; von Canstein et al., 2008; Wang et al., 2013) **(Figure 2.9)**. The precise pathway of EET has been demonstrated to be either through direct contact dependent (DET) which involved outer membrane c-type cytochromes (Okamoto et al., 2011), or alternatively mediated by soluble electron shuttles (mediators) (MET) (Marsili et al., 2008a; Schröder et al., 2015; von Canstein et al., 2008; Wang et al., 2010a). We hypothesized that Ldh1 may function as an electron donor transferring electrons through an yet uncharacterized mechanism involving the cytoplasmic membrane to iron oxides embedded in the biofilm matrix. In *E. faecalis*, this would involve demethylmenaquinone, since ubiquinone and menaquinone have not been identified in *E. faecalis* (Ramsey et al., 2014a). Alternatively, Ldh1 may indirectly influence expression or functions of yet uncharacterized mediators of electron transfer during EET.

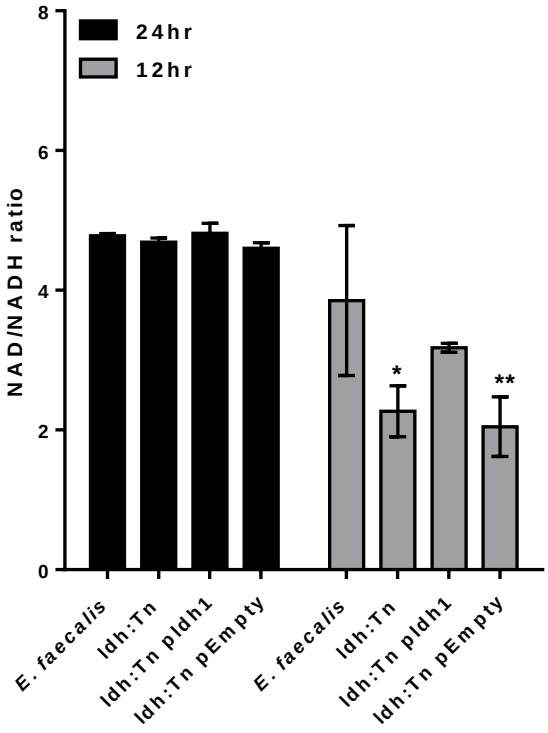

Figure 2.8: MALDI MS/MS analysis of NAD/NADH ratio. Biofilms grown for 12 hrs and 24 hrs respectively in 6 well microtiter plates were harvested, normalized and analyzed for total NAD and NADH quantification. Statistical significance was determined by two-way ANOVA with Sidak's test for multiple comparisons, N = 3. * $P \leq 0.05$, ** $P \leq 0.01$, *** $P \leq 0.001$, **** $P \leq 0.0001$, error bars represent standard error margin (SEM) from the mean.

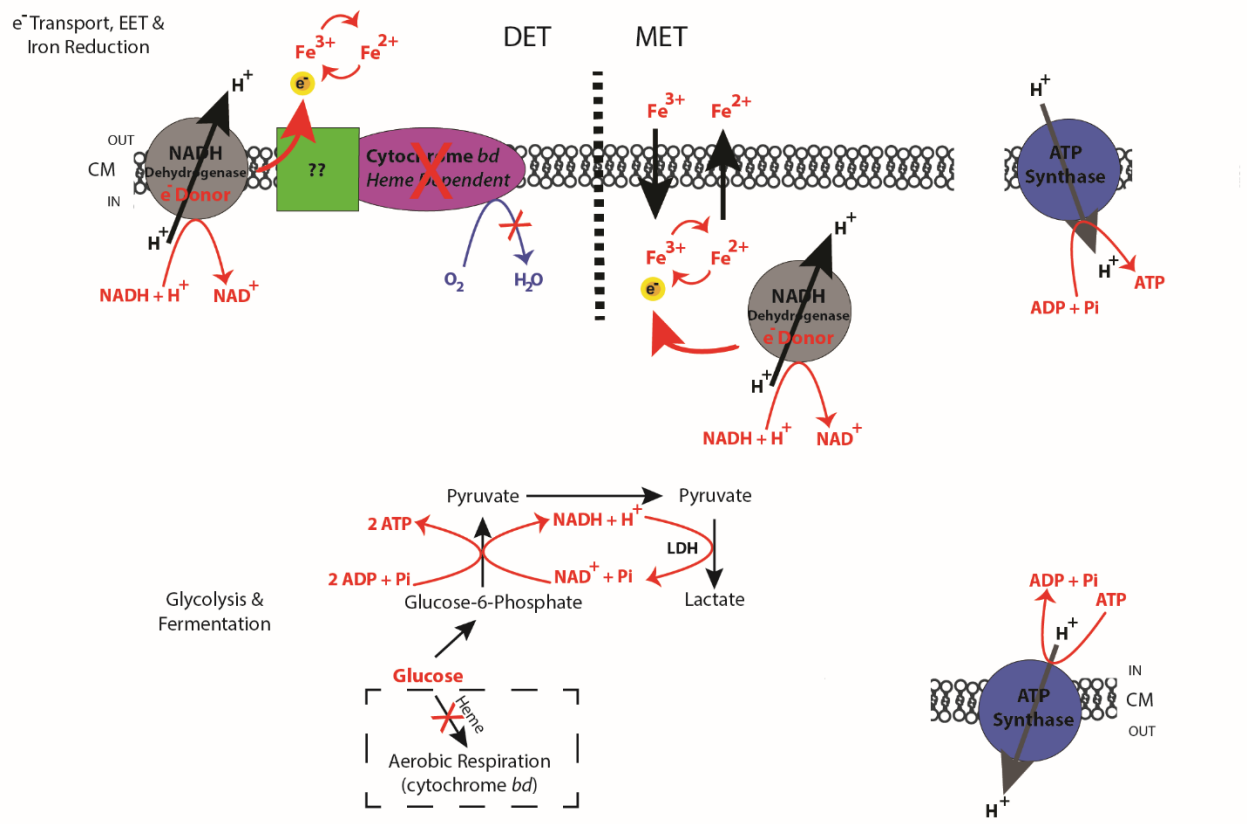

Figure 2.9: Model for fermentation and EET-dependent respiration metabolism in *E. faecalis* biofilm. Schematic model for *E. faecalis* biofilm metabolism describing EET through DET and MET mechanisms. ATP is generated by proton flow through membrane integrated ATP synthases. Glycolysis and fermentation are required prior to EET-dependent respiration. This generates the fermentation end-products required as substrates for dehydrogenases acting as electron donors. DET occurs in the absence of heme, where extracellular iron can be reduced and thereby serve as an iron sink for electrons of the respiratory electron transport chain. MET occurs in the absence of heme, when iron is transported intracellularly and reduced, thereafter being exported and serving as an electron mediator/shuttle.

2.5.7 Iron mediated extracellular electron transfer is biometal specific and genus specific mechanism

Given that our results indicate that iron-mediated *E. faecalis* biofilm growth is biometal specific, and that iron drives EET in *E. faecalis*, we hypothesized that electron transfer in *E. faecalis* biofilm also display biometal specificity. To address this, we performed chronocoulometry assay in *E.*

faecalis biofilm supplemented with manganese, magnesium and heme respectively. Consistent with our previous findings and our hypothesis, addition of manganese, magnesium and heme produce no or minimal current production, similar to our control *E. faecalis* biofilm in normal media **(Figure 2.10A)**. Moreover, we also observed that 200 µM iron concentration significantly enhanced current production, and addition of increasing iron concentration resulted in a dose dependent increase in current production **(Figure 2.10A)**. Based on literatures describing EET mechanism (Glasser et al., 2017), we also speculated that in the absence of iron, soluble electron shuttle can mediate electron transfer from *E. faecalis* cells. To test this, we supplemented 50 µM hydroxy-1,4-naphthoquinone (HNQ), which serves as soluble electron shuttles; however, we observed no significant increase in current production **(Figure 2.10A)**, which suggest that presence of iron is required for EET in *E. faecalis* biofilm.

To further characterize the specificity of iron mediated EET and determine whether this mechanism is broadly utilized by other bacterial species, we performed similar experiments using *E. coli* and *S. saprophyticus*, which are not known to utilize EET, and *P. aeruginosa* (Wang et al., 2010b), which is able to utilize EET but not yet characterized to utilize iron for EET. We observed no significant increase in current production in these bacterial species, however; when we tested using *E. faecium*, we observed significant increase in current production **(Figure 2.10B)**. Taken together, these findings demonstrate that EET using iron as final electron acceptor may be a unique mechanism utilize by *Enterococcus spp*.

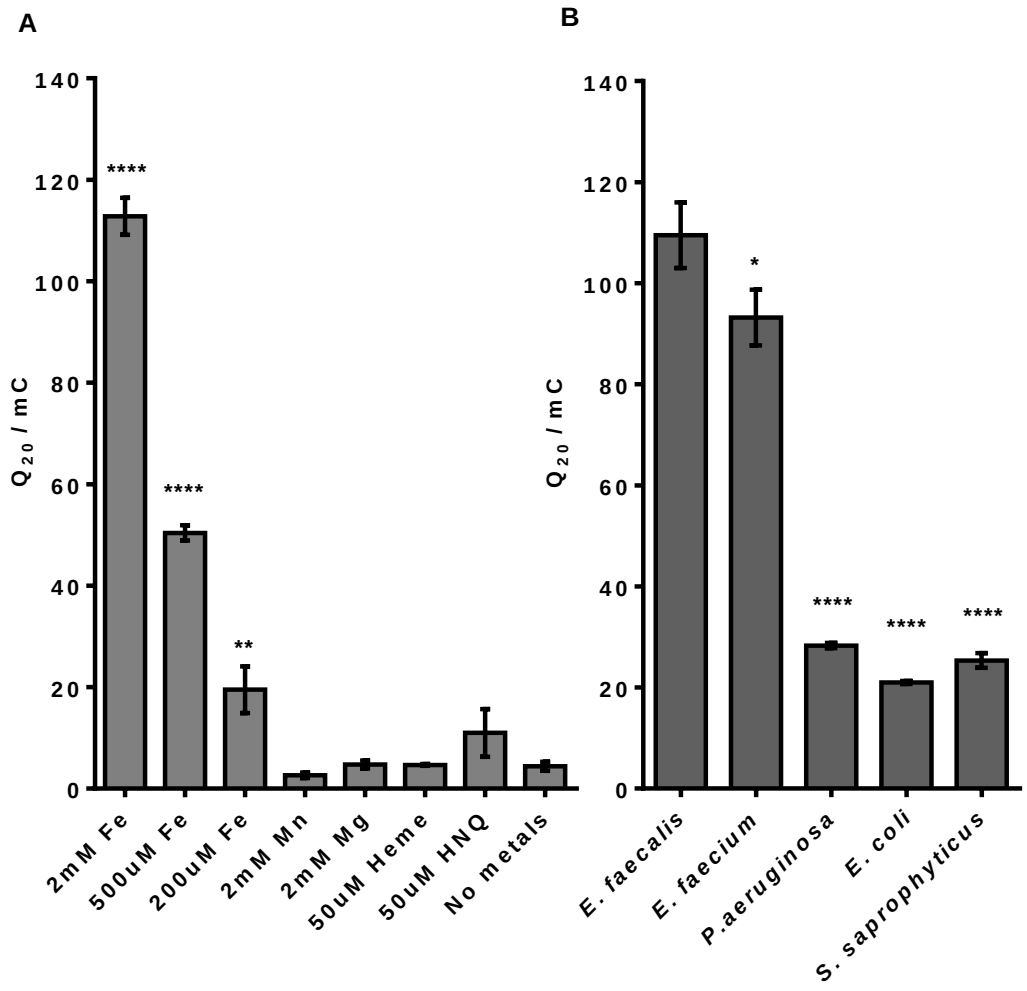

Figure 2.10: Biometal specificity of extracellular electron transfer in *Enterococcus spp*. Chronocoulometry current (Q) measurement, expressed in milicoulomb (mC), of *E. faecalis* biofilm on a screen-printed electrode over 20 hr in TSBG (Supplemented). (A) Biometal specificity of EET, (B) strain specificity of iron mediated EET. Statistical significance was determined by one-way ANOVA with LSD Fisher's test, N=6, error bars represent SEM from the mean, * $P \leq 0.05$, ** $P \leq 0.01$, *** $P \leq 0.001$, **** $P \leq 0.0001$

2.6 Discussion

In this study, we have shown that iron mediated EET drive metabolism and energy production, which resulted in enhanced *E. faecalis* biofilm growth. Using an array of interdisciplinary approaches, we have also demonstrated that iron mediated EET is a unique mechanism employed by Enterococci and involved L-lactate dehydrogenase (Ldh1) in electron transfer. Although the precise mechanism of electron transfer from Ldh1 and the subsequent release of electron from cell wall surface has not been characterized, from our findings, we proposed our working model in which fermentation and EET-dependent respiration drive the flow of electron transfer in the absence of oxygen as the final electron acceptor. We reasoned that oxidization of pyruvate, by L-lactate dehydrogenase, drive the production of lactate. Accompanying the oxidization of the substrate, conversion of NADH to NAD^+ also occurs. We hypothesized that the small molecules, NADH and NAD^+ are important for EET-dependent respiration, and the absence of Ldh1 limited the availability of these molecules, which attenuate the flow of electron from the cell membrane. Additionally, lactic acid producing bacteria such as *E. faecalis*, rely on fermentation to produce NADH, in contrast to most bacteria species that utilize tricarboxylic acid cycle (TCA) (Pedersen et al., 2012). Moreover, we also speculate that *E. faecalis* likely take advantage of Fe(III)/Fe(II) redox coupling to transfer electrons extracellularly, however the mechanism we employed in this study does not allow for detection of iron speciation. Nevertheless, our findings indicate that likely Fe(III)/Fe(II) oxyhydroxide mixture serves as iron sink as seen in our TEM images whereby iron deposits are embedded in the biofilm matrix.

Extracellular electron transfer (EET), generally are employed by metal-reducing anaerobic bacterial species, as alternative mechanism for respiration and growth. The most well characterized model organisms, *Geobacter spp.* and *Shewanella spp.*, have been extensively studied for their application in microbial fuel cells (Shi et al., 2016). A vast majority of studies in EET are characterized in gram negative bacteria, and only a select few gram positive bacteria such as *Thermincola potens* and *Desulfotomaculum reducens* have been characterized (Wrighton et al., 2011). Moreover, *Corynebacterium* sp. (Liu et al., 2010) and *E. faecalis* itself have been shown to be electro-active in microbial fuel cells when supplied with redox mediators AQDS and riboflavin (Zhang et al., 2014) respectively. Additionally, *E. gallinarum* can use iron as an electron acceptor but the impact on growth was not determined (Kim et al., 2005). The precise pathway of EET has

been demonstrated to be either through direct contact dependent (DET) which involved outer membrane c-type cytochromes (Okamoto et al., 2011), or alternatively mediated by soluble electron shuttles (mediators) (MET) (Marsili et al., 2008a; Schröder et al., 2015; von Canstein et al., 2008; Wang et al., 2010a). Moreover, the mechanism of EET has been shown to involve membrane embedded menaquinone as well (Shi et al., 2009).

Enterococcus faecalis, like all lactic acid bacteria, possess the aerobic respiration pathway in addition to glycolysis, for generation of ATP. The components of aerobic respiration include: (1) NADH dehydrogenases functioning as electron donors, (2) a quinone pool to transfer electrons to (Brooijmans et al., 2009) (3) the terminal electron acceptor complex cytochrome oxidase (Richardson, 2000). The *E. faecalis* cytochrome *bd* enzyme use oxygen as a terminal electron acceptor when exogenous heme are available (Baureder and Hederstedt, 2012; Winstedt et al., 2000). *E. faecalis* does not synthesize porphyrin and, in the absence of heme, relies on fermentation for respiration. Moreover, our results demonstrate that supplementing heme does not mediate EET. In the context of *E. faecalis*, this is the first study documenting iron mediated EET using iron as terminal electron acceptor. While we did not detect demenaquinone (DMQ) pathway associated mutant with altered biofilm formation in our library screen, we reasoned that this may be due to redundancies inherent in aerobic respiration chain, or substitution of enzyme function to compensate for absence of functional DMQ (Chen et al., 2017a; Poole and Cook, 2000). Substitution of heme with copper as the cofactor for menaquinone has been demonstrated in *Lactococcus lactis* and consequently drive respiration (Rezaiki et al., 2008).

Owing to its metabolic versatility and inherent oxidative stress tolerance, Enterococci can thrive in iron-limiting and iron-enriched environment. Although further investigation is needed to clarify the yet not fully understood mechanism of iron mediated EET, the findings in this study given us a deeper understanding of the mechanisms that can be employed by *E. faecalis* in colonizing niches. To what extent does this mechanism play a role in clinical context, we do not yet understand but we do know that niches such as the human gastrointestinal tract (Abbaspour et al., 2014) or the natural environment (Byappanahalli and Fujioka, 2004; Giraffa, 2002; Ratan et al., 2017) where iron is abundant, may be the reason for the emergence of this mechanism either for survival or to thrive in these niches. Colonization and persistence in clinical infections requires

metabolic adaptability to exploit the nutrients available, and our study highlight that an alternative form of metabolism employed by *E. faecalis*, an opportunistic pathogen involved in numerous nosocomial infections, which may have implication on virulence and pathogenicity. To address this, future work should include a deeper understanding of how iron impact virulence and colonization in *in vivo* models. In addition to *ldh1*, several other genes have been identified in the library screen and contribute to iron-augmented biofilm growth. In **Chapter 3 and 4**, the role of these genes will be further characterized and discussed.

2.7 Acknowledgements

This work was supported by the National Research Foundation and Ministry of Education Singapore under its Research Centre of Excellence Programme, by the National Research Foundation under its Singapore NRF Fellowship programme (NRF-NRFF2011-11), and by the Ministry of Education Singapore under its Tier 2 programme (MOE2014-T2-2-124). We thank Kenneth Beckman (University of Minnesota) and colleagues for sequencing of the *E. faecalis* transposon library, and Wandy Beatty (Washington University in St. Louis) for performing TEM. We thank SCELSE members Sumitra Debina Mitra, Irina Afonina, Shu Sin Chng, Hans-Kurt Fleming, Scott Rice, and Staffan Kjelleberg, as well as Jeff Gralnick (University of Minnesota) for their critical assessment of the manuscript for this study.

2.8 Supplementary figures and tables

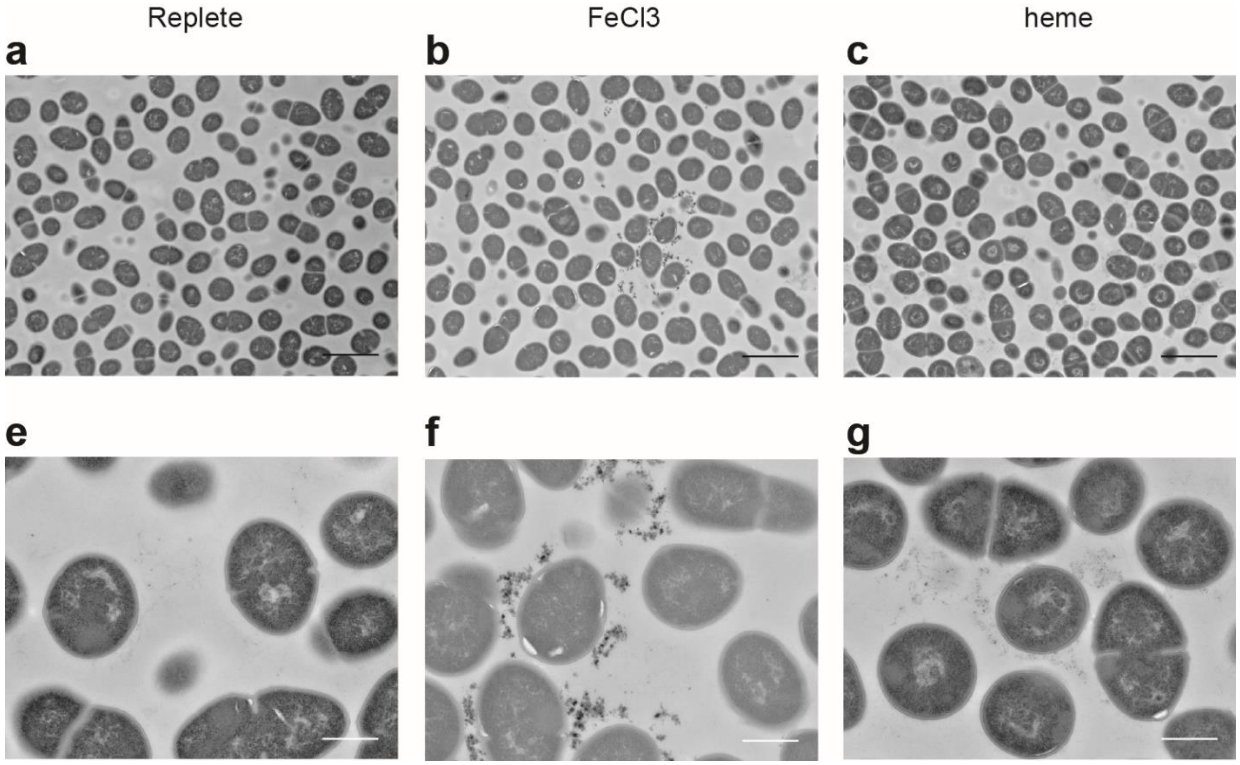

Figure S2.1: Electron micrographs of the *E. faecalis* biofilm matrix in the absence or presence of metal supplementation. Representative images from TEM of *E. faecalis* biofilm from 24 hr static biofilms **(A, E)** grown in normal TSBG, **(B, E)** TSBG supplemented with 2 mM $FeCl_3$, or **(C, F)** 50 µM heme. Scale bars represent 2 µm (black) and 0.5 µm (white).

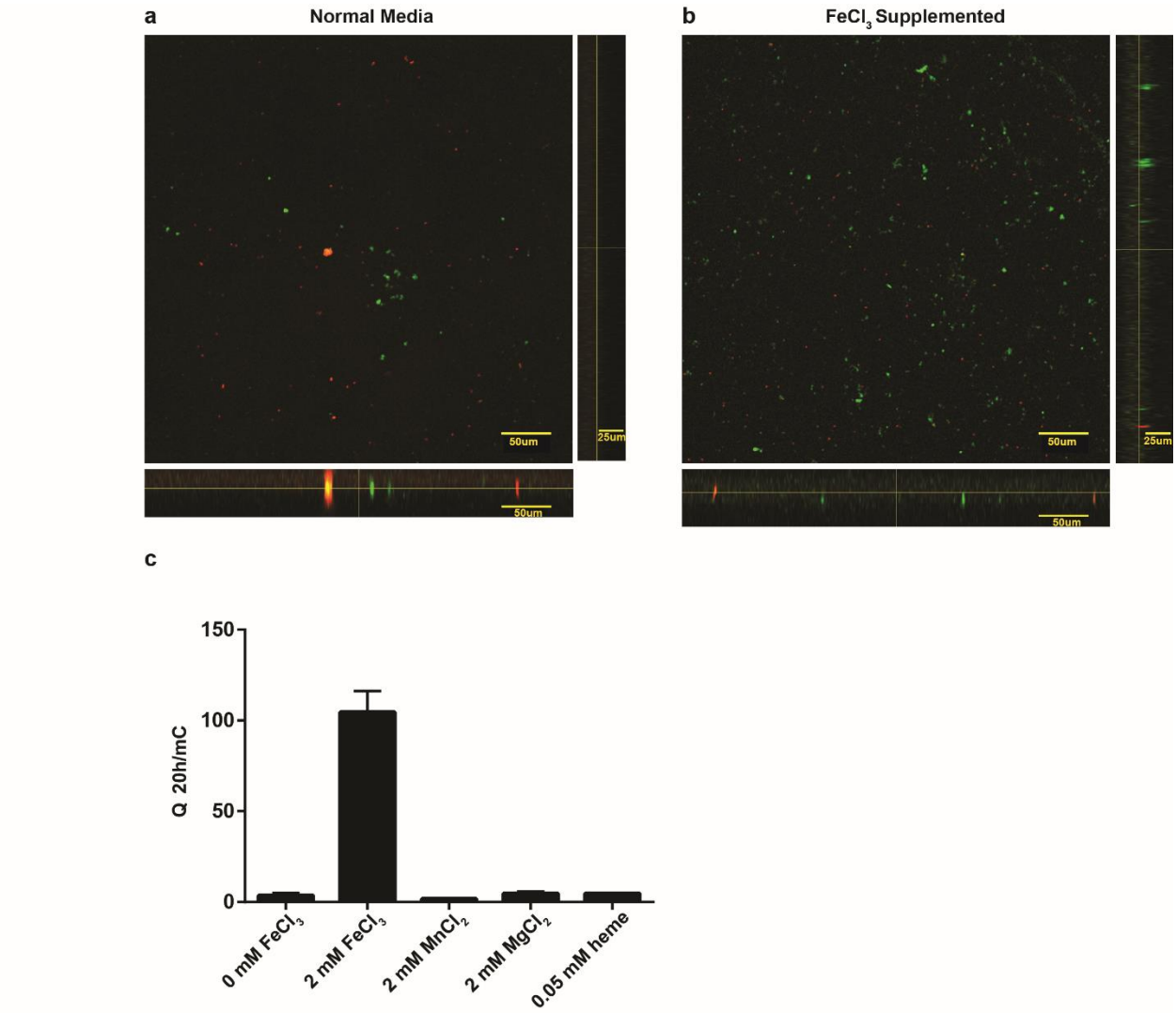

Figure S2.2: Biofilm biomass and metal-dependence of *E. faecalis* EET. CLSM images of *E. faecalis* biofilm on screen-printed electrode at the end of chronocoulometry measurements after 20 hrs growth in **(A)** normal TSBG or **(B)** TSBG supplemented with 2 mM $FeCl_3$. **(C)** Charge (mC) transferred from *E. faecalis* biofilm to the SPE after 20 hr in normal TSBG, TSBG supplemented with 2mM $FeCl_3$, 2mM manganese chloride ($MnCl_2$), 2 mM magnesium sulphate ($MgSO_4$), or 50µM heme. These results were measured in glass electrochemical cells filled with 11 mL growth medium. All the other parameters are the same described in the Materials and Methods section. The working electrode was poised at 200 mV vs the silver pseudoreference electrode of the SPE.

Chapter 3: Iron-pili interaction facilitates electron transfer, biofilm augmentation and intracellular iron accumulation to promote *Enterococcus faecalis* biofilm formation

3.1 Statement of contribution

L.N.L conceptualized the study. L.N.L, E.M and K.A.K designed the experiments, analyzed the data and prepared the manuscript. L.N.L performed biofilm experiments, immuno-fluorescence assays and analyzed the data. A.M analyzed the confocal data and generated 3D reconstruction models. L.N.L performed ICP-MS and analyzed the ICP-MS data. L.N.L, P.M.L and E.M performed the electrochemistry experiments and analyzed the data. L.N.L and J.J.W performed the murine GI colonization model and analyzed the data. L.N.L prepared the RNA samples for RNA sequencing and K.K.L.C analyzed the data. Manuscript for this work is in preparation.

3.2 Abstract

Enterococcus-associated biofilm infections are clinically important. An in depth understanding of enterococcal biofilm physiology is crucial in contributing to advancement in anti-biofilm therapeutics. Previously we have shown that iron mediated extracellular electron transfer (EET) promotes *E. faecalis* biofilm growth; however, the role of iron and EET in a clinical context has yet to be explored. Moreover, for colonization and persistence in clinical infections, expression of biofilm associated virulence factors is necessary. Type IV pili have been shown to function as microbial nanowires which aid electron transfer in other bacteria species. Hence, it is not implausible that *E. faecalis* pili may also contribute to electron transfer.

Here, we report an alternative role for *E. faecalis* endocarditis and biofilm associated pili (Ebp), in addition to their role in adhesion, in binding iron to promote EET and iron-mediated biofilm growth. We show that increased *ebp* expression is essential for iron-mediated biofilm augmentation, restructuring of biofilm, and EET. Deletion of *ebp* results in attenuated iron-mediated biofilm growth and electron transfer. We also show that MenB and Ndh3 which are essential for demethylmenaquinone (DMK) biosynthesis and flavin-mediated electron transfer respectively are involved in iron-mediated EET. Moreover, we postulate that iron interacts with the pilus at the EbpA subunit, specifically at the MIDAS motif of the VWA domain in the N terminus, which is a conserved motif for cationic metal binding. We show that the MIDAS motif contributes to iron-mediated biofilm growth and electron transfer because the *ebpA*^{AWAGA} mutant, which is defective in ligand binding due to three alanine substitutions in the MIDAS motif, is attenuated for these phenotypes. Furthermore, we show that iron co-purifies with Ebp expressed on cell surface, and presence of Ebp on cell surface is essential for iron uptake in *E. faecalis* biofilm cells. Moreover, a global transcriptional analysis of *E. faecalis* biofilm revealed 90 genes that were differentially regulated in response to iron supplementation, and we show that the iron transporter *feoB* is upregulated in the presence of iron and FeoB is essential for iron uptake. The transcriptional response to iron in the *ebpA*^{AWAGA} MIDAS mutant resulted in 734 genes differentially regulated as compared to the wild type OG1RF. Lastly, we also demonstrated that a high iron diet promoted *E. faecalis* gastrointestinal tract (GI) colonization in the murine colon, in an *ebp*-dependent manner. These findings represent the first description of a contribution of endocarditis and biofilm associated pili to EET and gut colonization, *in vitro* and *in vivo*, respectively. Moreover, this is the

first study looking at the role of the MIDAS motif of EbpA in EET. Collectively, these data demonstrate that iron-pili interaction facilitate electron transfer and contributes to biofilm augmentation and intracellular iron accumulation in *Enterococcus faecalis* biofilm.

3.3 Introduction

Enterococcus faecalis biofilm contributes to several opportunistic infections including endocarditis, urinary tract infections, bacteremia, wound and medical implant-associated infections. A number of *E. faecalis* virulence factors have been phenotypically characterized for their contribution to pathogenesis (Ch'ng et al., 2018; Garsin et al., 2014). Among these virulence factors, the endocarditis and biofilm associated pilus (Ebp) is one of the best characterized. The vast majority of studies have focused on pilus biogenesis, assembly, and the role of Ebp in *E. faecalis* biofilm formation and host colonization.

The Ebp, which is composed of subunits EbpA (the tip of the pilus), EbpB (basal unit of the pilus polymer which is anchored to cell wall), and EbpC (major subunit which contributes to the varying length of the pilus). The *ebpABC* operon is transcriptionally regulated by EbpR, a transcriptional regulator upstream of *ebpABC*, and deletion of *ebpR* significantly reduces *ebpABC* gene transcripts (Bourgogne et al., 2007). Additionally, studies have shown that the *fsr* quorum sensing system regulates pilus expression. Deletion of *fsr* results in an absence of pilus expression, and consequently results in reduced surface adherence and *in vitro* biofilm formation (Dunny et al., 2014). Pilus biogenesis proceeds via polymerization of the subunits by the sortase C enzyme, followed by the anchoring of the polymerized pilus polymer to the cell wall by sortase A (Kline et al., 2009; Nielsen et al., 2013b; Sillanpaa et al., 2013). Deletion of *ebpABC* results in attenuated *in vitro* biofilm formation; binding to ligands such as fibrinogen, collagen, and platelets; and attenuated colonization in urinary tract infection (UTI), catheter-associated UTI (CAUTI), and infective endocarditis models (Nallapareddy et al., 2011a; Nallapareddy et al., 2006; Nallapareddy et al., 2011b; Nielsen et al., 2013b).

In addition to EbpR, environmental cues can drive pilus gene expression, however this is less well-studied. Bourgogne and colleagues have shown that bicarbonate increased *ebpR-ebpABC* expression, independent of *fsr* repression (Bourgogne et al., 2010). Moreover, growth in serum also resulted increased pilus gene expression (Nallapareddy et al., 2006). A separate study demonstrated that deletion of *rnjB*, a putative RNase J2, resulted in decreased *ebpC* gene transcript levels and reduced biofilm formation, which is phenotypically similar to an *ebpABC* deletion

mutant (Gao et al., 2010). In addition, whether and how pilus gene expression responds to environmental cues in the host remains to be explored.

Previously, we have shown that iron mediated extracellular electron transfer (EET) promotes *E. faecalis* biofilm growth (Keogh et al., 2018). In other species, microbial nanowires, which are typically extracellular filamentous protein structures, aid electron transfer by direct contact from the cell surface to extracellular metal oxides, or alternatively, interact with extracellular soluble redox mediators to mediate electron transfer (Sure et al., 2016; Weber et al., 2006). In *Geobacter spp*, deletion of *pilA*, the type IV pilus major subunit, resulted in attenuated ability for long range electron transfer (Smith et al., 2014b). By contrast, expression of *pilA* in other *Geobacter spp* lacking pilin-encoding genespromoted electron transfer (Tan et al., 2017). Tan and colleagues recently also showed that the organization of the aromatic amino acids in the pilus structure contribute to the conductivity of the pili (Tan et al., 2017). Alanine substitution of each of the five amino acids in the carboxy terminus of PilA resulted in attenuated long range electron transfer in *Geobacter sulfurreducens* (Vargas et al., 2013), and this attenuated electron transfer is independent of the ability of the pilus to bind the multiheme c-type cytochrome OmcS, which is essential for iron oxide reduction (Leang et al., 2010).

Based on the role for pili in EET in the model organism *Geobacter*, we hypothesized that *E. faecalis* endocarditis and biofilm associated pili (Ebp) may contribute to iron-mediated EET. The underlying final step for EET is to promote the release of electrons from the cell wall to an extracellular electron acceptor, in this case, ferric iron oxide. We postulate that the pili either directly contact iron oxides at close proximity to allow for electron transfer, or alternatively, they interact with an electron shuttle or iron reductase which facilitate the electron transfer. It is not yet known whether the *E. faecalis* pilus binds extracellular cytochromes; however, the N terminus of EbpA consists of the von Willebrand factor A domain which contains a MIDAS motif. In eukaryotes, the MIDAS motif is a metal ion-dependent adhesion site important for metal (Mg^{2+}) and ligand binding (Plow et al., 2000), and it is conserved in cell adhesion and extracellular matrix (ECM) proteins (Whittaker and Hynes, 2002). However, the role of MIDAS in bacterial ligand binding has not been characterized. We hypothesize that the MIDAS motif of EbpA plays a role in iron binding, iron mediated biofilm growth, and electron transfer. We show that *ebp* expression,

and specifically the MIDAS motif in EbpA, is essential for iron-mediated biofilm augmentation, restructuring of biofilm architecture, and EET. Moreover, biofilm growth in iron-supplemented media results in a global transcriptional response which involves modulation of virulence genes, metabolism genes, and iron acquisition systems. Furthermore, iron co-purifies with Ebp, and the presence of Ebp anchored on cell surface is essential for iron uptake in *E. faecalis* biofilm. Finally, using an *in vivo* murine GI colonization model, we demonstrated that high iron diets result in enhanced *E. faecalis* colonization in the murine colon in an *ebp*-dependent manner. Together, these data demonstrate that iron-pili interaction facilitate electron transfer, and contributes to biofilm augmentation and intracellular iron accumulation in *Enterococcus faecalis* biofilm.

3.4 Materials and methods

3.4.1 Bacterial Strains and Growth Conditions

Enterococcus faecalis was grown in Brain Heart Infusion broth (BHI) and cultured at 37 ^{o}C under static and shaking (200rpm) conditions where appropriate. Preparation of inoculum for biofilm and planktonic assays were performed as previously described (Keogh et al., 2018). Bacterial strains used were listed in **Table 3.1**. Where appropriate, strains harbouring pGCP123 plasmids were selected using 1000 ug/mL kanamycin (Sigma Aldrich, USA). The reagents used for bacterial growth were listed as below. BHI was supplied by Becton, Dickinson and Company, Franklin Lakes, NJ. TSB and agar was supplied by Oxoid Inc., Ontario, Canada. Metals for supplementation were added during medium preparation. Ferric citrate hydrate ≥98%, magnesium chloride anhydrous ≥98%, copper chloride dihydrate ≥99%, ferrous sulphate heptahydrate ≥99%, ferric sulphate hydrate ≥97%, ferric chloride anhydrous ≥99%, heme ≥90% and the chelator 2,2'dipyridyl ≥99% were supplied by Sigma Aldrich, St Louis, MO, USA. Manganese chloride tetrahydrate and zinc chloride were supplied by Merck Millipore, Singapore.

Table 3.1: List of bacterial strains used

Strains used	Relevant characteristics	Reference or source
***E. faecalis* OG1RF wild type**	Laboratory strain, Rif^R, Fus^R	(Bourgogne et al., 2008)
OG1RF Δ*ebpABC*	*ebpABC* triple deletion mutant; Rif^R, Fus^R	(Nielsen et al., 2012; Nielsen et al., 2013b)
OG1RF Δ*ebpA*	*ebpA* single deletion mutant; Rif^R, Fus^R	
OG1RF Δ*ebpB*	*ebpB* single deletion mutant; Rif^R, Fus^R	
OG1RF Δ*ebpC*	*ebpC* single deletion mutant; Rif^R, Fus^R	
OG1RF Δ*ebpABC* *gcp123::ebpABCsrtC*	Complement mutation; Rif^R, Fus^R	
OG1RF Δ*ebpABC* gcp123	*ebpABC* triple deletion mutant; Rif^R, Fus^R, Kan^R	
OG1RF gcp123	Laboratory strain, Rif^R, Fus^R, Kan^R	
OG1RF ebpA^{AWAGA} (MIDAS)	ebpA allelic replacement with ebpA^{AWAGA} (coding for Ala^{315}-Trp-Ala^{317}-Gly-Ala^{319}); Rif^R, Fus^R	
***menB*::Tn**	Rif^R, Fus^R, Erm^R (ID: 15.2I2 E11 Tn mutant)	(Kristich et al., 2008)
***menB*::Tn pMSP3535**	Rif^R, Fus^R, Erm^R	This paper
menB*::Tn pMSP3535::*menB	Rif^R, Fus^R, Erm^R Complement mutation	This paper
***ndh3*::Tn**	Rif^R, Fus^R, Erm^R	(Kristich et al., 2008)

	(ID: 3.2A1 E10 Tn mutant)	
***ndh3*::Tn pMSP3535**	Rif^R, Fus^R, Erm^R	This paper
ndh3*::Tn pMSP3535::*ndh3	Rif^R, Fus^R, Erm^R Complement mutation	This paper
ndh3::Tn* Δ*menB	Deletion mutant	This paper
OG1RF pMSP3535	Laboratory strain, Rif^R, Fus^R, Erm^R	This paper

3.4.2 Immunofluorescence Imaging and 3D Reconstruction of Biofilm

Bacterial cultures were normalized to OD 0.7 and diluted 1000 times prior inoculating into each well of µ-Slide 8 well glass bottom (ibiTreat coated) (ibidi Inc., USA) containing 40% v/v TSBG for incubation at 37^{o}C under static conditions for 24 hours. Post incubation, adherence biofilm was fixed in 4% paraformaldehyde (Sigma Aldrich, USA)-PBS for 30 minutes, blocked with 3% bovine serum album (Sigma Aldrich, USA) (BSA)-PBS for 30 minutes, and incubated with primary antibody (Rabbit Anti-Group D antigen or Guinea Pig Anti-EbpC, Thermo Scientific Singapore) at 1:500 dilution for 30 minutes. Post incubation, adherence biofilm was washed with 3% bovine serum album (Sigma Aldrich, USA) (BSA)-PBS and incubated with secondary antibody (IgG horse radish peroxidase-conjugated anti rabbit or anti guinea pig, Thermo Scientific Singapore) at 1:500 dilution for 30 minutes, and washed with 3% Bovine serum album (Sigma Aldrich, USA) (BSA)-PBS. Biofilms were hydrated with PBS prior to imaging. Biofilm morphology, biomass, and cell distribution were analysed by confocal laser scanning microscopy (CLSM). Images were acquired using LSM780 confocal microscope (Zeiss, Germany) equipped with 63x/1.4 Oil DIC M27 and controlled by ZEN software. Samples were illuminated with 488 nm and 561nm Argon laser line; GFP emitted fluorescence was collected in the 493-580 nm range and RFP emitted fluorescence was collected in the 568-712 nm range. Optical sections (134.95x134.95 µm) were collected every 0.637 µm through the entire biofilm thickness and signal from each section was averaged 4 times. Fiji software was used for further processing (levels adjustment, stack resliced). To visualize the biofilm matrix and spatial organization coordinates were plotted as spheres with cell-size diameter and color coded Z-depth.

3.4.3 Static Biofilm Assay

Bacterial cultures were normalized as previously described (Keogh et al., 2018) and inoculated in TSBG in a 96-well flat bottom transparent microtiter plate (Thermo Scientific, Waltman, MA,

USA), at 37°C under static conditions. Staining of adherence surface biofilm biomass was performed using 0.1% w/v crystal violet (Sigma-Aldrich, St Louis, MO, USA), and incubated at 4 °C for 30 minutes. The microtitre plate was washed twice with PBS followed by crystal violet solubilization with ethanol-acetone (4:1) for 45 minutes at room temperature. Quantification of adherence biofilm biomass was performed by measuring absorbance at OD_{595nm} using a Tecan Infinite 200 PRO spectrophotometer (Tecan Group Ltd., Männedorf, Switzerland).

3.4.4 Planktonic Growth Assay

Bacterial cultures were normalized as previously described (Keogh et al., 2018) and serial diluted by dilution factor of 200. Diluted cultures were inoculated into the media at a ratio of 1:25, which is 8 µL of inoculum in 200 µL of media, incubated at 37°C for 18 hours, and absorbance at OD_{600nm} was measured using a Tecan Infinite 200 PRO spectrophotometer (Tecan Group Ltd., Männedorf, Switzerland) at 15 minutes interval. Growth curve was plotted to determine the exponential growth.

3.4.5 Quantification of Pilus Expressing Population

Biofilms were grown in 6 well microtiter plate 37°C under static conditions for 24 hours in TSBG, and TSBG supplemented with metals where appropriate, and planktonic cultures were grown similarly under shaking condition (200 rpm). Immunoblotting was performed as described previously (Kline et al., 2009) with some modification. Spent media was removed, and adherence biofilm was suspended in PBS. Cell scraper was used to dislodge the biofilm, and biofilms were centrifuged at 14,000 rpm for 2 minutes at room temperature to remove supernatant. Biofilms was suspended in PBS, and normalized to OD1.0. Normalized cultures were fixed in 4% paraformaldehyde (Sigma Aldrich, USA)-PBS for 20 minutes at 4 °C and the supernatant was discarded. Normalized biofilm cultures were washed with PBS, centrifuged at 14,000 rpm for 2 minutes and the supernatant was discarded again. Immunofluorescence microscopy was performed as described previously(Kline et al., 2009) with the following modifications: 1:500 dilution of guinea pig anti-EbpC (Thermo Scientific, Singapore) in PBS-3% bovine serum albumin, and 1:500 dilution of goat Anti-guinea pig AlexaFluor-568 (Invitrogen Inc., USA) incubation for 30 minutes. After washing with PBS twice, resuspended cells were aliquot to the pre-treated poly-L-lysine slides (Polysciences Inc., USA), dried in the hybridisation oven for 5 minutes, mounted with

Vectashield® mounting media and sealed with a cover slip. Images were acquired using inverted Epi-fluorescence microscope (Zeiss Axio observer Z1, Germany) equipped with EC Plan-Neofluar 100x/1.3 Oil objective and controlled by ZEN software. For each biological sample, 5 images were acquired and percentage of cell population expressing pili was quantified. At least 300 bacterial cells per strain per experiment were scored for pilus expression.

3.4.6 Thin-section Transmission Electron Microscopy (TEM)

Biofilms were grown in a 6-well plate for 24 hours at 37^{o}C under static conditions. Post incubation, adherence biofilms were suspended in PBS and dislodged using cell scraper. Biofilm cultures were centrifuged at 14,000 rpm for 2 minutes at room temperature to remove supernatant and were suspended in a 2 % paraformaldehyde-2.5 % glutaraldehyde solution (Polysciences Inc., Warrington, PA) in 100 mM PBS (pH 7.4) for 1 hr at room temperature. Samples were rinsed in distilled water (dH_2O) prior to *en bloc* staining with 1 % aqueous uranyl acetate (Ted Pella, Inc., Redding, CA, USA) for 1 hour. Post *en bloc* staining, samples were dehydrated in a graded series of ethanol and embedded in Eponate 12 resin (Ted Pella, Inc., Redding, CA, USA). Sections of 95 nm were cut with a Leica Ultracut UCT ultramicrotome (Leica Microsystems, Inc., Bannockburn, IL, USA), stained with uranyl acetate and lead citrate, and viewed on a JEOL 1200 EX transmission electron microscope (JEOL USA, Inc., Peabody, MA, USA).

3.4.7 Quantitative Real time PCR (qRT-PCR) and RNA sequencing

Biofilms were grown in a 6-well plate for 24 hours at 37^{o}C under static conditions. Post incubation, spent media was removed and biofilms were suspended in PBS prior being dislodged using cell scraper. Biofilm cultures were centrifuged at 14,000 rpm for 2 minutes at room temperature to remove supernatant. Biofilm cell pellet was incubated with lysozyme solution containing lysozyme from chicken egg white (10mg/ml) (Sigma Aldrich, USA) for 30 minutes at 37^{o}C, and centrifuged at 14,000 rpm for 2 minutes at room temperature to remove supernatant prior to cell lysis. RNA extraction was performed in a Purifier® filtered PCR enclosure using the PureLink™ RNA mini kit (Invitrogen, USA) according to the manufacturer's instructions. RNA purification and removal of DNA was performed using TURBO DNA-free™ kit (Thermo Fisher, USA) and Agencourt® RNAClean® XP Kit (Beckman Coulter, USA). Measurement of RNA yield and quality was performed using Qubit® RNA HS assay kit (Thermo Fisher, USA) and RNA

ScreenTape System and 2200 TapeStation (Agilent, USA). Synthesis of cDNA was performed using SuperScript III First-strand (Invitrogen, USA). Quantitative real-time PRC using cDNA was performed using KAPA SYBR fast qPCR master mix kit (Sigma Aldrich, USA) and Applied Biosystems StepOne Plus Real-Time PCR system. The expression of *ebpC*, *ebpR*, *srtA*, *srtC* and *gyrA* were analysed using primer pairs listed in **Table 3.2**. For each primer set, a standard curve was established using genomic DNA from *E. faecalis* OG1RF. Normalized amount of cDNA were used to determine relative fold change in gene expression as compared to *E. faecalis* OG1RF biofilm grown in TSBG. For RNA sequencing, ribosomal RNA depletion was performed after RNA purification using Ribo-Zero™ rRNA removal kit (Illumina, USA). cDNA library synthesis was performed using NEBNext RNA First-strand and NEBNext Ultra directional RNA Second-strand synthesis module (New England BioLab, US). Transcriptome library preparation was performed using 300bp paired end Illumina sequencing. All genes that were differentially regulated, with p-value of less than 0.05 and false discovery rate (FDR) of less than 0.05 were included. Pathway enrichment analysis was done by annotating genes in *E. faecalis* OG1RF to the KEGG database (KEGG identifier: efi). Gene classification was done based on their gene membership according to KEGG pathways. KEGG gene set enrichment analysis was performed using the Bioconductor package, clusterprofiler (version 3.8.1) (Yu et al., 2012).

Table 3.2: Primers used in qRT-PCR

Gene	5' – 3'
gyrA F'	TGTTCGTCGGGATGTGAGTG
gyrA R'	GGTACGCCTTTTTCGATGGC
ebpR F'	TAAACAGCGTTGGGGCGAAA
ebpR R'	TGGGTGGTCGTTGACGTTTT
ebpC F'	CGGTCATACCGACGACCAAA
ebpC R'	TGTCACATCGCCATCGACTT
srtA F'	TCGTACGCCGTTAGCAAGTT
srtA R'	TTCATCACCGCTTCTGTGCT

srtC F'	ACACATGCGGTCATTTCAGG
srtC R'	GCGTCTTCCCATTGACTTCG
ahrC F'	CCACTATTTACAAGAAAAGGGCGT
ahrC R'	CGCGAGAAATCGTTGCTTGT

3.4.8 Pilus Extraction And Visualization Using Native Gel Blot

Cell surface protein extracts from biofilms were prepared as described previously (Nallapareddy et al., 2006) with minor modifications. Biofilms were grown in 6 well microtiter plates for 24 hours at 37^{o}C under static conditions. Post incubation, spent media was removed and biofilms were suspended in PBS prior being dislodged using cell scraper. Biofilm cultures were centrifuge at 3300 g for 4 minutes, 15 ^{o}C, washed with Tris buffer (10 mM Tris-HCl pH 8, 1 mM EDTA, 1 mM DTT) and suspended in protoplast buffer with Pierce™ protease inhibitors (Thermo Scientific, USA). Mutanolysin from *Streptomyces globisporus* ATCC 21553 (Sigma Aldrich, USA) and benzonase nuclease (Sigma Aldrich, USA) were added and incubated at 37^{o}C for 6 hours with shaking (200 rpm). Post incubation, biofilm cultures were centrifuged at 3300 g for 4 minutes, 15 ^{o}C to obtain the supernatant. Supernatant were filtered through a 0.45µm Supor® membrane (Sigma Aldrich, USA) and loaded into Corning Spin-X UF concentrators (MWCO 100kDa) (Sigma Aldrich, USA), centrifuge for 20 minutes, 15 ^{o}C at 6000 g, and dialysis using Tris buffer using Spectra/Por® Float-A-Lyzer® G2 dialysis device (MWCO 300kDa) (Spectrum Labs, USA). Pilus extract were collected, quantified using Nanodrop 2000 Spectrophotometer (Thermofisher, USA), and normalized to 5 ug per sample. Samples were mixed with equal volume of NuPAGE® Tris-glycine native sample buffer (Novex®) and loaded on to NuPAGE™ 3-8% Tris-acetate gel (Thermofisher, USA). Gel blots were run at 150 V for 3 hours. Western blotting was performed as described previously(Nielsen et al., 2013a) with minor modification. Membrane was block in 0.05% v/v Tween-3% v/v bovine serum albumin-PBS (Sigma Aldrich, USA) overnight at 4 ^{o}C and washed twice with 0.05% v/v Tween (Sigma Aldrich, USA)-PBS prior to incubation with primary and secondary antibodies, and prior to incubation with detection substrate. Primary antibody (guinea pig Anti-EbpC or rabbit Anti-SecA) (Thermo Scientific, Singapore) at dilution of 1:1500, and secondary antibody (IgG guinea pig or rabbit conjugated horseradish peroxidase) (Thermo

Scientific, USA) at dilution of 1:4000 were used. Detection of protein bands were obtained using SuperSignal® west femto maximum sensitivity substrate kit (Thermo Scientific, USA).

3.4.9 Inductive-Coupled Plasma Mass Spectrometry (ICP-MS).

Pilus extracts, normalized to 5ug per sample, were prepared and run under native condition as previously described above. Using the western blot prepared gel as a reference, a separate identical NuPAGE™ Tris-acetate gel (Thermofisher, USA) was cut to isolate pilus extract at above molecular weight of 100 kDa. For intracellular metal quantification, biofilms are cultured under static condition at 37°C for 24 hrs. After incubation, biofilms are scraped, resuspended in 1mL PBS and normalized to OD 1. Normalized biofilms are pelleted at 14,000 rpm for 2 minutes, and supernatant was discarded. Cell pellets are washed with 1 mL of 0.5 mM EDTA. Next, the cell pellets are suspended in 300 uL of lysozyme from chicken egg white (20 mg/ml) (Sigma Aldrich, USA) (20mg/mL) for 30 minutes at 37°C, washed with 1 mL PBS and pelleted. At a ratio of 2:1, 70% nitric acid (Sigma Aldrich, USA) and 30% hydrogen peroxide (Sigma Aldrich, USA) was added to the excised gel containing the pilus protein, and left under room temperature for 3 days to allow complete digestion. The digested samples were diluted with LC-MS grade water and filtered using 0.2 µm membrane, prior to analysis using ICP-MS. For tissue ICP-MS, tissues (cecum, colon, small intestines) are emptied of its content and suspended in 1 mL PBS. Digestion of tissues was performed using 2 mL 70% nitric acid (Sigma Aldrich, USA) and 500 uL 30% hydrogen peroxide (Sigma Aldrich, USA) at 37°C for 3 days, and then 65°C for 5 hours. Digested tissues were diluted with 9 mL LC-MS grade water and filtered using 0.2 µm membrane, prior to analysis using ICP-MS. Analysis of trace metals in samples were performed using ICP-MS model Elan-DRCe, Meinhard Nebulizer model TR-30-C3 (Perkin Elmer; Model: N8122006 (Elan Standard Torch)).

3.4.10 Electrochemical Setup and Analysis

Screen printed electrodes (SPE) (model DRP-C110; DropSens, Spain) consisting of a carbon working electrode, carbon counter electrode, and Ag pseudo-reference electrode were controlled by a multichannel potentiostat (VSP, Bio-Logic, France) in an electrochemical cell of 9 mL working volume sealed with a Teflon cap. Chronocoulometry was performed as previously described with minor modifications (Keogh et al., 2018). All electrochemical experiments were

conducted at 37 ^{o}C using TSBG medium supplemented with 1 mM $FeCl_3$ unless otherwise stated. Chronocoulometry was also performed on electrochemical cell set up in a continuous flow system previously described with minor modifications (Keogh et al., 2018).

3.4.11 Ferric iron reduction assay

Bacterial cultures were normalized as previously described (Keogh et al., 2018) and serial diluted by dilution factor of 200. Diluted cultures were inoculated into the media at a ratio of 1:25, which is 8 µL of inoculum in 200 µL of media supplemented with 0.5 mM ferrozine, incubated at 37^{o}C for 10 hours, and absorbance at OD_{562nm} was measured using a Tecan Infinite 200 PRO spectrophotometer (Tecan Group Ltd., Männedorf, Switzerland) at 2 minutes interval.

3.4.12 High Iron Diet Murine Gastrointestinal Tract (GI) Colonization Model

Three weeks old male C57BL/6NTac mice were placed on customized synthesized diets (C1038 iron deficient diet with 200 mg/kg ferric chloride as control diet, C1038 iron deficient diet with 2000 mg/kg ferric chloride as high iron diet) (Altromin, Germany) for 5 weeks. Ampicillin is spiked in the drinking water (1 g/L) for 5 days after 3 weeks of consuming the synthesized diets. Mice were then given one day of recovery prior to administration of approximately 1-5 x 10^8 CFU/ml *E. faecalis* (OD 0.5) in drinking water for 3 days. Bacterial spiked drinking water is removed and allowed to rest for one day. Prior and post infection, mice were monitored for signs of disease and weight loss. All animal experiments were approved and performed in compliance with the Institutional Animal Care and Use Committee (IACUC). Post infection, small intestine, colon and cecum were harvested. Tissue samples were homogenised in PBS, serial diluted in PBS and spot-plated on BHI agar with 10 mg/L colistin, 10 mg/L nalidixic acid, 100 mg/L rifampicin, 25 mg/L fusidic acid. All selective agents were obtained from Sigma Aldrich, USA.

3.5 Results

3.5.1 Iron-augmented *E. faecalis* biofilm formation requires pilus expression

To test the hypothesis that pilus expression contributes to iron-mediated biofilm growth, we performed static biofilm assays in normal media and media supplemented with 2 mM ferric chloride ($FeCl_3$), and quantified total adherent biofilm biomass of wild type *E. faecalis* in comparison with a panel of pilus mutants after 120 hrs of incubation using a crystal violet assay. In iron supplemented media, Δ*ebpABC*, Δ*ebpA* and Δ*ebpC* deletion mutants displayed significantly reduced biofilm growth (**** $P \leq 0.0001$) as compared to the wild type control **(Figure 3.1)**. An Δ*ebpB* deletion mutant also displayed significantly reduced biofilm growth (** $P \leq 0.01$) as compared to the wild type control in iron supplemented media; however, it is not as dramatically attenuated as compared to the other pilus mutants **(Figure 3.1)**. These results indicate that both EbpA and EbpC subunits are essential for iron-mediated biofilm growth, and the contribution of EbpB is not as great. Moreover, since pili contribute to initial surface adherence via the EbpA subunit, it is not unexpected that deletion of *ebpA* and *ebpABC* resulted in significantly reduced (** $P \leq 0.01$) biofilm formation in normal media, as previously shown (Sillanpaa et al., 2013). However, deletion of *ebpB* and *ebpC* consequently do not attenuate biofilm formation in normal media **(Figure 3.1)**. Moreover, since deletion of *ebpA* attenuates iron mediated biofilm growth, we speculated that the metal ion domain adhesin site (MIDAS) may contribute to biofilm formation To address this, we tested an MIDAS ($ebpA^{AWAGA}$) mutant, which results in three alanine substitutions within the MIDAS domain (Ala^{315}-Trp-Ala^{317}-Gly-Ala^{319}), for iron-mediated biofilm growth and observed that it was significantly attenuated (**** $P \leq 0.0001$) similar to the *ebpABC* null mutant **(Figure 3.1)**. Collectively, these results demonstrate that both EbpA and EbpC are essential for iron mediated biofilm growth, while EbpB is dispensable.

To validate that pili contribute to iron-mediated biofilm growth, a complemented Δ*ebpABC* deletion mutant with pGCP123:e*bpABCsrtC* was tested using the iron-supplemented biofilm assay. Indeed, we observe partial restoration of iron-mediated biofilm formation **(Figure 3.1)**. Western blot analysis showed that the complemented strain displayed lower EbpC expression from the plasmid as compared to wild type OG1RF **(Figure 3.2)**. Overnight cultures for strains harboring the pGCP123 plasmids are incubated with 500 ug/mL kanamycin; however since

kanamycin has an effect on iron precipitation (data not shown), hence kanamycin is not added during the biofilm assay. We reasoned that the inability to include kanamycin for maintaining plasmid expression and reduced Ebp expression from the plasmid are likely reasons for the observed partial restoration of iron-mediated biofilm growth phenotype.

A

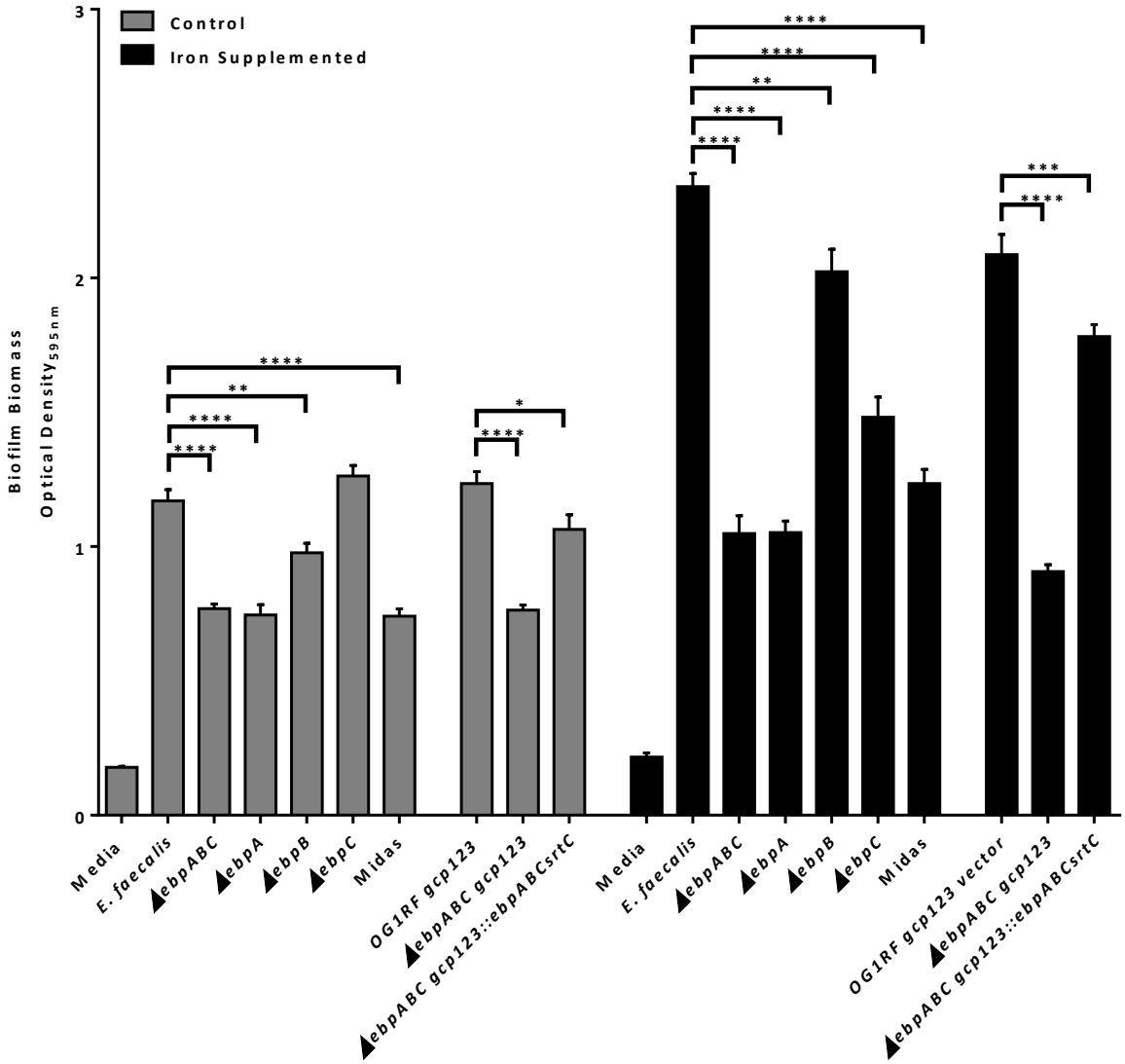

B

Condition	Strains	Fold change in biofilm biomass
Control	*E. faecalis* OG1RF	1.000
	Δ*ebpABC*	0.657
	Δ*ebpA*	0.637
	Δ*ebpB*	0.835
	Δ*ebpC*	1.078
	Midas	0.632
	E. faecalis OG1RF gcp123	1.054
	Δ*ebpABC* gcp123	0.652
	Δ*ebpABC* gcp123::ebpABCsrtC	0.909
Iron supplemented	*E. faecalis* OG1RF	1.000
	Δ*ebpABC*	0.448
	Δ*ebpA*	0.449
	Δ*ebpB*	0.864
	Δ*ebpC*	0.633
	Midas	0.527
	E. faecalis OG1RF gcp123	0.891
	Δ*ebpABC* gcp123	0.387
	Δ*ebpABC* gcp123::ebpABCsrtC	0.761

Figure 3.1. Contribution of pilus to iron mediated *E. faecalis* biofilm growth. (A) *E. faecalis* biofilm biomass quantification at 120 hrs in 96-well microtiter plate using crystal violet staining. N=9 repeated on non-consecutive days. **(B)** Fold change in biofilm biomass relative to wild type type control in control and iron supplemented media respectively. Strains harboring pGCP123 plasmids are not maintained using kanamycin (Sigma, USA) (500 ug/mL) during the experiment as kanamycin has an effect on iron precipitation (data not shown). Statistical significance was determined by two-way ANOVA. * $P \leq 0.05$, ** $P \leq 0.01$, *** $P \leq 0.001$, **** $P \leq 0.0001$. Error bar represents standard error margin (SEM).

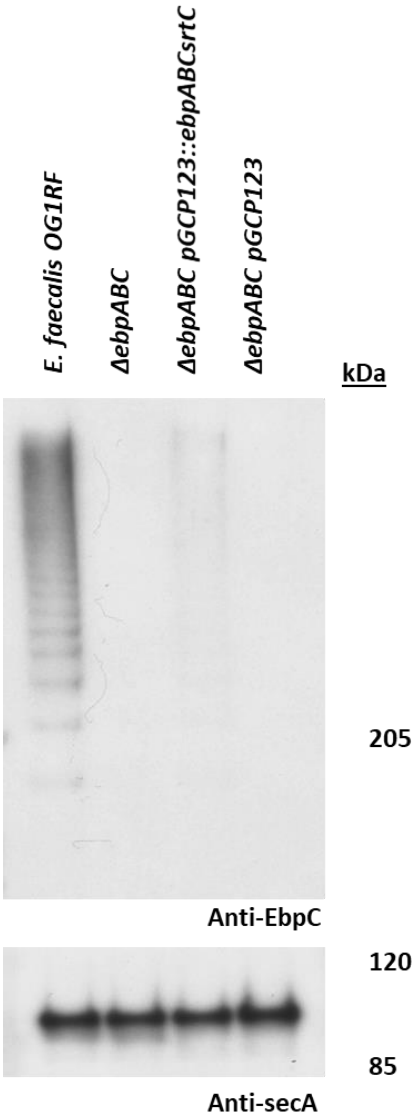

Figure 3.2. Analysis of complemented ΔebpABC pGCP123::ebpABCsrtC ability to form biofilm in iron supplemented media. Western blot analysis of whole cell lysates probed with EbpC antibodies on SDS-PAGE Tris-acetate 3-8% gel. N=3. The blot shown is representative of three biological replicates. Strains harboring pGCP123 plasmids are maintained using kanamycin (Sigma, USA) (500 ug/mL).

3.5.2 Iron drives aggregation of pilus-expressing cells in *E. faecalis* biofilm

Since our results demonstrated that pilus expression was required for iron-mediated biofilm growth, and our previous study showed that iron-mediated biofilm growth involved alteration in biofilm structure, we hypothesized that pilus expression may contribute to the biofilm restructuring during growth in iron-supplemented media. To address this, we grew *E. faecalis* biofilm in diluted (40% (v/v)) normal media and with the addition of 0.2 mM iron, we fixed and stained the cells with antibodies conjugated fluorophores (EbpC labelled as red, Group D antigen labeled as green), and performed confocal microscopy to visualize the pilus-expressing cell population in the biofilm. In the iron supplemented media, we observed increased biofilm depth and thickness which we did not observe in normal media **(Figure 3.3A-B)**, which is consistent with our previous findings demonstrating that iron supplementation alters the *E. faecalis* biofilm matrix (Keogh et al., 2018). Moreover, neither the Δ*ebpABC* deletion mutant nor the MIDAS ($ebpA^{AWAGA}$) mutant show the altered biofilm depth and thickness observed for the wild type strain **(Figure 3.3A-B)**. Using 3D reconstruction of the z-stack confocal data, we observed more pilus-expressing cells in the population and aggregation of the pilus-expressing cells in iron supplementation media as compared to normal media, which we did not observe in the Δ*ebpABC* deletion mutant or the $ebpA^{AWAGA}$ mutant **(Figure 3.3C)**. Taken together, these results indicate that cell aggregation is dependent on pilus expression and the MIDAS motif of EbpA pilin subunit.

A

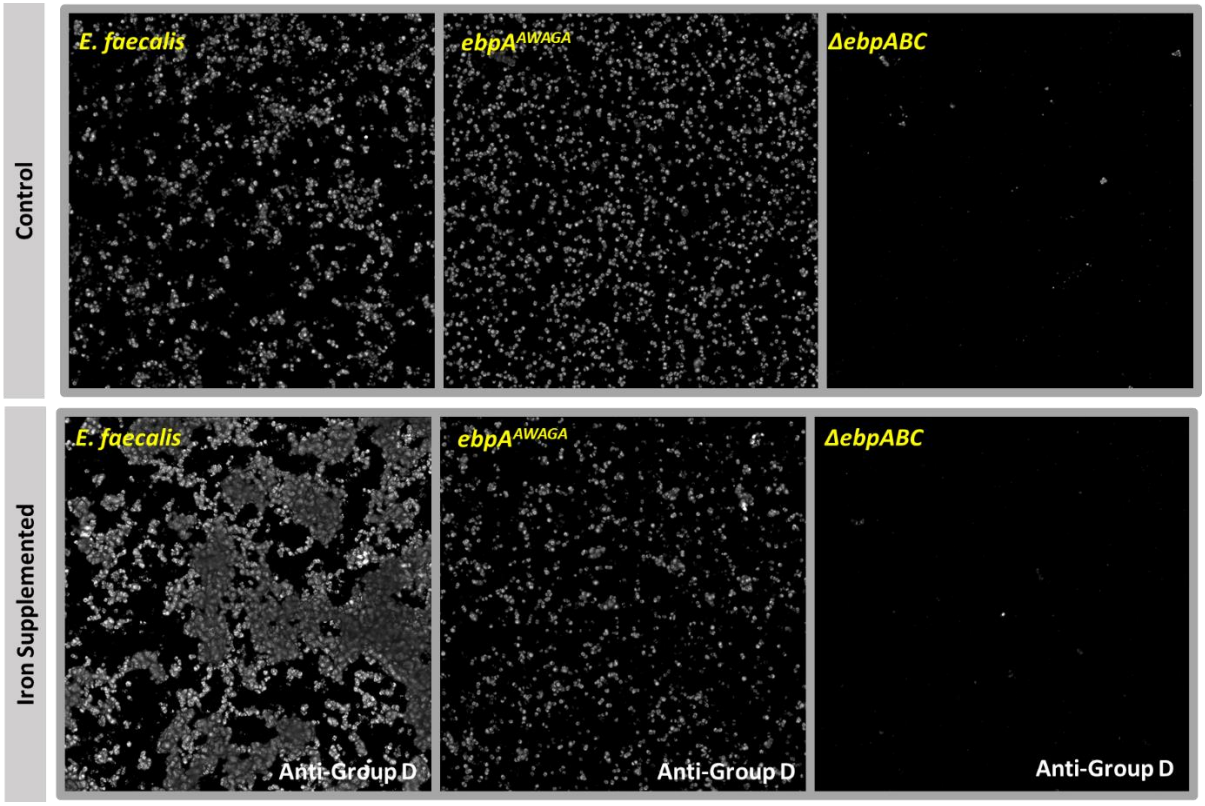
Control
E. faecalis
ebpA^AWAGA
ΔebpABC
Iron Supplemented
E. faecalis
ebpA^AWAGA
ΔebpABC
Anti-Group D
Anti-Group D
Anti-Group D

B

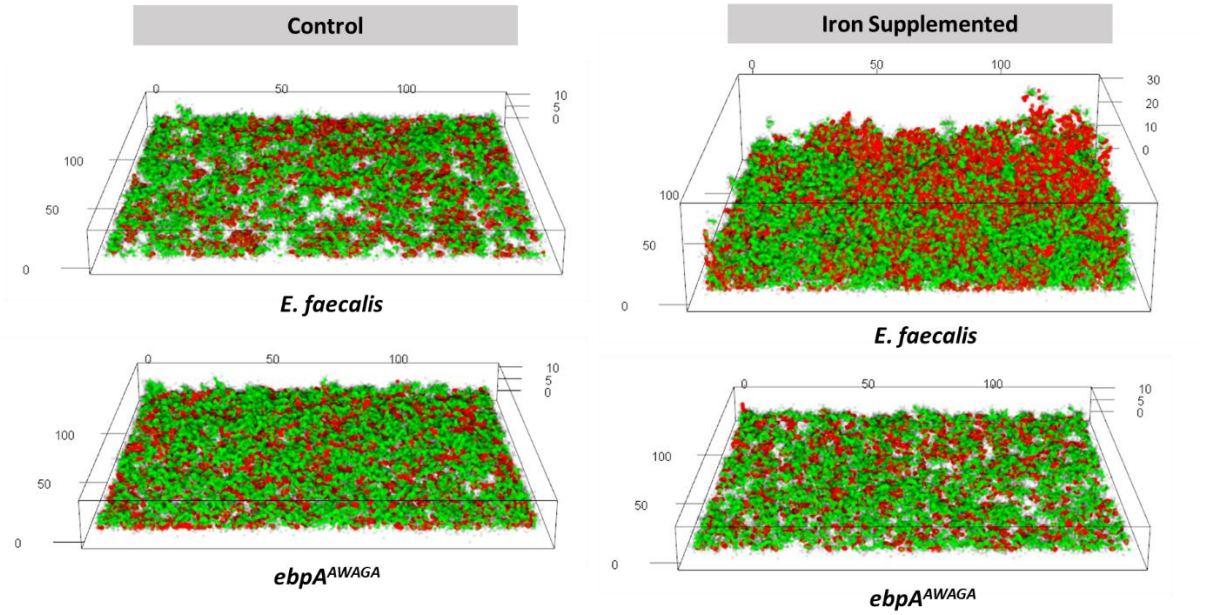
Control
Iron Supplemented
E. faecalis
E. faecalis
ebpA^AWAGA
ebpA^AWAGA

C

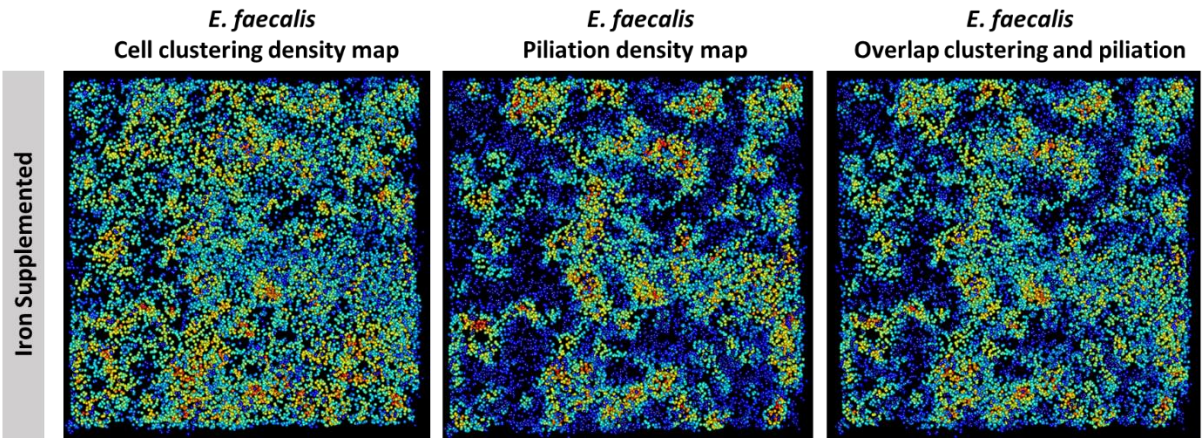

Figure 3.3. *E. faecalis* biofilm in iron supplemented media. (A) Volume viewer of CSLM images 63x magnification of *E. faecalis* biofilm at 24 hr for control (40% TSBG) and iron supplemented (40% TSBG, 0.2 mM $FeCl_3$). Cells are tagged with antibody against Group D antigen. **(B)** Comparison of wild type OG1RF and *ebpA*^{AWAGA} mutant biofilm piliation cell population distribution. Cells labeled with anti-EbpC AF568 are red color, cells labeled with group D AF488 are green color. **(C)** Overlap cell aggregation density map with piliated cell population density map using 3D reconstruction of CLSM z-stack images of iron supplemented *E. faecalis* biofilm. N=3, repeated on non-consecutive days.

3.5.3 Iron induces pilus expression in *E. faecalis* in a biometal specific manner

The presence of an increased pilus-expressing cell population in iron-supplemented media *E. faecalis* biofilm **(Figure 3.3A-B)** suggests that pili are upregulated. To test the hypothesis that pilus expression is iron responsive, we quantified the number of cells expressing pili in 24hr *E. faecalis* biofilm by immuno-labeling cells expressing EbpC on cell surface. In biofilms, we observed a significantly increased (*** $P \leq 0.001$) pilus-expressing cell population in the presence of 2 mM ferric iron, but not in alternative sources of iron such as ferrous iron and heme, or with other cation metals **(Figure 3.4A)**.

A

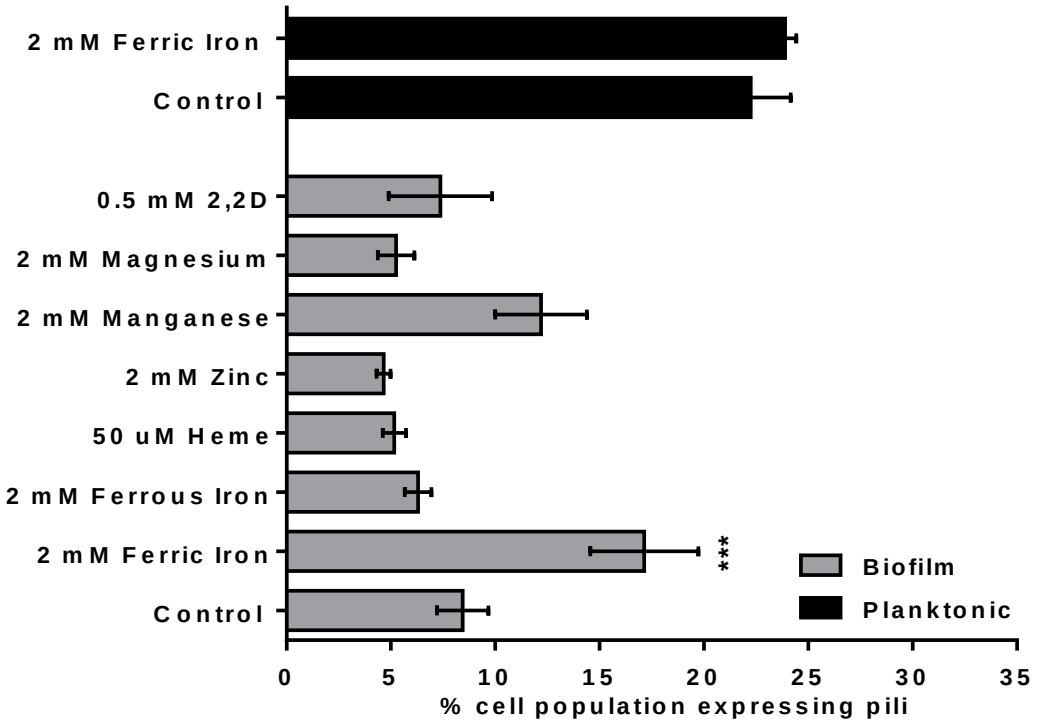
2 mM Ferric Iron
Control
0.5 mM 2,2D
2 mM Magnesium
2 mM Manganese
2 mM Zinc
50 uM Heme
2 mM Ferrous Iron
2 mM Ferric Iron
Control
***
Biofilm
Planktonic
0
5
10
15
20
25
30
35
% cell population expressing pili

B

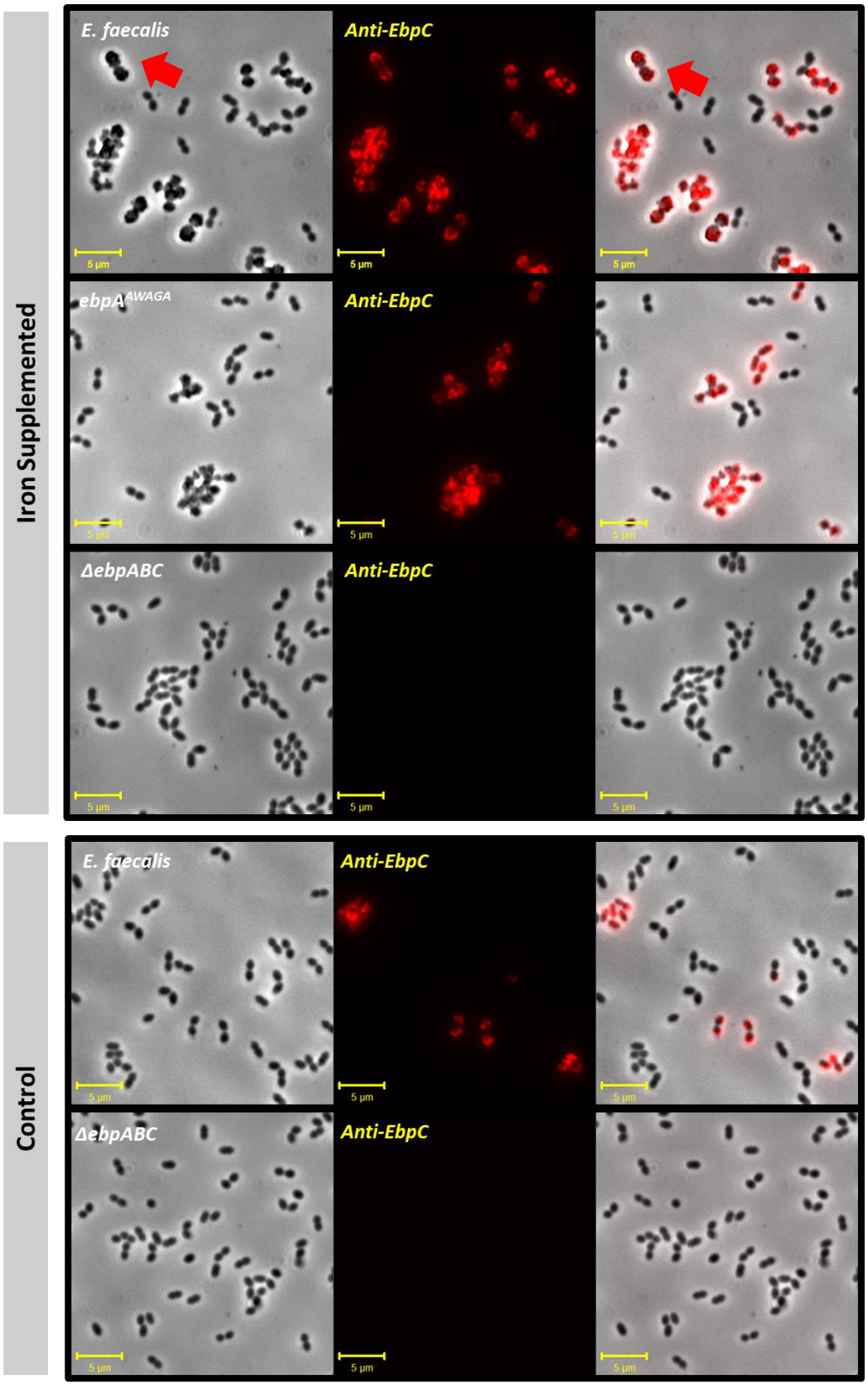
Iron Supplemented
E. faecalis
Anti-EbpC
ebpA^AWAGA
Anti-EbpC
ΔebpABC
Anti-EbpC
Control
E. faecalis
Anti-EbpC
ΔebpABC
Anti-EbpC
5 µm

Figure 3.4. Quantification of pilus-expressing cell population in *E. faecalis* biofilm. (A) Quantification of immuno-fluorescent labelled anti-EbpC *E. faecalis* cells from 6-well microtiter plate 24hr biofilm and planktonic grown under 37 degrees in control and metal supplemented conditions, **(B)** Representative images of *E. faecalis* and pilus mutants from 6-well microtiter plate 24hr biofilm grown under 37 degrees in control and iron supplemented. N=6, with 5 images per biological replicate, capturing approximately 100-300 cells per images, repeated on non-consecutive days. Red arrow indicates electron dense deposits. * $P \leq 0.05$, ** $P \leq 0.01$, *** $P \leq 0.001$, **** $P \leq 0.0001$. Error bar represents standard error margin (SEM).

Moreover, under planktonic condition, we observed no significant difference in the pilus-expressing cell population in either the control or iron-supplemented conditions. The metal concentrations used was determined based on the highest concentration in which *E. faecalis* cells did not exhibit growth defects (data not shown). Furthermore, we also observed that in iron-supplemented media, dense deposits could be seen at the poles of *E. faecalis* OG1RF cells, which co-localized to sites EbpC deposition, suggesting that these dense deposits may be interacting with the pilus **(Figure 3.4B)**. Additionally, we observed these dense deposits less frequency in the *ebpA*^{AWAGA} mutant and they were completely absence in Δ*ebpABC* deletion mutant **(Figure 3.4B)**.

3.5.5 Iron co-localized to pili on cell surface and is dependent on MIDAS motif on EbpA

Another hallmark of iron-mediated EET is the presence of iron sinks in the biofilm matrix, which has been demonstrated in **Chapter 2**. We therefore postulated that iron deposits in the matrix are interacting with the pilus, as suggested by our immuno-fluorescence images (**Figure 3.4B**). To address this hypothesis, we cultured biofilms in 6-well microtiter plates for 24hrs at 37^{o}C and analyzed the disrupted biofilm cells using TEM. We did not observe iron deposits in the matrix of the Δ*ebpABC* deletion mutant, whereas iron deposits were visible in the extracellular matrix of the wild type control biofilms in iron- supplemented media. By contrast, MIDAS (*ebpA*^{AWAGA}) mutant biofilm did have extracellular iron deposits but they were far more dispersed in the biofilm as compared to the wild type where the deposits appeared more organized around the cells **(Figure 356A-D).** Using imageJ to analyze the number of dense iron deposits within proximity of 100 pixels from cell surface (n>100 cells), we observed that there were significantly fewer iron deposits surrounding MIDAS (*ebpA*^{AWAGA}) mutant **(Figure 3.5E)**. Together, these

results suggest that presence of iron deposits at cell surface is dependent on the MIDAS motif within EbpA.

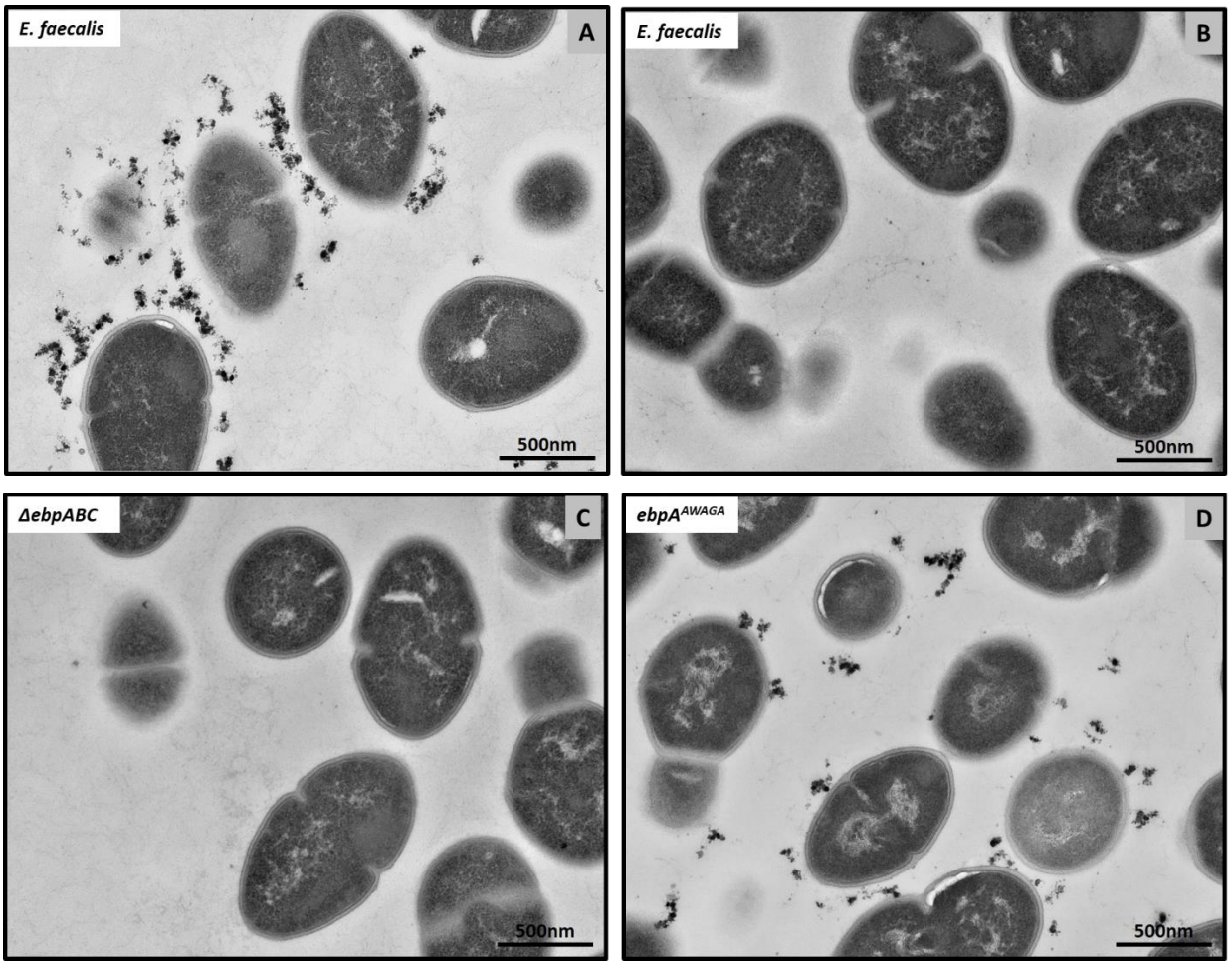

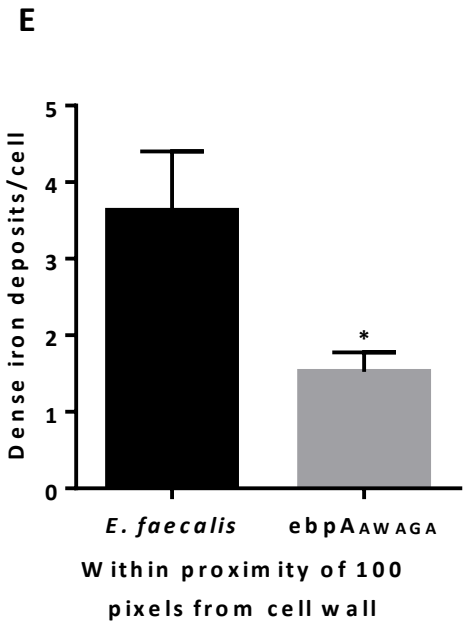

Figure 3.5. Electron micrographs of *E. faecalis* biofilm. Representative images from TEM of 24 hr *E. faecalis* biofilm from 6-well microtiter plate biofilm. **(A)** wild type OG1RF 2mM iron, **(B)** wild type OG1RF control, **(C)** Δ*ebpABC* 2mM iron and **(D)** $ebpA^{AWAGA}$ 2mM iron. **(E)** Quantification of iron deposits within proximity of 100 pixels from cell surface, n>100. Statistical significance was determined by Mann Whitney test. * $P \leq 0.05$, ** $P \leq 0.01$, *** $P \leq 0.001$, **** $P \leq 0.0001$. Error bar represents standard error margin (SEM). Black bar indicate 500nm. Red arrow indicates iron deposits.

The absence of iron deposits in pilus null biofilms **(Figure 3.5C)** suggested that either the iron deposits are associated with the pilus. To test whether pili were interacting with iron, we extracted pili from *E. faecalis* biofilms grown in normal or iron-supplemented media and performed ICP-MS on those samples to determine pilus-associated iron levels.

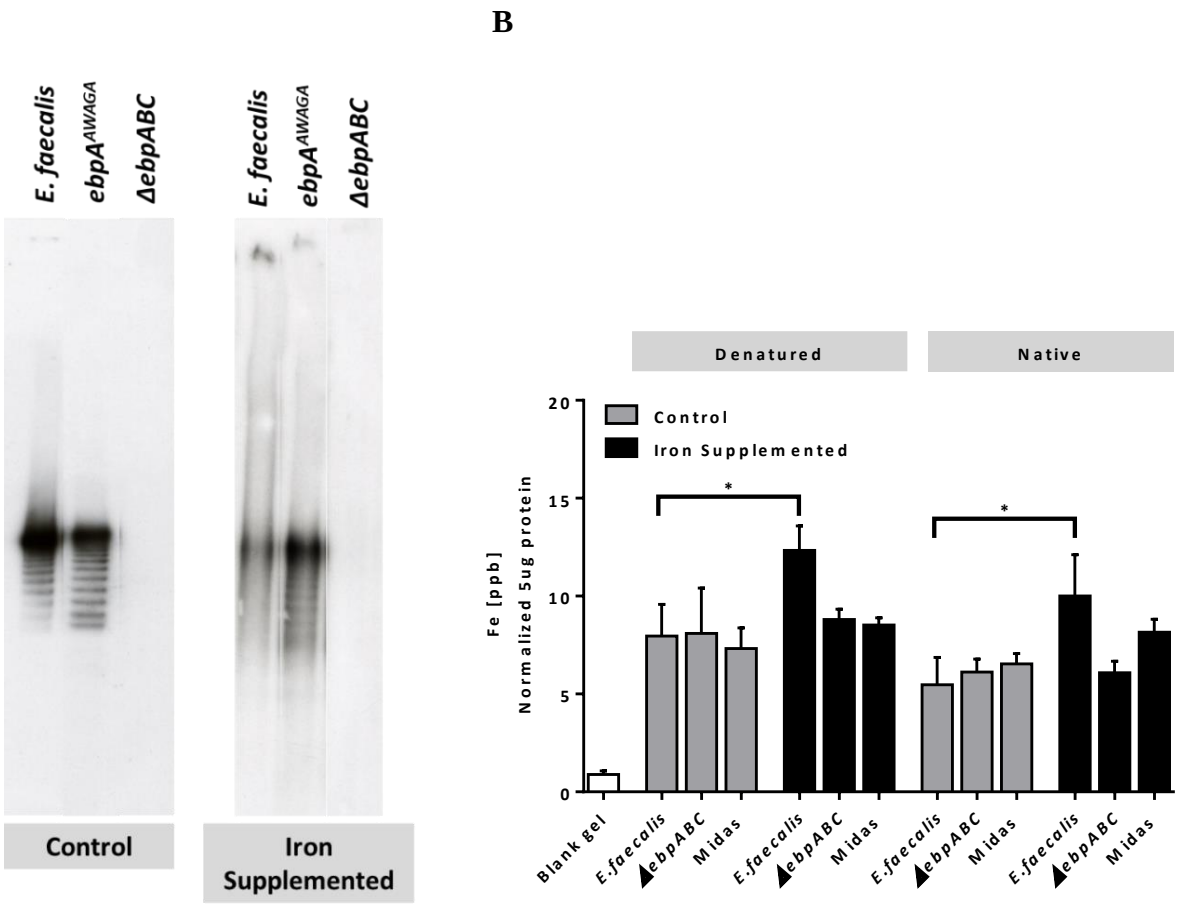

Figure 3.6. Iron quantification in pilus extract from *E. faecalis* biofilm. (A) Western blots and immunostaining of EbpC on purified mutanolysin cell wall extracts from biofilm cultures (300kDa). N=3. Above shown is a representative gel blot from one experiment. **(B)** ICP-MS analysis of iron concentrations (ppb) from digested tris-acetate gel run under native Tris-glycine buffer and denaturing SDS tris-acetate buffer. N=6. Statistical analysis is performed using two-way ANOVA Fisher LSD test. * $P \leq 0.05$. Error bar represents standard error margin (SEM).

We ran the purified pilus extract on tris-glycine gels and performed immunoblot usingEbpC antisera to identify the high molecular weight pilus ladder, and then excised the corresponding pilus ladder from a duplicate gel for ICP-MS to determine the total iron content **(Figure 3.6A)**. From the ICP-MS analysis, we observed significantly increased iron content in pilus extract from iron-supplemented *E. faecalis* wild type biofilm as compared to the normal media **(Figure 3.6B)**. Moreover, the iron content in the pilus preps from cells biofilm grown in normal media was similar

to "pilus preps" from the Δ*ebpABC* biofilm cells regardless of iron supplementation. "Pilus preps" from the pilus null strain reflect the background iron content in the gel and serve as a negative control during extraction in the assay. In addition, a blank gel control also has base level of iron detected. By contrast, there was a non-significant increase in iron content in pilus extracts from iron supplemented MIDAS (*ebpA*^{AWAGA}) mutant biofilm as compared to the iron supplemented wild type OG1RF which was ran in native condition **(Figure 3.6B)**. Moreover, we also observed similar results using samples obtained from SDS denaturing run condition **(Figure 3.6B)**, which demonstrate that increased pilus-associated iron levels detected was not due to transient protein-protein interactions vulnerable to detergent treatment. Together, these data suggest that the increased iron level detected in pilus extracts isolated from iron supplemented biofilm, very likely comes from co-isolated iron deposits.

3.5.4 Pili and electron transport systems contribute to extracellular electron transfer (EET)

Since we now know that pilus expression is iron responsive and biofilm restructuring occurs in the presence of iron, we hypothesized that iron-mediated EET requires pilus expression. To address this, we grew biofilms in in iron supplemented media and performed chronocoulometry to measure both current and cumulative charge production in the pilin mutants as compared to the wild type control. We observed that both the wild type OG1RF and pilin mutants showed increased current at similar rates during the first 8 hours of incubation before reaching thier maximum current peak **(Figure 3.7A-C)**. In both 0.5 mM and 1 mM iron-supplemented media, current production by the Δ*ebpABC* deletion mutant started to decrease at later timepoints as compared to the MIDAS (*ebpA*^{AWAGA}) mutant in which the current started to drop immediately after reaching the max current peak. Both pilin mutants exhibited an inability to sustain current production as compared to the wild type control **(Figure 3.7A-B)**. However, in 2 mM iron-supplemented media, the Δ*ebpABC* deletion mutant displayed a higher maximum current peak as compared to the wild type control and sustained current production over time, even though the wild type control showed exponential drop in current production from approximately 15 hrs onward **(Figure 3.7C)**. By contrast, only the MIDAS (*ebpA*^{AWAGA}) mutant displayed consistent attenuation in sustained current production across all three concentrations of iron tested **(Figure 3.7A-C)**. In addition to quantification of current produced over time, we also quantified cumulative charge produced at the end of the 20 hrs incubation. Under 0.5 mM iron concentration, we observed significant attenuation in

cumulative charge produced by Δ*ebpABC* deletion mutant. By contrast, MIDAS (*ebpA*^{AWAGA}) mutant display attenuated charge production in all iron concentrations tested **(Figure 3.7D)**. We did not observe restoration of charge production using the complemented Δ*ebpABC* deletion mutant with pGCP123:e*bpABCsrtC*. We reasoned that the lower Ebp expression and inability to use kanamycin to maintain plasmid expression may contribute to this. Moreover, alteration in the curren production in Δ*ebpABC* deletion mutant is only observed in the later timepoints. Since the absence of Ebp did not significantly alter current production at early time points, we therefore postulate that even though the pilus contributes to EET, but other yet uncharacterized mechanisms also contribute to *E. faecalis* electron transfer.

It has been reported that *L. monocytogenes*, a gram positive bacterium, uses flavin to mediate extracellular electron transfer, and this mechanism is encoded by an eight-gene locus (Light et al., 2018). Since *E. faecalis* genome also encode homologs (*OG1RF_12507-12513*) to this eight-gene locus, we speculate that *E. faecalis* is able to use flavin-mediated extracellular electron transfer in the presence of iron. In our previous study, we also speculated that demethylmenaquinone (DMK), which is produced via menaqunione biosynthesis pathway that is encoded by *OG1RF_10330-10335* (Ramsey et al., 2014a), could drives iron-mediated EET. We hypothesized that *ndh3*, encoded by *OG1RF_12510* and *menB*, encoded by *OG1RF_10330*, which are involved in flavin-mediated electron transfer and DMK biosynthesis respectively contribute to iron-mediated EET. Using *ndh3*::Tn mutant and *menB*::Tn mutant respectively, we tested for cumulative charge production using chronocoulometry. We observed attenuated charge production in both *ndh3*::Tn and *menB*::Tn mutants **(Figure 3.7E)**. Complementing *ndh3* and *menB* using nisin inducible plasmid partially restored charge production. We reasoned that optimizing the nisin concentration supplemented may be crucial to fully restore charge production to level similar to wild type control. Since the flavin-mediated EET associated gene locus is not identified in **Chapter 2**, this uncouples the iron-mediated biofilm growth phenotype and the ability to use iron for EET as two separate phenotypes. Moreover, absence of either *menB* or *ndh3* does not completely abolish charge production in *E. faecalis* biofilm **(Figure 3.7E)**, hence we reasoned that both electron transport systems work in concomitant effort, to drive iron-mediated EET. Indeed, charge production is significantly reduced in the *ndh3::Tn* Δ*menB* mutant as compared to the single deletion mutants **(Figure 3.7E)**. Collectively, these findings demonstrate that *E. faecalis* uses both the DMK and

flavin-mediated mechanisms, together with pilus expression in concomitant effort, to drive iron-mediated EET.

A **B** **C**

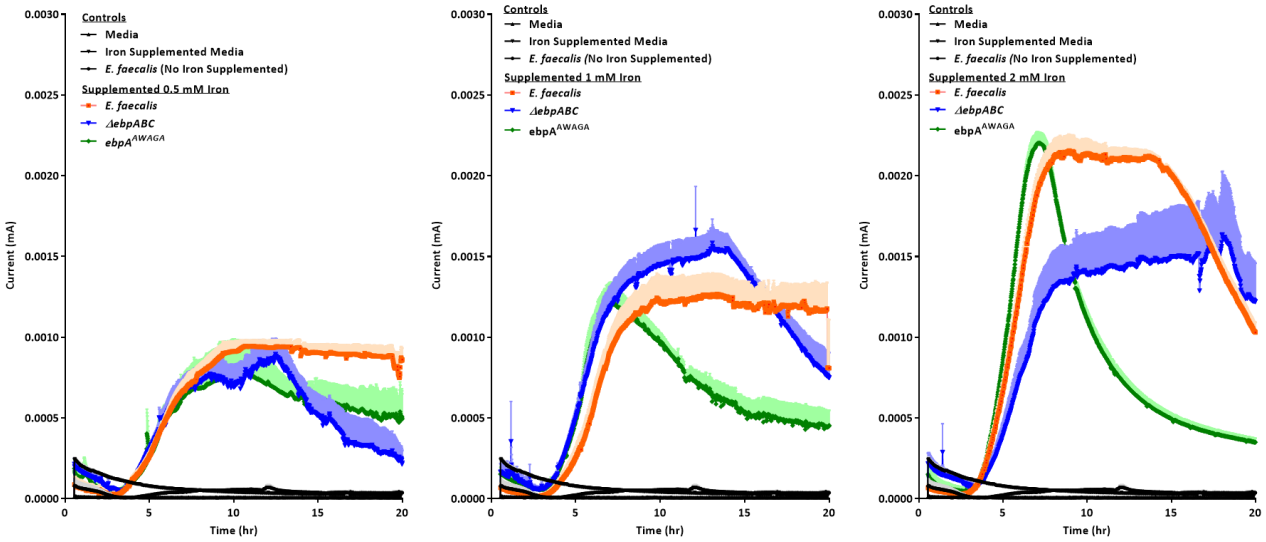

D

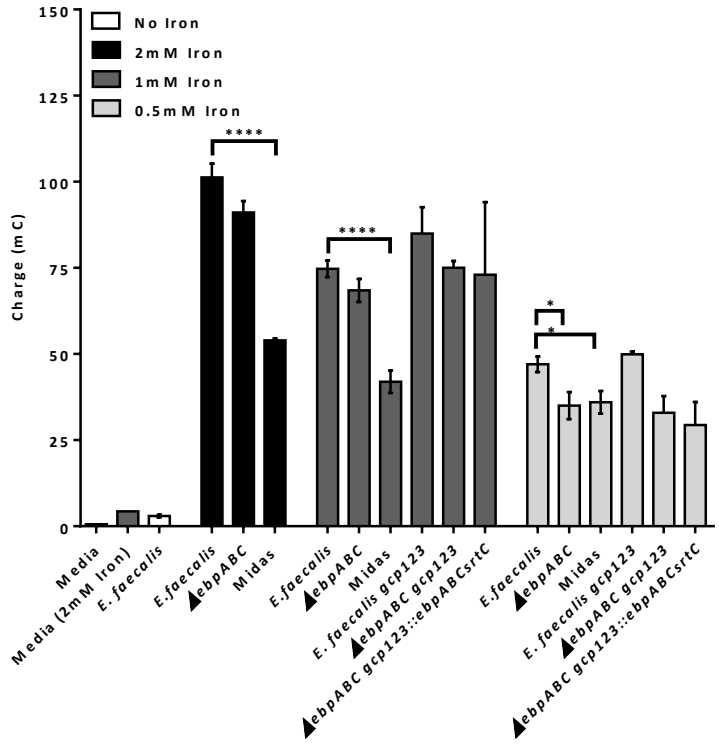

E

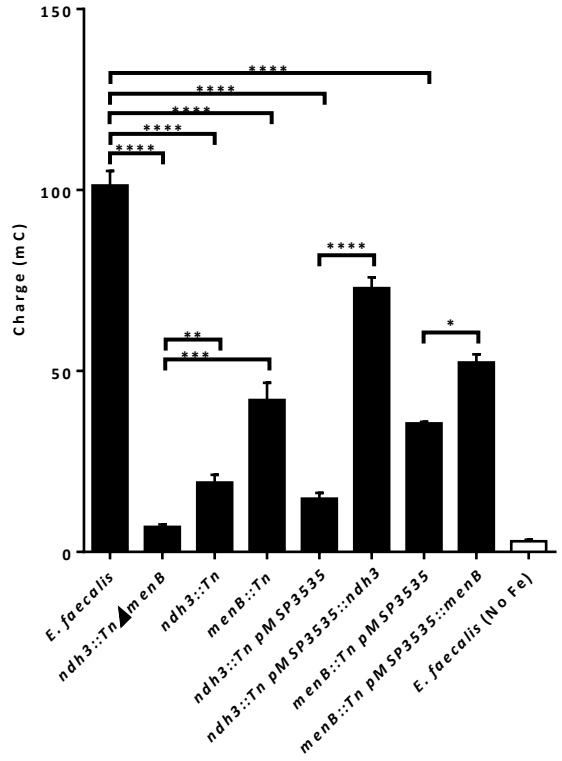

Figure 3.7. Extracellular electron transfer in *E. faecalis* biofilm. Chronocoulometry current (mA) measurement over time of *E. faecalis* biofilm grown on a screen-printed carbon mini-electrode over 20 hr in closed static system at 37^{o}C, at **(A)** 0.5 mM iron, **(B)** 1 mM iron and **(C)** 2 mM iron. Experiments were repeated on non-consecutive days with wild type (N=12) and pilin mutants (N=6). Chronocoulometry end point cumulative charge production in **(D)** pilin mutants and **(E)** flavin-mediated EET associated and DMK associated mutants. N=3. Strains harboring pGCP123 are not maintained with kanamycin as kanamycin has an effect on iron precipitation (data not shown). Strains harboring pMSP3535 plasmid are maintained on 100 µg/ml erythromycin and genes expression are induced using 5 µg/ml nisin. Abiotic controls and media controls are indicated.

3.5.6 Global transcriptional analysis of iron supplemented *E. faecalis* biofilm reveal 90 genes which are differentially regulated in response to iron

To determine genes that contribute to iron mediated biofilm growth, we used RNA sequencing to characterize the global transcriptional response of *E. faecalis* biofilm exposed to iron for 24 hrs at

37 ^{o}C under static conditions. We defined genes that were differentially regulated, as those with p-value of less than 0.05 and false discovery rate (FDR) of less than 0.05 were in response to iron. A total of 90 genes are differentially regulated, of which 51 genes were down regulated and 39 genes were up regulated in response to iron. The differentially expressed genes were categorized based on their predicted function and associated metabolic pathway using the KEGG genome database **(Figure 3.8)**. Of these 90 genes, the majority of the differentially regulated genes in response to iron were involved in carbon and sugar metabolism, and cell wall synthesis and modification. We also observed down regulation of several genes associated with purine/pyrimidine metabolism (*OG1RF_11489-11498*) and up regulation of genes associated with galactose metabolism (*OG1RF_10544-10545, OG1RF_10549, OG1RF_10551*) and sugar uptake (*OG1RF_11774-11778*). Additionally, the putative iron associated transporters *hmnVUT (OG1RF_11352-11354), fhuDCBG (OG1RF_10136-10139), yclQPN* (*OG1RF_12351-12354), feoA (OG1RF_10359)* and ferric iron regulator (*fur*) were transcriptionally unchanged. By contrast, *feoB (OG1RF_10360)* was up-regulated **(Table 3.4),** which indicates that *E. faecalis* biofilm may be importing iron intracellularly in the presence of 2 mM iron. Although Lopez and colleagues have shown that *OG1RF_10589* (annotated as cation efflux transporter, this gene is studied in **Chapter 4** of this this where it is renamed *mntE*, and therefore we refer to it as such going forward) was transcriptionally upregulated in planktonic conditions in the presence of 1 mM iron (Lopez et al., 2012), under biofilm conditions, *mntE* remains transcriptionally unchanged. Coupled with the up regulation of *feoB*, this suggests that iron uptake is favored when iron is in excess in biofilms. In support of this, in **Chapter 2** we showed that *E. faecalis* biofilm grown in 2 mM iron resulted in increased intracellular iron content (Keogh et al., 2018).

Furthermore, *OG1RF_10838-10839* (*mntH, uspA*) annotated as a manganese/iron antiporter, which belongs to the NRAMP family, was downregulated, suggesting that iron efflux and corresponding uptake of manganese was restricted **(Table 3.4)**. Moreover, *perR* and *zurR*, which are part of *fur* family of transcriptional regulators, are all unchanged, indicating that these genes are not iron responsive under biofilm conditions, and that *E. faecalis* biofilm is not eliciting a global oxidative stress response since PerR is a global regulator of several oxidative-stress associated genes as described in *Bacillus spp* and *Neisseria spp* (Brenot et al., 2005; Faulkner et al., 2012; Wu et al., 2006). However, *ohrA* which encodes an organic hydroperoxide resistance

protein, was down regulated **(Table 3.4)**. Furthermore, *OG1RF_11677-11679* (*efaCBA* operon) and *OG1RF_11058-11063* (phage associated genes) were down regulated, whereas to *OG1RF_10870-10871* (endocarditis and biofilm associated pilus - *ebpA*, *ebpB*) were up regulated; together suggesting that iron sensing modulates virulence genes expression **(Table 3.4)**.

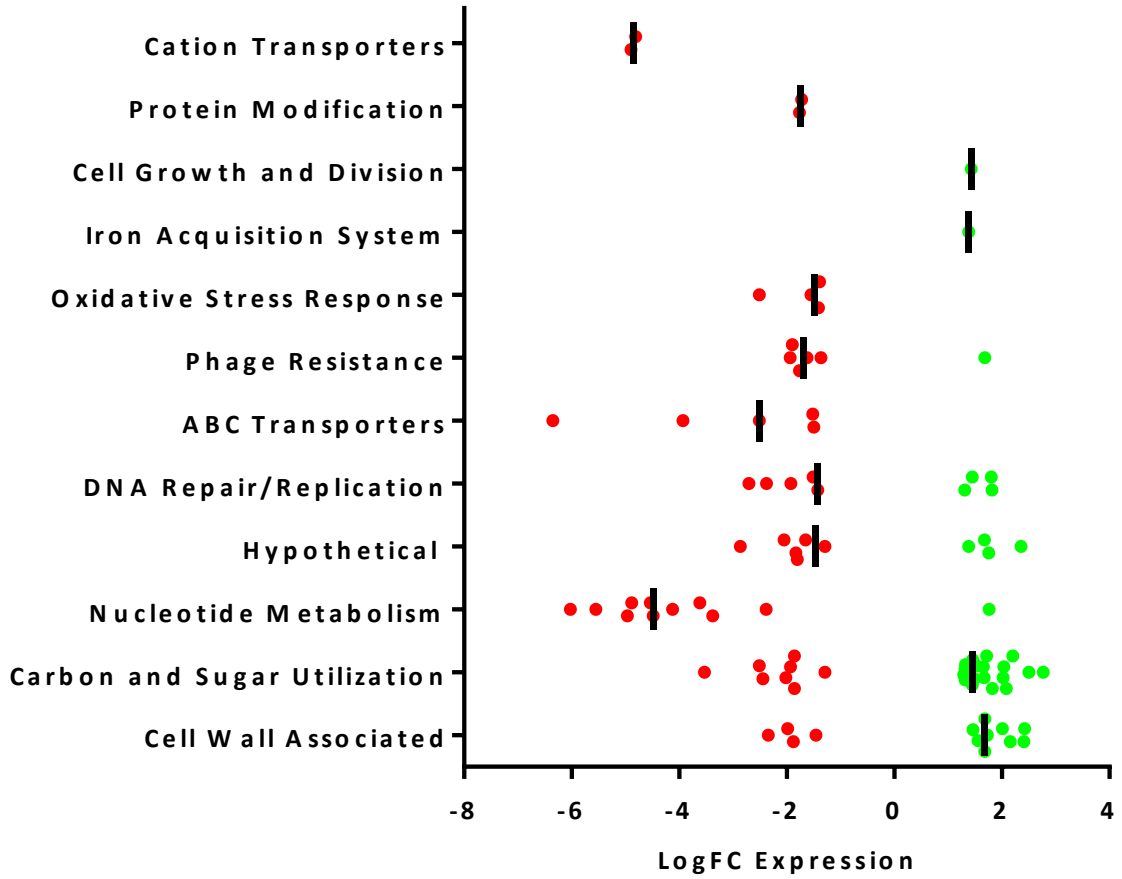

Figure 3.8: Global transcriptional response of *E. faecalis* biofilm exposed to 2 mM iron for 24 hrs. All genes that were differentially regulated, with p-value of less than 0.05 and false discovery rate (FDR) of less than 0.05 were included. Red dots indicate genes that are down-regulated and green dots indicate genes that are up-regulated. Pathway enrichment analysis was done by annotating genes in *E. faecalis* OG1RF to the KEGG database (KEGG identifier: efi). Gene classification was done based on their gene membership according to KEGG pathways. KEGG gene set enrichment analysis was performed using the Bioconductor package, clusterprofiler (version 3.8.1) (Yu et al., 2012).

Table 3.3: *E. faecalis* iron uptake and oxidative stress homeostasis genes transcriptionally regulated in response to 2 mM iron

Gene Locus	Gene Name	Annotated Function	LogFC Expression
OG1RF_10360	ferrous iron transport protein B *(feoB)*	Iron uptake	1.383982236
OG1RF_10338	organic hydroperoxide resistance protein *(ohrA)*	Oxidative stress response	-1.4098355

Table 3.4: List of *E. faecalis* virulence gene transcriptionally regulated in response to iron

Gene Locus	Gene Name	Annotated Function	$_{Log2FC}$ Expression
OG1RF_10838	Putative manganese transporter (*mntH2*)	Manganese transport	-4.899583016
OG1RF_10839	universal stress protein *(uspA)*	Stress response	-4.806902878
OG1RF_11677	ABC transporter ATP-binding protein *(efaC)*	Manganese transport	-3.928198377
OG1RF_11678	membrane protein *(efaB)*		-2.511805781
OG1RF_11679	endocarditis specific antigen *(efaA)*		-6.349307685
OG1RF_11058	hypothetical protein	-	-1.89475629
OG1RF_11059	tail protein	phage tail protein	-1.937213114
OG1RF_11060	structural protein	transglycosylase associated protein	-1.765286253
OG1RF_11061	hypothetical protein	E1-E2 family cation-transporting ATPase	-1.62124439
OG1RF_11062	holin	cold shock protein CspA	-1.364703691
OG1RF_11063	N-acetylmuramoyl-L-alanine amidase	transglycosylase associated protein	-1.98517425
OG1RF_10870	Endocarditis and biofilm associated subunit EbpA	Surface adherence and host colonization	1.685043432
OG1RF_10871	Endocarditis and biofilm associated subunit EbpB		1.556727874
OG1RF_10072	putative NRAMP Mn/Fe transporter	Manganese transport	-1.387202011
OG1RF_10073	membrane protein		-1.54795265

To validate that the endocarditis and biofilm associated pilus is up regulated when iron is supplemented, we next performed qRT-PCR to determine the fold change in RNA transcript abundance in comparison against normal unsupplemented media. Indeed, we observed increased abundance of *ebpC* gene transcript in *E. faecalis* biofilm grown in 2 mM iron supplemented media **(Figure 3.9)**. Since our previous findings revealed increased pilus-expressing cells in *E. faecalis* biofilm **(Figure 3.4A)**, we hypothesized that the increased expression of gene transcripts of sortases (*srtC*, *srtA*) may result in increased SrtA and SrtC, which consequently contribute to

increased EbpC anchored on the cell surface. To address this hypothesis, we next compared *srtA* and *srtC* transcript abundance in *E. faecalis* biofilm grown in 2 mM iron supplemented media; however, neither sortase is upregulated **(Figure 3.9)**. This indicates that the increased abundance of pili anchored on the cell surface is solely dependent on increased *ebp* gene transcripts. We also speculate that upregulation of *ebp* gene transcripts is dependent on up regulation of *ebpR* (transcriptional regulator for *ebpABC* operon); however, *ebpR* is not up regulated **(Figure 3.9)** indicating that upregulation of *ebpC* is driven by alternative (not characterized yet) transcriptional factors. Recently, a separate study showed that AhrC promotes initial surface attachment and biofilm growth in *E. faecalis* (Frank et al., 2013); and *ahrC* up regulation directly activates *ebpR* expression which results in increased pilus expression (Manias and Dunny, 2018). We postulate that up regulation of *ebp* gene transcripts is dependent on up-regulation of *ahrC* (transcriptional regulator for *ArgR*); however we observed that *ahrC* gene transcripts are not increased which suggests that up regulation of *ebp* gene transcripts is not a result of up regulation of *ahrC*.

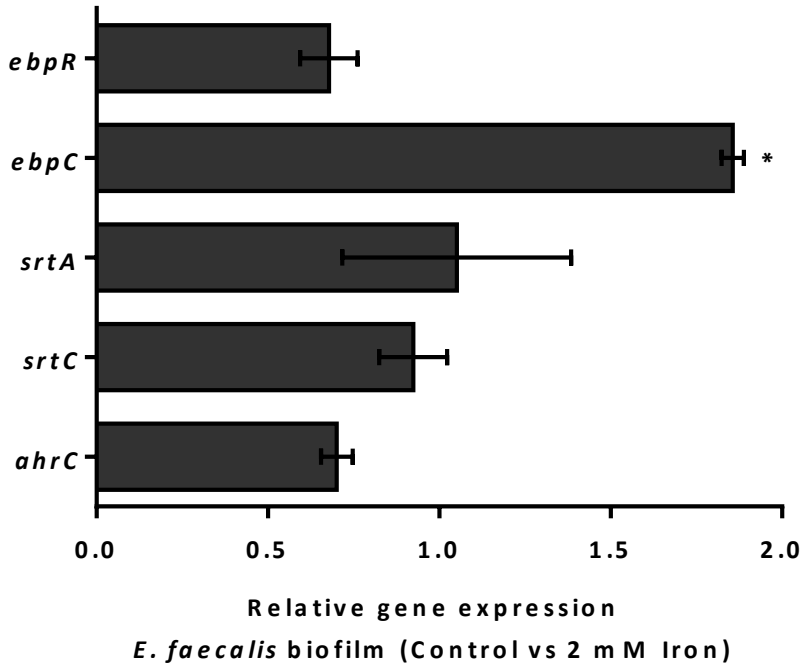

Figure 3.9. qRT-PCR of RNA transcript abundance of genes associated with pilus biogenesis. N=6, repeated on non-consecutive days. Statistical analysis is performed using one-way ANOVA Fisher LSD test. * $P \leq 0.05$, ** $P \leq 0.01$, *** $P \leq 0.001$, **** $P \leq 0.0001$.

The simultaneous up-regulation of *ebpABC* and *feoB* as the sole iron-responsive transporter, along with our observations that Ebp co-purify with iron and are required for EET suggest a model in which pilus-associated iron may be reduced and subsequently taken up by the ferrous iron transporter FeoB for promoting biofilm growth. Since ferric iron reduction to ferrous iron is the last step in EET, we reasoned that inability to perform EET coincide with attenuation in ferric reduction activity, which may lead to reduced extracellular ferrous iron pool for iron uptake via FeoB in *E. faecalis* biofilm. To test this hypothesis, we performed ICP-MS to determine the intracellular iron content in pilus mutants and *feoB* mutant grown in iron-supplemented media. Since Ldh1 has been previously shown to be important for EET in **Chapter 2** (Keogh et al., 2018), we postulate that absence of *ldh1* also may result in reduced intracellular iron. In agreement with our hypothesis, we observed significantly reduced intracellular iron in Δ*ebpA* deletion mutant (7.18-fold), Δ*ebpB* deletion mutant (2.36-fold), Δ*ebpC* deletion mutant (3.25-fold), Δ*ebpABC* deletion mutant (3.56-fold) and MIDAS ($ebpA^{AWAGA}$) mutant (3.66-fold) **(Figure 3.10)**. Complementation with pGCP123::*ebpABCsrtC* increased intracellular iron by 1.91-fold as compared to Δ*ebpABC* deletion mutant with pGCP123, but did not completely restore to levels observed in wild type OG1RF with pGCP123 vector. We also observed 2.15-fold and 2.48-fold reduction in intracellular iron in *feoB* mutant and *ldh1* mutant. However, we did not observe any significant differences in intracellular iron in both *menB::Tn* and *ndh3::Tn* mutants **(Figure 3.10)**. The presence of reduced intracellular iron in the *feoB* mutant indicate that iron uptake via *feoB* contributes to intracellular iron accumulation. We reasoned that reduced intracellular iron observed is a direct consequence of decreased availability of ferrous iron pool due to reduced ferric iron being reduced to ferrous iron extracellularly. To address this, we next performed ferric iron reductase assay. We observed significantly decrease ability in ferric iron reduction in both *ndh3::Tn* and *menB::Tn* mutant, but not in Δ*ebpABC* deletion mutant **(Figure 3.11)**. We also observed significantly reduced ability in ferric iron reduction in the *ndh3::Tn* Δ*menB* mutant as compared to its singe deletion mutant counterparts. No ferric iron reduction is detectable in the absence of iron supplementation **(Figure 3.11)**. We reasoned that presence of either *menB* or *ndh3* is sufficient to reduce extracellular ferric iron, hence we do not observed significant changes in intracellular iron. To address this, we will be performing ICP-MS on *ndh3::Tn* Δ*menB* mutant to quantify intracellular iron. Since absence of *ebpABC* do not drastically attenuates EET, we speculate that this ferric iron reduction assay which measures absorbance readings may not be

sensitive to detect small differences in ferric iron reduction. Collectively, we showed that inability to perform EET coincide with attenuation in ferric reduction activity, which may lead to reduced extracellular ferrous iron pool for iron uptake. However, the role of Ebp in ferric iron reduction remains unanswered.

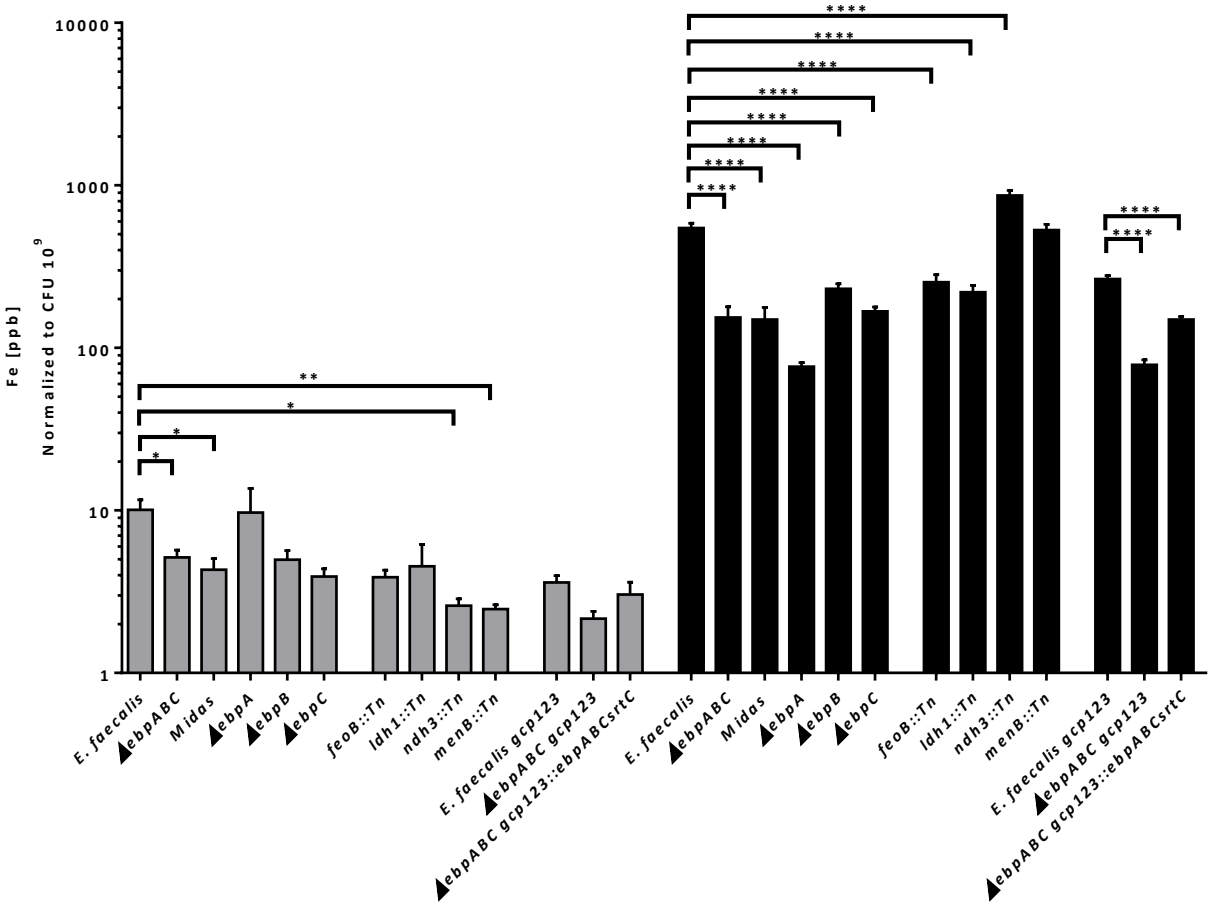

Figure 3.10. Intracellular iron quantification of *E. faecalis* mutants. ICP-MS analysis of iron concentrations (ppb) from *E. faecalis* biofilm normalized to 10^9 CFU. N=9. Statistical significance was determined by one-way ANOVA. * $P \leq 0.05$, ** $P \leq 0.01$, *** $P \leq 0.001$, **** $P \leq 0.0001$. Error bar represents standard error margin (SEM).

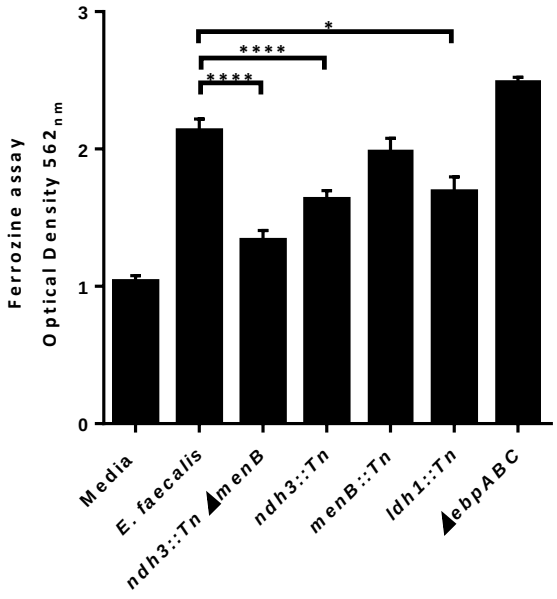

Figure 3.11. Quantification of ferric iron reduction in E. faecalis mutants. *E. faecalis* is grown in TSBG supplemented with 2 mM iron, with 0.5 mM ferrozine added to detect extracellular ferrous iron. Absorbance is taken at OD_{562nm}. Statistical significance was determined by one-way ANOVA. * $P \leq 0.05$, ** $P \leq 0.01$, *** $P \leq 0.001$, **** $P \leq 0.0001$. Error bar represents standard error margin (SEM). N=9.

3.5.7 Global transcriptional analysis of iron supplemented *ebpA*^{AWAGA} (MIDAS) mutant biofilm reveal 734 genes which are differentially regulated compared to wild type OG1RF

Since the MIDAS (*ebpA*^{AWAGA}) mutant was significantly attenuated in EET and *in vitro* iron-mediated biofilm growth, we hypothesized that the transcriptional response to iron would be different in MIDAS (*ebpA*^{AWAGA}) mutant compared to wild type OG1RF. To address this, we compared global transcriptional changes in MIDAS (*ebpA*^{AWAGA}) mutant biofilm with wild type OG1RF biofilm, both grown in 2mM iron supplemented media. We observed 734 genes which were differentially regulated **(Figure 3.12)** in MIDAS (*ebpA*^{AWAGA}) mutant. By contrast, Δ*ebpABC* deletion mutant which was not significantly attenuated in electron transfer was transcriptionally identical to wild type OG1RF biofilm (data not shown). The majority of the transcriptional changes were in central metabolism (data not shown). Moreover, putative iron uptake systems including the ferrichrome ABC transporter substrate-binding protein *fhuD* (*OG1RF_10136*), iron ABC transporter *hmuVUT* (*OG1RF_11352-11354*), and *ycl* (*OG1RF_12353-12354*) were

downregulated, which suggest reduced iron uptake **(Table 3.5)** in the MIDAS (*ebpA*^{AWAGA}) mutant compared to wild type.

Since 734 genes were differentially in MIDAS (*ebpA*^{AWAGA}) mutant and we know that 90 genes were iron-responsive in *E. faecalis* OG1RF, we next ask whether there is a common cluster of genes which are transcriptionally regulated. Indeed, we observed 45 genes which are transcriptionally changed **(Figure 3.13)**. Among these 45 genes, 13 genes are similarly up- and down-regulated in the same direction. By contrast, 32 genes are differentially regulated **(Figure 3.13)**. Majority of the differentially regulated genes are involved in metabolism **(Table 3.6)**. This suggest that altering the MIDAS motif has an effect on metabolism, however the mechanism underlying this transcriptionally switch remains unclear.

Table 3.5: *E. faecalis ebpA*^{AWAGA} mutant iron uptake and oxidative stress homeostasis genes transcriptionally regulated in response to 2 mM iron

Gene Locus	Gene Name	Annotated Function	Log_2FC Expression
OG1RF_10136	ferrichrome ABC transporter substrate-binding protein (*fhuD*)	Iron uptake	-1.354515148
OG1RF_11352	iron ABC transporter ATP-binding protein (*hmuV*)	Iron uptake	-2.131325463
OG1RF_11353	corrinoid ABC transporter permease (*hmuU*)		-1.16957636
OG1RF_11354	iron ABC transporter substrate-binding protein (*hmuT*)		-1.693620127
OG1RF_12353	iron ABC transporter permease	Iron uptake	-1.446182834
OG1RF_12354	iron ABC transporter permease		-1.283411187
OG1RF_12355	hypothetical protein		-1.542974935

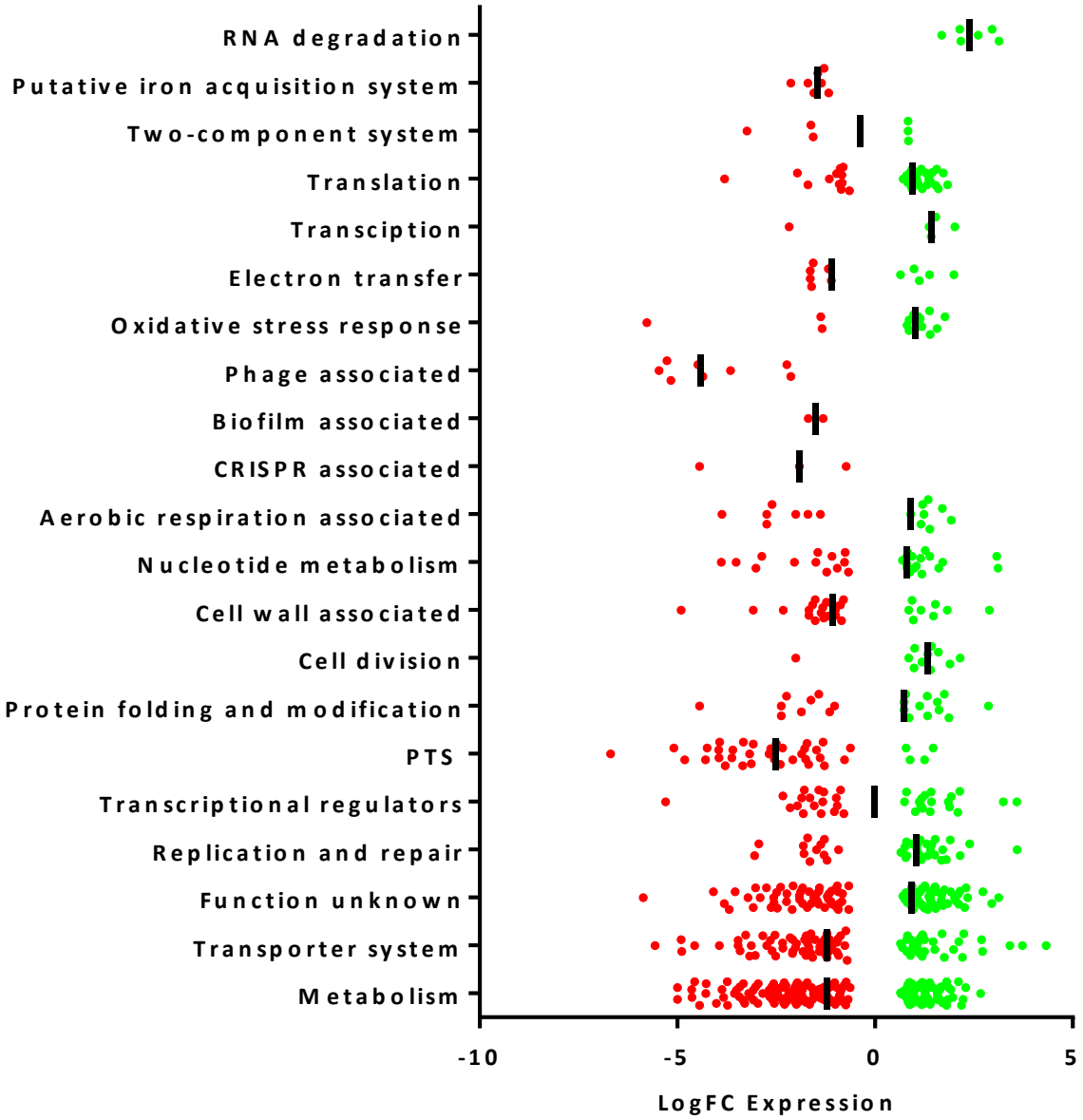

Figure 3.12: Global transcriptional response of *E. faecalis ebpA*^{AWAGA} deletion mutant biofilm exposed to iron for 24 hrs. All genes that were differentially regulated, with p-value of less than 0.05 and false discovery rate (FDR) of less than 0.05 were included. Red dots indicate genes that are down-regulated and green dots indicate genes that are up-regulated. Pathway enrichment analysis was done by annotating genes in *E. faecalis* OG1RF to the KEGG database (KEGG identifier: efi). Gene classification was done based on their gene membership according to KEGG pathways. KEGG gene set enrichment analysis was performed using the Bioconductor package, clusterprofiler (version 3.8.1) (Yu et al., 2012).

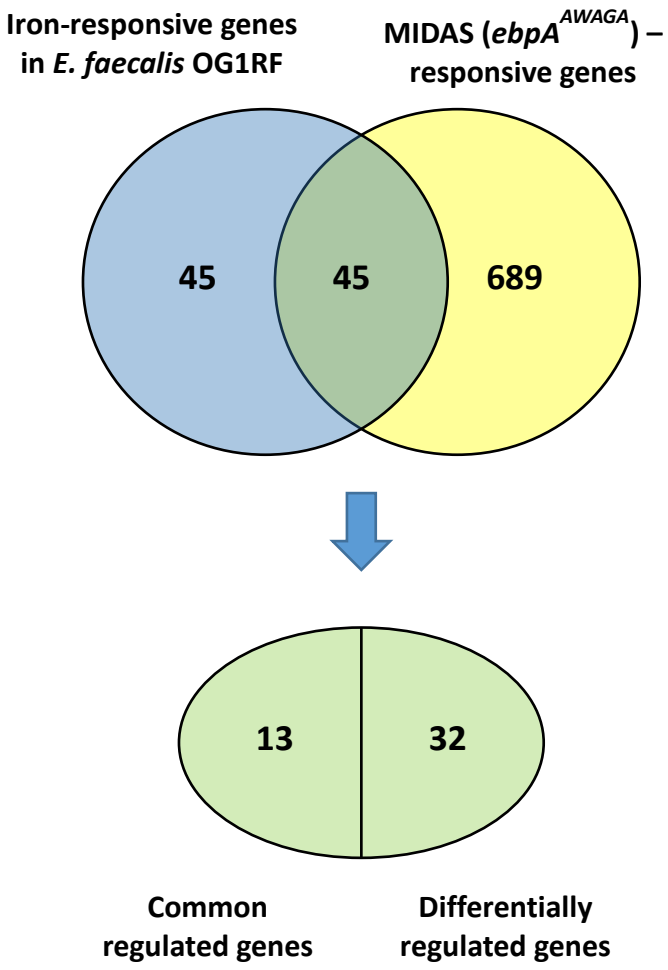

Figure 3.13. Venn diagram of genes responsive to iron and MIDAS motif. All genes that were differentially regulated, with p-value of less than 0.05 and false discovery rate (FDR) of less than 0.05 were included.

Table 3.6: List of gene transcriptionally regulated in response to iron and MIDAS motif

Gene Locus	Gene Name	Annotated Function	Log_2FC Expression (No Fe vs Fe)	Log_2FC Expression (Fe WT vs Fe MIDAS)
OG1RF_10171	preprotein translocase subunit SecY	Secretion	**1.463183338**	**-0.842434321**
OG1RF_10172	adenylate kinase	Metabolism and PTS system	**1.432931662**	**-0.683137179**
OG1RF_10269	esterase		**1.287597933**	**1.001469517**
OG1RF_10296	PTS mannitol transporter subunit IICB		**2.022681132**	**-1.77872166**
OG1RF_10338	osmotically inducible protein C		**-1.4098355**	**1.568682889**

OG1RF_10340	PTS sorbose transporter subunit IIC		**2.204807616**	**-4.813528416**
OG1RF_10544	glucuronyl hydrolase		**1.821271601**	**-2.22733774**
OG1RF_10545	beta-galactosidase		**2.037322632**	**-1.462189744**
OG1RF_10549	PTS fructose transporter subunit IID		**2.773313165**	**-3.595821812**
OG1RF_10565	PTS cellbiose transporter subunit IIC		**2.412544502**	**-4.243498537**
OG1RF_10567	hypothetical protein	Unknown	**2.155121669**	**-4.084386682**
OG1RF_10859	excinuclease ABC subunit A	DNA replication	**1.806135291**	**-2.936141805**
OG1RF_10860	hypothetical protein	Unknown	**1.814250122**	**-2.38564749**
OG1RF_10870	Endocarditis and biofilm associated subunit EbpA	Pilus assembly	**1.685043432**	**-1.581735057**
OG1RF_10871	Endocarditis and biofilm associated subunit EbpB		**1.556727874**	**-2.323720432**
OG1RF_10874	DUF378 domain-containing protein	Unknown	**-2.047982376**	**-2.484069644**
OG1RF_11036	ATPase P	ATP dependent ion pump	**-1.51488775**	**1.510927005**
OG1RF_11058	hypothetical protein	Phage	**-1.89475629**	**-5.159324486**
OG1RF_11059	tail protein		**-1.937213114**	**-5.465503674**
OG1RF_11060	structural protein		**-1.765286253**	**-5.259291425**
OG1RF_11061	hypothetical protein		**-1.62124439**	**-3.653527798**
OG1RF_11062	holin		**-1.364703691**	**-4.355677265**
OG1RF_11063	N-acetylmuramoyl-L-alanine amidase		**-1.98517425**	**-4.477589949**
OG1RF_11167	alanine--tRNA ligase	Metabolism	**1.309472725**	**-1.965869889**
OG1RF_11246	type I glyceraldehyde-3-phosphate dehydrogenase		**-2.018386574**	**2.671380329**
OG1RF_11269	transcriptional regulator	Transcription	**-1.924999394**	**-1.364114638**
OG1RF_11400	adenine phosphoribosyltransferase	Metabolism	**1.450694973**	**-1.549050066**
OG1RF_11437	cold-shock protein	Stress response	**-1.509404959**	**0.967491542**
OG1RF_11489	phosphoribosylamine--glycine ligase	Metabolism	**-5.547202144**	**-2.566607855**
OG1RF_11490	bifunctional phosphoribosylaminoimidazolecarboxamide formyltransferase/inosine monophosphate cyclohydrolase	Metabolism	**-4.88560125**	**-1.425786538**
OG1RF_11493	amidophosphoribosyltransferase		**-4.126158265**	**-2.464177309**
OG1RF_11506	hypothetical protein	Unknown	**-1.4594454**	**1.134563485**
OG1RF_11564	50S ribosomal protein L19	Translation	**-2.376731034**	**1.840708695**
OG1RF_11584	C4-dicarboxylate ABC transporter	Metabolism	**1.668889537**	**-3.266779711**
OG1RF_11752	hypothetical protein	Unknown	**1.755185503**	**-3.687548287**
OG1RF_11753	PTS maltose transporter subunit IIBC	PTS system and maltose metabolism	**1.321262579**	**-3.943118057**
OG1RF_11774	sugar ABC transporter substrate-binding protein	ABC transporter	**2.084800985**	**1.195502445**

OG1RF_11794	hypothetical protein	Unknown	**1.764765218**	**-1.420625949**
OG1RF_11976	PTS beta-glucoside transporter subunit EIIBCA	PTS system	**1.719928**	**-3.167570078**
OG1RF_12046	adapter protein MecA	DNA replication	**-1.760184516**	**1.317999166**
OG1RF_12243	D-ribose pyranase	Energy production	**1.457500468**	**-3.17253863**
OG1RF_12244	ribokinase		**1.318904557**	**-3.728710567**
OG1RF_12280	allantoin permease	Lipid metabolism	**2.504490153**	**-3.338919103**
OG1RF_12310	peptidase		**-1.722455554**	**1.624977261**
OG1RF_12425	glycosyl hydrolase	Metabolism	**1.686195755**	**-3.509158163**

**Genes are indicated in green (upregulated), red (downregulated) and black (not changed).*

3.5.8 High iron diet promotes Ebp-dependent *E. faecalis* colonization in the murine colon

We previously demonstrated that iron-mediated EET promoted *in vitro E. faecalis* biofilm growth (Keogh et al., 2018), and in this chapter (**Figures 3.3 and 3.8**) we have so far shown that pilus expression plays a role in EET and iron-mediated biofilm growth. Since iron modulates *E. faecalis* biofilm growth and transcriptional responses which impact virulence gene expression including Ebp, we speculate that pilus- and iron-mediated biofilm growth may be relevant during gastrointestinal colonization (GI). Although *E. faecalis* is one of the first colonizers in the infant GI tract of mammals and humans, determinants which promote GI colonization have not been well-characterized. We therefore hypothesize that iron-mediated *E. faecalis* biofilm growth could be observed in the gastrointestinal tract (GI), a physiologically relevant niche where the majority of unabsorbed dietary iron is stored prior to being excreted out of the host. Since Ebp contribute to EET and iron-mediated biofilm growth, we also postulate that presence of Ebp would also contribute to GI colonization in an iron-dependent manner. To address this hypothesis, we compared two experimental iron diets containing either 200 mg/kg ferric chloride (control group) or 2000 mg/kg ferric chloride (high iron group), and fed these diets to 3 weeks old male mice for 5 weeks **(Figure 3.14A)**. At the end of the 3rd week, mice are given ampicillin for 5 days. After resting for 24 hrs *E. faecalis* is inoculated in drinking water for 3 days. After resting for 24 hrs, the mice are sacrificed and tissues (cecum, colon, small intestine) were homogenized to determine bacterial titers and iron content using ICP-MS **(Figure 3.14A)**.

We observed significantly increased bacterial titres recovered from the mouse colon in mice fed with high iron diet as compared to the control group. However, no significant differences was

observed in either the small intestine or cecum. By contrast, we observed similar bacteria titres of the Δ*ebpABC* deletion mutant in animals fed both diets. However, importantly, we observed a significant decrease in the CFU of the Δ*ebpABC* deletion mutant as compared to wild type mice fed high iron diets **(Figure 3.14B)**. These data suggest that dietary iron promote *E. faecalis* colonization in murine colon, in an Ebp-dependent manner. Furthermore, we speculate that Fe levels in each region of the GI tract may be different, and analysis of the Fe content in each region will clarify whether the Fe levels contribute to the increased colonization in murine colon. To address this, we acid digested tissues and analyzed the Fe content using ICP-MS. We observed significant increases in Fe levels in the colon of mice fed a high Fe diet **(Figure 3.14C)**. This phenotype correlates with high iron-mediated colon colonization observed.

A

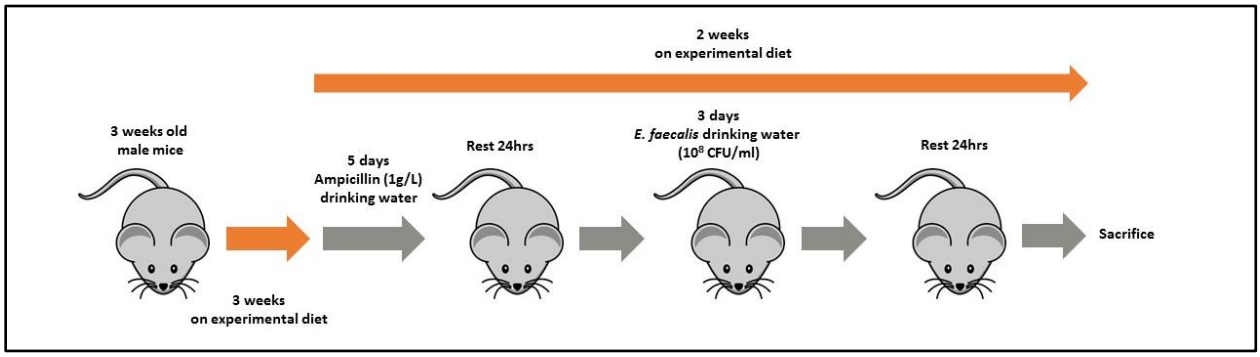

B

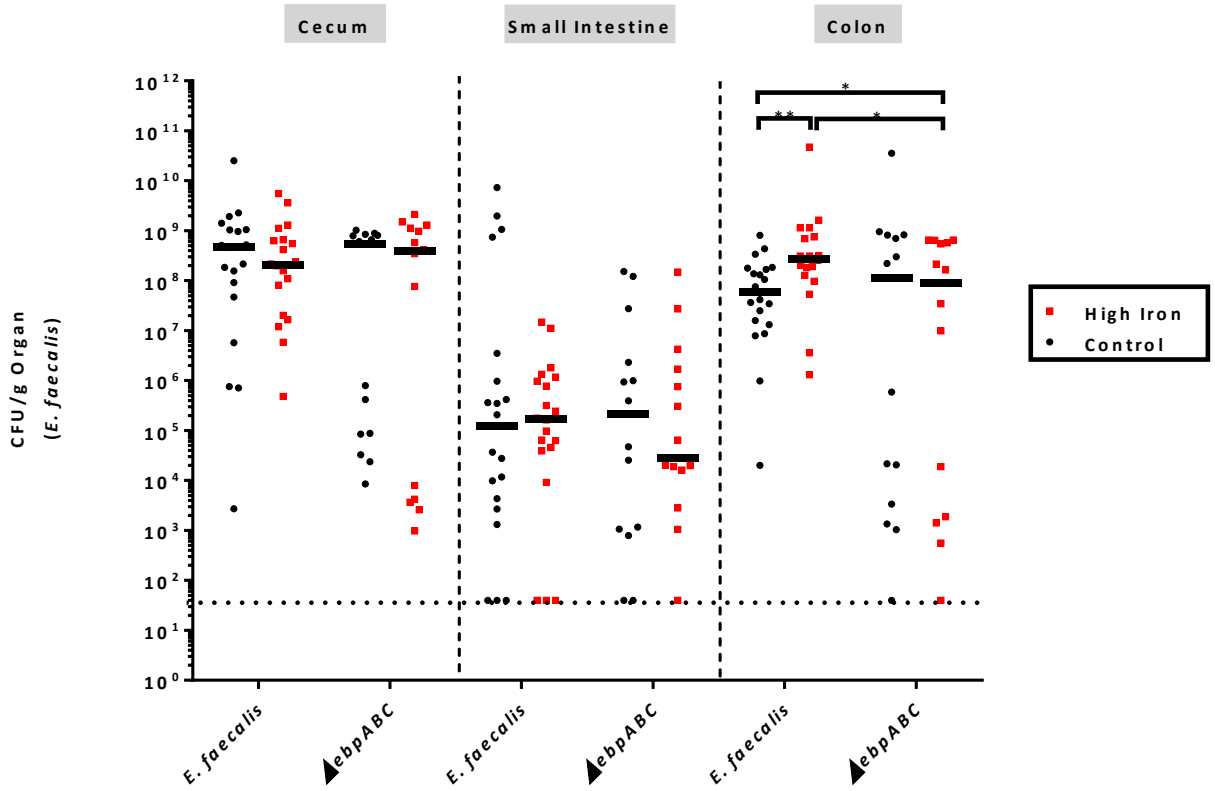

C

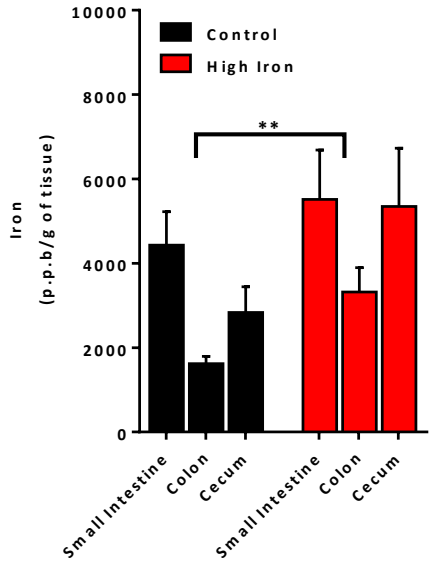

Figure 3.13. *E. faecalis* colonization in lower gastrointestinal tract. (A) Schematic of diet associated GI colonization model, **(B)** Bacterial titers recovered from murine tissues, N=3, n=5

repeated on non-consecutive days. **(C)** Iron content in murine tissues colonized by *E. faecalis* (emptied of its content). N=2, n=5. Statistical significance was determined by Mann-Whitney test. * $P \leq 0.05$, ** $P \leq 0.01$, *** $P \leq 0.001$, **** $P \leq 0.0001$. Black line indicate median. Dotted line indicate limitation of detection of CFU <40.

3.6 Discussion

In **Chapter 2**, we showed that iron-mediated EET promotes *in vitro E. faecalis* biofilm growth and identified novel genes which play a role in iron-mediated biofilm growth (Keogh et al., 2018). In that study, however, we observed that absence of *ebpR-ABC* and *srtC* attenuated iron-mediated biofilm growth (data not shown). However, because Ebp also mediates biofilm formation in normal (unsupplemented media) we excluded it from further analysis because it was not iron-specific. Since extracellular filamentous protein structures, such as type IV pili, contribute to EET in other organisms (Holmes et al., 2016), we hypothesized that *E. faecalis* Ebp may play similar role in iron-mediated biofilm growth and EET.

Although conservation of the type IVa pilin has been shown in several gram negative anaerobic bacteria (Reardon and Mueller, 2013b), gram positive bacterial pili has not been closely examined. We therefore examined single deletion of *ebp* subunits, and we observed that both *ebpA* and *ebpC* mutants, but not the *ebpB* mutant, were attenuated for *in vitro* iron-mediated biofilm growth. Although previous studies have shown that deletion of any single *ebp* gene had no effect on expression of other *ebp* genes and that growth kinetics were not significantly altered, *ebpA* deletion mutant had significantly reduced surface displayed EbpC and EbpB compared to the parent strain (Nielsen et al., 2012; Sillanpaa et al., 2013). By contrast, *ebpB* and *ebpC* deletion mutants do not show significant differences in other surface displayed pilin subunits (Sillanpaa et al., 2013). Hence, the attenuated iron-mediated biofilm formation observed in *ebpA* deletion mutant may be due to reduced surface anchored EbpC, since the absence of EbpB alone does not drastically impact iron-mediated biofilm growth. Together, these results suggest that the EbpC major subunit is essential for *in vitro* iron mediated biofilm growth. Since deletion of *ebpA* impacts display of EbpC on the cell surface, we next sought to determine the role of a putative metal ion binding site in EbpA in iron-mediated biofilm growth, using a MIDAS ($ebpA^{AWAGA}$) mutant. We observed that the MIDAS ($ebpA^{AWAGA}$) mutant displayed flat monolayer of a 2-3 cell thickness biofilms. This result shows that the absence of a functional MIDAS motif prevent iron responsive biofilm growth and re-structuring. Additionally, the MIDAS mutant is attenuated in iron-mediated biofilm growth and EET. Since in *Geobacter spp*, alanine substitution of each of the five amino acids in the carboxyl terminus of PilA resulted in attenuated ability for long range electron transfer in *Geobacter sulfurreducens* (Vargas et al., 2013), it will be interesting to examine whether specific

Ebp amino acid residues contribute to EET in a similar manner. We also show that matrix-associated iron deposits require pilus expression, and ICP-MS of pilus preps from *E. faecalis* biofilm cells grown in iron-supplemented media show increased iron levels, whereas the MIDAS mutant did not. These results suggest that iron directly interacts with the pilus or, alternatively, iron interacts with another protein that co-purifies with the pili. To address this, mass spectrometric analysis of the pilus preps should be done to allow us to test the second hypothesis.

Furthermore, we have identified that *ndh3* and *menB* contribute to iron-mediated EET, and absence of both these genes impact ability to reduce ferric iron extracellularly. Since *ldh1* has been shown in **Chapter 2** to be involved in EET, here we show that absence of *ldh1* also resulted in reduced intracellular iron. Together, these findings suggest that likely ferric iron reduction extracellularly is important for iron uptake. However, the role of pili in ferric iron reduction and ferrous iron import is still unclear since absence of *ebpABC* does not impact extracellular ferric iron reduction. To address this, deletion of both *ndh3* and *menB* in *ebpABC* deletion mutant may be needed. An alternative hypothesis is that the pili does not play a role in ferric iron reduction, but contributes to iron biomineralization. Since iron drives *E. faecalis* biofilm growth, having ferric iron localized at close proximity to cell surface allow for ferric iron reduction to ferrous iron which is subsequently used for iron uptake. In other iron oxidizing bacteria, extracellular organic polymers have been shown to be important for iron encrustation and this provides iron specific redox gradient (Fe^{2+} and Fe^{3+}) along the polymer (Miot et al., 2009). Both marine Zetaproteobacterium and Betaproteobacterium deposit ferric iron on to extracellular organic-rich stalks to prevent iron encrustation on cell surface (Chan et al., 2011; Comolli et al., 2011). This structural adaptation has been proposed to be important for survival and growth in iron riched environment.

Although we observed attenuated EET for both the *ebpABC* deletion mutant and the MIDAS (*ebpA*^{AWAGA}) mutant, the kinetics of current production were different between the two strains, suggesting that the pili may contribute to EET by multiple mechanisms. We speculate that changes in global gene expression may contribute to EET. To address this, we performed expression profiling for these strains compared to wild type biofilm grown in iron-supplemented media. While we observed no transcriptional differences between wild type and the *ebpABC* deletion mutant, we observed massive transcriptional changes associated with the mutated MIDAS motif. While we

observed many differentially regulated genes in the MIDAS mutant, and understanding the reasons for this are an important future direction, for many of the genes we observed a complete inverse transcriptomic profile as compared to wild type OG1RF biofilm grown in iron supplemented media as well as a skewing toward induction of genes involved in aerobic respiration and down-regulation of the flavin-mediated electron transfer gene locus (encoded by *OG1RF_12507-12513*) **(Table S3.1, S3.2)**, which likely influence the ability of MIDAS (*ebpA*^{AWAGA}) mutant to contribute to EET and iron-mediated biofilm growth. We have also shown that majority of genes which are differentially regulated due to alteration in MIDAS motif are involved in metabolism **(Table 3.6)**.

We observed attenuated iron-mediated biofilm growth and EET phenotype in the MIDAS (*ebpA*^{AWAGA}) mutant. One explanation for this could be simply the reduced ability of the mutant to interact with iron. Alternatively, changes in the MIDAS motif could impact overall pilus structure which could, in turn, result in altered biofilm structure. A third possibility is that global transcriptional changes associated with the MIDAS (*ebpA*^{AWAGA}) mutant could attenuate EET and biofilm formation, although it is unclear how this would occur. However, we speculate that the underlying mechanism for altered gene expression could be somewhat similar to the mechano-sensing reported in gram negative bacterium. For example, sheer force mechanosensing through the *P. aeruginosa* PilY1 protein, which contains a region with low similarity to the von Willebrand factor A (VWA) domain, can result in accumulation of c-di-GMP (3′-5′ cyclic diguanylate monophosphate) leading to increased virulence gene expression and biofilm formation (Rodesney et al., 2017). Although several reports have demonstrated that c-di-GMP contributes to surface sensing and adhesion by type IV pilus in *P. aeruginosa* (Ribbe et al., 2017), mechano-sensing in gram positive bacteria including *E. faecalis* has not been previously reported. To better understand whether the tertiary structure of the pilus itself is altered in the MIDAS mutant and whether this in turn results in attenuated EET, further studies should focus on pilus structure prediction and modeling to decipher the role that pilus plays in extracellular electron and the potential iron interaction sites.

We also compared transcriptional changes in wild type OG1RF biofilm in the presence of supplemented iron. A global transcriptional analysis revealed 90 genes that were differentially regulated. Several putative iron acquisition systems have been described in *E. faecalis* genome;

we observed that only *feoB* (involved in ferrous iron import) was upregulated, indicating that an active iron import system may be important in iron-supplemented biofilm growth. However, no efflux genes or oxidative stress associated genes were upregulated, which indicate that *E. faecalis* biofilm is tolerant of iron at this concentration. Moreover, the manganese transporter *mntH2* and manganese dependent virulence factor *efaA* are downregulated. A previous study by Abrantes and colleagues have shown transcriptional network crosstalk in manganese, copper and zinc regulation (Abrantes et al., 2011); however, ours is the first study showing downregulation of manganese-associated genes in response to iron. - The upregulation of *ebp* genes further support that pilus expression is iron responsive. The simultaneous up-regulation of *ebpABC* and *feoB* as the sole iron-responsive transporter, along with our observations that Ebp co-purify with iron and are required for EET suggest a model in which pilus-associated iron may be reduced and subsequently taken up by the ferrous iron transporter FeoB for promoting biofilm growth.

Since our findings demonstrate that iron impacts virulence gene expression, we next sought to determine whether iron can influence *E. faecalis* colonization *in vivo*. Iron is considered an essential metal utilised by both the host and invading pathogens; and is obtained in the form of dietary iron. Moreover, less than 10% of dietary iron consumed is absorbed at the duodenum in the lower gastrointestinal tract which leaves the majority of unabsorbed iron directed for excretion. (Benito and Miller, 1998). Using high iron diet in a murine GI colonization model, we showed that high iron consumption promotes colonization in the colon, in an Ebp-dependent manner.

Together, these findings represent the first description of Ebp contributions to EET and iron-mediated biofilm growth. This supports our hypothesis that iron enhances *E. faecalis* colonization in the gastrointestinal tract. However, the GI tract is home to several other bacterial species as well. To what extent does iron-mediated *E. faecalis* colonization affects colonization fitness of other bacteria species remains to be explored; and whether dietary iron-mediated shifts in GI microbiota composition impacts host health remains to be characterized. Future studies should focus on understanding the role of iron-mediated *E. faecalis* biofilm growth in the context of mixed species studies, both *in vitro* and *in vivo*.

3.7 Acknowledgements

This work was supported by the National Research Foundation and Ministry of Education Singapore under its Research Centre of Excellence Programme, by the National Research Foundation under its Singapore NRF Fellowship programme (NRF-NRFF2011-11), and by the Ministry of Education Singapore under its Tier 2 programme (MOE2014-T2-2-124). We thank Wandy Betty (Washington University, St Louis, USA) for performing TEM, and Hailyn V. Nielsen and Scott Hultgren (Washington University, St Louis, USA) for providing the pilus mutants.

3.8 Supplementary figures and tables

Table 3.1: List of *E. faecalis* virulence gene transcriptionally regulated in response to iron in *E. faecalis ebpA*^{AWAGA} mutant

Gene Locus	Gene Name	Annotated Function	Log_2FC Expression
OG1RF_10404	type II CRISPR RNA-guided endonuclease (*csn1*)	CRISPR	-0.73145319
OG1RF_10405	subtype II CRISPR-associated endonuclease (*cas1*)		-1.911995098
OG1RF_10406	CRISPR-associated endonuclease (*cas2*)		-4.436473521
OG1RF_10413	arginine repressor (*argR2*)	Arginine metabolism transcriptional regulator	-1.545373261
OG1RF_10373	L lactate dehydrogenase 2 (*ldh2*)	glycolysis	-2.054920722
OG1RF_10868	Ebp transcriptional regulator (*ebpR*)	pilus	-3.081424943
OG1RF_10869	Pilus subunit (*ebpA*)		-1.066800425
OG1RF_10870	Pilus subunit (*ebpB*)		-1.581735057
OG1RF_10871	Pilus subunit (*ebpC*)		-2.323720432
OG1RF_10872	Sortase C (*srtC*)	Polymerization of pilus	-1.324219355
OG1RF_11525	Serine protease (*sprE*)	Matrix modification	-1.687864622
OG1RF_11526)	Gelatinase E (*gelE*)	Matrix modification	-1.31390395
OG1RF_11051	hypothetical protein	Phage associated resistance	-1.877500908
OG1RF_11054	structural protein		-2.226406895
OG1RF_11055	phage major tail protein, TP901-1 family		-2.132298763
OG1RF_11056	hypothetical protein		-3.538368904
OG1RF_11058	hypothetical protein		-5.159324486
OG1RF_11059	tail protein		-5.465503674
OG1RF_11060	structural protein		-5.259291425
OG1RF_11061	hypothetical protein		-3.653527798
OG1RF_11062	holin		-4.355677265
OG1RF_11063	N-acetylmuramoyl-L-alanine amidase		-4.477589949

Table 3.2: List of cell division and respiration-associated genes transcriptionally regulated in response to iron in *E. faecalis ebpA*^{AWAGA} mutant

Gene Locus	Gene Name	Annotated Function	Log_2FC Expression
OG1RF_10723	cell division protein FtsL	Cell division	1.606430554
OG1RF_10729	cell division protein FtsA		1.404344346
OG1RF_10730	cell division protein FtsZ		1.425748593
OG1RF_10731	YggS family pyridoxal phosphate enzyme		1.35983141
OG1RF_10733	cell division protein		1.001832791
OG1RF_10734	RNA-binding protein S4		0.93581213
OG1RF_10735	cell division protein DivIVA		0.856193644
OG1RF_10737	glucose-6-phosphate dehydrogenase	glycolysis	1.265380697
OG1RF_10738	Cro/Cl family transcriptional regulator	Regulator	1.928924078
OG1RF_11663	amino acid ABC transporter ATP-binding protein	Aerobic respiration	1.206833563
OG1RF_11664	thiol reductant ABC exporter subunit (*cydD*)		1.237286574
OG1RF_11665	cytochrome c oxidase assembly protein (*cydB*)		1.386928882
OG1RF_11666	cytochrome d ubiquinol oxidase subunit I (*cydA*)		1.158501265
OG1RF_12507	1,4-dihydroxy-2-naphthoate polyprenyltransferase (*ubiA2*)	Flavin-mediated extracellular electron transfer	-1.102380325
OG1RF_12508	thiamine biosynthesis protein ApbE		-1.634110047
OG1RF_12509	FMN-binding domain-containing protein		-1.604582332
OG1RF_12510	NADH dehydrogenase (*ndh3*)		-1.177969213
OG1RF_12513	geranylgeranyl pyrophosphate synthase (*hepT*)		-1.560946242

Chapter 4: *E. faecalis* manganese efflux transporter (MntE) prevents manganese toxicity and contributes to fitness in murine gastrointestinal (GI) colonization

4.1 Statement of Contribution

L.N.L conceptualized the study. L.N.L and K.A.K designed the experiments, analyzed the data and prepared the manuscript. L.N.L performed the experiments and analyzed the data. L.N.L performed ICP-MS and analyzed the ICP-MS data. L.N.L performed the qRT-PCR experiment and analyzed the data. L.N.L and J.J.W performed the murine GI colonization model and L.N.L analyzed the data. L.N.L prepared the RNA samples for RNA sequencing and K.K.L.C analyzed the data. Manuscript for this work is in preparation.

4.2 Abstract

The ability to regulate intracellular metal concentration is crucial to prevent metal toxicity-mediated growth inhibition. Being inherently resilient to oxidative stress, *Enterococcus faecalis* is equipped with an array of antioxidant enzymes for dealing with intracellular oxygen radicals arising from metals. Even though metal efflux pumps have been documented in several bacterial species as alternative strategy for intracellular metal homeostasis, metal efflux pumps are understudied in *E. faecalis*.

In **Chapter 2**, we showed that the absence of *mntE* (predicted to encode an efflux pump) resulted in significantly enhanced iron-mediated biofilm growth, which is independent of extracellular electron transfer (EET). Uncoupling EET and iron-mediated biofilm growth suggests that alternative mechanisms contribute to biofilm growth under these conditions. In this chapter, we have determined that MntE, which belongs to the cation diffusion facilitator (CDF) family, functions as a manganese (Mn) efflux transporter in *Enterococcus faecalis*. Further *in vitro* characterization demonstrate that the absence of MntE results in sensitivity to manganese and, consequently, mutant cells display growth inhibition under both planktonic and biofilm condition in Mn-supplemented media. Additionally, absence of *mntE* results in intracellular Mn accumulation, and Mn-mediated growth inhibition can be alleviated with magnesium (Mg) supplementation. This likely suggests that Mg-dependent biological processes are targets of intracellular Mn. Interestingly, the absence of *mntE* also leads to intracellular iron (Fe) accumulation, which suggest that MntE exhibits dual specificity for both Mn and Fe. Global transcriptional analysis of *mntE::Tn* mutant under growth in iron-supplemented media revealed that three glycerol catabolic genes (*glpF2, glpK, glpO*) are upregulated which likely contributed to significantly enhanced iron-mediated biofilm growth. Although *mntE* is not upregulated in biofilms in iron-supplemented media, upregulation of *mntE* under Mn supplementation observed and associated with upregulation of endocarditis and biofilm associated pilus (Ebp) and downregulation of the glycerol catabolic genes (*glpF2, glpK, glpO*). The absence of *mntE* also resulted in attenuated GI colonization *in vivo*. However, absence of *mntE* did not alter sensitivity to oxidative stress nor hydrogen peroxide production *in vitro*. Together, these findings demonstrate that MntE plays an important role in regulation of intracellular iron and manganese, and contributes to fitness in *E. faecalis* gastrointestinal tract colonization.

4.3 Introduction

Manganese (Mn) is important for metabolism, signal transduction, and protection against oxidative stress (Jakubovics and Jenkinson, 2001). The role of Mn in oxidative stress responses has been established, yet the importance of Mn in *E. faecalis* physiology and virulence has been understudied. In many lactic acid bacterial species, including Enterococci, the requirement of manganese for growth can be substituted by other transition metals, with iron (Fe) being the most widely characterized for manganese substitution (Archibald, 1986; Bruyneel et al., 1989; Marcelis et al., 1978; Weinberg, 1997). Given the similarity in ionic radius between manganese and iron, it is not unexpected that these cations are interchangeable (Nies and Grass, 2009).

In many bacterial species, manganese is important for alleviating oxidative stress as bacterial antioxidant enzymes including superoxide dismutase (*sodA*) utilise Mn as cofactor (Abrantes et al., 2013). Huycke and colleagues have previously shown that extracellular superoxide and 5,5-dimethyl-1-pyrroline N-oxide adducts of hydroxyl and thiol radicals can be detected in stools of rats colonized by *E. faecalis* and the production of these radicals by *E. faecalis* is associated with increased DNA damage in rat colonic epithelial cells (Huycke et al., 2002). This support that superoxide is present in the colon and *E. faecalis* has the ability to withstand oxidative stress. Deletion of *sodA* resulted in increased sensitivity to vancomycin and penicillin (Bizzini et al., 2009), which demonstrate that antibiotic resistance involves the ability to withstand oxidative stress. Additionally, a *sodA* deletion mutant is impaired in intracellular murine peritoneal macrophage survival (Verneuil et al., 2006) and is susceptible to *in vitro* microglial killing (Peppoloni et al., 2011) which demonstrate that Mn dependent *sodA* is important for virulence. Aside from its role in SodA activity, the contribution of Mn on *E. faecalis* physiology has not been clearly elucidated.

Manganese dependent uptake systems in Enterococci, to date, involve the ABC-type permease *efaCBA* and two Nramp transporters (*mntH1, mntH2*). In *E. faecalis*, the *efaCBA* operon is dependent on EfaR, a transcriptional repressor which is depressed in Mn-depleted media (Abrantes et al., 2013). The *efaCBA* operon encodes the adhesion lipoprotein EfaA (endocarditis-associated antigen) and an ATP dependent ABC transporter. The role of *efaCBA* operon as a virulence factor in *E. faecalis* was established given that *efaR* deletion mutant was impaired in intracellular

macrophage survival and biofilm formation *in vitro*, and the mutant exhibits increased sensitivity to hydrogen peroxide killing (Abrantes et al., 2013). An earlier study also demonstrated that infection using *efaA* deletion mutant resulted in delayed murine mortality as compared to the wild type in an intraperitoneal murine infection model (Singh et al., 1998).

Since *E. faecalis* possesses both the ABC-type transporter *efaCBA* and two Nramp transporters (*mntH1, mntH2*), it is not inconceivable that these transporters may serve redundant functions in transport of Mn under Mn-starved conditions. Recently, Colomer-Winter and colleagues demonstrated that deletion of all three transporter systems (*efaCBA, mntH1, mntH2*) resulted in significantly reduced intracellular Mn levels, *in vitro* biofilm formation, and growth defects which could be restored upon supplementation with Mn (Colomer-Winter et al., 2018). Although deletion of *mntH2* with either *efaCBA* or *mntH1* resulted in reduced intracellular Mn levels, most notably, intracellular Mn levels were below the detectable limit in the triple deletion mutant. Since single deletion of these systems did not result in impaired growth *in vitro*, this indicates that these three systems, in concomitant effort, promote Mn uptake for normal cellular growth. Expression of any one of the three transporters rescued growth under Mn depleted conditions (Colomer-Winter et al., 2018). Additionally, the triple deletion mutant exhibited attenuated colonization in rabbit endocarditis and murine catheter-associated urinary tract infection (CAUTI) models, as well as attenuated killing in a *G. mellonella* model (Colomer-Winter et al., 2018).

Together, these findings demonstrated that Mn acquisition contributes to biofilm formation and virulence. However, Mn efflux systems in *E. faecalis* have not been characterized. Although Mn uptake systems play crucial role in acquiring Mn, inversely Mn efflux systems potentially play important role in regulating intracellular Mn homeostasis. The cation diffusion facilitators (CDFs) is a large family of membrane bound proteins involved in exporting metal ions out of cells. CDF proteins typically possess a transmembrane domain (TMD) and a C-terminal domain that protrudes into the cytoplasm (Kolaj-Robin et al., 2015). Metal specificity for the CDF protein is broad, and can involve one or more cationic metal. To decipher the role of each CDF protein, an in depth phenotypic characterization on metal sensitivity is essential.

A previous study demonstrated that *mntE* is upregulated in response to 1 mM iron under planktonic condition (Lopez et al., 2012). In this chapter, we show that MntE, which belongs to the cation diffusion facilitator (CDF) family, functions as a Mn efflux pump with dual specificity for Fe in *E. faecalis*. Alleviating Mn mediated toxicity by supplementing with Mg demonstrates that competition for Mg rescues growth inhibition in an *mntE* mutant. Additionally, in iron-supplemented media, the absence of *mntE* results in upregulation of glycerol catabolic genes (*glpF2, glpK, glpO*). Conversely, wild type growth in Mn-supplemented media results in down regulation of glycerol catabolic genes and upregulation of endocarditis and biofilm associated pilus expression. We also demonstrate that MntE plays an important role in regulation of intracellular iron and manganese, and contributes to fitness in *E. faecalis* gastrointestinal tract colonization

4.4 Material and method

4.4.1 Bacterial Strains and Growth Conditions

Enterococcus faecalis was grown in Brain Heart Infusion broth (BHI) and cultured at 37 ^{o}C under static and shaking (200rpm) conditions where appropriate. Preparation of inoculum for biofilm and planktonic assays were performed as previously described (Keogh et al., 2018). Bacterial strains used were listed in **Table 4.1**. Where appropriate, strains harbouring pMSP3535 plasmids were selected using 100 ug/mL erythromycin (Sigma Aldrich, USA) and induction of gene expression was performed using 5 ug/mL nisin from *Lactococcus lactis* (Sigma Aldrich, USA). The reagents used for bacterial growth were listed as below. BHI was supplied by Becton, Dickinson and Company, Franklin Lakes, NJ. TSB and agar was supplied by Oxoid Inc., Ontario, Canada. Metals for supplementation were added during medium preparation. Ferric citrate hydrate ≥98%, magnesium chloride anhydrous ≥98%, copper chloride dihydrate ≥99%, ferrous sulphate heptahydrate ≥99%, ferric sulphate hydrate ≥97%, ferric chloride anhydrous ≥99% and heme ≥90% were supplied by Sigma Aldrich, St Louis, MO, USA. Manganese chloride tetrahydrate and zinc chloride were supplied by Merck Millipore, Singapore.

Table 4.1: List of bacterial strains used

Strains used	Relevant characteristics	Reference or source
***E. faecalis* OG1RF wild type**	Laboratory strain, Rif^R, Fus^R	(Bourgogne et al., 2008)
***E. faecalis* OG1RF pMSP3535**	Rif^R, Fus^R, Erm^R	This paper
mntE::Tn	Rif^R, Fus^R, Erm^R (ID: 4.2A1 F1 Tn mutant)	(Kristich et al., 2008)
mntE::Tn pMSP3535	Rif^R, Fus^R, Erm^R	This paper
mntE::Tn pMSP3535::mntE	Rif^R, Fus^R, Erm^R	This paper

4.4.2 Static Biofilm Assay

Bacterial cultures were normalized as previously described (Keogh et al., 2018) and inoculated in TSBG in a 96-well flat bottom transparent microtiter plate (Thermo Scientific, Waltman, MA, USA), at 37^{o}C under static conditions. Staining of adherence surface biofilm biomass was performed using 0.1% w/v crystal violet (Sigma-Aldrich, St Louis, MO, USA), and incubated at 4 ^{o}C for 30 minutes. The microtitre plate was washed twice with PBS followed by crystal violet solubilization with ethanol-acetone (4:1) for 45 minutes at room temperature. Quantification of

adherence biofilm biomass was performed by measuring absorbance at OD_{595nm} using a Tecan Infinite 200 PRO spectrophotometer (Tecan Group Ltd., Männedorf, Switzerland).

4.4.3 Planktonic Growth Assay

Bacterial cultures were normalized as previously described (Keogh et al., 2018) and serial diluted by dilution factor of 200. Diluted cultures were inoculated into the media at a ratio of 1:25, which is 8 µL of inoculum in 200 µL of media, incubated at 37ºC for 18 hours, and absorbance at OD_{600nm} was measured using a Tecan Infinite 200 PRO spectrophotometer (Tecan Group Ltd., Männedorf, Switzerland) at 15 minutes interval. Growth curve was plotted to determine the exponential growth.

4.4.4 Planktonic Growth Kinetics

Bacterial cultures were normalized and inoculated into the media at a ratio of 1:1000 in 30 mL of media. The falcon tubes were incubated in the shaking incubator for 8 hours at 200 rpm, 37°C. At every time interval, 100 µL and 1 mL of culture was aliquot for colony forming units (CFU) enumeration and optical density measurement respectively for each time point.

4.4.5 Macro-Colony Assay

Bacterial cultures were normalized and spotted onto TSBG agar plate at 5µL per spot. Agar plates were supplemented with metals where appropriate and incubated for 120 hours at 37°C. Macro-colonies were excised and resuspended in 3 mL PBS. 100µL of the cell suspension was added to the wells of the 96-well plates and serial dilution of up to 10^{-7} was performed for colony forming units (CFU) enumeration. 5µL of diluent from each well was spotted onto the agar plates and incubated at 37°C overnight. After incubation, the number of colonies formed for each bacterial strain was counted and recorded to determine CFU/mL.

4.4.6 Inductively Coupled Plasma Mass Spectrometry (ICP-MS)

Biofilms are cultured under static condition at 37°C for 24 hrs. After incubation, biofilms are scraped, resuspended in 1mL PBS and normalized to OD 1. Normalized biofilms are pelleted at 14,000 rpm for 2 minutes, and supernatant was discarded. Cell pellets are washed with 1 mL of 0.5 mM EDTA. Next, the cell pellets are suspended in 300 uL of lysozyme from chicken egg white

(20 mg/ml) (Sigma Aldrich, USA) (20mg/mL) for 30 minutes at 37°C, washed with 1 mL PBS and pelleted. At a ratio of 2:1, 70% nitric acid (Sigma Aldrich, USA) and 30% hydrogen peroxide (Sigma Aldrich, USA) was added to normalized lysozyme treated biofilm cells and left under room temperature for 3 days to allow complete digestion. The digested samples were diluted with 3.4 mL LC-MS grade water and filtered using 0.2 um membrane, prior to analysis using ICP-MS. For tissue ICP-MS, tissues (cecum, colon, small intestines) are emptied of its content and suspended in 1 mL PBS. Digestion of tissues was performed using 2 mL 70% nitric acid (Sigma Aldrich, USA) and 500 uL 30% hydrogen peroxide (Sigma Aldrich, USA) at 37°C for 3 days, and then 65°C for 5 hours. Digested tissues were diluted with 9 mL LC-MS grade water and filtered using 0.2 um membrane, prior to analysis using ICP-MS. Analysis of trace metals in samples were performed using ICP-MS model Elan-DRCe, Meinhard Nebulizer model TR-30-C3 (Perkin Elmer; Model: N8122006 (Elan Standard Torch)).

4.4.7 Quantitative Real time PCR (qRT-PCR) and RNA sequencing

Biofilms were grown in a 6-well plate for 24 hours at 37^{o}C under static conditions. Post incubation, spent media was removed and biofilms were suspended in PBS prior being dislodged using cell scraper. Biofilm cultures were centrifuged at 14,000 rpm for 2 minutes at room temperature to remove supernatant. Biofilm cell pellet was incubated with lysozyme solution containing lysozyme from chicken egg white (10mg/ml) (Sigma Aldrich, USA) for 30 minutes at 37^{o}C, and centrifuged at 14,000 rpm for 2 minutes at room temperature to remove supernatant prior to cell lysis. RNA extraction was performed in a Purifier® filtered PCR enclosure using the PureLink™ RNA mini kit (Invitrogen, USA) according to the manufacturer's instructions. RNA purification and removal of DNA was performed using TURBO DNA-free™ kit (Thermo Fisher, USA) and Agencourt® RNAClean® XP Kit (Beckman Coulter, USA). Measurement of RNA yield and quality was performed using Qubit® RNA HS assay kit (Thermo Fisher, USA) and RNA ScreenTape System and 2200 TapeStation (Agilent, USA). Synthesis of cDNA was performed using SuperScript III First-strand (Invitrogen, USA). Quantitative real-time PRC using cDNA was performed using KAPA SYBR fast qPCR master mix kit (Sigma Aldrich, USA) and Applied Biosystems StepOne Plus Real-Time PCR system. The expression of *ebpC*, *ebpR*, *mntE* and *gyrA* were analysed using primer pairs listed in **Table 4.2**. For each primer set, a standard curve was established using genomic DNA from *E. faecalis* OG1RF. Normalized amount of cDNA were

used to determine relative fold change in gene expression as compared to *E. faecalis* OG1RF biofilm grown in TSBG. For RNA sequencing, ribosomal RNA depletion was performed after RNA purification using Ribo-Zero™ rRNA removal kit (Illumina, USA). cDNA library synthesis was performed using NEBNext RNA First-strand and NEBNext Ultra directional RNA Second-strand synthesis module (New England BioLab, US). Transcriptome library preparation was performed using 300bp paired end 130llumine sequencing. Pathway enrichment analysis was done by annotating genes in *E. faecalis* OG1RF to the KEGG database (KEGG identifier: efi). Gene classification was done based on their gene membership according to KEGG pathways. KEGG gene set enrichment analysis was performed using the Bioconductor package, clusterprofiler (version 3.8.1) (Yu et al., 2012).

Table 4.2: Primers used in qRT-PCR

Gene	5' – 3'
gyrA F'	TGTTCGTCGGGATGTGAGTG
gyrA R'	GGTACGCCTTTTTCGATGGC
ebpC F'	CGGTCATACCGACGACCAAA
ebpC R'	TGTCACATCGCCATCGACTT
mntE F'	ACAGCATTCGGTGCTTTTGC
mntE R'	ACACTACCTGAAAGCAAGCCA

4.4.8 Oxidant Stress Challenge

Bacterial cultures were normalized to OD 0.7, and added at 1:25 ratio to media. Supplementation of menadione or hydrogen peroxide stimulate oxidative stress. Bacterial cultures were allowed to grow for 2 h at 37°C static condition prior to CFU enumeration.

4.4.9 Hydrogen Peroxide Quantification

Bacterial cultures were normalized to OD 0.7, and added at 1:25 ratio to media. Bacterial cultures were allowed to grow for 2 h at 37°C static condition. After incubation, hydrogen peroxide quantification was performed using ROS-Glo™ H2O2 Assay (Promega, USA) according to manufacturer's instructions.

4.4.10 Mouse Gastrointestinal Tract (GI) Colonization Model

Six weeks old male C57BL/6NTac mice were given ampicillin spiked drinking water (1 g/L) for 5 days. Mice were then given one day of recovery prior to administration of approximately 1-5 x 10^8 CFU/ml *E. faecalis* (OD 0.5) in drinking water for 3 days. Bacterial spiked drinking water is removed and allowed to rest for one day. Prior and post infection, mice were monitored for signs of disease and weight loss. All animal experiments were approved and performed in compliance with the Institutional Animal Care and Use Committee (IACUC). Post infection, small intestine, colon and cecum were harvested. Tissue samples were homogenised in PBS, serial diluted in PBS and spot-plated on BHI agar with 10 mg/L colistin, 10 mg/L nalidixic acid, 100 mg/L rifampicin, 25 mg/L fusidic acid. All selective agents were obtained from Sigma Aldrich, USA.

4.5 Results

4.5.1 *OG1RF_10589* cation efflux transporter is a manganese efflux pump (MntE)

Enterococcus faecalis OG1RF encodes a putative cation efflux transporter (OG1RF_10589) which displays 28% similarity to the *S. pneumoniae* manganese exporter MntE (Rosch et al., 2009). Additionally, this transporter, which belongs to the CDF family of metal efflux pumps, is conserved among several gram positive and gram negative bacteria including *S. aureus*, *C. botulinum*, *E. coli*, and *B. subtilis*. The CDF family has been extensively characterized in several bacterial species; however, metal specificity for each CDF protein may be different. The *E. faecalis* cation efflux transporter also share 25-28% protein similarity to MntR in *B. subtilis* (Huang et al., 2017) and FieF in *E. coli* (Grass et al., 2005) which have been demonstrated to be specific for manganese and ferrous iron export, respectively.

We hypothesize that the *mntE* efflux pump exhibits biometal specificity. To address this, we performed growth kinetic assays using *mntE::Tn* mutant to characterize its sensitivity to manganese (Mn), iron (Fe), zinc (Zn), copper (Cu) and magnesium (Mg), and our results show that *mntE::Tn* display Mn sensitivity **(Figure 4.1A-F)**. The reduced optical density measured in wild type OG1RF grown in 4 mM Mn suggest that at this concentration, growth kinetics are altered. However, similar altered growth kinetics was observed in the *mntE::Tn* mutant when grown in only 0.5 mM Mn. These results suggest that the absence of *mntE* increases Mn sensitivity by 8-fold **(Figure 4.1A)**. Complementing the *mntE::Tn* mutantwith *mntE* under control of a nisin-inducible promoter rescues Mn-mediated growth inhibition and restores growth similar to wild type OG1RF **(Figure 4.1F)**. We also show that *mntE::Tn* is not sensitive to Mg, Zn, Fe, or Cu, as the growth kinetic profiles are completely similar to the wild type OG1RF **(Figure 4.1B-E)**. To validate that absence of *mntE* results in Mn sensitivity leading to growth inhibition, we next performed planktonic growth assays which allow colony-forming unit (CFU) quantification. Cultures were grown under constant shaking conditions (200 rpm) for 8 hours, and at specific time intervals, optical density and the CFU enumeration was performed. At an early 4 hr time point, optical density readings of *mntE::Tn* under as little as 0.5 mM Mn, resulted in delayed growth **(Figure 4.2A, 4.2C)**. However, there was no significant difference in CFU at the 4 hr time point. Significantly decreased CFU of *mntE::Tn* was observed at both the 6^{th} and 8^{th} time points for all concentration of Mn that were tested **(Figure 4.2A, 4.2C)**. Complementing the *mntE::Tn* with

mntE on a nisin-inducible plasmid rescued Mn-mediated growth inhibition and restored CFU to wild type OG1RF levels **(Figure 4.2B, 4.2D-E)**. Even though the optical density reading showed that wild type OG1RF exhibited delayed growth at 1mM Mn and above, there was no significant decrease in CFU **(Figure 4.22A)**.

A

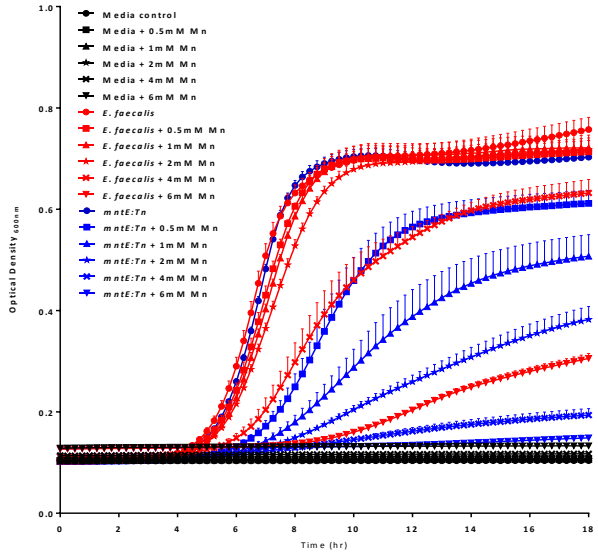

B

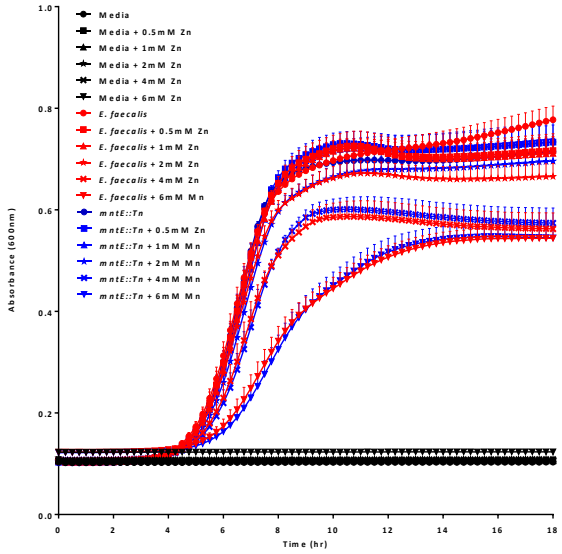

C

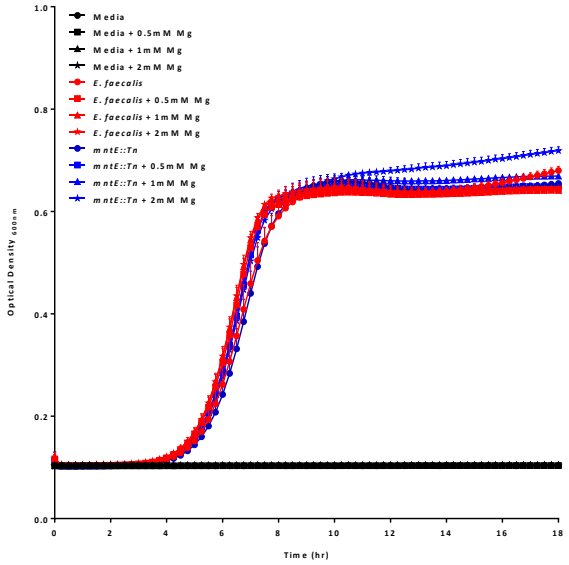

D

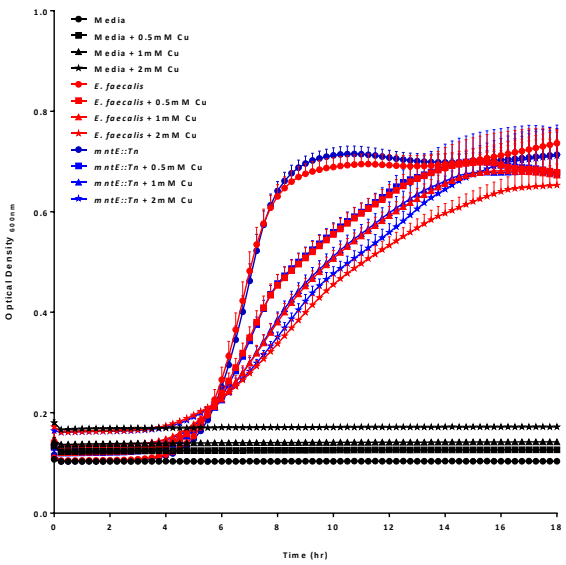

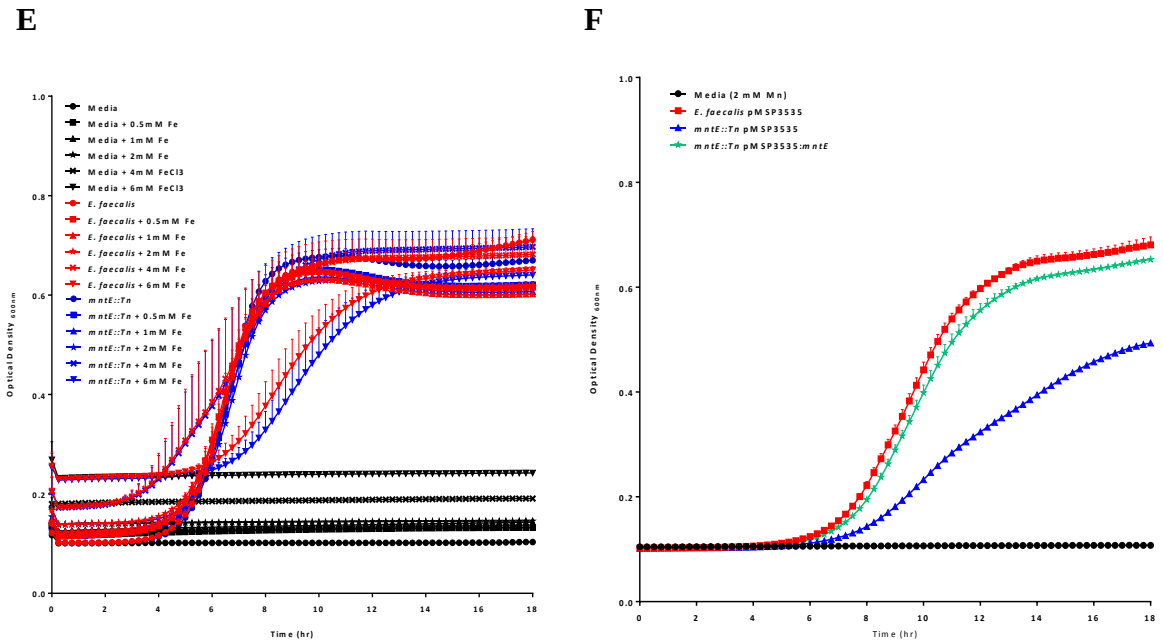

Figure 4.1. Cation sensitivity of MntE transposon mutant. Planktonic growth of *E. faecalis* in TSBG and TSBG supplemented with increasing **(A)** manganese, **(B)** zinc, **(C)** magnesium, **(D)** copper, **(E)** iron and **(F)** manganese (complemented strain). N=9, repeated on non-consecutive days.

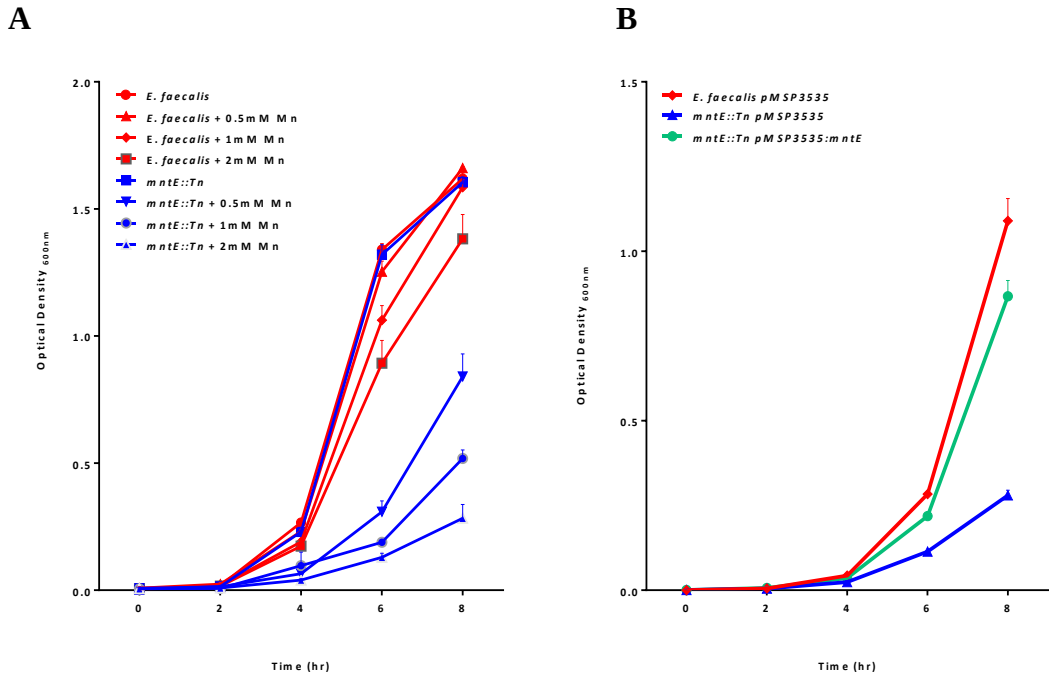

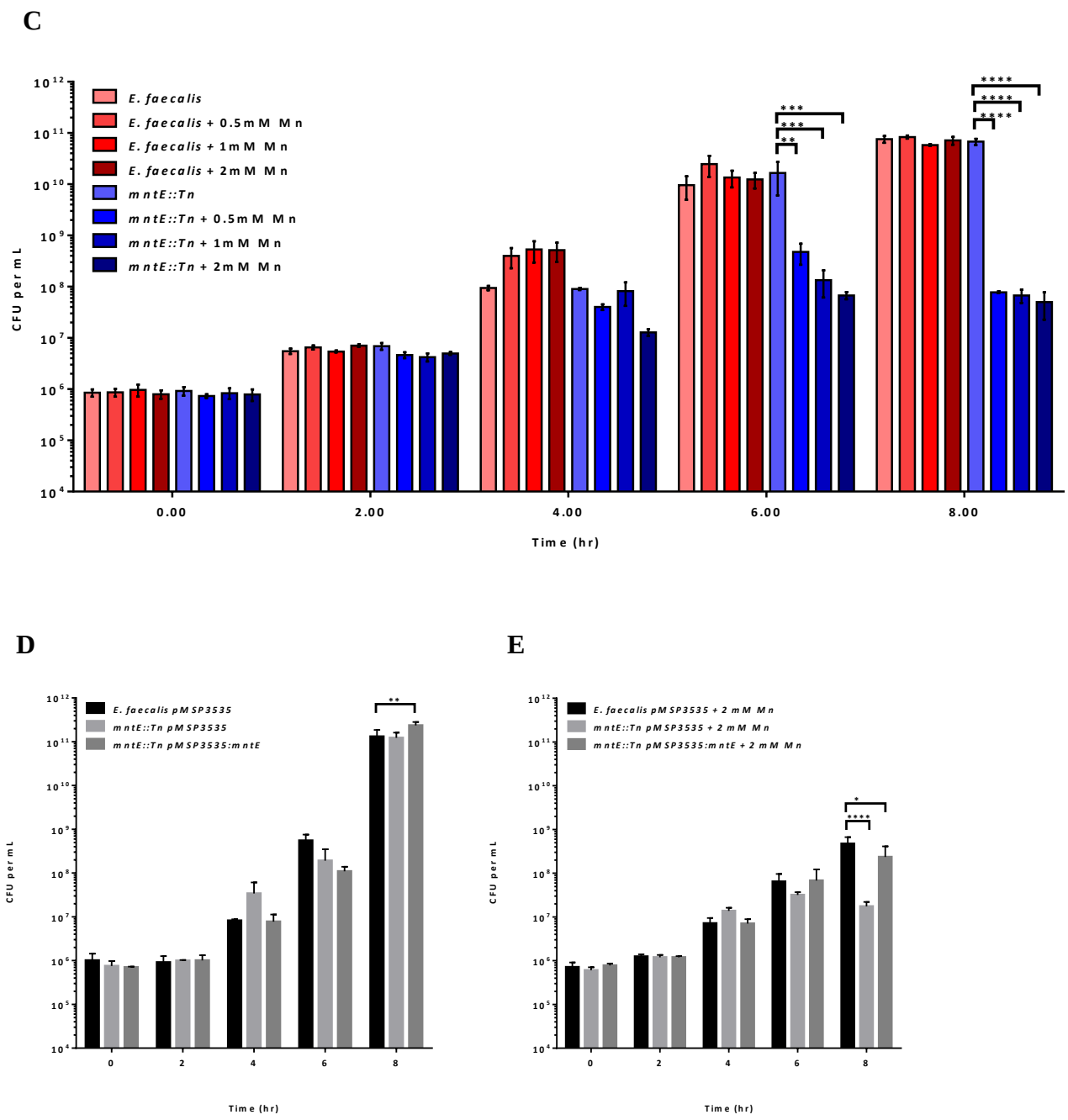

Figure 4.2. Manganese supplementation results in planktonic growth inhibition. Planktonic growth of *E. faecalis* in TSBG and TSBG supplemented with manganese for 8 hrs. Optical density measurement of (A) wild type and (B) complement, CFU enumeration of (C) wild type and (D-E) complement. N=9, repeated on non-consecutive days. Statistical analysis was performed using two-way ANOVA Fisher's LSD. * $P \leq 0.05$, ** $P \leq 0.01$, *** $P \leq 0.001$, **** $P \leq 0.0001$. Error bar represents standard error margin (SEM).

Since we have demonstrated that 0.5 mM Mn is sufficient to cause growth inhibition in *mntE::Tn* **(Figure 4.2A)**, we next speculated that this growth inhibition should also be observed under biofilm conditions. To address this, we performed static *in vitro* biofilm assays and macro-colony assays. Measurement of adherent biofilm biomass and CFU enumeration was performed after 120 hrs incubation. In both biofilm assays, the wild type OG1RF exhibited moderate sensitivity to 1 mM and 2 mM Mn; however; the *mntE::Tn* mutant exhibited increased sensitivity as compared to the wild type control in both assays at both Mn concentrations **(Figure 4.3A-B)**. For reasons that we don't yet understand, the empty complementation vector pMSP3535 augments biofilm biomass accumulation of the *mntE::Tn* in the static CV biofilm assay and the complementation vector returns biofilm biomass levels to that of wild type (**Figure 4.3C**). However, in the macrocolony biofilm assay, complementing the *mntE::Tn* with *mntE in trans* rescued Mn mediated growth inhibition and restored biofilm formation and CFU to wild type OG1RF levels **(Figure 4.3D)**. Collectively, our results support that absence of *mntE* consequently leads to increased sensitivity to Mn.

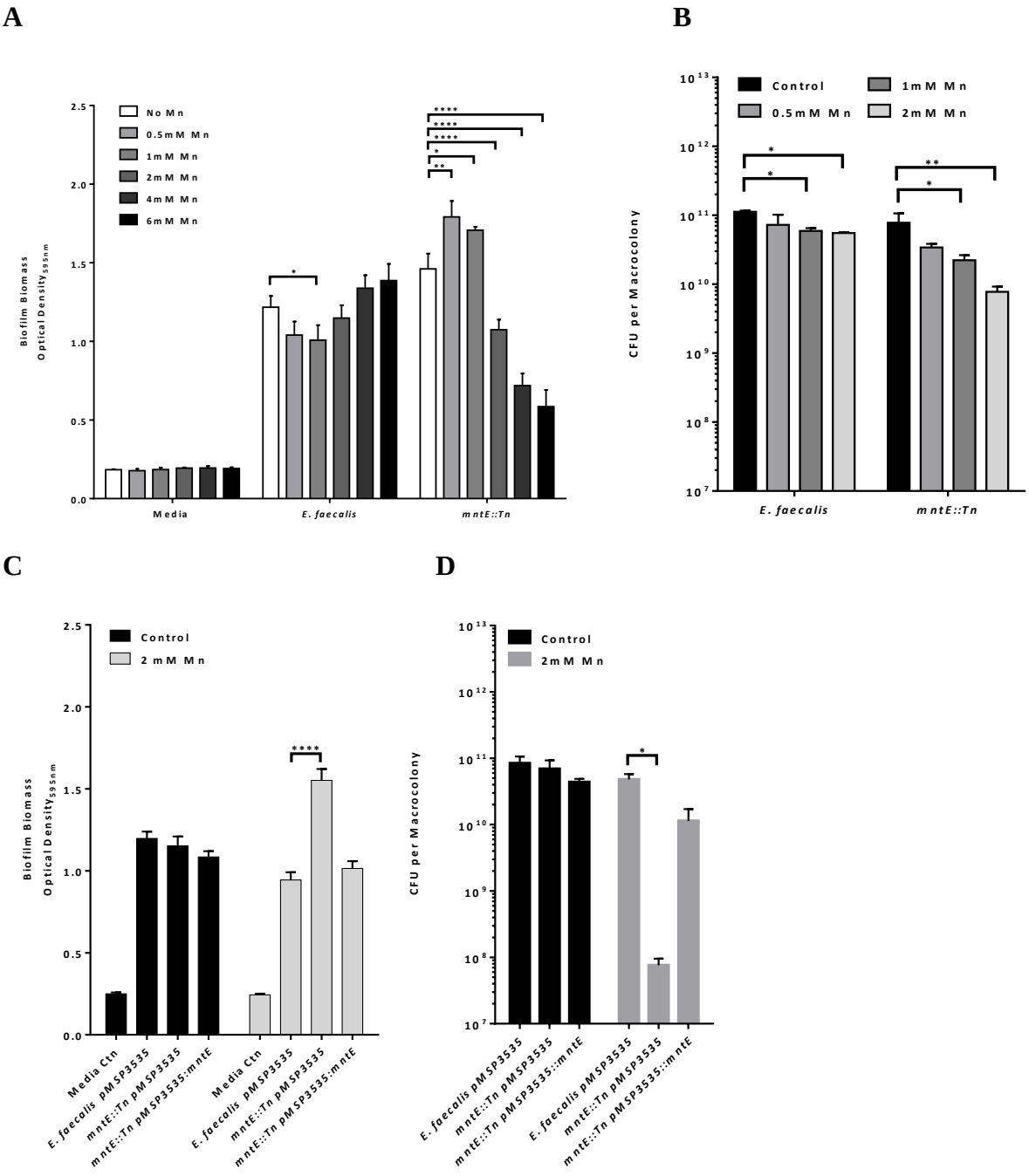

Figure 4.3. Manganese supplementation results in biofilm growth inhibition. 120 hr biofilms grown under increasing manganese supplementation. Adherence biofilm biomass quantification, CFU enumeration per macro-colony of wild type (A-B) and complement (C-D). N=3, n=3, repeated on non-consecutive days. Statistical analysis was performed using two-way ANOVA Fisher's LSD. * $P \leq 0.05$, ** $P \leq 0.01$, *** $P \leq 0.001$, **** $P \leq 0.0001$. Error bar represents standard error margin (SEM).

4.5.2 Upregulation of *mntE* in manganese supplemented media alleviates intracellular metal accumulation and modulates *E. faecalis* pathogenicity

The ability to regulate intracellular Mn is a key determinant in cell survival and growth. We postulate that the absence of MntE, which functions to export intracellular Mn during high Mn stress, consequently leads to increased intracellular Mn. To test this hypothesis, we performed ICP-MS on static 24 hr biofilms grown in 2 mM Mn-supplemented media. ICP-MS results revealed that *E. faecalis* wild type OG1RF has higher intracellular Mn (25-fold) concentrations when grown in 2 mM Mn supplemented media; however, the *mntE::Tn* mutant accumulates significantly more Mn (57-fold) as compared to wild type OG1RF under the same growth conditions. Notably, increased intracellular Mn (1494-fold) in the *mntE::Tn* mutant was also accompanied with increased intracellular Mg (8.13-fold), which was not observed in wild type OG1RF **(Figure 4.4A)**. We speculate that the increased Mg accumulation in the *mntE::Tn* mutant occurs as a consequence of increased Mn uptake. We reasoned that presence of *mntE* should results in decreased Mn and Mg accumulation in *mntE::Tn* mutant grown in 2 mM Mn supplemented media. Complementing *mntE* back to *mntE::Tn* mutant indeed decreased Mn accumulation (5.7-fold) significantly as compared to *mntE::Tn* pMSP3535 harboring empty vector **(Figure 4.4B)**. However, again, for reasons we don't understand, compared to the *mntE::Tn* mutant without pMSP3535, we did not observe reduction in intracellular Mg in *mntE::Tn* pMSP3535 harboring empty vector grown in 2 mM Mn supplemented media, and wild type OG1RF had significantly increased intracellular Mn in both control and Mn-supplemented media as compared to *mntE::Tn* pMSP3535 and *mntE::Tn* pMSP3535::*mntE* **(Figure 4.4B)**.

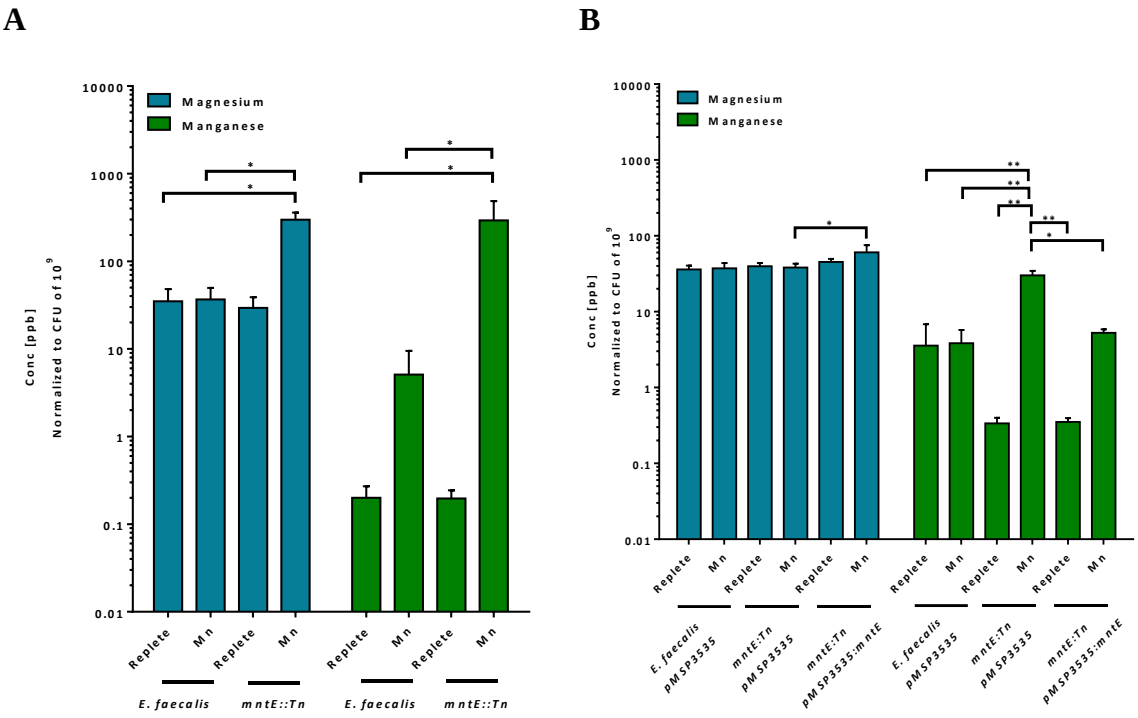

Figure 4.4. Intracellular manganese and magnesium content in 24 hr *E. faecalis* biofilm. (A) 24 hr wild type OG1RF and *mntE::Tn* mutant biofilms, N=6 and **(B)** complemented strains grown under 2 mM manganese, N=6, repeated on non-consecutive days. Statistical analysis was performed using two-way ANOVA Bonferroni multiple test. * $P \leq 0.05$, ** $P \leq 0.01$, *** $P \leq 0.001$, **** $P \leq 0.0001$. Error bar represents standard error margin (SEM).

4.5.3 Magnesium supplementation alleviate manganese mediated growth inhibition

Since we did not observe *E. faecalis* growth inhibition in 2 mM Mg (**Figure 4.1**), we reasoned that increased intracellular Mg was a bacterial response against the Mn accumulation, because intracellular Mn accumulation could affect Mg-dependent biological processes resulting in growth inhibition. By supplementing Mg in Mn-supplemented media, we would increase Mg availability which could alleviate Mn competition. To address this, we performed *in vitro* static planktonic growth assays, static 120hr biofilm assays, and macro-colony assays using 2 mM Mn-supplemented media with additional supplementation of increasing Mg. Indeed, our results showed that supplementing Mg to Mn-supplemented media restored growth to the *mntE::Tn* mutant **(Figure 4.5A-C)**. Although the wild type OG1RF exhibited attenuated biofilm formation with increasing Mg supplementation, planktonic growth did not appear to be inhibited. ICP-MS analysis

of intracellular Mn and Mg in both wild type OG1RF and *mntE::Tn* grown in 2 mM Mn-supplemented media, which is then supplemented with increasing Mg, revealed that both intracellular Mg (3-fold) and Mn (2.19-fold) are reduced **(Figure 4.5D-E)**. Collectively, these observations demonstrate that Mg supplementation results in reduced intracellular Mn and Mg levels, and rescues growth inhibition, but the reasons for this remain unclear **(Figure 4.5D-E)**.

A

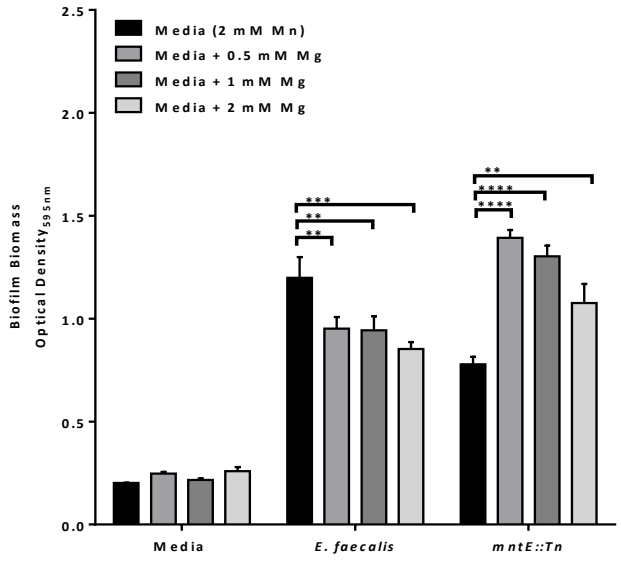

B

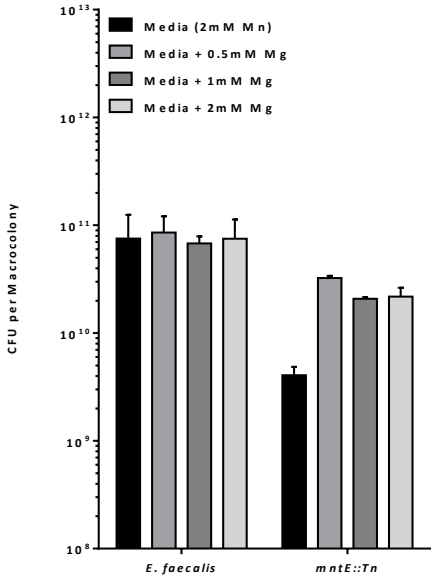

C

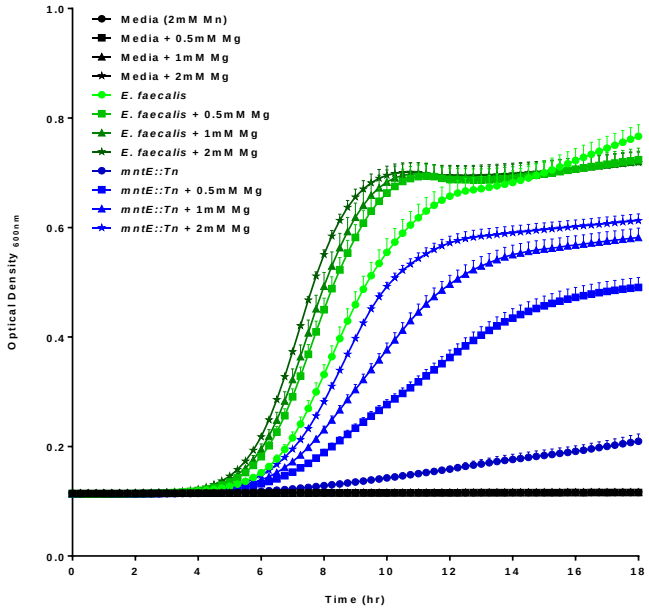

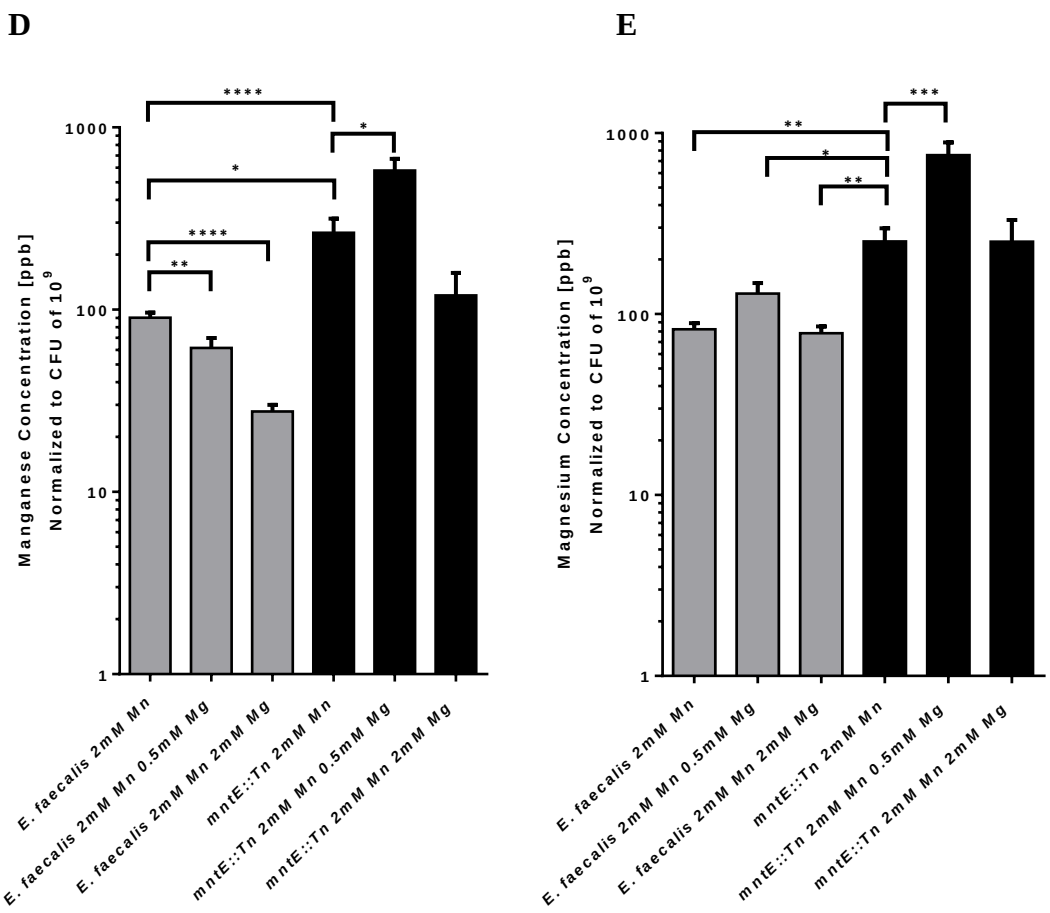

Figure 4.5. Magnesium supplementation rescue manganese mediated growth inhibition. (A) Adherence biofilm biomass quantification, (B) CFU enumeration per macro-colony and (C) planktonic growth kinetic. N=9, repeated on non-consecutive days. Statistical analysis was performed using two-way ANOVA Fisher's LSD. (D) ICP-MS analysis of intracellular manganese, (E) ICP-MS analysis of intracellular magnesium. N=6. Statistical analysis was performed using one-way ANOVA Fisher's LSD. * $P \leq 0.05$, ** $P \leq 0.01$, *** $P \leq 0.001$, **** $P \leq 0.0001$. Error bar represents standard error margin (SEM). N=6.

4.5.4 MntE efflux pump exhibit dual manganese and iron specificity which modulate growth and virulence gene expression

Since complementation of *mntE* alleviates intracellular Mn accumulation, we hypothesized that upregulation of *mntE* expression is an adaptive response for growing in high Mn environments. To address this, we performed qRT-PCR to determine *mntE* gene expression in wild type OG1RF biofilm grown in 2 mM Mn-supplemented media. Additionally, since upregulation of *S.*

pneumoniae MntE efflux pump modulates pilus gene expression (Rosch et al., 2009), we hypothesized that this might be similar in the case of *E. faecalis* as well. We observed that *mntE* and *ebpC* are upregulated in Mn-supplmented media **(Figure 4.6)**. Previously we have shown that the absence of the MntE efflux pump resulted in significantly enhanced iron-mediated biofilm growth independent of EET (Keogh et al., 2018). We therefore hypothesized that absence of *mntE* would consequently result in intracellular Fe accumulation driving iron-mediated biofilm growth. Indeed, ICP-MS analysis of *mntE::Tn* grown in iron–supplemented media showed significantly increased intracellular Fe (3.5-fold) as compared to wild type OG1RF. Complementing *mntE* back to *mntE::Tn* decreased intracellular Fe by 0.5-fold **(Figure 4.7)**. Global transcriptional analysis of *mntE::Tn* biofilm in comparison with wild type OG1RF biofilm in iron-supplemented mediarevealed that glycerol catabolic genes (*glpF2, glpO, glpK*) were the only genes which are significantly different **(Table 4.3)**. Since glycerol uptake and subsequently break down produces carbon metabolites which will be funneled towards glycolysis for energy production, upregulation of glycerol catabolic genes suggests that increased energy production and growth may drive enhanced biofilm growth in iron-supplemented media for the *mntE::Tn* mutant. In comparison, these three glycerol catabolic genes (*glpF2, glpO, glpK*) are not upregulated under Mn supplemented conditions **(Figure 4.6)** and previous global transcriptional analysis (**Chapter 3**) revealed that these genes are not iron responsive in wild type OG1RF. Collectively, these results indicate that upregulation of glycerol catabolic genes is specifically observed in the absence of *mntE* efflux pump when Fe levels are high.

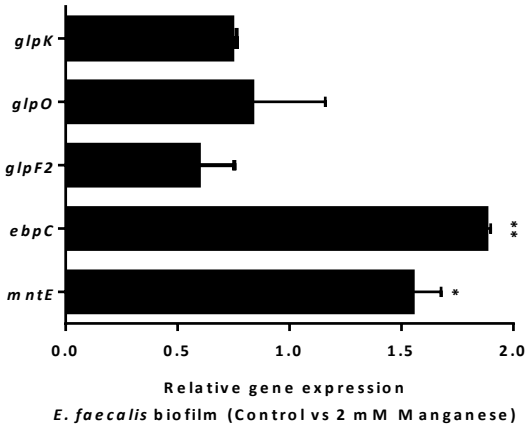

Figure 4.6. Comparison of gene expression in *E. faecalis* biofilm under manganese condition. (A) qRT-PCR of *E. faecalis* OG1RF biofilm grown in 2 mM manganese. N=6, repeated on non-

consecutive days. Statistical analysis is performed using one-way ANOVA Fisher LSD test. * $P \leq 0.05$, ** $P \leq 0.01$, *** $P \leq 0.001$, **** $P \leq 0.0001$.

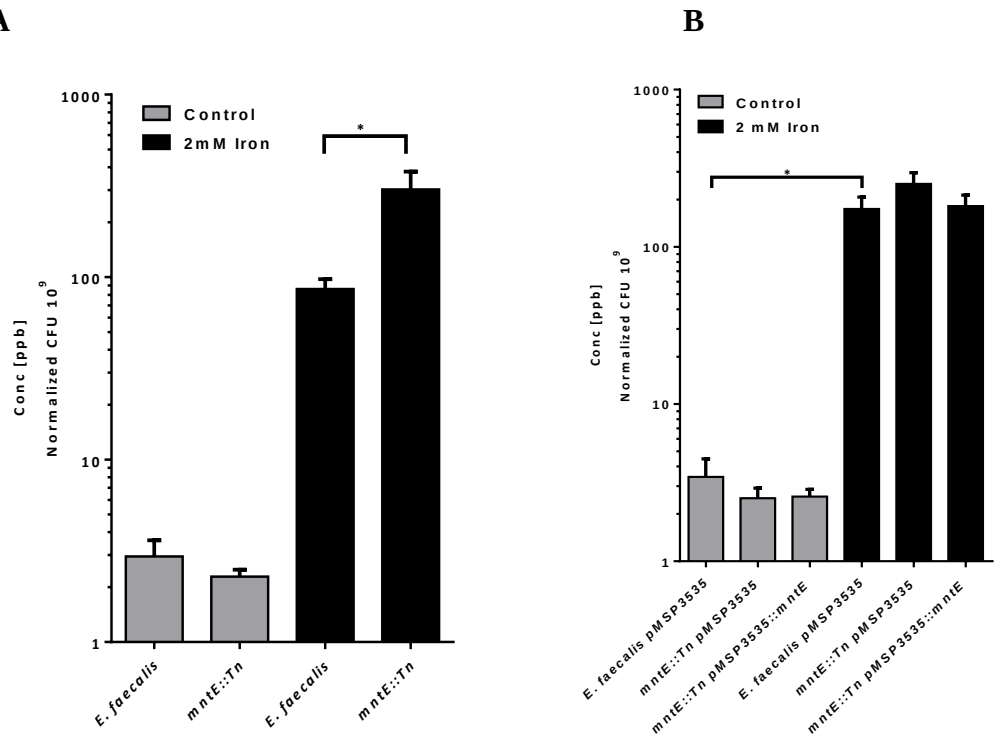

Figure 4.7. Iron quantification in *E. faecalis* biofilm grown in 2 mM iron. ICP-MS analysis of intracellular iron concentrations (ppb) in (A) normalized 10^9 cells in OG1RF and *mntE::Tn*, N=6 (B) complemented strain. N=9. Statistical analysis is performed using one-way ANOVA Fisher LSD test. * $P \leq 0.05$, ** $P \leq 0.01$, *** $P \leq 0.001$, **** $P \leq 0.0001$.

Table 4.3. Global transcriptional changes in *mntE::Tn* grown in 2 mM iron in comparison with OG1RF.

Gene Locus	Gene Name	Annotated Function	Log_2FC Expression
OG1RF_11590	glycerol transporter (*glpF2*)	Glycerol import	1.38628235
OG1RF_11591	alpha-glycerophosphate oxidase (*glpO*)	Conversion of L-alpha-glycerol-3-P to dihydroxyacetone-P	1.495219557
OG1RF_11592	glycerol kinase (*glpK*)	Conversion of glycerol to L-alpha-glycerol-3-P	1.906223762

All genes that were differentially regulated, with p-value of less than 0.05 and false discovery rate (FDR) of less than 0.05 were included. Red dots indicate genes that are down-regulated and green

dots indicate genes that are up-regulated. Pathway enrichment analysis was done by annotating genes in *E. faecalis* OG1RF to the KEGG database (KEGG identifier: efi). Gene classification was done based on their gene membership according to KEGG pathways. KEGG gene set enrichment analysis was performed using the Bioconductor package, clusterprofiler (version 3.8.1).

4.5.5 Absence of MntE do not alter oxidative stress tolerance

Since the absence of MntE results in intracellular Mn accumulation, we speculated that accumulation of Mn may enhance oxidative stress tolerance due to increase availability of Mn for Mn dependent antioxidant defenses against oxygen radicals. To address this, we performed oxidative stress tests to determine the sensitivity of the *mntE::Tn* mutant towards oxidizing reagents such as menadione and hydrogen peroxide. The *mntE::Tn* mutant did not display altered sensitivity to oxidizing agents **(Figure 4.8)** and hydrogen peroxide production did not significantly change either **(Figure 4.9)**.

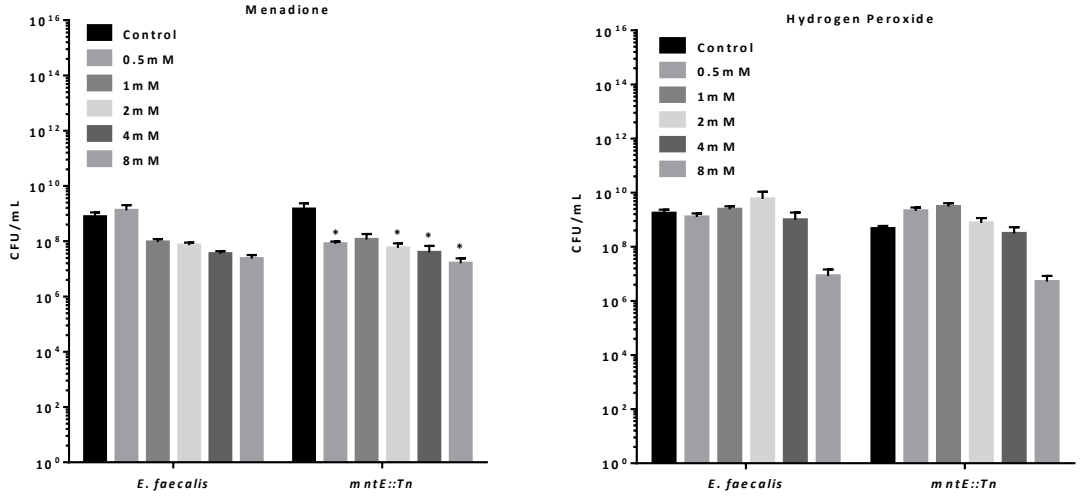

Figure 4.8. Oxidative stress tolerance against menadione and hydrogen peroxide. CFU enumeration 2 hrs post exposure to oxidizing agents. N=12, repeated on non-consecutive days. Statistical analysis is performed using two-way ANOVA Bonferroni multiple comparison test. * $P \leq 0.05$, ** $P \leq 0.01$, *** $P \leq 0.001$, **** $P \leq 0.0001$.

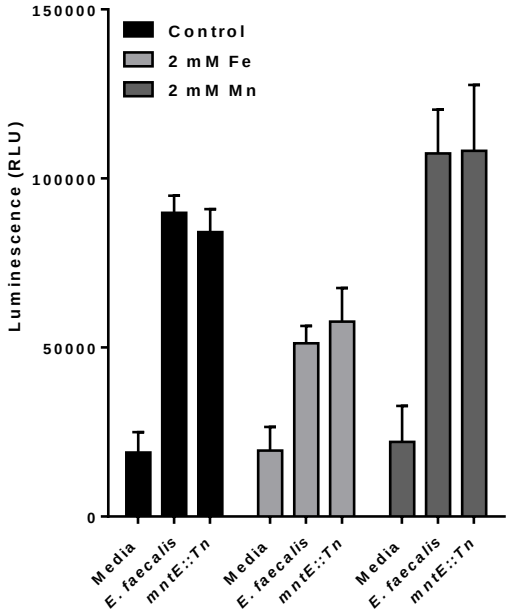

Figure 4.9. Hydrogen peroxide production under manganese and iron stress. Hydrogen peroxide quantification based on arbitrary luminescence readings. N=12, repeated on non-consecutive days. Statistical analysis is performed using two-way ANOVA Bonferroni multiple comparison test. * $P \leq 0.05$, ** $P \leq 0.01$, *** $P \leq 0.001$, **** $P \leq 0.0001$.

4.5.6 MntE efflux pump contributes to fitness in murine gastrointestinal (GI) tract colonization

Since the MntE Mn exporter protects *E. faecalis* from Mn stress, we next sought to address the contribution of MntE in mouse GI colonization. The *mntE::Tn* mutant displayed significantly reduced colonization in cecum, colon and small intestine as compared to wild type OG1RF **(Figure 4.10A)**. Our results demonstrate that MntE Mn exporter play a role in *E. faecalis* GI colonization.

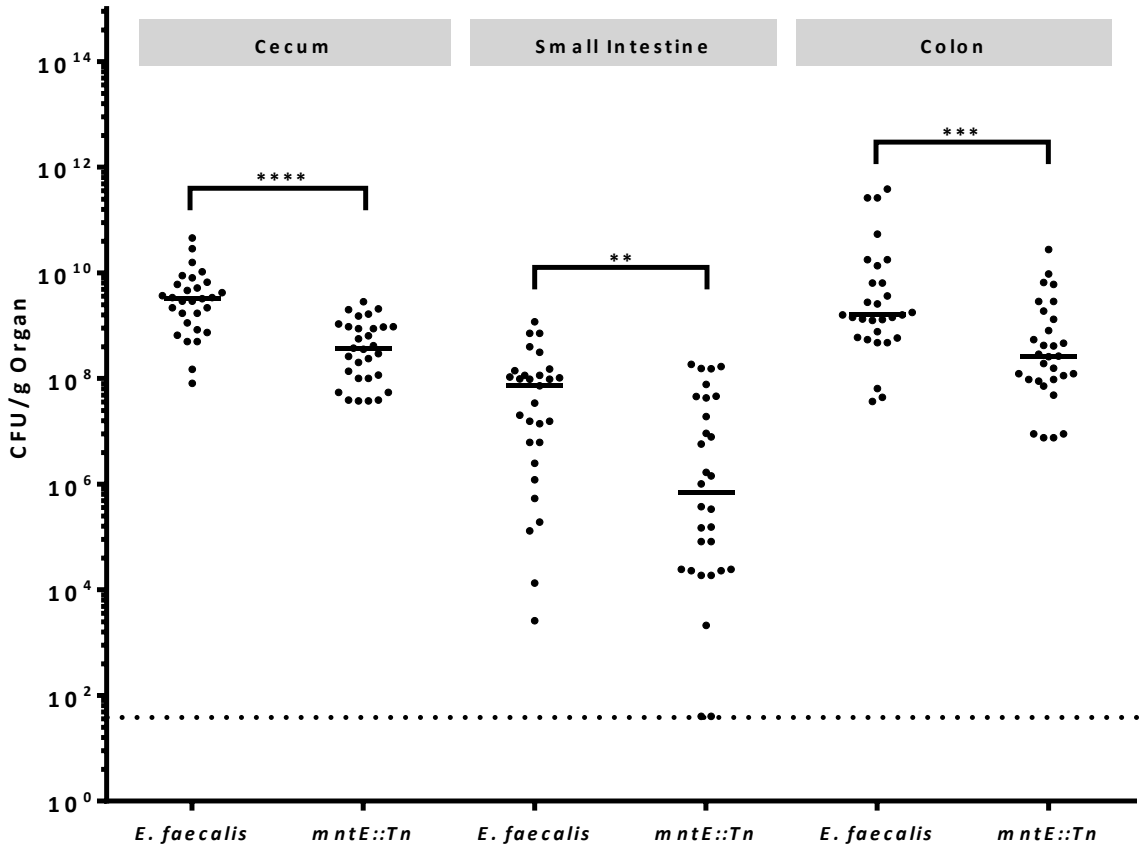

Figure 4.10. *E. faecalis* colonization in lower gastrointestinal tract of murine. N=6, n=5. Statistical significance was determined by Mann-Whitney test. * $P \leq 0.05$, ** $P \leq 0.01$, *** $P \leq 0.001$, **** $P \leq 0.0001$. Black line indicates median. Dotted line indicate limitation of detection of CFU <40.

4.6 Discussion

Manganese functions as a co-factor for enzymes involved in metabolism, signal transduction, and oxidative stress responses. Several studies have demonstrated the importance of Mn in bacterial physiology (Jakubovics and Jenkinson, 2001; Papp-Wallace and Maguire, 2006). Since Mn acquisition plays an important role in *E. faecalis* physiology (Colomer-Winter et al., 2018), the ability to import and efflux Mn must be regulated as well. While Mn import has been studied, Mn efflux has not been described in *E. faecalis*. Our results demonstrate that *E. faecalis* encodes a CDF protein which functions as a Mn efflux pump.

We show that MntE is a Mn exporter, and absence of *mntE* results in Mn-mediated growth inhibition and intracellular Mn accumulation. However, it is interesting to note that absence of *mntE* under high Fe conditions also resulted in intracellular Fe accumulation, but no growth inhibition was observed. Since Lopez and colleagues have shown that *mntE* is upregulated in 1 mM iron under planktonic shaking conditions (Lopez et al., 2012), this indicates that *mntE* is also iron responsive. However, in biofilms, *mntE* is not upregulated in iron-supplemented media (**Chapter 3**). Since absence of *mntE* in iron-supplemented media resulted in significantly enhanced biofilm growth (**Chapter 2**) (Keogh et al., 2018), we speculate that the increased intracellular Fe may modulate transcriptional changes which drive enhanced biofilm growth. Global transcriptional analysis revealed that glycerol catabolic genes (*glpF2, glpO, glpK*) are upregulated. The upregulation of the glycerol importer (*glpF2*), alpha-glycerophosphate oxidase (*glpO*), and glycerol kinase (*glpK*) suggest that increased uptake of glycerol precursors occurs, which in turn are converted to glycerol-3-phosphate (G3P) in glycolysis for energy production. The regulation of *glpK* is conserved in several gram positive and gram negative bacteria, and typically is regulated by carbon catabolite repression and sugar phosphotransferase system (PTS) (Yeh et al., 2009). In *E. coli*, glycerol catabolism is upregulated in the presence of glycerol and repressed in the presence of glucose (Voegele et al., 1993). It is unclear how iron stimulates upregulation of the glycerol catabolic genes, and future work should focus on characterizing the role of Fe on glycerol kinase (*glpK*) and alpha-glycerophosphate oxidase (*glpO*). Nevertheless, we speculate that Fe function as catalyst which drives glycerol catabolism. To validate that the upregulation in glycerol catabolic genes is a direct consequence of Fe accumulation in the absence of *mntE*, we are currently working on generating *mntE* deletion in glycerol catabolic gene (*glpF2, glpO, glpK*) transposon mutants,

as well as performing glycerol supplementation in the presence of Fe in the wild type OG1RF background to test whether enhanced biofilm growth in iron-supplemented media is due to increased expression of the glycerol catabolic genes.

Rosch and colleagues have previously shown that in *S. pneumoniae*, absence of the Mn exporter *mntE,* which consequently led to increased intracellular Mn, resulted in increased oxidative stress resilience, increased hydrogen peroxide production, and enhanced pilus expression on the cell surface (Rosch et al., 2009). We reasoned that since *S. pneumoniae* MntE shares 25% protein similarity with *E. faecalis* MntE, the absence of *mntE* should alter oxidative stress resilience and pilus expression. However, we did not observe significant difference in either of these phenotypes. We propose that since *E. faecalis* possess a number of antioxidant enzymes which collectively contribute to oxidative stress resilience (Flahaut et al., 1998; Riboulet et al., 2007b), that the absence of *mntE* is not sufficient to render it vulnerable to oxidative stress. By contrast, we observed that pilus expression is upregulated in the presence of Mn which suggests that Mn stress may promote virulence in host colonization since pilus expression impacts surface adherence and initial biofilm attachment. Although upregulation of pilus expression indeed can impact virulence, the *mntE::Tn* mutant is attenuated in GI colonization which indicate that inability to export Mn in the GI tract attenuate virulence. Even though it is unclear how absence of *mntE* impact colonization, we speculate that glycerol import may be involved since glycerol catabolic genes are upregulated in *mntE::Tn* mutant in the presence of Fe abundance. It is likely that glycerol is present in the GI tract, since glycerol has been previously described to be liberated from butyrate, a by-product from microbial fermentation by GI commensals (Bedford and Gong, 2017). Another study has also shown that glycerol accumulates in the colon which can be utilized by GI microbiota to form reuterin (De Weirdt et al., 2010) which has antimicrobial properties and protects the host from invading pathogenic *Salmonella spp* (De Weirdt et al., 2012). However, in the GI, there exist both Fe and Mn abundance. It is also likely that presence of Mn may lead to growth inhibition of *mntE::Tn* mutant. Notably, *E. faecalis* colonization titer differ in the different region of the GI tract, which may be due to the host microenvironment and/or the commensals which inhabit each region. Since the small intestine has a microenvironment which significantly differ to the lower GI region such as the colon (Said, 2018), *E. faecalis* may utilize different survival mechanisms for colonization in each site.

Additionally, since Mn stress in the absence of *mntE* results in growth inhibition, we sought to understand the underlying mechanism of inhibition. The observed increased in intracellular Mg suggested that uptake of Mg is essential in the absence of *mntE*. Indeed, we observed restoration of growth upon Mg supplementation. There is limited literature describing the interaction between Mg and Mn in prokaryotes. However, since both cation metals are redox-active and serve as catalysts for biological processes, it is not implausible that mismetallation of metalloproteins may be the causal agent for growth inhibition. Metal binding preferences of most metalloproteins often involve more than one metal, though with different affinity. It has been reported that Mg often competes with zinc for binding, and this metal competition may lead to inactivation of enzymes (Foster et al., 2014). Another study in *Bradyrhizobium japonicum* demonstrated that Mg dependent enzyme activities are inhibited by Mn when Mn is more abundant and Mg is limited, which support that Mg and Mn can bind to the same metalloprotein (Hohle and O'Brian, 2014).

Together, these findings suggest that MntE is a dual Mn and Fe responsive exporter with selective affinity. Future studies need to focus on elucidating the protein sequence that determine metal ion specificity for this transporter. We speculate that since Fe and Mn share similar ionic radii, both these metals are able to be transported by MntE. Since the MntE Mn exporter is conserved across a number of gram positive and gram negative bacteria, we propose that this Mn efflux system is a common strategy for Mn homeostasis. Moreover, absence of *mntE* also has a downstream effect on Fe associated signalling, as both our transcriptional analysis and previous studies in other bacteria suggest a significant degree of cross-talk between these pathways (Guedon et al., 2003; Hanks et al., 2006; Rosch et al., 2009). Nevertheless, this is the first study characterizing the role of *E. faecalis* Mn exporter and our findings demonstrate that the Mn exporter MntE contributes to *E. faecalis* fitness in GI colonization.

4.7 Acknowledgements

This work was supported by the National Research Foundation and Ministry of Education Singapore under its Research Centre of Excellence Programme, by the National Research Foundation under its Singapore NRF Fellowship programme (NRF-NRFF2011-11), and by the Ministry of Education Singapore under its Tier 2 programme (MOE2014-T2-2-124).

Chapter 5: Conclusion

5.1 Significance of findings

Enterococcus faecalis, as an opportunistic pathogen, is the causal agent for several clinical infections including bacteremia, endocarditis, wound and urinary tract infections. Of these infections, many are often biofilm associated and thus display biofilm associated virulence traits such as increased tolerance to antibiotics and reduced killing by immune cells. Additionally, iron accounts for one of the environmental cues in the host which can influence virulence and disease outcome, depending on the colonization niche and its iron availability.

In **Chapter 1** of this thesis, we have discussed on the gaps in current knowledge on the role of iron in E. faecalis biofilm physiology. Using an array of interdisciplinary approaches, we have shown that Fe impacts virulence and growth of *E. faecalis* biofilm. In **Chapter 2**, we have shown that *E. faecalis* utilise extracellular electron transfer (EET), a form of iron-dependent metabolism to promote biofilm growth. We have elucidated the EET mechanism which involves Ldh1. Subsequently, in **Chapter 3**, we also showed that both MenB and Ndh3, which are involved in demethylmenaquinone biosynthesis and flavin-mediated electron transfer respectively, contribute to iron-mediated EET. Together, these findings represent the first mechanistic description of EET by *E faecalis*, a gastrointestinal tract commensal and opportunistic pathogen. Moreover, we also show that an alternative role for *E. faecalis* endocarditis and biofilm associated pili (Ebp), a cell surface virulence factor, in addition to its role in adhesion, in binding iron to promote EET and iron-mediated biofilm growth. The co-purification of Fe with pilus, as well as the importance of pilus and *feoB* iron transporter for iron uptake suggest a model in which both ferric and ferrous iron are simultaneously being used by *E. faecalis* biofilm for EET and biofilm growth respectively. We have also shown that exposure to Fe resulted in 90 genes that are differentially regulated. By contrast, the transcriptional response to Fe in the MIDAS ($ebpA^{AWAGA}$) mutant resulted in 734 genes differentially regulated as compared to the wild type OG1RF. Furthermore, 32 genes that are iron-responsive, are differentially regulated due to altering MIDAS motif.

In **Chapter 4**, we show that regulation of Fe export have a profound impact on biofilm growth. Consistent with the inherent robust nature of *E. faecalis*, we also show Mn efflux pump (*mntE*) is

important for Mn tolerance. Phenotypic characterization of MntE Mn exporter support dual specificity to Mn and Fe, and impact glycerol catabolism (GlpF2, GlpO, GlpK) and pilus expression. Additionally, MntE is essential for mouse GI colonization.

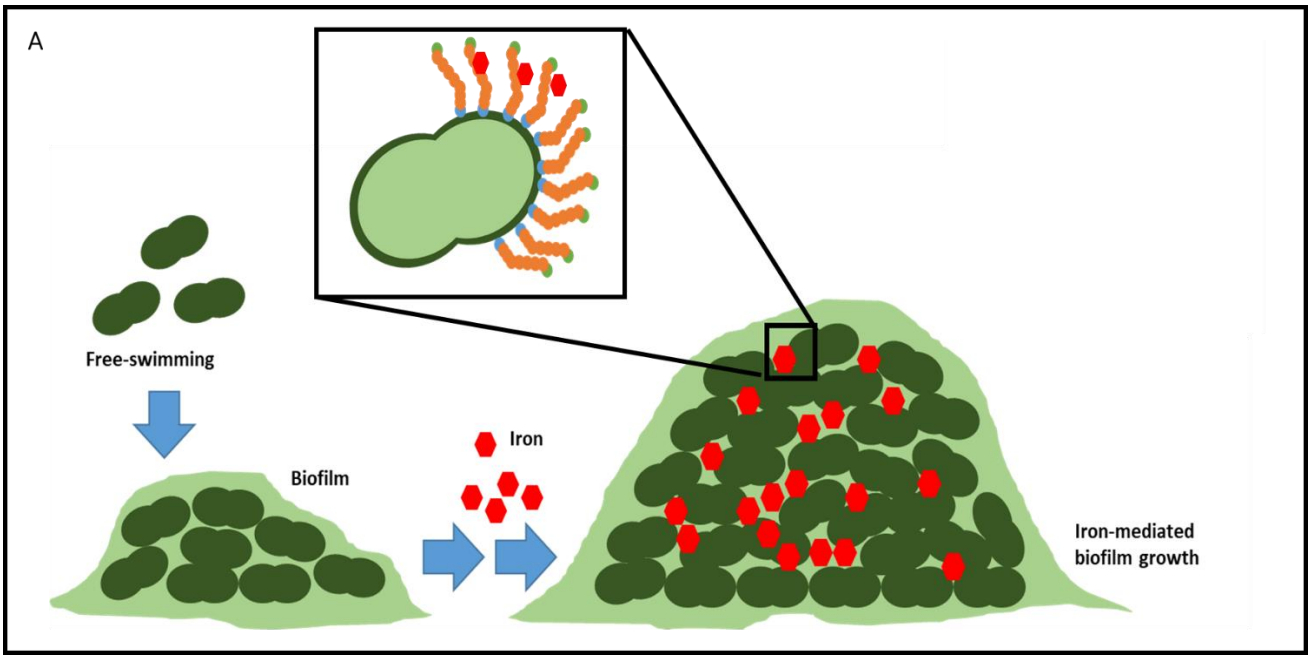

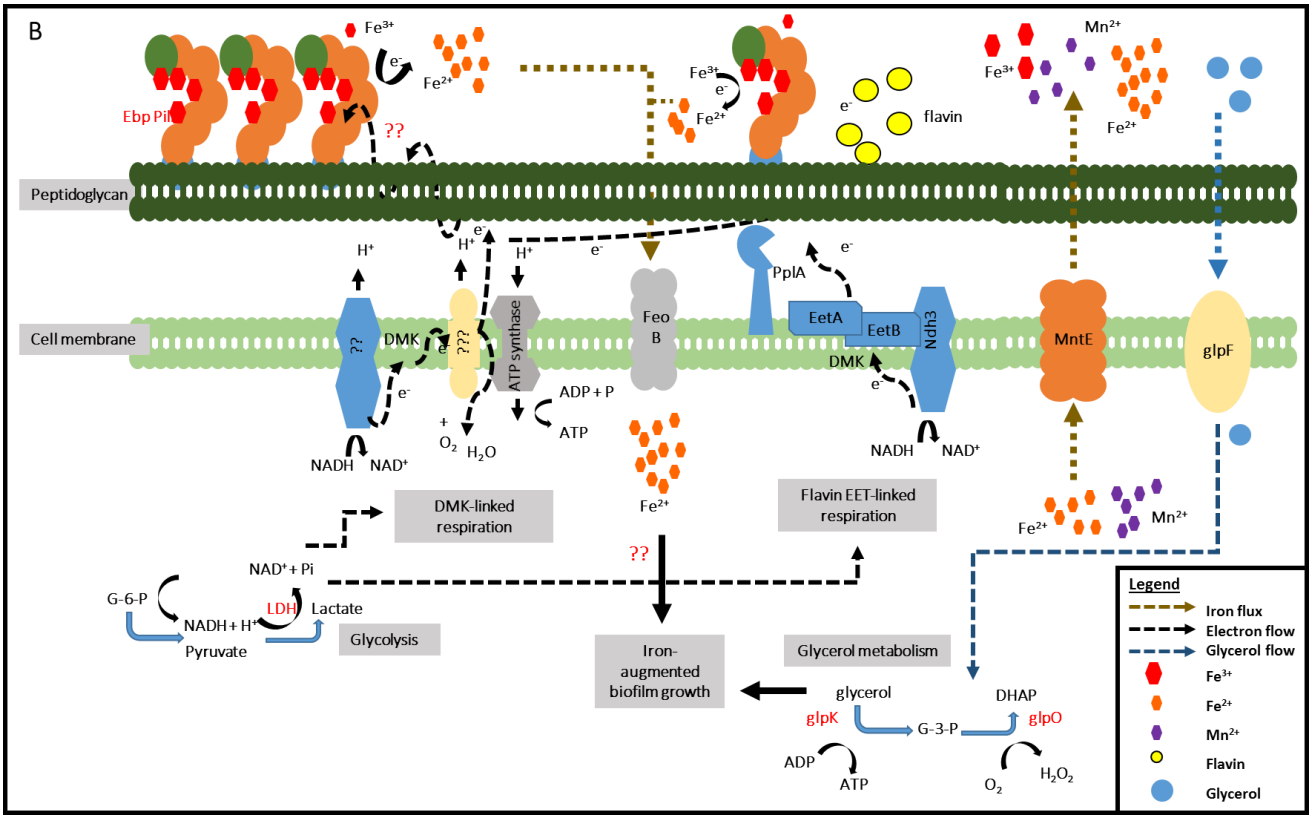

Figure 5.1 Model for the role of iron in *E. faecalis* biofilm. (A) Iron promote *E. faecalis* biofilm growth and **(B)** mechanisms underlying the role of iron in EET and iron-mediated biofilm growth.

Collectively, we also demonstrate that Fe and Mn play important roles in *E. faecalis* colonization of the mouse gastrointestinal tract. In summary, these findings have shed insights into the mechanisms governing iron-mediated biofilm growth in *E. faecalis*. Based on the above findings discussed, we present a schematic model on the role of iron in *E. faecalis* biofilm **(Figure 5.1)**. We now appreciate that several genes and pathways contribute to iron acquisition, iron tolerance, and metabolic switches which consequently may lead to iron-mediated biofilm growth. To abolish *E. faecalis* biofilm growth under such circumstances, treatment strategies should focus on eliminating the ability of *E. faecalis* in sensing and acquiring iron.

5.2 Future direction

We have shown that extracellular electron transfer (EET), an iron dependent form of metabolism, benefits *E. faecalis* biofilm formation, and we have elucidated the genetic factors that play a role in EET. However, there still exist several questions to be answered. Although we have shown that absence of L-lactate dehydrogenase (encoded by *ldh1*), NADH dehydrogenase (encoded by *ndh3*), DMK (synthesized by *menB*) and endocarditis and biofilm associated pilus (encoded by *ebpABC*) attenuate electron transfer respectively, electron transfer is not completely abolished in all circumstances. Deletion of both *menB* and *ndh3* completely abolish ability for EET. Moreover, in **Chapter 2**, several genes involved in iron-mediated biofilm growth are not attenuated for EET which uncouples iron-augmented biofilm phenotype and EET as two separate phenotypes. This is not unexpected since the initial library screen is not selective for iron-mediated EET. To identify all the genetic factors which may play a role in electron transfer, a library screen using ferric reductase assay which has been described previously (Light et al., 2018) that specifically look at reduction of ferric iron to ferrous iron, will allow us to identify alternative mechanisms of EET and address the redundancy mechanisms potentially used by *E. faecalis*. Using the mouse GI model, the absence of *ldh1* and *ndh3* respectively resulted in attenuated colonization **(Figure 5.2)**. This suggest that EET-mediated respiration play an important role in host GI colonization and is not due to general growth defect since absence of *ldh1* and *ndh3* do not impact growth *in vitro*

(data not shown). However, to what extent and how does EET contribute to *E. faecalis* GI colonization remains to be further characterized.

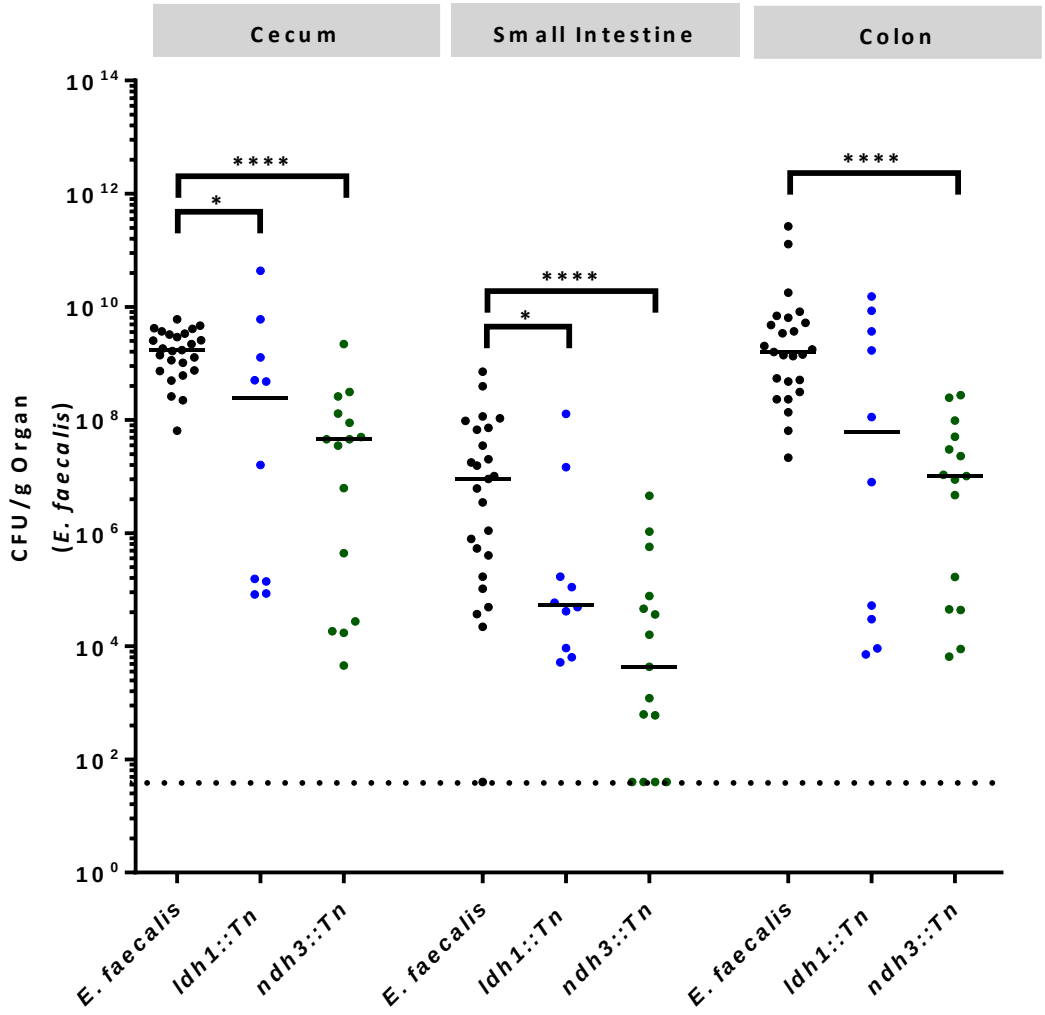

Figure 5.2. *E. faecalis ldh1::Tn* colonization in lower gastrointestinal tract of murine. GI tract colonization in mice fed with **(A)** high Mn diet and **(B)** high Fe diet Statistical significance was determined by Mann-Whitney test. For wild type N=5, n=5; for *ldh1*::Tn N=2, n=5; for *ndh3*::Tn N=3, n=5. * $P \leq 0.05$, ** $P \leq 0.01$, *** $P \leq 0.001$, **** $P \leq 0.0001$. Black line indicates median. Dotted line indicate limitation of detection of CFU <40.

Since type IV pilus have been shown to function as microbial nanowires which contributes to electron transfer in other bacteria species, we hypothesized that *E. faecalis* pili may contribute to electron transfer as well. Indeed, we showed that the pilus is involved in electron transfer. However, the mechanistic role of pili in this process remains to be clearly elucidated. Although

controversial since current literature indicate that the MIDAS motif binds divalent Mg^{2+}, it is plausible that the tertiary structure of the pilus allows for iron binding (Fe^{3+}). It has been hypothesized that the arrangement of aromatic amino acids due in part to the tertiary structure allow for electron hopping. To determine the binding affinity of iron to MIDAS motif, we could employ isothermal titration calorimetry on purified pilus extracts. Additionally, to determine the amino acid sequence arrangement that contributes to electron transfer, we could generate mutants with truncated pilus expression.

Lastly, we have also shown that the MntE efflux pump contribute to Mn tolerance. Although we have demonstrated that Mn mediated growth inhibition can be rescued upon Mg supplementation, the underlying mechanism of Mn mediated growth inhibition remains to be explored. We hypothesized that Mn competitively binds to Mg dependent metalloproteins which render these proteins inactivated, which leads to growth inhibition. Future work should focus on identifying Mg dependent enzymes and compare binding affinities of Mg and Mn to support our hypothesis. Collectively, these future experiments will further support our hypotheses.

Conference participation

- Lam L.N, Keogh D., Kline K. A. *Electrogenic Enterococcus faecalis biofilm: Elucidating the mechanism of ferric iron mediated extracellular electron transfer.* 15th International Congress of Bacteriology and Applied Microbiology, IUMS, Singapore, 17-21 July 2017. (Oral presentation)
- Lam L.N, Matysik A., Chong K.K.L, Low J. P. M, Marsili E., Kline K.A. *Endocarditis and biofilm associated pilus contributes to iron mediated augmented Enterococcus faecalis biofilm and extracellular electron transfer.* 6th ASM Conference on Cell-Cell Communication in Bacteria, Athens, Georgia, United States of America, 16-19 October 2017. (Poster presentation)
- Lam L.N, Matysik A., Chong K.K.L, Wong J.J, Low J. P. M, Marsili E., Kline K.A. *Endocarditis and biofilm associated pilus contributes to iron mediated augmented Enterococcus faecalis biofilm and extracellular electron transfer.* 5th International Conference on Enterococci, Chamonix, France, 15-19 April 2018. (Poster presentation)
- Lam L.N, Matysik A., Chong K.K.L, Wong J.J, Low J. P. M, Marsili E., Kline K.A. *Endocarditis and biofilm associated pilus contributes to iron mediated augmented Enterococcus faecalis biofilm and extracellular electron transfer.* Gordon Research Seminar, Waterville valley, NH, USA, 7-8th July 2018. (Oral presentation)

- Lam L.N, Matysik A., Chong K.K.L, Wong J.J, Low J. P. M, Marsili E., Kline K.A. *Endocarditis and biofilm associated pilus contributes to iron mediated augmented Enterococcus faecalis biofilm and extracellular electron transfer.* Gordon Research Conference, Waterville valley, NH, USA, 8-13th July 2018. (Poster presentation)

Publication

- **Keogh D[#], Lam L.N[#]**, Doyle L, Matysik A, Pavagadhi S, Umashankar S, Dale J.L, Boothroyd C.B, Dunny G.M, Swarup S, Williams R.B.H, Marsili E, Kline K.A. *Extracellular Electron Transfer Powers Enterococcus faecalis Biofilm Metabolism.* doi: 10.1128/mBio.00626-17 10 April 2018 mBio vol. 9 no. 2 e00626-17
- Ch'ng J.H, Chong K.K.L, **Lam L.N**, Wong J.J, Kline K.A. *Biofilm-associated Infection in Enterococci.* 18 October 2018 Nature Review Micro.1740-1534
- **Lam L.N**, Matysik A, Chong K.K.L, Wong J.J, Low P.M, Marsili E., Kline K.A. *Endocarditis and Biofilm Associated Pilus Contributes to Iron Mediated Augmented Enterococcus faecalis biofilm and Extracellular Electron Transfer*. (in preparation)
- **Lam L.N**, Chong K.K.L, Wong J.J, Kline K.A. *Enterococcus faecalis Cation Efflux Transporter Prevents Manganese Toxicity and contribute to fitness in murine gastrointestinal tract colonization.* (in preparation)
- **Lam L.N**, Tay W.H, Veleba M., Kline K.A. *Host-Associated Environmental Cues to Enterococci.* Frontier Review (in preparation)

References

Abbaspour, N., Hurrell, R., Kelishadi, R., 2014. Review on iron and its importance for human health. Journal of research in medical sciences : the official journal of Isfahan University of Medical Sciences 19, 164-174.

Abrantes, M.C., Lopes Mde, F., Kok, J., 2011. Impact of manganese, copper and zinc ions on the transcriptome of the nosocomial pathogen Enterococcus faecalis V583. PloS one 6, e26519.

Abrantes, M.C., Kok, J., Lopes Mde, F., 2013. EfaR is a major regulator of Enterococcus faecalis manganese transporters and influences processes involved in host colonization and infection. Infection and immunity 81, 935-944.

Aggarwal, C., Jimenez, J.C., Lee, H., Chlipala, G.E., Ratia, K., Federle, M.J., 2015. Identification of Quorum-Sensing Inhibitors Disrupting Signaling between Rgg and Short Hydrophobic Peptides in Streptococci. mBio 6.

Ahmed, E., Holmstrom, S.J., 2014. Siderophores in environmental research: roles and applications. Microbial biotechnology 7, 196-208.

Ali, L., Goraya, M.U., Arafat, Y., Ajmal, M., Chen, J.L., Yu, D., 2017. Molecular Mechanism of Quorum-Sensing in Enterococcus faecalis: Its Role in Virulence and Therapeutic Approaches. International journal of molecular sciences 18.

An, F.Y., Sulavik, M.C., Clewell, D.B., 1999. Identification and characterization of a determinant (eep) on the Enterococcus faecalis chromosome that is involved in production of the peptide sex pheromone cAD1. Journal of bacteriology 181, 5915-5921.

Andrews, S.C., Robinson, A.K., Rodriguez-Quinones, F., 2003. Bacterial iron homeostasis. FEMS microbiology reviews 27, 215-237.

Archibald, F., 1986. Manganese: its acquisition by and function in the lactic acid bacteria. Crit Rev Microbiol 13, 63-109.

Arias, C.A., Murray, B.E., 2012. The rise of the Enterococcus: beyond vancomycin resistance. Nature reviews. Microbiology 10, 266-278.

Bao, Y., Sakinc, T., Laverde, D., Wobser, D., Benachour, A., Theilacker, C., Hartke, A., Huebner, J., 2012. Role of mprF1 and mprF2 in the pathogenicity of Enterococcus faecalis. PloS one 7, e38458.

Barcelona-Andres, B., Marina, A., Rubio, V., 2002. Gene structure, organization, expression, and potential regulatory mechanisms of arginine catabolism in Enterococcus faecalis. Journal of bacteriology 184, 6289-6300.

Barnes, A.M., Ballering, K.S., Leibman, R.S., Wells, C.L., Dunny, G.M., 2012. Enterococcus faecalis produces abundant extracellular structures containing DNA in the absence of cell lysis during early biofilm formation. mBio 3, e00193-00112.

Barnes, A.M.T., Dale, J.L., Chen, Y., Manias, D.A., Greenwood Quaintance, K.E., Karau, M.K., Kashyap, P.C., Patel, R., Wells, C.L., Dunny, G.M., 2017. Enterococcus faecalis readily colonizes the entire gastrointestinal tract and forms biofilms in a germ-free mouse model. Virulence 8, 282-296.

Baureder, M., Hederstedt, L., 2012. Genes important for catalase activity in Enterococcus faecalis. PLoS One 7, e36725.

Bedford, A., Gong, J., 2017. Implications of butyrate and its derivatives for gut health and animal production. Animal Nutrition.

Benito, P., Miller, D., 1998. Iron absorption and bioavailability: An updated review. Nutrition Research 18, 581-603.

Bird, A.J., 2015. Cellular sensing and transport of metal ions: implications in micronutrient homeostasis. The Journal of nutritional biochemistry 26, 1103-1115.

Bizzini, A., Zhao, C., Auffray, Y., Hartke, A., 2009. The Enterococcus faecalis superoxide dismutase is essential for its tolerance to vancomycin and penicillin. The Journal of antimicrobial chemotherapy 64, 1196-1202.

Borgna-Pignatti, C., Marsella, M., 2015. Iron Chelation in Thalassemia Major. Clinical therapeutics.
Borisov, V.B., Gennis, R.B., Hemp, J., Verkhovsky, M.I., 2011. The cytochrome bd respiratory oxygen reductases. Biochim Biophys Acta 1807, 1398-1413.
Bourgogne, A., Thomson, L.C., Murray, B.E., 2010. Bicarbonate enhances expression of the endocarditis and biofilm associated pilus locus, ebpR-ebpABC, in Enterococcus faecalis. BMC microbiology 10, 17.
Bourgogne, A., Singh, K.V., Fox, K.A., Pflughoeft, K.J., Murray, B.E., Garsin, D.A., 2007. EbpR is important for biofilm formation by activating expression of the endocarditis and biofilm-associated pilus operon (ebpABC) of Enterococcus faecalis OG1RF. Journal of bacteriology 189, 6490-6493.
Bourgogne, A., Garsin, D.A., Qin, X., Singh, K.V., Sillanpaa, J., Yerrapragada, S., Ding, Y., Dugan-Rocha, S., Buhay, C., Shen, H., Chen, G., Williams, G., Muzny, D., Maadani, A., Fox, K.A., Gioia, J., Chen, L., Shang, Y., Arias, C.A., Nallapareddy, S.R., Zhao, M., Prakash, V.P., Chowdhury, S., Jiang, H., Gibbs, R.A., Murray, B.E., Highlander, S.K., Weinstock, G.M., 2008. Large scale variation in Enterococcus faecalis illustrated by the genome analysis of strain OG1RF. Genome biology 9, R110.
Brenot, A., King, K.Y., Caparon, M.G., 2005. The PerR regulon in peroxide resistance and virulence of Streptococcus pyogenes. Molecular microbiology 55, 221-234.
Britton, L., Malinowski, D.P., Fridovich, I., 1978. Superoxide dismutase and oxygen metabolism in Streptococcus faecalis and comparisons with other organisms. J Bacteriol 134, 229-236.
Brooijmans, R., Smit, B., Santos, F., van Riel, J., de Vos, W.M., Hugenholtz, J., 2009. Heme and menaquinone induced electron transport in lactic acid bacteria. Microbial cell factories 8, 28.
Bruyneel, B., Vandewoestyne, M., Verstraete, W., 1989. Lactic-Acid Bacteria - Microorganisms Able to Grow in the Absence of Available Iron and Copper. Biotechnol Lett 11, 401-406.
Bullen, J.J., Rogers, H.J., Spalding, P.B., Ward, C.G., 2006. Natural resistance, iron and infection: a challenge for clinical medicine. Journal of medical microbiology 55, 251-258.
Byappanahalli, M., Fujioka, R., 2004. Indigenous soil bacteria and low moisture may limit but allow faecal bacteria to multiply and become a minor population in tropical soils. Water Science and Technology 50, 27-32.
Cabiscol, E., Tamarit, J., Ros, J., 2000. Oxidative stress in bacteria and protein damage by reactive oxygen species. International microbiology : the official journal of the Spanish Society for Microbiology 3, 3-8.
Camilli, A., Bassler, B.L., 2006. Bacterial small-molecule signaling pathways. Science (New York, N.Y.) 311, 1113-1116.
Carrondo, M.A., 2003. Ferritins, iron uptake and storage from the bacterioferritin viewpoint. The EMBO journal 22, 1959-1968.
Cassat, J.E., Skaar, E.P., 2013. Iron in infection and immunity. Cell Host Microbe 13, 509-519.
Ch'ng, J.-H., Chong, K.K.L., Lam, L.N., Wong, J.J., Kline, K.A., 2018. Biofilm-associated infection by enterococci. Nature Reviews Microbiology.
Chan, C.S., Fakra, S.C., Emerson, D., Fleming, E.J., Edwards, K.J., 2011. Lithotrophic iron-oxidizing bacteria produce organic stalks to control mineral growth: implications for biosignature formation. The ISME journal 5, 717-727.
Chandler, J.R., Dunny, G.M., 2008. Characterization of the sequence specificity determinants required for processing and control of sex pheromone by the intramembrane protease Eep and the plasmid-encoded protein PrgY. Journal of bacteriology 190, 1172-1183.
Chávez de Paz, L.E., Lemos, J.A., Wickström, C., Sedgley, C.M., 2012. Role of (p)ppGpp in Biofilm Formation by Enterococcus faecalis. Applied and environmental microbiology 78, 1627-1630.
Chen, G.Y., McDougal, C.E., D'Antonio, M.A., Portman, J.L., Sauer, J.-D., 2017a. A Genetic Screen Reveals that Synthesis of 1, 4-Dihydroxy-2-Naphthoate (DHNA), but Not Full-Length Menaquinone, Is Required for Listeria monocytogenes Cytosolic Survival. mBio 8, e00119-00117.

Chen, Y., Bandyopadhyay, A., Kozlowicz, B.K., Haemig, H.A.H., Tai, A., Hu, W.S., Dunny, G.M., 2017b. Mechanisms of peptide sex pheromone regulation of conjugation in Enterococcus faecalis. MicrobiologyOpen 6.
Chong, K.K.L., Tay, W.H., Janela, B., Yong, A.M.H., Liew, T.H., Madden, L., Keogh, D., Barkham, T.M.S., Ginhoux, F., Becker, D.L., Kline, K.A., 2017. Enterococcus faecalis Modulates Immune Activation and Slows Healing During Wound Infection. J Infect Dis 216, 1644-1654.
Colomer-Winter, C., Gaca, A.O., Lemos, J.A., 2017. Association of Metal Homeostasis and (p)ppGpp Regulation in the Pathophysiology of Enterococcus faecalis. Infection and immunity 85.
Colomer-Winter, C., Flores-Mireles, A.L., Baker, S.P., Frank, K.L., Lynch, A.J.L., Hultgren, S.J., Kitten, T., Lemos, J.A., 2018. Manganese acquisition is essential for virulence of Enterococcus faecalis. PLOS Pathogens 14, e1007102.
Comolli, L.R., Luef, B., Chan, C.S., 2011. High-resolution 2D and 3D cryo-TEM reveals structural adaptations of two stalk-forming bacteria to an Fe-oxidizing lifestyle. Environmental microbiology 13, 2915-2929.
Cook, L.C., Federle, M.J., 2014. Peptide pheromone signaling in Streptococcus and Enterococcus. FEMS microbiology reviews 38, 473-492.
Corrigan, R.M., Campeotto, I., Jeganathan, T., Roelofs, K.G., Lee, V.T., Gründling, A., 2013. Systematic identification of conserved bacterial c-di-AMP receptor proteins. Proceedings of the National Academy of Sciences 110, 9084-9089.
Creti, R., Koch, S., Fabretti, F., Baldassarri, L., Huebner, J., 2006. Enterococcal colonization of the gastro-intestinal tract: role of biofilm and environmental oligosaccharides. BMC microbiology 6, 60.
Dale, J.L., Nilson, J.L., Barnes, A.M.T., Dunny, G.M., 2017. Restructuring of Enterococcus faecalis biofilm architecture in response to antibiotic-induced stress. NPJ Biofilms Microbiomes 3, 15.
Dale, J.L., Cagnazzo, J., Phan, C.Q., Barnes, A.M., Dunny, G.M., 2015. Multiple roles for Enterococcus faecalis glycosyltransferases in biofilm-associated antibiotic resistance, cell envelope integrity, and conjugative transfer. Antimicrob Agents Chemother 59, 4094-4105.
De Weirdt, R., Possemiers, S., Vermeulen, G., Moerdijk-Poortvliet, T.C., Boschker, H.T., Verstraete, W., Van de Wiele, T., 2010. Human faecal microbiota display variable patterns of glycerol metabolism. FEMS microbiology ecology 74, 601-611.
De Weirdt, R., Crabbe, A., Roos, S., Vollenweider, S., Lacroix, C., van Pijkeren, J.P., Britton, R.A., Sarker, S., Van de Wiele, T., Nickerson, C.A., 2012. Glycerol supplementation enhances L. reuteri's protective effect against S. Typhimurium colonization in a 3-D model of colonic epithelium. PloS one 7, e37116.
Debroy, S., van der Hoeven, R., Singh, K.V., Gao, P., Harvey, B.R., Murray, B.E., Garsin, D.A., 2012. Development of a genomic site for gene integration and expression in Enterococcus faecalis. J Microbiol Methods 90, 1-8.
Drakesmith, H., Nemeth, E., Ganz, T., 2015. Ironing out Ferroportin. Cell metabolism 22, 777-787.
Dunny, G.M., Brown, B.L., Clewell, D.B., 1978. Induced cell aggregation and mating in Streptococcus faecalis: evidence for a bacterial sex pheromone. Proc Natl Acad Sci U S A 75, 3479-3483.
Dunny, G.M., Hancock, L.E., Shankar, N., 2014. Enterococcal Biofilm Structure and Role in Colonization and Disease. In: Gilmore, M.S. (Ed.), Enterococci: From Commensals to Leading Causes of Drug Resistant Infection. Massachusetts Eye and Ear Infirmary, Boston.
Fabretti, F., Theilacker, C., Baldassarri, L., Kaczynski, Z., Kropec, A., Holst, O., Huebner, J., 2006. Alanine esters of enterococcal lipoteichoic acid play a role in biofilm formation and resistance to antimicrobial peptides. Infection and immunity 74, 4164-4171.
Faulkner, M.J., Ma, Z., Fuangthong, M., Helmann, J.D., 2012. Derepression of the Bacillus subtilis PerR Peroxide Stress Response Leads to Iron Deficiency. Journal of bacteriology 194, 1226-1235.
Fisher, K., Phillips, C., 2009. The ecology, epidemiology and virulence of Enterococcus. Microbiology (Reading, England) 155, 1749-1757.

Flahaut, S., Laplace, J.M., Frere, J., Auffray, Y., 1998. The oxidative stress response in Enterococcus faecalis: relationship between H2O2 tolerance and H2O2 stress proteins. Letters in applied microbiology 26, 259-264.
Flemming, H.-C., Wingender, J., Szewzyk, U., Steinberg, P., Rice, S.A., Kjelleberg, S., 2016. Biofilms: an emergent form of bacterial life. Nature Reviews Microbiology 14, 563.
Foster, A.W., Osman, D., Robinson, N.J., 2014. Metal Preferences and Metallation. The Journal of biological chemistry 289, 28095-28103.
Frank, K.L., Barnes, A.M., Grindle, S.M., Manias, D.A., Schlievert, P.M., Dunny, G.M., 2012. Use of recombinase-based in vivo expression technology to characterize Enterococcus faecalis gene expression during infection identifies in vivo-expressed antisense RNAs and implicates the protease Eep in pathogenesis. Infection and immunity 80, 539-549.
Frank, K.L., Vergidis, P., Brinkman, C.L., Greenwood Quaintance, K.E., Barnes, A.M., Mandrekar, J.N., Schlievert, P.M., Dunny, G.M., Patel, R., 2015. Evaluation of the Enterococcus faecalis Biofilm-Associated Virulence Factors AhrC and Eep in Rat Foreign Body Osteomyelitis and In Vitro Biofilm-Associated Antimicrobial Resistance. PloS one 10, e0130187.
Frank, K.L., Guiton, P.S., Barnes, A.M., Manias, D.A., Chuang-Smith, O.N., Kohler, P.L., Spaulding, A.R., Hultgren, S.J., Schlievert, P.M., Dunny, G.M., 2013. AhrC and Eep are biofilm infection-associated virulence factors in Enterococcus faecalis. Infection and immunity 81, 1696-1708.
Frankenberg, L., Brugna, M., Hederstedt, L., 2002a. Enterococcus faecalis heme-dependent catalase. Journal of bacteriology 184, 6351-6356.
Frankenberg, L., Brugna, M., Hederstedt, L., 2002b. Enterococcus faecalis Heme-Dependent Catalase. Journal of Bacteriology 184, 6351-6356.
Frawley, E.R., Fang, F.C., 2014. The ins and outs of bacterial iron metabolism. Molecular microbiology 93, 609-616.
Ganz, T., Nemeth, E., 2012a. Hepcidin and iron homeostasis. Biochimica et biophysica acta 1823, 1434-1443.
Ganz, T., Nemeth, E., 2012b. Iron metabolism: interactions with normal and disordered erythropoiesis. Cold Spring Harbor perspectives in medicine 2, a011668.
Gao, P., Pinkston, K.L., Nallapareddy, S.R., van Hoof, A., Murray, B.E., Harvey, B.R., 2010. Enterococcus faecalis rnjB is required for pilin gene expression and biofilm formation. Journal of bacteriology 192, 5489-5498.
Garsin, D.A., Frank, K.L., Silanpää, J., Ausubel, F.M., Hartke, A., Shankar, N., Murray, B.E., 2014. Pathogenesis and Models of Enterococcal Infection. In: Gilmore, M.S. (Ed.), Enterococci: From Commensals to Leading Causes of Drug Resistant Infection. Massachusetts Eye and Ear Infirmary, Boston.
Gentry-Weeks, C.R., Karkhoff-Schweizer, R., Pikis, A., Estay, M., Keith, J.M., 1999. Survival of Enterococcus faecalis in mouse peritoneal macrophages. Infection and immunity 67, 2160-2165.
Giraffa, G., 2002. Enterococci from foods. FEMS microbiology reviews 26, 163-171.
Glasser, N.R., Saunders, S.H., Newman, D.K., 2017. The Colorful World of Extracellular Electron Shuttles. Annual review of microbiology 71, 731-751.
Gloag, E.S., Turnbull, L., Huang, A., Vallotton, P., Wang, H., Nolan, L.M., Mililli, L., Hunt, C., Lu, J., Osvath, S.R., Monahan, L.G., Cavaliere, R., Charles, I.G., Wand, M.P., Gee, M.L., Prabhakar, R., Whitchurch, C.B., 2013. Self-organization of bacterial biofilms is facilitated by extracellular DNA. Proceedings of the National Academy of Sciences of the United States of America 110, 11541-11546.
Gorby, Y.A., Yanina, S., McLean, J.S., Rosso, K.M., Moyles, D., Dohnalkova, A., Beveridge, T.J., Chang, I.S., Kim, B.H., Kim, K.S., Culley, D.E., Reed, S.B., Romine, M.F., Saffarini, D.A., Hill, E.A., Shi, L., Elias, D.A., Kennedy, D.W., Pinchuk, G., Watanabe, K., Ishii, S., Logan, B., Nealson, K.H., Fredrickson, J.K., 2006. Electrically conductive bacterial nanowires produced by Shewanella oneidensis strain MR-1 and other

microorganisms. Proceedings of the National Academy of Sciences of the United States of America 103, 11358-11363.
Grass, G., Otto, M., Fricke, B., Haney, C.J., Rensing, C., Nies, D.H., Munkelt, D., 2005. FieF (YiiP) from Escherichia coli mediates decreased cellular accumulation of iron and relieves iron stress. Archives of microbiology 183, 9-18.
Gries, C.M., Bruger, E.L., Moormeier, D.E., Scherr, T.D., Waters, C.M., Kielian, T., 2016. Cyclic di-AMP Released from Staphylococcus aureus Biofilm Induces a Macrophage Type I Interferon Response. Infection and immunity 84, 3564-3574.
Guedon, E., Moore, C.M., Que, Q., Wang, T., Ye, R.W., Helmann, J.D., 2003. The global transcriptional response of Bacillus subtilis to manganese involves the MntR, Fur, TnrA and sigmaB regulons. Molecular microbiology 49, 1477-1491.
Guilhen, C., Forestier, C., Balestrino, D., 2017. Biofilm dispersal: multiple elaborate strategies for dissemination of bacteria with unique properties. Molecular microbiology 105, 188-210.
Guiton, P.S., Hung, C.S., Kline, K.A., Roth, R., Kau, A.L., Hayes, E., Heuser, J., Dodson, K.W., Caparon, M.G., Hultgren, S.J., 2009. Contribution of autolysin and Sortase a during Enterococcus faecalis DNA-dependent biofilm development. Infect Immun 77, 3626-3638.
Hallberg, L., 2001. Perspectives on nutritional iron deficiency. Annual review of nutrition 21, 1-21.
Hallgren, A., Claesson, C., Saeedi, B., Monstein, H.J., Hanberger, H., Nilsson, L.E., 2009. Molecular detection of aggregation substance, enterococcal surface protein, and cytolysin genes and in vitro adhesion to urinary catheters of Enterococcus faecalis and E. faecium of clinical origin. International journal of medical microbiology : IJMM 299, 323-332.
Hancock, L.E., Perego, M., 2004a. Systematic inactivation and phenotypic characterization of two-component signal transduction systems of Enterococcus faecalis V583. Journal of bacteriology 186, 7951-7958.
Hancock, L.E., Perego, M., 2004b. The Enterococcus faecalis fsr two-component system controls biofilm development through production of gelatinase. J Bacteriol 186, 5629-5639.
Hanks, T.S., Liu, M., McClure, M.J., Fukumura, M., Duffy, A., Lei, B., 2006. Differential regulation of iron- and manganese-specific MtsABC and heme-specific HtsABC transporters by the metalloregulator MtsR of group A Streptococcus. Infection and immunity 74, 5132-5139.
Hassan, K.A., Fagerlund, A., Elbourne, L.D.H., Vörös, A., Kroeger, J.K., Simm, R., Tourasse, N.J., Finke, S., Henderson, P.J.F., Økstad, O.A., Paulsen, I.T., Kolstø, A.-B., 2017. The putative drug efflux systems of the Bacillus cereus group. PloS one 12, e0176188.
He, Z., Liang, J., Zhou, W., Xie, Q., Tang, Z., Ma, R., Huang, Z., 2016. Effect of the quorum-sensing luxS gene on biofilm formation by Enterococcus faecalis. Eur J Oral Sci 124, 234-240.
Hentze, M.W., Muckenthaler, M.U., Andrews, N.C., 2004. Balancing acts: molecular control of mammalian iron metabolism. Cell 117, 285-297.
Higuita, N.I.A., Huycke, M.M., 2014. Enterococcal Disease, Epidemiology, and Implications for Treatment. In: Gilmore, M.S. (Ed.), Enterococci: From Commensals to Leading Causes of Drug Resistant Infection. Massachusetts Eye and Ear Infirmary, Boston.
Hirt, H., Greenwood-Quaintance, K.E., Karau, M.J., Till, L.M., Kashyap, P.C., Patel, R., Dunny, G.M., 2018. Enterococcus faecalis Sex Pheromone cCF10 Enhances Conjugative Plasmid Transfer In Vivo. mBio 9.
Hohle, T.H., O'Brian, M.R., 2014. Magnesium-dependent processes are targets of bacterial manganese toxicity. Molecular microbiology 93, 736-747.
Hollenbeck, B.L., Rice, L.B., 2012. Intrinsic and acquired resistance mechanisms in enterococcus. Virulence 3, 421-433.
Holmes, D.E., Dang, Y., Walker, D.J., Lovley, D.R., 2016. The electrically conductive pili of Geobacter species are a recently evolved feature for extracellular electron transfer. Microbial genomics 2, e000072.

Hood, M.I., Skaar, E.P., 2012. Nutritional immunity: transition metals at the pathogen-host interface. Nature reviews. Microbiology 10, 525-537.
Huang, X., Shin, J.H., Pinochet-Barros, A., Su, T.T., Helmann, J.D., 2017. Bacillus subtilis MntR coordinates the transcriptional regulation of manganese uptake and efflux systems. Molecular microbiology 103, 253-268.
Hufnagel, M., Koch, S., Creti, R., Baldassarri, L., Huebner, J., 2004. A putative sugar-binding transcriptional regulator in a novel gene locus in Enterococcus faecalis contributes to production of biofilm and prolonged bacteremia in mice. J Infect Dis 189, 420-430.
Hufnagel, M., Liese, C., Loescher, C., Kunze, M., Proempeler, H., Berner, R., Krueger, M., 2007. Enterococcal colonization of infants in a neonatal intensive care unit: associated predictors, risk factors and seasonal patterns. BMC Infect Dis 7, 107.
Huycke, M.M., Abrams, V., Moore, D.R., 2002. Enterococcus faecalis produces extracellular superoxide and hydrogen peroxide that damages colonic epithelial cell DNA. Carcinogenesis 23, 529-536.
Jakubovics, N.S., Jenkinson, H.F., 2001. Out of the iron age: new insights into the critical role of manganese homeostasis in bacteria. Microbiology (Reading, England) 147, 1709-1718.
Jansen, B., Goodman, L.P., Ruiten, D., 1993. Bacterial adherence to hydrophilic polymer-coated polyurethane stents. Gastrointestinal endoscopy 39, 670-673.
Johnson, J.R., Clabots, C., Hirt, H., Waters, C., Dunny, G., 2004. Enterococcal aggregation substance and binding substance are not major contributors to urinary tract colonization by Enterococcus faecalis in a mouse model of ascending unobstructed urinary tract infection. Infection and immunity 72, 2445-2448.
Kajfasz, J.K., Mendoza, J.E., Gaca, A.O., Miller, J.H., Koselny, K.A., Giambiagi-Demarval, M., Wellington, M., Abranches, J., Lemos, J.A., 2012. The Spx regulator modulates stress responses and virulence in Enterococcus faecalis. Infection and immunity 80, 2265-2275.
Kammler, M., Schön, C., Hantke, K., 1993. Characterization of the ferrous iron uptake system of Escherichia coli. Journal of bacteriology 175, 6212-6219.
Keane, P.F., Bonner, M.C., Johnston, S.R., Zafar, A., Gorman, S.P., 1994. Characterization of biofilm and encrustation on ureteric stents in vivo. British journal of urology 73, 687-691.
Keogh, D., Tay, W.H., Ho, Y.Y., Dale, J.L., Chen, S., Umashankar, S., Williams, R.B., Chen, S.L., Dunny, G.M., Kline, K.A., 2016a. Enterococcal Metabolite Cues Facilitate Interspecies Niche Modulation and Polymicrobial Infection. Cell host & microbe 20, 493-503.
Keogh, D., Tay, W.H., Ho, Y.Y., Dale, J.L., Chen, S., Umashankar, S., Williams, R.B.H., Chen, S.L., Dunny, G.M., Kline, K.A., 2016b. Enterococcal Metabolite Cues Facilitate Interspecies Niche Modulation and Polymicrobial Infection. Cell Host Microbe 20, 493-503.
Keogh, D., Lam, L.N., Doyle, L.E., Matysik, A., Pavagadhi, S., Umashankar, S., Low, P.M., Dale, J.L., Song, Y., Ng, S.P., Boothroyd, C.B., Dunny, G.M., Swarup, S., Williams, R.B.H., Marsili, E., Kline, K.A., 2018. Extracellular Electron Transfer Powers Enterococcus faecalis Biofilm Metabolism. mBio 9.
Khan, F.A., Fisher, M.A., Khakoo, R.A., 2007. Association of hemochromatosis with infectious diseases: expanding spectrum. International Journal of Infectious Diseases 11, 482-487.
Kim, G., Hyun, M., Chang, I., Kim, H., Park, H., Kim, B., Kim, S., Wimpenny, J., Weightman, A.J., 2005. Dissimilatory Fe (III) reduction by an electrochemically active lactic acid bacterium phylogenetically related to Enterococcus gallinarum isolated from submerged soil. Journal of applied microbiology 99, 978-987.
Kline, K.A., Kau, A.L., Chen, S.L., Lim, A., Pinkner, J.S., Rosch, J., Nallapareddy, S.R., Murray, B.E., Henriques-Normark, B., Beatty, W., Caparon, M.G., Hultgren, S.J., 2009. Mechanism for Sortase Localization and the Role of Sortase Localization in Efficient Pilus Assembly in Enterococcus faecalis. Journal of bacteriology 191, 3237-3247.
Kolaj-Robin, O., Russell, D., Hayes, K.A., Pembroke, J.T., Soulimane, T., 2015. Cation Diffusion Facilitator family: Structure and function. FEBS letters 589, 1283-1295.

Kopani, M., Miglierini, M., Lancok, A., Dekan, J., Caplovicova, M., Jakubovsky, J., Boca, R., Mrazova, H., 2015. Iron oxides in human spleen. Biometals 28, 913-928.
Kowalski, W.J., Kasper, E.L., Hatton, J.F., Murray, B.E., Nallapareddy, S.R., Gillespie, M.J., 2006. Enterococcus faecalis adhesin, Ace, mediates attachment to particulate dentin. J Endod 32, 634-637.
Krasteva, P.V., Giglio, K.M., Sondermann, H., 2012. Sensing the messenger: the diverse ways that bacteria signal through c-di-GMP. Protein science : a publication of the Protein Society 21, 929-948.
Kristich, C.J., Rice, L.B., Arias, C.A., 2014. Enterococcal Infection—Treatment and Antibiotic Resistance. In: Gilmore, M.S. (Ed.), Enterococci: From Commensals to Leading Causes of Drug Resistant Infection. Massachusetts Eye and Ear Infirmary, Boston.
Kristich, C.J., Li, Y.H., Cvitkovitch, D.G., Dunny, G.M., 2004. Esp-independent biofilm formation by Enterococcus faecalis. Journal of bacteriology 186, 154-163.
Kristich, C.J., Nguyen, V.T., Le, T., Barnes, A.M., Grindle, S., Dunny, G.M., 2008. Development and use of an efficient system for random mariner transposon mutagenesis to identify novel genetic determinants of biofilm formation in the core Enterococcus faecalis genome. Applied and environmental microbiology 74, 3377-3386.
Kuo, C.H., Dai, Z.K., Wu, J.R., Hsieh, T.J., Hung, C.H., Hsu, J.H., 2009. Septic arthritis as the initial manifestation of fatal Vibrio vulnificus septicemia in a patient with thalassemia and iron overload. Pediatric blood & cancer 53, 1156-1158.
La Carbona, S., Sauvageot, N., Giard, J.C., Benachour, A., Posteraro, B., Auffray, Y., Sanguinetti, M., Hartke, A., 2007. Comparative study of the physiological roles of three peroxidases (NADH peroxidase, Alkyl hydroperoxide reductase and Thiol peroxidase) in oxidative stress response, survival inside macrophages and virulence of Enterococcus faecalis. Molecular microbiology 66, 1148-1163.
Lamarche, M.G., Wanner, B.L., Crepin, S., Harel, J., 2008. The phosphate regulon and bacterial virulence: a regulatory network connecting phosphate homeostasis and pathogenesis. FEMS microbiology reviews 32, 461-473.
Leang, C., Qian, X., Mester, T., Lovley, D.R., 2010. Alignment of the c-Type Cytochrome OmcS along Pili of Geobacter sulfurreducens. Applied and environmental microbiology 76, 4080-4084.
Lebreton, F., Willems, R.J.L., Gilmore, M.S., 2014. Enterococcus Diversity, Origins in Nature, and Gut Colonization. In: Gilmore, M.S., Clewell, D.B., Ike, Y., Shankar, N. (Eds.), Enterococci: From Commensals to Leading Causes of Drug Resistant Infection, Boston.
Lebreton, F., Riboulet-Bisson, E., Serror, P., Sanguinetti, M., Posteraro, B., Torelli, R., Hartke, A., Auffray, Y., Giard, J.C., 2009. ace, Which encodes an adhesin in Enterococcus faecalis, is regulated by Ers and is involved in virulence. Infection and immunity 77, 2832-2839.
Lee, K., Yoon, S.S., 2017. Pseudomonas aeruginosa Biofilm, a Programmed Bacterial Life for Fitness. Journal of microbiology and biotechnology 27, 1053-1064.
Lee, T., Clavel, T., Smirnov, K., Schmidt, A., Lagkouvardos, I., Walker, A., Lucio, M., Michalke, B., Schmitt-Kopplin, P., Fedorak, R., Haller, D., 2016. Oral versus intravenous iron replacement therapy distinctly alters the gut microbiota and metabolome in patients with IBD. Gut.
Li, J., Attila, C., Wang, L., Wood, T.K., Valdes, J.J., Bentley, W.E., 2007. Quorum Sensing in Escherichia coli Is Signaled by AI-2/LsrR: Effects on Small RNA and Biofilm Architecture. Journal of bacteriology 189, 6011-6020.
Light, S.H., Su, L., Rivera-Lugo, R., Cornejo, J.A., Louie, A., Iavarone, A.T., Ajo-Franklin, C.M., Portnoy, D.A., 2018. A flavin-based extracellular electron transfer mechanism in diverse Gram-positive bacteria. Nature.
Lisiecki, P., 2014. [Antibiotic resistance and siderophore production in enterococci]. Medycyna doswiadczalna i mikrobiologia 66, 1-10.
Lisiecki, P., Mikucki, J., 2006. Iron supply of enterococci by 2-oxoacids and hydroxyacids. Polish journal of microbiology / Polskie Towarzystwo Mikrobiologow = The Polish Society of Microbiologists 55, 195-202.

Lisiecki, P., Wysocki, P., Mikucki, J., 2000. Occurrence of siderophores in enterococci. Zentralblatt fur Bakteriologie : international journal of medical microbiology 289, 807-815.
Liu, M., Yuan, Y., Zhang, L.-x., Zhuang, L., Zhou, S.-g., Ni, J.-r., 2010. Bioelectricity generation by a Gram-positive Corynebacterium sp. strain MFC03 under alkaline condition in microbial fuel cells. Bioresource technology 101, 1807-1811.
Lopez, G., Latorre, M., Reyes-Jara, A., Cambiazo, V., Gonzalez, M., 2012. Transcriptomic response of Enterococcus faecalis to iron excess. Biometals : an international journal on the role of metal ions in biology, biochemistry, and medicine 25, 737-747.
Low, Y.L., Jakubovics, N.S., Flatman, J.C., Jenkinson, H.F., Smith, A.W., 2003. Manganese-dependent regulation of the endocarditis-associated virulence factor EfaA of Enterococcus faecalis. Journal of medical microbiology 52, 113-119.
Manias, D.A., Dunny, G.M., 2018. Expression of Adhesive Pili and the Collagen-binding Adhesin ACE is Activated by ArgR Family Transcription Factors in Enterococcus faecalis. Journal of bacteriology.
Marcelis, J.H., den Daas-Slagt, H.J., Hoogkamp-Korstanje, J.A., 1978. Iron requirement and chelator production of staphylococci, Streptococcus faecalis and enterobacteriaceae. Antonie Van Leeuwenhoek 44, 257-267.
Marsili, E., Rollefson, J.B., Baron, D.B., Hozalski, R.M., Bond, D.R., 2008a. Microbial biofilm voltammetry: direct electrochemical characterization of catalytic electrode-attached biofilms. Applied and environmental microbiology 74, 7329-7337.
Marsili, E., Baron, D.B., Shikhare, I.D., Coursolle, D., Gralnick, J.A., Bond, D.R., 2008b. Shewanella secretes flavins that mediate extracellular electron transfer. Proceedings of the National Academy of Sciences of the United States of America 105, 3968-3973.
Maskell, J.P., 1980. The functional interchangeability of enterobacterial and staphylococcal iron chelators. Antonie van Leeuwenhoek 46, 343-351.
Miot, J., Benzerara, K., Obst, M., Kappler, A., Hegler, F., Schädler, S., Bouchez, C., Guyot, F., Morin, G., 2009. Extracellular Iron Biomineralization by Photoautotrophic Iron-Oxidizing Bacteria. Applied and environmental microbiology 75, 5586-5591.
Mohamed, J.A., Teng, F., Nallapareddy, S.R., Murray, B.E., 2006. Pleiotrophic effects of 2 Enterococcus faecalis sagA-like genes, salA and salB, which encode proteins that are antigenic during human infection, on biofilm formation and binding to collagen type i and fibronectin. J Infect Dis 193, 231-240.
Monds, R.D., O'Toole, G.A., 2009. The developmental model of microbial biofilms: ten years of a paradigm up for review. Trends in microbiology 17, 73-87.
Montanaro, L., Poggi, A., Visai, L., Ravaioli, S., Campoccia, D., Speziale, P., Arciola, C.R., 2011. Extracellular DNA in biofilms. The International journal of artificial organs 34, 824-831.
Mostertz, J., Scharf, C., Hecker, M., Homuth, G., 2004. Transcriptome and proteome analysis of Bacillus subtilis gene expression in response to superoxide and peroxide stress. Microbiology (Reading, England) 150, 497-512.
Nakashige, T.G., Zhang, B., Krebs, C., Nolan, E.M., 2015. Human calprotectin is an iron-sequestering host-defense protein. Nat Chem Biol 11, 765-771.
Nakayama, J., Chen, S., Oyama, N., Nishiguchi, K., Azab, E.A., Tanaka, E., Kariyama, R., Sonomoto, K., 2006. Revised model for Enterococcus faecalis fsr quorum-sensing system: the small open reading frame fsrD encodes the gelatinase biosynthesis-activating pheromone propeptide corresponding to staphylococcal agrd. Journal of bacteriology 188, 8321-8326.
Nallapareddy, S.R., Singh, K.V., Duh, R.W., Weinstock, G.M., Murray, B.E., 2000a. Diversity of ace, a gene encoding a microbial surface component recognizing adhesive matrix molecules, from different strains of Enterococcus faecalis and evidence for production of ace during human infections. Infection and immunity 68, 5210-5217.

Nallapareddy, S.R., Qin, X., Weinstock, G.M., Hook, M., Murray, B.E., 2000b. Enterococcus faecalis adhesin, ace, mediates attachment to extracellular matrix proteins collagen type IV and laminin as well as collagen type I. Infection and immunity 68, 5218-5224.
Nallapareddy, S.R., Singh, K.V., Sillanpaa, J., Zhao, M., Murray, B.E., 2011a. Relative contributions of Ebp Pili and the collagen adhesin ace to host extracellular matrix protein adherence and experimental urinary tract infection by Enterococcus faecalis OG1RF. Infection and immunity 79, 2901-2910.
Nallapareddy, S.R., Singh, K.V., Sillanpaa, J., Garsin, D.A., Hook, M., Erlandsen, S.L., Murray, B.E., 2006. Endocarditis and biofilm-associated pili of Enterococcus faecalis. The Journal of clinical investigation 116, 2799-2807.
Nallapareddy, S.R., Sillanpaa, J., Mitchell, J., Singh, K.V., Chowdhury, S.A., Weinstock, G.M., Sullam, P.M., Murray, B.E., 2011b. Conservation of Ebp-type pilus genes among Enterococci and demonstration of their role in adherence of Enterococcus faecalis to human platelets. Infection and immunity 79, 2911-2920.
Nielsen, H.V., Guiton, P.S., Kline, K.A., Port, G.C., Pinkner, J.S., Neiers, F., Normark, S., Henriques-Normark, B., Caparon, M.G., Hultgren, S.J., 2012. The metal ion-dependent adhesion site motif of the Enterococcus faecalis EbpA pilin mediates pilus function in catheter-associated urinary tract infection. mBio 3, e00177-00112.
Nielsen, H.V., Flores-Mireles, A.L., Kau, A.L., Kline, K.A., Pinkner, J.S., Neiers, F., Normark, S., Henriques-Normark, B., Caparon, M.G., Hultgren, S.J., 2013a. Pilin and Sortase Residues Critical for Endocarditis- and Biofilm-Associated Pilus Biogenesis in Enterococcus faecalis. Journal of bacteriology 195, 4484-4495.
Nielsen, H.V., Flores-Mireles, A.L., Kau, A.L., Kline, K.A., Pinkner, J.S., Neiers, F., Normark, S., Henriques-Normark, B., Caparon, M.G., Hultgren, S.J., 2013b. Pilin and sortase residues critical for endocarditis- and biofilm-associated pilus biogenesis in Enterococcus faecalis. Journal of bacteriology 195, 4484-4495.
Nies, D.H., Grass, G., 2009. Transition Metal Homeostasis. EcoSal Plus 3.
O'Toole, G., Kaplan, H.B., Kolter, R., 2000. Biofilm formation as microbial development. Annual review of microbiology 54, 49-79.
Okamoto, A., Nakamura, R., Hashimoto, K., 2011. In-vivo identification of direct electron transfer from Shewanella oneidensis MR-1 to electrodes via outer-membrane OmcA-MtrCAB protein complexes. Electrochim Acta 56, 5526-5531.
Ollinger, J., Song, K.B., Antelmann, H., Hecker, M., Helmann, J.D., 2006. Role of the Fur regulon in iron transport in Bacillus subtilis. Journal of bacteriology 188, 3664-3673.
Paganelli, F.L., Willems, R.J., Jansen, P., Hendrickx, A., Zhang, X., Bonten, M.J., Leavis, H.L., 2013. Enterococcus faecium biofilm formation: identification of major autolysin AtlAEfm, associated Acm surface localization, and AtlAEfm-independent extracellular DNA Release. MBio 4, e00154.
Paiva, C.N., Bozza, M.T., 2014. Are reactive oxygen species always detrimental to pathogens? Antioxidants & redox signaling 20, 1000-1037.
Palmer, K.L., Schaik, W.V., Willems, R.J.L., Gilmore, M.S., 2014. Enterococcal Genomics. In: Gilmore, M.S. (Ed.), Enterococci: From Commensals to Leading Causes of Drug Resistant Infection. Massachusetts Eye and Ear Infirmary, Boston.
Palmer, L.D., Skaar, E.P., 2016. Transition Metals and Virulence in Bacteria. Annual review of genetics.
Papp-Wallace, K.M., Maguire, M.E., 2006. Manganese transport and the role of manganese in virulence. Annual review of microbiology 60, 187-209.
Paulsen, I.T., Banerjei, L., Myers, G.S., Nelson, K.E., Seshadri, R., Read, T.D., Fouts, D.E., Eisen, J.A., Gill, S.R., Heidelberg, J.F., Tettelin, H., Dodson, R.J., Umayam, L., Brinkac, L., Beanan, M., Daugherty, S., DeBoy, R.T., Durkin, S., Kolonay, J., Madupu, R., Nelson, W., Vamathevan, J., Tran, B., Upton, J., Hansen, T., Shetty, J., Khouri, H., Utterback, T., Radune, D., Ketchum, K.A., Dougherty, B.A., Fraser, C.M., 2003. Role of mobile DNA in the evolution of vancomycin-resistant Enterococcus faecalis. Science (New York, N.Y.) 299, 2071-2074.

Pedersen, M.B., Gaudu, P., Lechardeur, D., Petit, M.A., Gruss, A., 2012. Aerobic respiration metabolism in lactic acid bacteria and uses in biotechnology. Annu Rev Food Sci Technol 3, 37-58.
Peng, X., Zhang, Y., Bai, G., Zhou, X., Wu, H., 2016a. Cyclic di-AMP mediates biofilm formation. Molecular microbiology 99, 945-959.
Peng, X., Zhang, Y., Bai, G., Zhou, X., Wu, H., 2016b. Cyclic di-AMP mediates biofilm formation. Molecular microbiology 99, 945-959.
Peppoloni, S., Posteraro, B., Colombari, B., Manca, L., Hartke, A., Giard, J.C., Sanguinetti, M., Fadda, G., Blasi, E., 2011. Role of the (Mn)superoxide dismutase of Enterococcus faecalis in the in vitro interaction with microglia. Microbiology (Reading, England) 157, 1816-1822.
Phillips, P., Schultz, G., 2012. Molecular Mechanisms of Biofilm Infection: Biofilm Virulence Factors. 109-114 pp.
Pinkston, K.L., Gao, P., Diaz-Garcia, D., Sillanpaa, J., Nallapareddy, S.R., Murray, B.E., Harvey, B.R., 2011. The Fsr quorum-sensing system of Enterococcus faecalis modulates surface display of the collagen-binding MSCRAMM Ace through regulation of gelE. Journal of bacteriology 193, 4317-4325.
Plow, E.F., Haas, T.A., Zhang, L., Loftus, J., Smith, J.W., 2000. Ligand Binding to Integrins. Journal of Biological Chemistry 275, 21785-21788.
Poole, R.K., Cook, G.M., 2000. Redundancy of aerobic respiratory chains in bacteria? Routes, reasons and regulation. Advances in microbial physiology 43, 165-224.
Qin, X., Singh, K.V., Xu, Y., Weinstock, G.M., Murray, B.E., 1998. Effect of disruption of a gene encoding an autolysin of Enterococcus faecalis OG1RF. Antimicrobial agents and chemotherapy 42, 2883-2888.
Ramsey, M., Hartke, A., Huycke, M., 2014a. The physiology and metabolism of Enterococci.
Ramsey, M., Hartke, A., Huycke, M.M., 2014b. The Physiology and Metabolism of Enterococci. In: Gilmore, M.S. (Ed.), Enterococci: From Commensals to Leading Causes of Drug Resistant Infection. Massachusetts Eye and Ear Infirmary, Boston.
Ramsey, M., Hartke, A., Huycke, M., 2014c. The Physiology and Metabolism of Enterococci. In: Gilmore, M.S., Clewell, D.B., Ike, Y., Shankar, N. (Eds.), Enterococci: From Commensals to Leading Causes of Drug Resistant Infection. Massachusetts Eye and Ear Infirmary, Boston.
Rana, N.F., Sauvageot, N., Laplace, J.M., Bao, Y., Nes, I., Rince, A., Posteraro, B., Sanguinetti, M., Hartke, A., 2013. Redox balance via lactate dehydrogenase is important for multiple stress resistance and virulence in *Enterococcus faecalis*. Infection and Immunity 81, 2662-2668.
Ratan, A., Junqueira, A.C.M., Azeredo-Espin, A.M.L., Premkrishnan, B.N., Linz, B., Paulo, D.F., Drautz-Moses, D.I., Bryant, D.A., Acerbi, E., Gaultier, N.E., 2017. The microbiomes of blowflies and houseflies as bacterial transmission reservoirs. Scientific reports 7, 16324.
Reardon, P.N., Mueller, K.T., 2013a. Structure of the type IVa major pilin from the electrically conductive bacterial nanowires of Geobacter sulfurreducens. The Journal of biological chemistry 288, 29260-29266.
Reardon, P.N., Mueller, K.T., 2013b. Structure of the Type IVa Major Pilin from the Electrically Conductive Bacterial Nanowires of Geobacter sulfurreducens. Journal of Biological Chemistry 288, 29260-29266.
Reguera, G., Pollina, R.B., Nicoll, J.S., Lovley, D.R., 2007. Possible nonconductive role of Geobacter sulfurreducens pilus nanowires in biofilm formation. Journal of bacteriology 189, 2125-2127.
Reid, G., Denstedt, J.D., Kang, Y.S., Lam, D., Nause, C., 1992. Microbial adhesion and biofilm formation on ureteral stents in vitro and in vivo. The Journal of urology 148, 1592-1594.
Rezaiki, L., Lamberet, G., Derre, A., Gruss, A., Gaudu, P., 2008. Lactococcus lactis produces short-chain quinones that cross-feed Group B Streptococcus to activate respiration growth. Mol Microbiol 67, 947-957.
Ribbe, J., Baker, A.E., Euler, S., O'Toole, G.A., Maier, B., 2017. Role of Cyclic Di-GMP and Exopolysaccharide in Type IV Pilus Dynamics. Journal of bacteriology 199.

Riboulet, E., Verneuil, N., La Carbona, S., Sauvageot, N., Auffray, Y., Hartke, A., Giard, J.C., 2007a. Relationships between oxidative stress response and virulence in Enterococcus faecalis. Journal of molecular microbiology and biotechnology 13, 140-146.
Riboulet, E., Verneuil, N., La Carbona, S., Sauvageot, N., Auffray, Y., Hartke, A., Giard, J.C., 2007b. Relationships between oxidative stress response and virulence in Enterococcus faecalis. Journal of molecular microbiology and biotechnology 13, 140-146.
Richardson, D.J., 2000. Bacterial respiration: a flexible process for a changing environment. Microbiology 146 (Pt 3), 551-571.
Robbel, L., Helmetag, V., Knappe, T.A., Marahiel, M.A., 2011. Consecutive enzymatic modification of ornithine generates the hydroxamate moieties of the siderophore erythrochelin. Biochemistry 50, 6073-6080.
Roder, P.V., Wu, B., Liu, Y., Han, W., 2016. Pancreatic regulation of glucose homeostasis. Experimental & molecular medicine 48, e219.
Rodesney, C.A., Roman, B., Dhamani, N., Cooley, B.J., Katira, P., Touhami, A., Gordon, V.D., 2017. Mechanosensing of shear by Pseudomonas aeruginosa leads to increased levels of the cyclic-di-GMP signal initiating biofilm development. Proceedings of the National Academy of Sciences 114, 5906-5911.
Rolfe, M.D., Rice, C.J., Lucchini, S., Pin, C., Thompson, A., Cameron, A.D., Alston, M., Stringer, M.F., Betts, R.P., Baranyi, J., Peck, M.W., Hinton, J.C., 2012. Lag phase is a distinct growth phase that prepares bacteria for exponential growth and involves transient metal accumulation. J Bacteriol 194, 686-701.
Rosch, J.W., Gao, G., Ridout, G., Wang, Y.D., Tuomanen, E.I., 2009. Role of the manganese efflux system mntE for signalling and pathogenesis in Streptococcus pneumoniae. Molecular microbiology 72, 12-25.
Rozdzinski, E., Marre, R., Susa, M., Wirth, R., Muscholl-Silberhorn, A., 2001. Aggregation substance-mediated adherence of Enterococcus faecalis to immobilized extracellular matrix proteins. Microb Pathog 30, 211-220.
Saha, M., Sarkar, S., Sarkar, B., Sharma, B.K., Bhattacharjee, S., Tribedi, P., 2016. Microbial siderophores and their potential applications: a review. Environmental science and pollution research international 23, 3984-3999.
Said, H.M., 2018. Physiology of the Gastrointestinal Tract. Academic Press, 1812 pp.
Sbalzarini, I.F., Koumoutsakos, P., 2005. Feature point tracking and trajectory analysis for video imaging in cell biology. J Struct Biol 151, 182-195.
Schaible, U.E., Kaufmann, S.H., 2004. Iron and microbial infection. Nature reviews. Microbiology 2, 946-953.
Schindelin, J., Arganda-Carreras, I., Frise, E., Kaynig, V., Longair, M., Pietzsch, T., Preibisch, S., Rueden, C., Saalfeld, S., Schmid, B., Tinevez, J.Y., White, D.J., Hartenstein, V., Eliceiri, K., Tomancak, P., Cardona, A., 2012. Fiji: an open-source platform for biological-image analysis. Nat Methods 9, 676-682.
Schröder, U., Harnisch, F., Angenent, L.T., 2015. Microbial electrochemistry and technology: terminology and classification. Energy & Environmental Science 8, 513-519.
Sekirov, I., Russell, S.L., Antunes, L.C., Finlay, B.B., 2010. Gut microbiota in health and disease. Physiol Rev 90, 859-904.
Seneviratne, C.J., Yip, J.W., Chang, J.W., Zhang, C.F., Samaranayake, L.P., 2013. Effect of culture media and nutrients on biofilm growth kinetics of laboratory and clinical strains of Enterococcus faecalis. Arch Oral Biol 58, 1327-1334.
Shankar, N., Lockatell, C.V., Baghdayan, A.S., Drachenberg, C., Gilmore, M.S., Johnson, D.E., 2001. Role of Enterococcus faecalis surface protein Esp in the pathogenesis of ascending urinary tract infection. Infection and immunity 69, 4366-4372.

Shao, C., Shang, W., Yang, Z., Sun, Z., Li, Y., Guo, J., Wang, X., Zou, D., Wang, S., Lei, H., Cui, Q., Yin, Z., Li, X., Wei, X., Liu, W., He, X., Jiang, Z., Du, S., Liao, X., Huang, L., Wang, Y., Yuan, J., 2012. LuxS-dependent AI-2 regulates versatile functions in Enterococcus faecalis V583. Journal of proteome research 11, 4465-4475.
Shi, L., Richardson, D.J., Wang, Z., Kerisit, S.N., Rosso, K.M., Zachara, J.M., Fredrickson, J.K., 2009. The roles of outer membrane cytochromes of Shewanella and Geobacter in extracellular electron transfer. Environmental microbiology reports 1, 220-227.
Shi, L., Dong, H., Reguera, G., Beyenal, H., Lu, A., Liu, J., Yu, H.Q., Fredrickson, J.K., 2016. Extracellular electron transfer mechanisms between microorganisms and minerals. Nature reviews. Microbiology 14, 651-662.
Shiwei, L., Xiang, L., Feng, G., 2015. Progress of iron-chelating therapy for iron overload in patients after bone marrow transplantation. Yi chuan = Hereditas / Zhongguo yi chuan xue hui bian ji 37, 865-872.
Sillanpaa, J., Nallapareddy, S.R., Singh, K.V., Prakash, V.P., Fothergill, T., Ton-That, H., Murray, B.E., 2010. Characterization of the ebp(fm) pilus-encoding operon of Enterococcus faecium and its role in biofilm formation and virulence in a murine model of urinary tract infection. Virulence 1, 236-246.
Sillanpaa, J., Chang, C., Singh, K.V., Montealegre, M.C., Nallapareddy, S.R., Harvey, B.R., Ton-That, H., Murray, B.E., 2013. Contribution of individual Ebp Pilus subunits of Enterococcus faecalis OG1RF to pilus biogenesis, biofilm formation and urinary tract infection. PloS one 8, e68813.
Singh, K.V., Nallapareddy, S.R., Murray, B.E., 2007. Importance of the ebp (endocarditis- and biofilm-associated pilus) locus in the pathogenesis of Enterococcus faecalis ascending urinary tract infection. J Infect Dis 195, 1671-1677.
Singh, K.V., Coque, T.M., Weinstock, G.M., Murray, B.E., 1998. In vivo testing of an Enterococcus faecalis efaA mutant and use of efaA homologs for species identification. FEMS immunology and medical microbiology 21, 323-331.
Singh, K.V., Nallapareddy, S.R., Sillanpaa, J., Murray, B.E., 2010. Importance of the collagen adhesin ace in pathogenesis and protection against Enterococcus faecalis experimental endocarditis. PLoS pathogens 6, e1000716.
Smith, J.A., Tremblay, P.L., Shrestha, P.M., Snoeyenbos-West, O.L., Franks, A.E., Nevin, K.P., Lovley, D.R., 2014a. Going wireless: Fe(III) oxide reduction without pili by Geobacter sulfurreducens strain JS-1. Applied and environmental microbiology 80, 4331-4340.
Smith, J.A., Tremblay, P.-L., Shrestha, P.M., Snoeyenbos-West, O.L., Franks, A.E., Nevin, K.P., Lovley, D.R., 2014b. Going Wireless: Fe(III) Oxide Reduction without Pili by Geobacter sulfurreducens Strain JS-1. Applied and environmental microbiology 80, 4331-4340.
Solano, C., Echeverz, M., Lasa, I., 2014. Biofilm dispersion and quorum sensing. Current opinion in microbiology 18, 96-104.
Sprencel, C., Cao, Z., Qi, Z., Scott, D.C., Montague, M.A., Ivanoff, N., Xu, J., Raymond, K.M., Newton, S.M., Klebba, P.E., 2000. Binding of ferric enterobactin by the Escherichia coli periplasmic protein FepB. Journal of bacteriology 182, 5359-5364.
Stewart, P.S., 2002. Mechanisms of antibiotic resistance in bacterial biofilms. International journal of medical microbiology : IJMM 292, 107-113.
Stickler, D.J., King, J.B., Winters, C., Morris, S.L., 1993. Blockage of urethral catheters by bacterial biofilms. Journal of Infection 27, 133-135.
Sure, S.K., Ackland, L.M., Torriero, A.A., Adholeya, A., Kochar, M., 2016. Microbial Nanowires: An Electrifying Tale. Microbiology (Reading, England).
Sussmuth, S.D., Muscholl-Silberhorn, A., Wirth, R., Susa, M., Marre, R., Rozdzinski, E., 2000. Aggregation substance promotes adherence, phagocytosis, and intracellular survival of Enterococcus faecalis within human macrophages and suppresses respiratory burst. Infection and immunity 68, 4900-4906.
Taketani, S., 2005. Aquisition, mobilization and utilization of cellular iron and heme: endless findings and growing evidence of tight regulation. The Tohoku journal of experimental medicine 205, 297-318.

Tan, Y., Adhikari, R.Y., Malvankar, N.S., Ward, J.E., Woodard, T.L., Nevin, K.P., Lovley, D.R., 2017. Expressing the Geobacter metallireducens PilA in Geobacter sulfurreducens Yields Pili with Exceptional Conductivity. mBio 8.
Team, R.C., 2016. R: A Language and Environment for Statistical Computing.
Theilacker, C., Sanchez-Carballo, P., Toma, I., Fabretti, F., Sava, I., Kropec, A., Holst, O., Huebner, J., 2009. Glycolipids are involved in biofilm accumulation and prolonged bacteraemia in Enterococcus faecalis. Molecular microbiology 71, 1055-1069.
Thomas, V.C., Thurlow, L.R., Boyle, D., Hancock, L.E., 2008. Regulation of autolysis-dependent extracellular DNA release by Enterococcus faecalis extracellular proteases influences biofilm development. Journal of bacteriology 190, 5690-5698.
Thomas, V.C., Hiromasa, Y., Harms, N., Thurlow, L., Tomich, J., Hancock, L.E., 2009. A fratricidal mechanism is responsible for eDNA release and contributes to biofilm development of Enterococcus faecalis. Mol Microbiol 72, 1022-1036.
Thurlow, L.R., Thomas, V.C., Narayanan, S., Olson, S., Fleming, S.D., Hancock, L.E., 2010. Gelatinase contributes to the pathogenesis of endocarditis caused by Enterococcus faecalis. Infection and immunity 78, 4936-4943.
Toledo-Arana, A., Valle, J., Solano, C., Arrizubieta, M.J., Cucarella, C., Lamata, M., Amorena, B., Leiva, J., Penades, J.R., Lasa, I., 2001. The enterococcal surface protein, Esp, is involved in Enterococcus faecalis biofilm formation. Applied and environmental microbiology 67, 4538-4545.
Townsley, L., Yannarell, S.M., Huynh, T.N., Woodward, J.J., Shank, E.A., 2018. Cyclic di-AMP Acts as an Extracellular Signal That Impacts Bacillus subtilis Biofilm Formation and Plant Attachment. mBio 9.
Troxell, B., Hassan, H.M., 2013. Transcriptional regulation by Ferric Uptake Regulator (Fur) in pathogenic bacteria. Frontiers in cellular and infection microbiology 3, 59.
Valko, M., Morris, H., Cronin, M.T., 2005. Metals, toxicity and oxidative stress. Current medicinal chemistry 12, 1161-1208.
Varahan, S., Iyer, V.S., Moore, W.T., Hancock, L.E., 2013. Eep confers lysozyme resistance to enterococcus faecalis via the activation of the extracytoplasmic function sigma factor SigV. Journal of bacteriology 195, 3125-3134.
Varahan, S., Harms, N., Gilmore, M.S., Tomich, J.M., Hancock, L.E., 2014. An ABC Transporter Is Required for Secretion of Peptide Sex Pheromones in Enterococcus faecalis. mBio 5.
Vargas, M., Malvankar, N.S., Tremblay, P.L., Leang, C., Smith, J.A., Patel, P., Snoeyenbos-West, O., Nevin, K.P., Lovley, D.R., 2013. Aromatic amino acids required for pili conductivity and long-range extracellular electron transport in Geobacter sulfurreducens. mBio 4, e00105-00113.
Vebo, H.C., Snipen, L., Nes, I.F., Brede, D.A., 2009. The transcriptome of the nosocomial pathogen Enterococcus faecalis V583 reveals adaptive responses to growth in blood. PloS one 4, e7660.
Vebo, H.C., Solheim, M., Snipen, L., Nes, I.F., Brede, D.A., 2010. Comparative genomic analysis of pathogenic and probiotic Enterococcus faecalis isolates, and their transcriptional responses to growth in human urine. PloS one 5, e12489.
Verneuil, N., Rince, A., Sanguinetti, M., Auffray, Y., Hartke, A., Giard, J.C., 2005a. Implication of hypR in the virulence and oxidative stress response of Enterococcus faecalis. FEMS microbiology letters 252, 137-141.
Verneuil, N., Sanguinetti, M., Le Breton, Y., Posteraro, B., Fadda, G., Auffray, Y., Hartke, A., Giard, J.C., 2004. Effects of the Enterococcus faecalis hypR gene encoding a new transcriptional regulator on oxidative stress response and intracellular survival within macrophages. Infection and immunity 72, 4424-4431.
Verneuil, N., Rince, A., Sanguinetti, M., Posteraro, B., Fadda, G., Auffray, Y., Hartke, A., Giard, J.C., 2005b. Contribution of a PerR-like regulator to the oxidative-stress response and virulence of Enterococcus faecalis. Microbiology (Reading, England) 151, 3997-4004.

Verneuil, N., Maze, A., Sanguinetti, M., Laplace, J.M., Benachour, A., Auffray, Y., Giard, J.C., Hartke, A., 2006. Implication of (Mn)superoxide dismutase of Enterococcus faecalis in oxidative stress responses and survival inside macrophages. Microbiology (Reading, England) 152, 2579-2589.
Voegele, R.T., Sweet, G.D., Boos, W., 1993. Glycerol kinase of Escherichia coli is activated by interaction with the glycerol facilitator. Journal of bacteriology 175, 1087-1094.
von Canstein, H., Ogawa, J., Shimizu, S., Lloyd, J.R., 2008. Secretion of flavins by Shewanella species and their role in extracellular electron transfer. Applied and environmental microbiology 74, 615-623.
Vorkapic, D., Pressler, K., Schild, S., 2016. Multifaceted roles of extracellular DNA in bacterial physiology. Current genetics 62, 71-79.
Wang, V.B., Chua, S.-L., Cao, B., Seviour, T., Nesatyy, V.J., Marsili, E., Kjelleberg, S., Givskov, M., Tolker-Nielsen, T., Song, H., 2013. Engineering PQS biosynthesis pathway for enhancement of bioelectricity production in Pseudomonas aeruginosa microbial fuel cells. PloS one 8, e63129.
Wang, X., Davlieva, M., Reyes, J., Panesso, D., Arias, C.A., Shamoo, Y., 2017. A Novel Phosphodiesterase of the GdpP Family Modulates Cyclic di-AMP Levels in Response to Cell Membrane Stress in Daptomycin-Resistant Enterococci. Antimicrobial agents and chemotherapy 61, e01422-01416.
Wang, Y., Kern, S.E., Newman, D.K., 2010a. Endogenous phenazine antibiotics promote anaerobic survival of Pseudomonas aeruginosa via extracellular electron transfer. Journal of bacteriology 192, 365-369.
Wang, Y., Kern, S.E., Newman, D.K., 2010b. Endogenous Phenazine Antibiotics Promote Anaerobic Survival of Pseudomonas aeruginosa via Extracellular Electron Transfer. Journal of bacteriology 192, 365-369.
Waters, C.M., Antiporta, M.H., Murray, B.E., Dunny, G.M., 2003. Role of the Enterococcus faecalis GelE protease in determination of cellular chain length, supernatant pheromone levels, and degradation of fibrin and misfolded surface proteins. Journal of bacteriology 185, 3613-3623.
Waters, C.M., Hirt, H., McCormick, J.K., Schlievert, P.M., Wells, C.L., Dunny, G.M., 2004. An amino-terminal domain of Enterococcus faecalis aggregation substance is required for aggregation, bacterial internalization by epithelial cells and binding to lipoteichoic acid. Molecular microbiology 52, 1159-1171.
Weber, K.A., Achenbach, L.A., Coates, J.D., 2006. Microorganisms pumping iron: anaerobic microbial iron oxidation and reduction. Nature reviews. Microbiology 4, 752-764.
Weinberg, E.D., 1997. The Lactobacillus anomaly: total iron abstinence. Perspectives in biology and medicine 40, 578-583.
Weinberg, E.D., 1999. Iron loading and disease surveillance. Emerging infectious diseases 5, 346-352.
Weinberg, E.D., 2010. The hazards of iron loading. Metallomics 2, 732-740.
Whittaker, C.A., Hynes, R.O., 2002. Distribution and evolution of von Willebrand/integrin A domains: widely dispersed domains with roles in cell adhesion and elsewhere. Molecular biology of the cell 13, 3369-3387.
Winstedt, L., Frankenberg, L., Hederstedt, L., von Wachenfeldt, C., 2000. Enterococcus faecalis V583 contains a cytochrome bd-type respiratory oxidase. Journal of bacteriology 182, 3863-3866.
Wooldridge, K.G., Williams, P.H., 1993. Iron uptake mechanisms of pathogenic bacteria. FEMS microbiology reviews 12, 325-348.
Wrighton, K., Thrash, J., Melnyk, R., Bigi, J., Byrne-Bailey, K., Remis, J., Schichnes, D., Auer, M., Chang, C., Coates, J., 2011. Evidence for direct electron transfer by a Gram-positive bacterium isolated from a microbial fuel cell. Applied and environmental microbiology 77, 7633-7639.
Wu, H.J., Seib, K.L., Srikhanta, Y.N., Kidd, S.P., Edwards, J.L., Maguire, T.L., Grimmond, S.M., Apicella, M.A., McEwan, A.G., Jennings, M.P., 2006. PerR controls Mn-dependent resistance to oxidative stress in Neisseria gonorrhoeae. Molecular microbiology 60, 401-416.
Wyatt, T.D., 2014. Proteins and peptides as pheromone signals and chemical signatures. Animal Behaviour 97, 273-280.

Yan, X., Budin-Verneuil, A., Verneuil, N., Gilmore, M.S., Artigaud, S., Auffray, Y., Pichereau, V., 2015. Transcriptomic Response of Enterococcus faecalis V583 to Low Hydrogen Peroxide Levels. Current Microbiology 70, 156-168.
Yeh, J.I., Kettering, R., Saxl, R., Bourand, A., Darbon, E., Joly, N., Briozzo, P., Deutscher, J., 2009. Structural Characterizations of Glycerol Kinase: unraveling phosphorylation-induced long-range activation. Biochemistry 48, 346-356.
Yu, G., Wang, L.G., Han, Y., He, Q.Y., 2012. clusterProfiler: an R package for comparing biological themes among gene clusters. Omics : a journal of integrative biology 16, 284-287.
Zawadzka, A.M., Kim, Y., Maltseva, N., Nichiporuk, R., Fan, Y., Joachimiak, A., Raymond, K.N., 2009. Characterization of a Bacillus subtilis transporter for petrobactin, an anthrax stealth siderophore. Proceedings of the National Academy of Sciences of the United States of America 106, 21854-21859.
Zhang, E., Cai, Y., Luo, Y., Piao, Z., 2014. Riboflavin-shuttled extracellular electron transfer from Enterococcus faecalis to electrodes in microbial fuel cells. Can J Microbiol 60, 753-759.
Zhao, L., Xue, T., Shang, F., Sun, H., Sun, B., 2010. Staphylococcus aureus AI-2 Quorum Sensing Associates with the KdpDE Two-Component System To Regulate Capsular Polysaccharide Synthesis and Virulence. Infection and immunity 78, 3506-3515.